The Advanced Centre for Biochemical Engineering

Department of Biochemical Engineering

University College London

Microfabricated Devices for Adherent Stem Cell Culture

Thesis submitted towards Doctor of Philosophy by

Rhys Jarred Macown

28/03/2015

Supervisor: Dr Nicolas Szita

Advisor: Dr Farlan Veraitch

I, Rhys Jarred Macown, confirm that the work presented in this thesis is my own. Where information has been derived from other sources, I confirm that this has been indicated in the thesis.

Signature..... Date.....

Abstract

This thesis details the development of a system of microfabricated devices for the adherent culture of stem cells. The multipotency and self renewal of stem cells make them a potentially abundant source of valuable human cells, for both drug screening and regenerative medicine. However, processing stem cells is challenging due to the complexity of whole cell products, the number of process parameters, and the typical use of adherent culture. It is hypothesised that a microfabricated adherent culture system could facilitate process development with minimal use of resources. Furthermore, microfluidic systems offer advantages in spatial and temporal control over the microenvironment that would benefit process development.

An existing prototype culture system is critically evaluated by: assessing the design, modelling fluid flow and dissolved oxygen, and successfully co-culturing human embryonic stem cells, on inactivated mouse embryonic fibroblasts, under perfused conditions. The utilisation of reversible seals facilitates the use of standard tissue-culture polystyrene culture surfaces and manual seeding techniques. The evaluation of the prototype system is used to inform improvements to the design, making it easier to use, increasing the robustness, allowing monitoring of whole culture chambers by microscopy, and improving control over mean pericellular dissolved oxygen. Modelling shows the improved culture system also achieves more uniform distribution of both pericellular dissolved oxygen and fluid velocity.

The improved culture system shows similar mouse embryonic stem cell seeding behaviour to tissue culture flasks, but, with medium perfused at 300 $\mu l.h^{-1}$, mouse embryonic stem cells reach full confluency in less than 48 h, compared with 72 hours for cells maintained statically in flasks. There is also inconclusive data suggesting that the growth rate is limited by pericellular dissolved oxygen and is, therefore, increased and made more uniform by the inclusion of a gas permeable lid system. The reliability, ease of use, comparability with traditional culture systems, and control over process parameters of the improved system should make it a useful tool for stem cell process development.

Acknowledgements

I would like to thank University College London, the late Professor Peter Dunnill and his wife Pat for their financial support. I would like to thank my supervisors Professor Nicolas Szita and Dr Farlan Veraitch for their guidance and support throughout this project. I would also like to thank Dr Brian O'Sullivan and Mrs Ludmila Ruban for their technical support and advice, in microfluidics and cell culture respectively. I would like to acknowledge the work of Dr Marcel Reichen, which preceded this project, and thank him for the time he spent introducing me to the project. Finally, I would like to thank my fellow researchers in the microfluidics group, particularly Nicolas Jaccard, Alexandre Super, James Lawrence and Matt Davies, for sharing their time, advice, experience and jokes.

Table of Contents

List of Figures

List of Tables

Nomenclature

BIF	Basic Image Feature
CNC	Computer Numerical Control
DAPI	4',6-diamidino-2-phenylindole
DAQ	Data Acquisition Card
DMEM	Dulbecco’s Modified Eagle Medium
DO	Dissolved Oxygen (concentration)
DPBS	Dulbecco’s Phosphate Buffered Saline
ECM	Extra Cellular Matrix
EDTA	Ethylenediaminetetraacetic acid
ESC	Embryonic Stem Cell
FACS	Fluorescence Activated Cell Sorting
FBS	Foetal Bovine Serum
FGF2	Fibroblast Growth Factor 2
GMRES	Generalized Minimal Residual Method
hESC	Human Embryonic Stem Cell
iPSC	Induced Pluripotent Stem Cell
ITO	Indium-Tin-Oxide
LIF	Leukaemia Inhibitory Factor
MEF	Mouse Embryonic Fibroblast
mESC	Mouse Embryonic Stem Cell
NEAA	Non-essential Amino Acids
OUR	Oxygen Uptake Rate
PC	Polycarbonate
PDMS	poly(dimethylsiloxane)
PFA	Paraformaldehyde

PID	Proportional Integral Derivative (control)
pO_2	Partial pressure of Oxygen
PI	Propidium Iodide
PSC	Pluripotent Stem Cell
QbD	Quality by Design
SEM	Scanning Electron Microscope
qPCR	Quantitative Polymerase Chain Reaction
TC-PS	Tissue Culture Polystyrene
VI	(LabVIEW) Virtual Instrument

1. Introduction

Stem cells are a promising new area of medical research. Stem cells offer a potentially limitless supply of human cells due to their capacity to self-renew and their potential to turn into multiple cell types of the human body. Hence, they can potentially be utilised to repair and replace tissues treating or curing a wide variety of illnesses and injuries (Southwell et al., 2014, Daley, 2012). Stem cells also promise to provide highly relevant model systems for drug screening (Egawa et al., 2012, Huh et al., 2010, Thomson, 2007). However, few stem cell therapies have thus far made it to the market (FDA, 2015). This is due, in part, to the difficulty of developing efficient production processes.

Stem cell processing presents a number of additional challenges when compared with the established mammalian cell bioprocessing sector (Kirouac and Zandstra, 2008). In stem cell processes, the cell itself is the product rather than a protein or small molecule. Whole cells are significantly more complex products to characterise and must be kept viable, functional, and safe throughout processing (Peterson and Loring, 2014, Taapken et al., 2011, Mitalipova et al., 2005). Additionally, the potential of stem cells to differentiate introduces a requirement to produce the right cell phenotype (Lee et al., 2013a, Serra et al., 2012). However, cell growth and cell fate are influenced by a large number of physical, chemical and biological factors, the optimum values of which change over time (Chen et al., 2014, Serra et al., 2012, Wagers, 2012, Discher et al., 2009, Scadden, 2006). Consequently, there is a very large experimental space to explore.

Unfortunately, many of the factors required for stem cell culture are extremely expensive (Serra et al., 2012). Furthermore, most stem cells do not naturally grow in suspension culture (Thomson et al., 1998, Amit et al., 2000, Itskovitz-Eldor et al., 2000, Kehat et al., 2001, Takahashi and Yamanaka, 2006) and adaptation to suspension may impact product quality. While suspension culture is well established in the biopharmecuticals industry, adherent culture is less so. Adherent cultures are typically performed in culture wells, culture flasks, and multilayered flasks (Serra et al., 2012). These are poor analogies to the highly

controlled and automated reactors used for suspension culture at bench, pilot, and production scale. A potential solution is microfluidics, where volumes are reduced to the order of microliters allowing better control and requiring fewer resources (El-Ali et al., 2006). Such a culture device would need to be carefully designed to control the wide variety of relevant factors while remaining relatable to other culture systems.

1.1 What are Stem Cells?

The term ‘stem cell’ encompasses a relatively broad range of cells. Rather than having a structural or metabolic role in an organism, the role of a stem cell is to produce other cell types for growth, regeneration or repair. They achieve this by cell division and differentiation through indistinct intermediary stages to produce mature cell types. Accordingly, the two key properties of stem cells are: the ability to turn into another cell type, and the capacity for self-renewal to avoid depletion (Thomson et al., 1998, Cai et al., 2004).

1.1.1 Properties of Stem Cells

Multipotency

Multipotency is a property attributed to cells that are able to differentiate into multiple types of more committed cells. In the context of stem cells, differentiation is defined as progress, by changes in gene expression, towards any committed adult cell phenotype. Differentiation is typically discussed in terms of discrete steps, where steps often represent branch points in the commitment to different cell types. However, it should be recognised that the process occurs by continuous dynamic changes in gene expression rather than discrete jumps from one pattern of gene expression to the next.

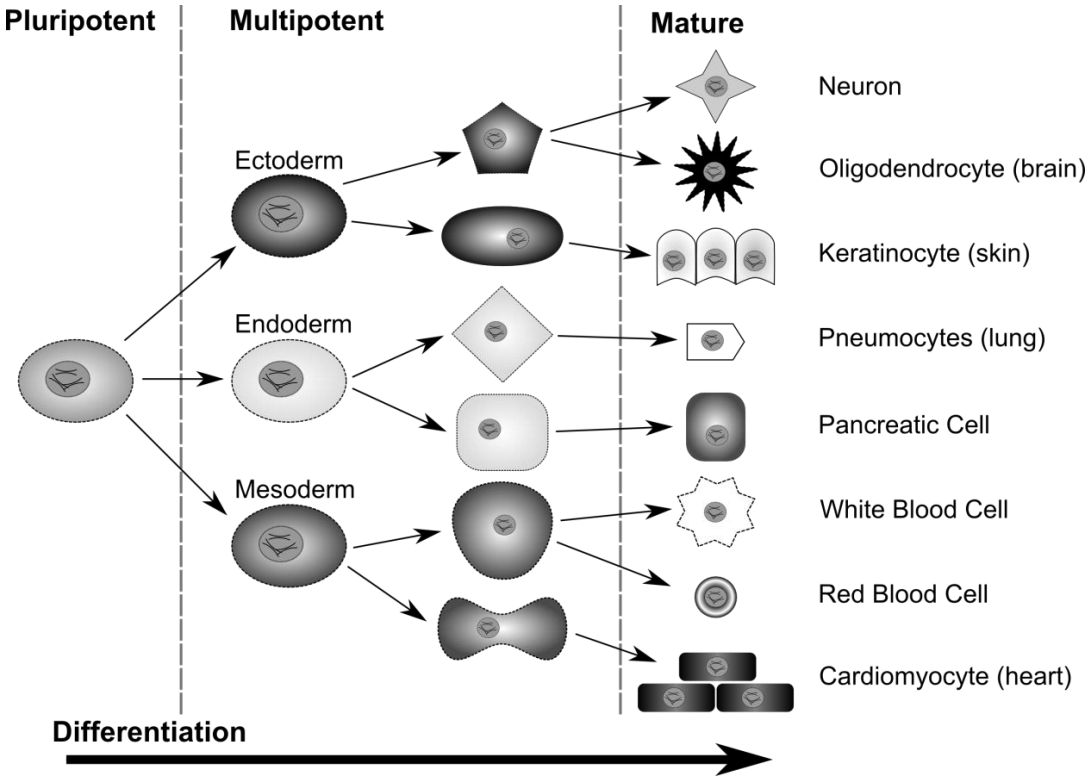

Figure 1.1 - Simplified schematic illustrating how cells progress through different stages of potency as they differentiate.

Adapted from Placzek *et al* (2009)

The level of potency attributed to cells can differ; as differentiation progresses, cells become committed to an increasingly narrow range of cell types. Cells are pluripotent if they are able to differentiate into any of the multipotent primary germ layers: endoderm, ectoderm and mesoderm (Osorno and Chambers, 2011). All adult cell types are in turn differentiated from one of these germ layers. The progression of differentiation from pluripotency through decreasing levels of potency to fully committed adult cells is illustrated in Figure 1.1.

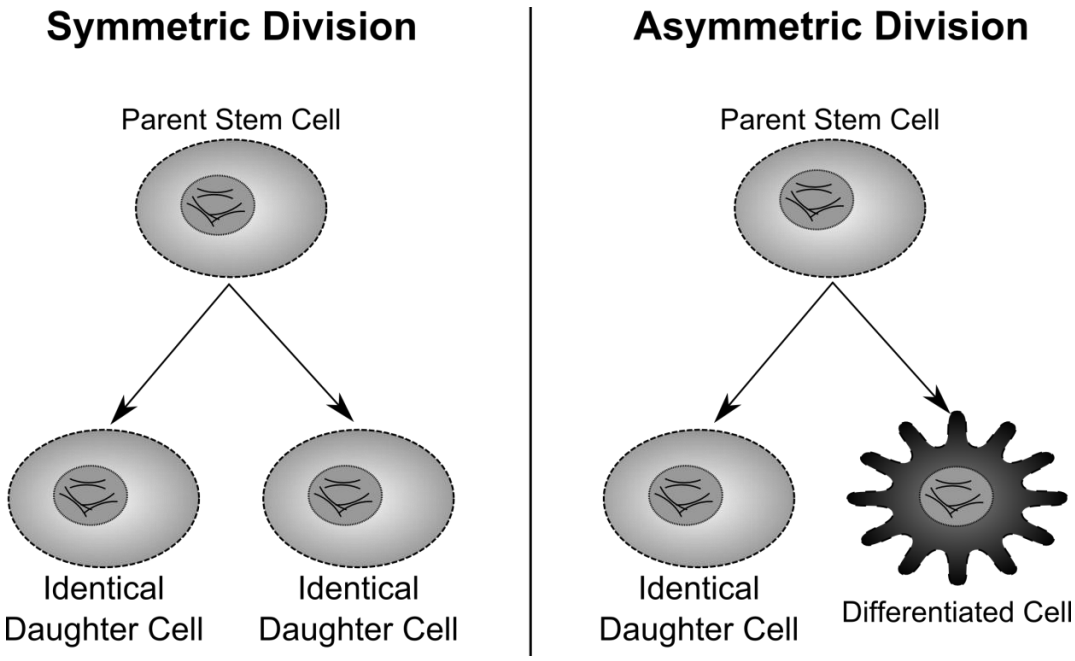

Figure 1.2 - Self-Renewal of stem cells by symmetric and asymmetric division.

Adapted from Morisson and Kimble (2006).

Self-Renewal

The process of self-renewal was reviewed in depth by Morrison and Kimble (2006). Self-renewal is the process through which identical daughter stem cells are produced by division of a parent stem cell. Stem cells can undertake either symmetric cell division, producing two identical daughter stem cells, or asymmetric cell division, producing a single identical daughter stem cell and another more differentiated daughter cell (Figure 1.2). Importantly, the identical daughter stem cells have the same potency and capacity for continued self-renewal as the parent cells. Pluripotent stem cells are considered immortal as they have the potential to indefinitely self-renew to expand or maintain their numbers. Stem cells express very high levels of telomerase activity, particularly embryonic stem cells (Hiyama and Hiyama, 2007). Telomerase adds telomere ends to chromosomes and is associated with cell immortality. Conversely, somatic cells express less telomerase activity and have a very limited lifespan.

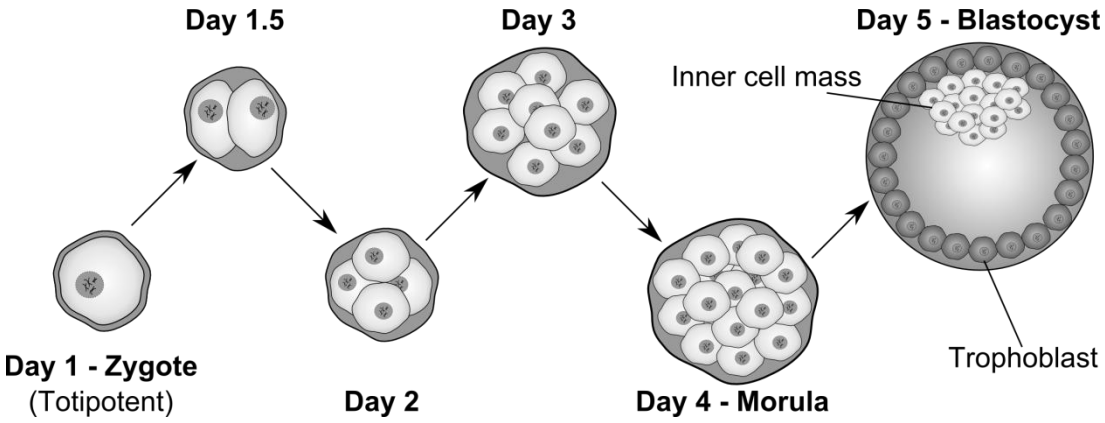

Figure 1.3 - Early embryonic development illustrating the inner cell mass form which embryonic stem cells are derived.

1.1.2 Pluripotent Stem Cells

Embryonic Stem Cells

Embryonic stem cells (ESCs) are pluripotent cells derived from the inner cell mass of a blastocyst (Figure 1.3) early in embryonic development. In normal development these cells go on to form all the tissues of the adult body. When undifferentiated ESCs are implanted into adult tissue they form teratomas (tumours containing cells from all three germ layers). When mouse ESCs are implanted into an immunodeficient blastocyst however, they play a normal role in development, producing a chimeric organism, with cells of both native and implanted origin present in every organ of the adult organism (Pease and Williams, 1990, Bradley et al., 1984). This is also true of teratoma cells implanted in a blastocyst (Brinster, 1976, Mintz and Illmensee, 1975). The presence of cells of implanted origin throughout chimera organisms illustrates the pluripotency of embryonic stem cells. Furthermore, the different outcomes of implantation in adult tissue and implantation in a blastocyst demonstrates the important influence of the microenvironment on the division and differentiation of ESCs (Zipori, 2009, p86-87).

Mouse embryonic stem cells were first derived in 1981 by Evans and Kaufman (Evans and Kaufman, 1981) while human ESC lines were first derived by Thompson *et al* in 1998 (Thomson et al., 1998). Human ESCs are derived from unneeded embryos prepared for in vitro fertilisation (IVF) treatment and donated

by the parents. Both mouse and human embryonic stem cell lines were first derived as adherent cultures. More recently, Steiner *et al* (2010) achieved the first derivation and expansion of human ESCs in suspension. Two of fifteen inner cell masses and one intact blastocyst proliferated in suspension to produce pluripotent cells with normal karyotypes.

Induced Pluripotent Stem Cells

A more recent development is the induced pluripotent stem cell (iPSC). Until recently, the loss of pluripotency by differentiation was considered irreversible. However, in 2006, Takahashi and Yamanaka showed that by introducing four genes into fully differentiated adult cells, those cells could be transformed into pluripotent stem cells similar to ESCs (Takahashi and Yamanaka, 2006). This new class of stem cells were classified induced pluripotent stem cells (iPSCs) and are often grouped with ESCs as pluripotent stem cells (PSCs). The original genes introduced to transform cells were Oct-4, Sox-2, Klf-4, and c-Myc in mouse and human fibroblasts cells and Oct-4, Sox-2, Nanog, and Lin28 in human fibroblasts (Yu et al., 2007, Takahashi et al., 2007, Takahashi and Yamanaka, 2006). Since then, induction of a pluripotent stem cell state has been demonstrated by various methods including introduction of proteins (Zhou et al., 2009), mRNA (Warren et al., 2010) and microRNAs (Miyoshi et al., 2011).

iPSCs are an important breakthrough for two key reasons. Firstly, as these pluripotent cells are not derived from human embryos they do not have the same ethical issues as ESCs. Secondly, iPSCs allow the production of pluripotent stem cells (PSCs) from any individual. This second point is important as it allows the production of more diverse cell line libraries for screening purposes and the production of autologous rather than allogeneic products for cell therapies (Both of these applications will be discussed further in section 1.2). However, concerns have recently been raised about genetic and epigenetic variations in iPSCs that may affect their suitability for clinical use (Serra et al., 2012, Lee et al., 2013a).

Tests for Pluripotent Stem Cells

ESCs and iPSCs are grouped together as pluripotent stem cells (PSCs). The ultimate test to identify cells as pluripotent stem cells is to implant them in immunodeficient embryos and show that they produce chimeras that have native and implanted cells present in all tissues of the adult organism (Zhang et al., 2013, Buta et al., 2013). This test has been applied to mouse PSCs but is not ethically possible with human PSCs and less exacting tests must be used. When implanted in immunodefficient mice, human PSCs will form teratomas containing tissues from all three germ layers (Zhang et al., 2013, Buta et al., 2013). Similarly, it is possible to direct differentiation of PSCs to all three germ layers *in vitro* or achieve all three germ layers through spontaneous differentiation in embryoid bodies (roughly spherical 3D aggregates of cells) (Zhang et al., 2013, Buta et al., 2013).

A more rapid if less rigorous assessment is to check for the expression of certain genes, which are expressed together in PSCs but not in more committed cells (Zhang et al., 2013, Buta et al., 2013). Among these genes the expression of Oct-4, Sox-2 and Nanog are common to both mouse and human PSCs, while SSEA-1 is expressed only in mouse PSCs and SSEA-3/4, Tra-1-81 and Tra-1-60 are expressed only in human PSCs (Zhang et al., 2013). In their review, Schnerch *et al* (2010) state that the Oct-4 and Nanog transcription factors are exclusively expressed in pluripotent cells of the developing human and mouse embryo, or its *in vitro* counterparts and are key to self-renewal and the maintenance of pluripotency. Sox-2 is also a marker of both mouse and human ESCs despite being expressed in some differentiated lineages (Schnerch et al., 2010). Human PSCs also express the stage specific surface markers SSEA-3, SSEA-4, Tra-1-60, and Tra-1-81, which are down regulated in differentiated cells (Draper et al., 2002), while mouse PSCs express SSEA-1 (Andrews, 1998).

Maintenance of Pluripotent Stem Cells

The maintenance of pluripotent stem cells requires the use of specific soluble growth factors that regulate the pathways involved in self renewal, pluripotency

and differentiation, as reviewed by Hyslop *et al* (2005). Maintenance of mouse PSCs requires Leukaemia Inhibitory Factor (LIF) and bone morphogenic protein 4 (BMP-4). BMP-4 can be supplied in serum, when serum is used to supplement medium, or added as a defined supplementary factor. BMP-4 induces genes that inhibit differentiation to neuroectoderm. LIF is always added as a defined supplementary factor and regulates genes to promote self-renewal and inhibit differentiation to mesoderm and endoderm. In contrast, maintenance of human PSCs requires Activin A and Transforming Growth Factor β (TGF-β), which can be supplemented or provided by co-cultured feeder cells, as well as Fibroblast Growth Factor 2 (FGF-2) as a defined supplementary growth factor. As with mouse PSCs, these factors regulate pathways that promote self-renewal and inhibit differentiation into the various germ lines.

1.1.3 Less Potent Stem Cells

Outside pluripotent stem cells, other stem cells exist that are more specified in the cell types they can produce (Volarevic et al., 2011). Adult stem cells are so called because they are found in the various tissues of the adult body (Volarevic et al., 2011). Similarly, foetal stem cells are derived from tissues of the foetus (Can and Karahuseyinoglu, 2007). The potency of these stem cells varies from multipotent haemopoietic stem cell to the unipotency of muscle progenitors. Like iPSCs, adult stem cells may be isolated from any individual, which allows the development of autologous treatments. Reduced potency could be considered a disadvantage as fewer cell types can be produced. However, reduced potency also results in easier processing as there is less potential to produce unwanted cells (Kirouac and Zandstra, 2008). As with PSCs, each type of stem cell expresses a certain combination of genes and requires a specific soluble environment to maintain their potency, self-renewal, and function (Scadden, 2006).

1.2 Why Stem Cells are Useful?

There are two broad uses for stem cells that take advantage of their unique properties. The first is as a source of cells and tissues for screening purposes

and the second is in regenerative medicine, either directly as stem cells or as a source of adult cells.

1.2.1 Cells and Tissues for Screening

Stem cells provide a new source of materials for biological screening. The development of new medicines currently necessitates animal trials followed by several phases of human trials. These trials are expensive and present a high risk both to the health of trial participants and the finances of the manufacturer. The development of a typical drug candidate currently takes approximately 13.5 years and costs $1.8 Billion USD (Paul et al., 2010). The continuing risk of failure throughout the development process contributes significantly to this high expense of drug development, a cost which is then passed on to the consumer. Stem cells may be able to significantly reduce the cost and risk of drug development as they provide a potentially unlimited source of all adult human cell types for screening purposes.

As stem cells can produce multiple cell types, drug candidates could be screened for their effects on both the cell types targeted by the drug candidate and other high risk tissues. Stem cells are also responsible for replacing senescent, damaged and missing cells throughout the body. They are therefore a useful tool to study processes such as wound healing and aging and how these are affected by different diseases and external factors. Furthermore, there is potential to generate complex 3D organoids to represent different organ systems in screening applications (Williamson et al., 2013, Huh et al., 2012, Huh et al., 2011). Some organoids have already been demonstrated including: vascular networks (Jeon et al., 2014, van der Meer et al., 2013), intestinal tissue (Kim and Ingber, 2013, Kimura et al., 2008), liver (Allen et al., 2005), lung (Douville et al., 2011, Huh et al., 2007), and cerebral organoids (Lancaster et al., 2013). iPSCs and adult stem cells are of particular interest for screening applications as cells can be derived with disease specific phenotypes and/or genotypes allowing patient specific drug screening (Yu et al., 2013, Egawa et al., 2012, Itzhaki et al., 2011, Liu et al., 2011).

The capacity to produce tissues from a wide range of human cell lines would allow extensive, species-specific testing of new medicines *in vitro* prior to *in vivo* testing. Consequently, it may be possible to eliminate or reduce animal trials and perform smaller, safer human trials. In addition to increasing safety for trial participants, this would reduce medicine development times and costs. Even if the length and cost of clinical trials remains the same, more representative pre-clinical trials would reduce the risks of clinical trials and, consequently, reduce the high costs incurred by drugs failing during clinical trials. In fact, models suggest that development costs are most sensitive to the success rate of phase II and III clinical trials (Paul et al., 2010).

1.2.2 Regenerative Medicine

The application with the potential for the most significant impact to human health is regenerative medicine. Regenerative medicine is the practice of replacing or regenerating damaged or missing cells (Mason and Dunnill, 2008). While this definition describes all transplants, the term is not generally applied to treatments where the donated cells are not required to expand in numbers (*in vivo* or *in vitro*) or promote proliferation of native cells (e.g. a heart or kidney transplant). Consequently, bone marrow transplants are often considered the original regenerative medicine; cells in the transplanted bone marrow expand to replenish and maintain blood cells in the recipient. Regenerative medicine includes the injection of cellular material (cell therapies) and the transplantation of grown tissues and organs (tissue engineering) (Mason and Dunnill, 2008).

Pluripotent stem cells have the potential to produce any cell type in the human body in large quantities. Hence, it should be possible to replace any damaged or missing cells (Hyslop et al., 2005) with cells produced from stem cells *in vitro* or produced *in vivo* from implanted stem cells. Further, due to their role in the natural maintenance and repair of tissues, the presence of certain types of stem cell may act to promote the body's natural healing processes (Kim et al., 2007b).

Cell therapies can be either autologous, where the cells originate from the patient, or allogeneic, where the cells originate from another donor (Serra et al., 2012). Autologous therapies are medically preferable for the treatment of non-genetic conditions as allogeneic therapies risk immune response and rejection. However, autologous therapies rely on the ability to derive healthy stem cells of the required type from the patient. Autologous therapies also require individual product batches for each patient (patient specific medicine), which is more demanding from a processing point of view (Serra et al., 2012).

Despite the promise of stem cells there are currently only 10 cell therapies on the market in the USA. 5 of these therapies are based on hematopoietic stem cells (FDA, 2015). These multipotent stem cells are responsible for the production of all blood cells. Bone marrow transplants, which have already been mentioned, are an example of a therapy based on the transplant of hematopoietic stem cells. However, bone marrow transplants are not classified as a cell therapy by the FDA. While originally only transplanted as bone marrow, in recent decades haematopoietic cells have been isolated from both umbilical cord blood (Broxmeyer et al., 1989) and peripheral blood (Kessinger, 1991) and expanded *in vitro (Brugger, 1993)*.

Stem cell therapies are currently being investigated for a wide range of conditions (Southwell et al., 2014, Daley, 2012). Because cell therapies are more complicated and expensive to produce than more traditional treatments, research is largely focused on conditions which are currently untreatable or difficult to manage with existing treatments. Table 1.1 lists some of the conditions currently under investigation for potential treatment by stem cell based cell therapies.

Table 1.1 - Conditions under investigation for treatment by stem cell based cell therapies.

Tissue Type	Disease
Endocrine	Diabetes
Blood	Immune Deficiencies
	Sickle Cell Anaemia
Liver	Liver Failure
Renal	Renal Failure
Neural	Spinal Cord Injuries
	Parkinson's Disease
	Motor Neuron Disease
	Alzheimer's Disease
	Ischemic Stroke
Musculoskeletal	Muscular Dystrophy
	Cartilage Injuries
	Large Bone Defects
Eye	Retinal Degeneration
	Corneal Injury
	Macular Degeneration
Cardiovascular	Myocardial Infarction
	Stroke
	Ischemic Limb Disease
Dermal	Acute Burns
	Diabetic Blisters

A non-exhaustive list conditions under investigation for treatment by stem cell based cell therapies categorised by the type of tissue affected (Volarevic et al., 2011, Martínez-Morales et al., 2013, Garbern and Lee, 2013, Schwartz et al., 2012, Touboul et al., 2010, Sun and Zweigerdt, 2009, Hernon et al., 2006, Cancedda et al., 2003, Koizumi et al., 2001).

1.3 The Processing Challenges of Stem Cells?

1.3.1 Product Attributes

The processing of stem cells presents a number of challenges unique from more traditional bioprocessing (Placzek et al., 2009, Kirouac and Zandstra, 2008). In stem cell processing the cells themselves are the product. Whole cells are significantly more difficult to characterise than proteins or small molecules. Furthermore, in traditional bioprocesses cells are deliberately altered to maximise the production of (a) target molecule(s). However, the potential applications of stem cells rely on the production of cells that are viable, functional, and representative of *in vivo* cells. As such care must be taken to avoid mutational changes to genotype and phenotype that can occur through adaptation to *in vitro* culture conditions (Peterson and Loring, 2014, Taapken et al., 2011, Mitalipova et al., 2005).

Karyotypic and other genotypic changes can occur when stem cells are cultured *in vitro,* and increase in frequency with increasing passage number (culture duration). It is important to test for these abnormalities and design processes that minimise their occurrence. Evidence suggests *in vitro* culture creates selective pressure for a variety of genotypic changes (Peterson and Loring, 2014, Baker et al., 2007). Different culture conditions can create selective pressures for different abnormalities, and the further from *in vivo* conditions they are, the more likely it is that selective pressures will be applied (Baker et al., 2007). Therefore, it is desirable to keep culture conditions as close to *in vivo* conditions as practical.

Stem cells also introduce an additional product attribute, relative to mature cells, through their ability to differentiate. Specific applications will require the production of specific cell types and the production of other cell types will not only decrease process efficiency but may present safety risks. Unintentionally introducing multipotent cells to a treatment site may result in tumour formation (Lee et al., 2013a) while introducing mature cells of the wrong type may cause other unforeseen side effects. Ultimately, trials and regulators will establish

whether certain levels of contaminating cells can be tolerated but the nature and quantities of these cells will no doubt require careful control (Serra et al., 2012).

1.3.2 Process Parameters

Another major problem with processing stem cells is the sheer breadth of biological, chemical, and physical factors which combine to control stem cell growth and differentiation (Chen et al., 2014, Cigognini et al., 2013, Serra et al., 2012, Wagers, 2012, Discher et al., 2009, Scadden, 2006). These factors include surface stiffness (Gonzalez-Garcia et al., 2012), hydrodynamic shear stress (Nsiah et al., 2014), concentrations of dissolved gases (Fynes et al., 2014, Forristal et al., 2013), nutrients and growth factors, cell density (Gage et al., 2013), and the presence of other cell types (Neto et al., 2014). *In vivo* stem cells reside in niches where all these factors are optimal for stem cells to carry out their functions. While it is relatively easy to control the initial values of many of these factors (e.g. seeding density, initial medium composition, etc), controlling them independently over multi-day periods is a major challenge.

Processes are increasingly being designed using quality by design (QBD) principles (Rathore and Winkle, 2009). QBD involves exploring a range of values for each processing parameter to define a design space that produces product of acceptable quality. A QBD approach allows some variation in processing parameters (within the design space) reducing the risk of failed batches (Rathore and Winkle, 2009). QBD also imparts a greater understanding of the process which can inform equipment design and scale-up processes (Rathore and Winkle, 2009). For these reasons a QBD approach to process development has become increasingly favoured by regulators (Rao et al., 2009, Rathore and Winkle, 2009). For stem cell process development, a QBD approach will mean exploring ranges of the above variables to investigate how they interact to affect product quality. This will obviously require a high quantity of experiments. It also necessitates the ability to control each parameter to precise values, and achieve those values as uniformly as possible across the culture area, so that the cultured cells are representative of the specific parameter set to be investigated.

The problematic variety of process parameters is compounded by a limited understanding of which factors a given process is sensitive to and how the optimal levels of these factors change through differentiation (Mondragon-Teran et al., 2011, Brack et al., 2008). Therefore a significant amount of process development will be required to design production processes for each stem cell product (van der Sanden et al., 2010). It will be expensive to perform this development at typical cell culture scales as the costs of some key materials are substantial (Serra et al., 2012). The cost of Leukaemia Inhibitory Factor (LIF), an essential growth factor for mouse ESC maintenance, is £84 per litre of mESC medium (ESG1107, Millipore, UK, April 2014). Similarly, recombinant human Lamini-511, a defined extra cellular matrix that helps maintain pluripotency of hESCs, costs $50 USD for sufficient material to coat a T-25 culture flask (N-892002, Iwai, USA, April 2014).

Culture substrate

One critical factor in the culture of stem cells is the culture substrate (Chowdhury et al., 2010, Melkoumian et al., 2010, Smith et al., 2009). For culture on flat surfaces this is typically a solid sheet of material with or without a coating of extra cellular matrix. In more complex cultures the substrate can involve microcarriers (Oh et al., 2009) or multi-component 3D scaffolds (Sung et al., 2010, Tibbitt and Anseth, 2009). Since the 1960s the majority of adherent culture systems have been made of polystyrene (Berthier et al., 2012). This polystyrene is typically treated with oxygen plasma to become more hydrophilic and is then classed as tissue culture polystyrene (TC-PS). Its role as the standard culture substrate over the past half century and the resulting wealth of trusted cell culture data mean polystyrene remains the culture substrate of choice for cell culture (Berthier et al., 2012). Significant research would be required to introduce a new material, particularly for clinical applications.

Tissue-culture polystyrene is often coated in an extracellular matrix (ECM) prior to cell culture. These extracellular matrices typically consist of hydrogels containing biopolymers, proteins and small molecules as reviewed extensively

by Tibbitt and Anseth (2009). Like culture medium extracellular matrices can be complex or defined and defined matrices can be of synthetic, human or animal origin. Common biopolymers in ECMs include gelatine, laminin, dextran, fibrin, cellulose, and alginate (Tibbitt and Anseth, 2009). Thicker 3D constructs of these same hydrogels are also used as scaffolds for 3D culture. Hydrogel scaffolds are also made using synthetic polymers such as poly(ethylene glycol) (Tibbitt and Anseth, 2009). Both biopolymers and polystyrene are also used to make Microcarriers (Martin et al., 2011). Microcarrier culture provides an intermediate between adherent and suspension culture. Cells are grown adherent to microcarriers that are, in turn, cultured in suspension.

The culture substrate interacts with cells in a variety of ways depending on its biological chemical and physical properties (Reilly and Engler, 2010). Culture substrates are bioactive where biopolymers, proteins and naturally derived small molecules are present (Tibbitt and Anseth, 2009). The presence of endogenous factors can affect viability, proliferation, and specific differentiation pathways. However, when using complex ECMs it is not clear what signalling pathways are involved. An example of a complex ECM is Matrigel, which is widely used to help maintain pluripotency in human embryonic stem cells. Extracellular matrices that mimic the stem cell niche are likely to have the most positive bioactive effect. For example decellularised heart tissue has been shown to be a favourable ECM for aortic smooth muscle cells and coronary artery endothelial cells (Singelyn et al., 2009).

The chemical composition of extra cellular matrices impact the transport of soluble factors, including nutrients, waste, and signalling molecules (Tibbitt and Anseth, 2009). Furthermore, chemical properties of culture substrate such as hydrophobicity and the availability of surface groups affect cell adherence and motility (Lee et al., 2013b, Peyton et al., 2011, Reilly and Engler, 2010). These factors in turn affect stem cell viability, proliferation, and differentiation. Similarly, physical properties of the substrate affect stem cells. Elastic modulus has been shown to influence differentiation (Lee et al., 2013b, Gonzalez-Garcia et al., 2012, Reilly and Engler, 2010), as have substrate geometry (Zhang and

Kilian, 2013, Kilian et al., 2010) and creep (Cameron et al., 2011). These properties determine the forces a cell can exert on its matrix.

Forces

As mentioned above, stem cells are sensitive to the elastic modulus and creep of the culture substrate which determine the forces a cell can exert on that substrate. Similarly, stem cells are sensitive to forces applied by both the culture substrate and the surrounding medium. Mechanical strain activates multiple signalling pathways (Zhou and Niklason, 2012) that can influence cell growth and fate. Cyclical uniaxial mechanical strain, applied through the culture substrate, affects proliferation, gene expression, and differentiation of stem cells (Li et al., 2012, Bayati et al., 2011, Kurpinski et al., 2006).

Another important stress in stem cell culture is due to the hydrodynamic force resultant from the flow of culture medium (Stolberg and McCloskey, 2009). At extreme levels, hydrodynamic shear can impact cell viability. Historically it was assumed that a major source of cell death in stirred culture systems was hydrodynamic shear generated by the impeller (up to 100 Pa) (Heath and Kiss, 2007, Nienow, 2006). Impellers can cause cell death when they generate micro-eddies smaller in scale than a suspended cell or microcarrier (Croughan et al., 1989). This requires significant agitation rates (Heath and Kiss, 2007) and can be prevented by increasing medium viscosity (e.g. with serum or dextran). It was later established that it is in fact bubble breakup (stresses >10,000 Pa) that is responsible for the majority of cell damage in gassed suspension reactors (Heath and Kiss, 2007, Kunas et al., 2009, Michaels et al., 1996, Jordan et al., 1994, Kunas and Papoutsakis, 1990). It was subsequently shown that the use of surfactants in culture medium can effectively eliminate shear induced cell death due to bubble break up by occupying the gas liquid interface.

Sustained shear stress can induce cell death at lower levels than the intermittent shear stress occurring in stirred bioreactors (Heath and Kiss, 2007). In laminar flow systems, hydrodynamic shear induced cell death in Chinese Hamster Ovary cells and in Human Embryonic Kidney cells with thresholds

between 0.59 and 1.19 Pa and between 1.19 Pa and 1.67 Pa respectively (Tanzeglock et al., 2009). Achieving these levels in a laminar flow culture system is unlikely unless the system utilises narrow capillaries. For example it would require a flow rate of ~100 $ml.s^{-1}$ between 10 cm wide parallel plates with 3 mm of separation, or ~300 $\mu l.s^{-1}$ between 1 cm wide parallel plates with 500 µm of separation. Consequently the design limitations of shear induced cell death on a potential culture device are minimal.

At lower levels hydrodynamic shear causes washout of adherent cells. Washout occurs when hydrodynamic shear overcomes the bonds attaching adherent cells to a culture surface (or other cells when not grown as a monolayer) (Korin et al., 2009a, Korin et al., 2009b).. Consequently, the exact threshold for washout will depend on the particular cells being cultured as well as the culture substrate. Furthermore, washout is more likely when the shear stress is maintained rather than delivered in a brief pulse (Korin et al., 2009a). Among measured washout thresholds (Toh and Voldman, 2011) report washout of mESC cells at sustained hydrodynamic shear of 0.1 Pa. Alternatively, CHO removal from microcarriers has been reported in stirred tank reactors with a maximum shear stress ~1 Pa (Heath and Kiss, 2007). These thresholds are more likely to be reached in a potential culture system and call for consideration in any system design.

Below the levels required for cell washout hydrodynamic shear can still affect cultures in a more subtle manner. As with mechanical strain, hydrodynamic shear can affect gene expression and hence stem cell differentiation. Among a number of studies into these effects (Stolberg and McCloskey, 2009, Yamamoto et al., 2005), Nsiah et al. (2014) report shear stresses of 0.5 Pa promote the expression of endothelial associated genes in mESCs and Toh and Voldman (2011) report shear stresses as low as 1.6×10^{-3} Pa priming mESC for differentiation. Currently, it has not been established what minimum level, if any, prevents any shear effect on stem cell gene expression. Without a clear goal in mind, any system for the development of stem cell culture processes should aim to allow the lowest possible hydrodynamic shear levels. It is a relatively simple matter to increase shear stress by increasing medium flow rates thus,

the lower the shear stress achievable at a low flow rate, the broader the range of shear levels that can be explored.

Dissolved Gases

The concentrations of dissolved oxygen and carbon dioxide are important in all cell cultures. Dissolved carbon dioxide is widely used in cell culture to maintain the pH within a range representative of *in vivo* conditions. Cells are typically cultured in equilibrium with 5% gaseous CO_2. Dissolved oxygen (DO) is required for cellular respiration and can limit cell growth if not maintained at a sufficient concentration. Further to this, dissolved oxygen concentration affects the oxidative state of cells and the production of hypoxia inducible transcription factors, and, through these mechanisms, stem cell differentiation (Yanes et al., 2010, Simon and Keith, 2008, Smith et al., 2000). The concentration of dissolved oxygen has different affects at different stages through differentiation (Mondragon-Teran et al., 2011) and can even precondition cells towards certain fates without actually initiating differentiation (Fynes et al., 2014, Mathieu et al., 2014, Forristal et al., 2013, Yanes et al., 2010, Smith et al., 2000).

Adherent cell culture has typically been carried out with medium in contact with 20% gaseous oxygen (1 atm total pressure) (Mondragon-Teran et al., 2011). The role of dissolved oxygen in embryogenesis was reviewed by Simon and Keith (2008). In contrast to typical laboratory practice, typical physiological dissolved oxygen is in equilibrium with 2%-9% oxygen and subtle differences in dissolved oxygen levels are involved in the spatially defined development of tissues and organs during embryogenesis. Furthermore, early in mammalian embryogenesis uterine dissolved oxygen is in equilibrium with approximately 2.5% gaseous oxygen but increases to 8.6% with connection to maternal vasculature. As with spatial variations these different dissolved oxygen concentrations are associated with the control of embryogenesis. *In vitro*, low oxygen (3-5% gaseous) has been shown to promote pluripotency of hESCs (Ezashi et al., 2005). In contrast, both high (40% gaseous oxygen) and very low levels of dissolved oxygen (1% gaseous oxygen) have been shown to decrease

growth rate and the expression of pluripotency markers in mESCs (Powers et al., 2008).

Other Soluble Factors

Stem cells are also influenced by a wide variety of other soluble factors (Hazeltine et al., 2013). As with all cells sufficient nutrients (glucose, glutamine, pyruvate, amino acids) must be supplied for cell survival and growth. Similarly, over-accumulation of waste molecules such as lactate can inhibit cell growth and survival. In addition, stem cells are sensitive to a wide variety of signalling molecules. These molecules can be added to the medium or secreted by cells in culture (Hazeltine et al., 2013, Titmarsh et al., 2012, Przybyla and Voldman, 2012). Secreted molecules can interact with the secreting cell (autocrine signalling) or neighbouring cells (paracrine signalling). Furthermore, signalling can occur between similar cells or between cells of different phenotypes or even different species (e.g. human embryonic stem cells co cultured on mouse embryonic fibroblasts) (Hyslop et al., 2005).

As discussed in section 1.12, molecules can also be added to culture medium either individually or as part of a complex ingredient such as serum. Specific ‘growth factors' are often added in different stem cell culture protocols to promote or repress various differentiation pathways. For example leukaemia inhibitor factor (LIF) is used to maintain pluripotency in mouse embryonic stem cells while basic fibroblast growth factor (FGF2) is used to the same end with human embryonic stem cells. Stem cells are sensitive to the concentration of all these soluble factors (autocrine, paracrine and exogenous) with relatively narrow ranges of concentration having optimal effects (Titmarsh et al., 2012).

Cell Density

The concentration of secreted factors is partly dependent on the cell density making it another key factor in stem cell culture (Gage et al., 2013, Whyte et al., 2011, Ghosh et al., 2010, Lu et al., 2009, Bitar et al., 2007, Reubinoff et al., 2000). Cell density affects the rate at which nutrients are consumed and waste

and signalling molecules released (Csaszar et al., 2012, Fong et al., 2005). Cell density also affects the transport of these molecules with dense multi-cell layers preventing free exchange between inner cells and culture medium, concentrating secreted molecules and depleting those supplied by the medium. Finally, cell density also affects the extent of physical interaction between cells; adhering to, pulling on, and pushing against each other. Cell density has been shown to influence a variety of stem cell culture protocols such as: the differentiation of human ESCs to pancreatic endocrine cells (Gage et al., 2013), the vascular differentiation of human bone marrow stromal cells (Whyte et al., 2011), the endocrine potential of adipose derived stem cells (Ghosh et al., 2010), the adipogenic differentiation of human bone marrow-derived mesenchymal stem cells (Lu et al., 2009), and the derivation of human ESCs (Reubinoff et al., 2000).

Cell density varies throughout a culture as cells expand, starting at the seeding density and continuing to increase until the cells are passaged. This makes the passaging method critical. Passaging when cell density reaches a certain upper limit helps to limit the level of cell signalling and waste accumulation while maintaining minimum levels of nutrients and dissolved oxygen. Likewise, the density the cells are re-seeded at determines the initial levels of cell signalling. In some cases cells seeded as individuals perform significantly worse than cells seeded in clumps (e.g. hESCs in the absence of rock inhibitor) (Watanabe et al., 2007, Pyle et al., 2006). Where this is the case physical dissociation may be necessary (e.g. cutting colonies into small clumps) rather than enzymatic dissociation.

1.3.3 Culture Systems

The requirements of stem cell culture systems have been reviewed in depth by Kirouac and Zandstra (2008) and Serra *et al* (2012) amongst others. The challenging product attributes and process parameters of stem cells necessitate certain requirements from any potential culture system. In bioprocessing cells are grown in free suspension or on microcarriers wherever possible. However, suspension culture would require adaptation of most stem cell types (with the

notable exception of cells occurring in the blood). Unfortunately, adaptation (as previously mentioned) may increase the likelihood of changes in cell phenotype and karyotype rendering them inappropriate for some applications (Peterson and Loring, 2014, Taapken et al., 2011, Mitalipova et al., 2005). Suspension culture also results in higher amounts of shear damage (Kehoe et al., 2010, Cherry and Kwon, 1990). Culture on microcarriers may require less adaptation than suspension culture but results in a less controlled microenvironment, with variable cell densities and transport distances in and around the microcarriers. Microcarrier culture also makes cell recovery challenging as cells must be detached, freed, and separated from the microcarriers. (Serra et al., 2012).

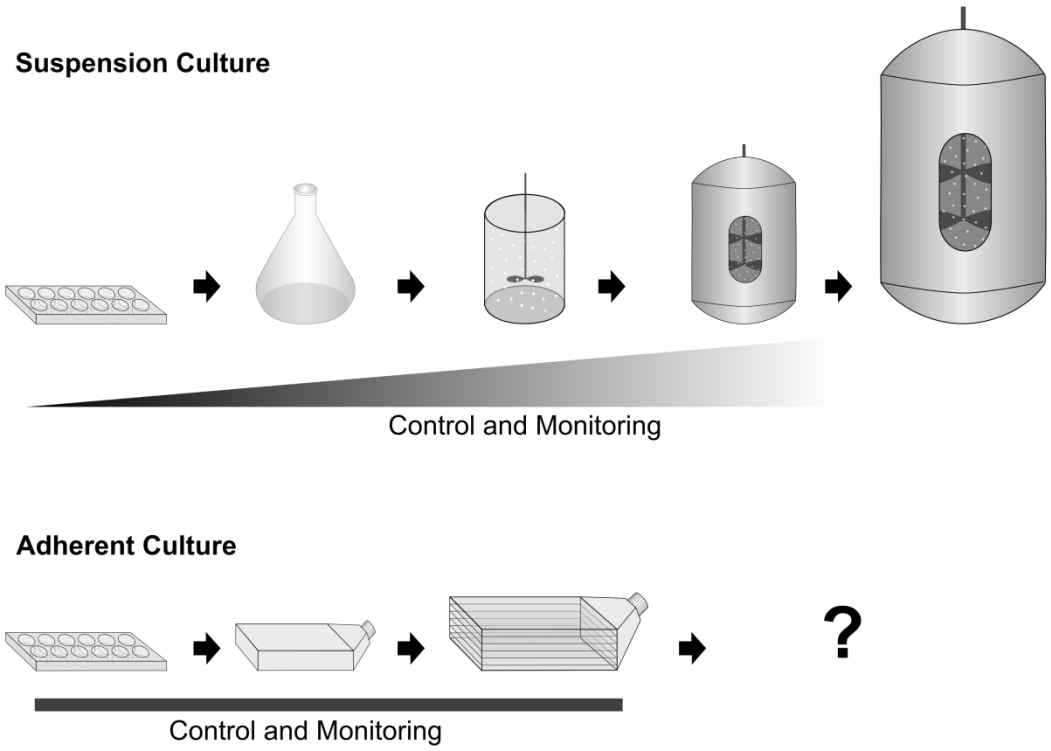

Figure 1.4 - Suspension and adherent culture scale-up trains.

A typical suspension culture scale-up train compared to the available scale-up train for adherent culture. For suspension culture scale, control and monitoring increase from shaken microwell plates through shake flasks, bench-top reactors, and pilot reactors to full scale bioreactors. For adherent culture it is possible to scale up from wells to multi-layer systems but control and monitoring are similar at all scales.

Initially, pluripotent stem cells could only be isolated, maintained, and differentiated in adherent culture (Thomson et al., 1998, Amit et al., 2000, Itskovitz-Eldor et al., 2000, Kehat et al., 2001, Takahashi and Yamanaka, 2006). More recently some processes have been demonstrated in suspension and on microcarriers (dos Santos et al., 2014, Serra et al., 2012, Fluri et al., 2012, Sun et al., 2011, Steiner et al., 2010). However, adherent culture remains a mainstay of stem cell processing, particularly in the later differentiation stages of a process. A variety of systems are available for adherent culture, though none reach the same scale as industrial suspension. These systems include culture wells and flasks, and multilayer systems (e.g. Cell Factories by Thermo Fischer Scientific, Millicell HY Flasks by Millipore, and HYPERFlasks, CellStacks, and CellCubes by Corning). However, these are poor analogies to the highly controlled and automated reactors used for suspension culture at bench, pilot, and production scale (Figure 1.4).

Hollow fibre bioreactors are a notable exception to the above points. Hollow fibre bioreactors were first developed in the 1970s for mammalian cell culture (Knazek et al., 1972). Typically medium is perfused through multiple narrow tubes made of a semi-permeable material, while cells grow in the space surrounding these fibres. Alternatively, cells can be grown inside the fibres and medium perfused in the external space (Roberts et al., 2012). Soluble components, bellow a certain size, are exchanged through the fibre walls. In this way nutrients can be supplied and waste molecules removed while the cells are shielded from any shear stress. Hollow fibre bioreactors offer significantly higher culture areas than flat sheet culture systems. However, hollow fibre bioreactors do not allow continuous non-invasive monitoring of cultured cells by microscopy. Cell recovery may also be suboptimal as hollow fibre bioreactors were initially designed for the production of secreted molecules rather than whole cells.

A major challenge with current adherent systems is control of soluble microenvironment. The majority of adherent culture systems do not perfuse medium. Therefore there is limited control over the concentration of nutrient, waste, and signalling molecules. The concentrations of these soluble factors will

rise and fall between medium exchanges at variable rates depending on cell density (Csaszar et al., 2012, Fong et al., 2005). In systems where medium is perfused, velocity distributions are non-uniform and flow paths are long resulting in a highly variable soluble environment (Aunins et al., 2003). Furthermore, as adherent systems are not well mixed the concentration of dissolved molecules will vary with distance from the cultured cells. This includes dissolved oxygen (DO). Even when there is an external source of oxygen it must diffuse from that gas supply or head space (Millman et al., 2009, Serra et al., 2010).

A second challenge with adherent systems is monitoring (Jaccard et al., 2014a). The well established monitoring methods employed with suspension culture systems are often unsuitable for adherent culture as they assume a well mixed system. Monitoring of the soluble environment typically involves measuring at a single point and assuming that point is representative of conditions throughout the culture system. As outlined above, adherent systems are not well mixed and conditions vary with distance from culture surfaces. Additionally, monitoring of cell density and quality rely on measuring a representative cell suspension which is clearly not possible without significant disruption in an adherent system (Jaccard et al., 2014a).

1.4 What is Microfluidics?

One promising technology for stem cell culture is microfluidics. Microfluidics makes use of microfabrication techniques to reduce unit operations to the scale of microlitres or smaller (Whitesides, 2006). Microfluidic or microfabricated systems have advantages for stem cell culture in terms of both reduced size and high levels of control. This makes them well suited for the development of stem cell processes.

1.4.1 Microfabrication Techniques and Materials

The field of microfluidics makes use of a variety of solid materials. One of the origins of microfluidics is microelectronics and as such it makes extensive use of silicon and silicon oxide (Becker and Gartner, 2008, Whitesides, 2006).

However, microfabrication techniques have expanded to use glass, metals, and thermosetting and thermoplastic polymers (Becker and Gartner, 2008, Whitesides, 2006). The most notable polymer used in microfluidics is poly(dimethylsiloxane) (PDMS) (Berthier et al., 2012); an elastomeric, thermosetting polymer which is ubiquitous in modern microfluidics. PDMS is a low-cost, non-toxic polymer that is highly gas permeable, has a low stiffness, and is optically transparent to wavelengths greater than 230 nm (Berthier et al., 2012, Sia and Whitesides, 2003). These properties are well suited to microfabrication techniques, gas delivery, and optical and fluorescent analysis. However, PDMS has been shown to absorb small hydrophobic molecules and leach unlinked oligomers, which can impact on biological applications (Regehr et al., 2009). Thermoplastic polymers are also popular in microfluidics due to their low cost, ease of manufacture and optical transparency (Becker and Gartner, 2008).

Microfabrication techniques are focused on introducing micro-scale features to solid substrates and the bonding of those substrates. Microfabrication techniques for polymers have been thoroughly reviewed by Becker and Gartner (2008). One common technique to introduce features is photolithography. Photolithography uses a mask to protect part of a surface from electromagnetic radiation. The surface hit by the radiation is altered such that it is harder or easier to remove, by a method such as a chemical wash, and leaves a structure corresponding to the mask. Photolithography can use lenses to shrink mask features and wavelengths including UV light or x-ray radiation depending on the substrate material. A similar technique is etching which uses a chemical to strip material from some areas while other areas are protected from the chemical by a mask. It can be difficult to deliver vertical feature edges, using both these techniques, as the etching chemical or light used can spread under the protective mask. This problem worsens with increasing channel depth.

Other techniques for targeted removal of material are laser ablation (Becker and Gartner, 2008), which uses focused electromagnetic radiation to remove material, and micro-milling, which uses small milling cutters to physically remove material. Micro-milling can give very high dimensional accuracy and

vertical feature boundaries. However it is very time consuming as the rate of tool travel is limited by the force that can be applied to the tool and the heat the tool generates. Micro-milling also has a minimum tool size limit of 5 μm in diameter (PMT, 2014), limiting the minimum feature size. Conversely, laser ablation is rapid and can achieve much smaller feature sizes (Pronko et al., 1995). However, laser ablation typically uses non-square intensity profiles (e.g. Gaussian for CO_2 lasers) and produces unclean feature boundaries due to alteration of adjacent material.

Alternatively, some techniques introduce material. Techniques such as vapour deposition, electroplating, printing, and spin coating can be used to add thin layers of material. For thicker features, replication methods such as casting (Whitesides et al., 2001), injection moulding (McCormick et al., 1997) and hot embossing (Martynova et al., 1997) are more suitable (Becker and Gartner, 2008). These three methods all require the use of a negative mould. These moulds are typically fabricated by techniques such as photolithography, laser ablation or micro-milling. Injection moulding and hot embossing are typically used with thermoplastics, which are also compatible with techniques such as micro-milling and laser ablation. However, a single mould can be used repeatedly to rapidly produce multiple identical parts. Casting is used with thermosetting polymers such as PDMS, which are not compatible with techniques that remove material such as micro-milling.

Fabricated parts can be bonded together into more complex assemblies by a variety of techniques (Tsao and DeVoe, 2009, Becker and Gartner, 2008). These techniques include; adhesive bonding, eutectic bonding, anodic bonding, direct silicon-silicon bonding, thermal bonding, and plasma bonding. The choice of bonding technique depends on the materials to be bonded. Parts made of the same thermoplastic can be thermally bonded by applying pressure and heating them near or above their glass transition temperature. PDMS, on the other hand, can be bonded to some materials (such as PDMS and glass) by exposing the surfaces to be bonded to air plasma before contacting them. Both these techniques are superior to adhesive bonding as the added adhesive may alter feature dimensions and/or leach.

1.4.2 Advantages of Microfluidics

General Advantages

The most obvious advantages of microfluidic systems are reduction in the size and, consequently, the capital and spatial requirements of equipment, the use of consumables, and the size of samples (Whitesides, 2006). This can have benefits in terms of both operating costs and safety (when dealing with hazardous mixtures or intermediates). Furthermore, because of the small distances involved, microfluidic systems are well suited to finely controlled heat and mass transfer by diffusion (Berthier et al., 2012, Whitesides, 2006). Finally, the less obvious advantages of microfluidic systems are the physical phenomena that occur at when surface effects are much more significant than bulk effects, e.g. laminar flow (Whitesides, 2006).

Advantages for Stem Cell Processes

Microfluidic culture devices have small culture areas and small culture chamber volumes. Furthermore, culture chambers are typically fully enclosed allowing large culture area to volume ratios (Paguirigan and Beebe, 2008). Consequently, microfluidic systems can allow significant reductions in the required quantities of both expensive growth factors, and difficult to isolate stem cells (Berthier et al., 2012). In addition, the fully enclosed chambers eliminate meniscus effects, and reduce evaporation compared to open vessels. In any culture system evaporation will increase the concentration of soluble factors over time. Additionally, in static systems with a medium/gas interface (e.g. culture wells and flasks) evaporation can reduce the height through which gases must diffuse affecting pericellular concentrations. Menisci similarly create non-uniform medium heights as well as interfering with imaging of the cultured cells (Paguirigan and Beebe, 2008).

Microfluidic systems also offer advantages in control over a number of factors important to stem cell fate and function (Berthier et al., 2012). The short characteristic lengths in microfluidic systems facilitate rapid heat and mass

transfer by diffusion (Paguirigan and Beebe, 2008). Rapid heat and mass transfer in turn allows fine control over temperature and concentration of dissolved gases. Similarly, fine spatial and temporal control over the concentration of soluble factors is possible thanks to the laminar flow typical in microfluidic systems (Paguirigan and Beebe, 2008). Laminar flow can be used to establish highly uniform fluid velocity fields as well as spatially precise concentration gradients (Dertinger et al., 2001).

1.5 What are the Requirements of a Microfluidic System for the Development of Adherent Stem Cell Processes?

There are two major requirements of a microfluidic system for the development of stem cell processes. Firstly, the system must deliver a controlled and uniform microenvironment. As discussed previously, this is both a key advantage of microfluidics and a chief requirement of process development. Secondly, the system must have comparability with large-scale systems to allow validation (Young and Simmons, 2010). Furthermore, a system should be comparable to existing culture wells and plates to take advantage of pre-existing research.

1.5.1 A Controlled and Uniform Microenvironment

To achieve a controlled microenvironment, medium must be perfused. Perfusion of medium replenishes consumed nutrients while controlling the accumulation of waste and signalling molecules (Yeo et al., 2013). Further to this the medium must be perfused with a uniform fluid velocity field. Assuming the initial seeding of cells is uniform, non-uniform velocities will result in variation of the soluble microenvironment across the width of the growth surface. In addition, perfused medium introduces shear stress, which must also be kept uniform by delivering a uniform velocity field. As well as being uniform, the magnitude of shear stress at the culture plane should be controlled, as shear stress can affect stem cell growth and fate (section 1.3.2).

Another key factor in stem cell growth and fate is the concentration of dissolved oxygen (Fynes et al., 2014, Mathieu et al., 2014, Forristal et al., 2013), as

previously discussed in section 1.3.2. In culture wells and flasks oxygen is delivered through the direct gas medium interface above the culture surface. This method achieves poor control in these systems due to the large height of medium through which oxygen must diffuse (relative to the diffusivity). Furthermore, this method of oxygen supply is not possible in enclosed microfluidic systems. Nevertheless, dissolved oxygen must be delivered in a uniform and controlled manner. Likewise, as with all culture systems, methods to control pH and temperature are required (Veraitch et al., 2008). These are typically controlled by an incubator that heats the culture system and utilises 5% gaseous CO_2 for pH control. Incubators may be compatible with microfabricated culture devices depending on their design and periphery systems.

1.5.2 Compatibility with Other Systems

To be compatible with other culture systems a microfluidic system must allow the use of the same materials and methods. The key material in adherent cell culture devices is the growth surface. Growth surfaces for monolayer culture have traditionally been tissue culture polystyrene (TC-PS). However, this material is not common in microfluidics as it is difficult to bond (Berthier et al., 2012). A microfabricated device for process development should facilitate use of TC-PS substrates. Stem cells are also increasingly cultures in 3D scaffolds such as hydrogels (Chen et al., 2013, Sung et al., 2010, Tibbitt and Anseth, 2009). Therefore it would be desirable if both TC-PS and 3D scaffolds could be readily integrated.

Beyond the medium exchange regime, stem cell methods include cell seeding, inspection, passaging, harvesting and immunostaining. Cell seeding is typically conducted statically, with a cell suspension being introduced directly to the culture surface by pipette. Conversely, microfluidic culture systems commonly use dynamic seeding due to their fully enclosed culture chambers (Kim et al., 2007a). In dynamic seeding a cell suspension is introduced to the culture chamber through channels at a defined flow rate. The flow is then stopped allowing cells to settle and attach. Care must be taken to avoid cells settling and persisting outside the culture chamber as well as ensuring cells are evenly

distributed above all of the culture chamber before flow is stopped. Static seeding typically allows finer control over the density and spatial confinement of seeded cells as a uniform suspension can be introduced to only the culture chamber (Kim et al., 2007a).

As with static seeding, passaging, harvesting, and immunostaining typically rely on direct access to the culture surface. Immunostaining and enzymatic dissociation of cells could be performed via perfused channels but larger reagent volumes would be required and higher cell loss may be expected. Furthermore, enzymatic dissociation requires adaptation and has been shown more likely to impact cell karyotype than manual dissociation (Ellerstrom et al., 2007, Mitalipova et al., 2005). Manual dissociation is also necessary where cells cannot be passaged as single cells e.g. hESC passaged as colony fragments (Ellerstrom et al., 2007). Consequently, direct access to the culture chamber is a key requirement of a microfabricated culture system for process development.

On the other hand visual inspection does not require direct physical access to the culture chamber. It does, however, require clear optical access to the cells. Many of the materials used in microfluidics are transparent but a system must be designed so that the cells are not optically obstructed by opaque materials or complex features (Cimetta et al., 2009). Furthermore, while most materials are transparent to visible light fewer are transparent to the UV light which may be required when immunostaining. To allow in-situ immunostaining all materials in the light path should be transparent to wave lengths above 320 nm (for DAPI staining).

Finally, in addition to comparability with existing systems, it may be advantageous if the microfluidic system could be scaled up directly. While processes developed on the proposed system could inform processing in other existing systems, they may not be able to achieve desired levels of control. Therefore, a microfabricated system which could be scaled up and/or out to production scale may provide a useful future production system.

1.6 Existing Microfluidic Adherent Stem Cell Culture Systems

A variety of microfluidic culture devices have been developed either to culture cells for drug screening applications, or to study specific aspects of stem cell culture. However, these devices have not been manufactured as complete process development tools that meet all the above requirements.

Screening devices include those of Tan *et al* (2013) for high-density hepatocyte culture, Jeon *et al* (2014) for the generation of vascular networks from mesenchymal stem cells, and Peng *et al* (2013) for screening the effect of drugs on cells at different dissolved oxygen concentrations. Unfortunately, most of these devices do not meet the need for comparability. This is due, in part, to their inability to incorporate TC-PS and use of static cell seeding and recovery. In addition, they are not all designed to precisely and uniformly control key parameters of stem cell process such as shear stress, dissolved oxygen, and the concentration of soluble molecules.

Other devices have been developed to control and investigate specific parameters. For example, Yoshimitsu *et al* (2014) investigated different defined media and extra cellular matrices as well as the effects of different perfusion rates. Xu *et al* (2013) produced a device to screen soluble factor concentrations with no hydrodynamic shear. Titmarsh *et al* (2012) investigated exogenous factors and paracrine signalling. Giulitti *et al* (2013) produced a device to investigate medium perfusion strategies. However, these devices focus only on the parameter of interest while other parameters are either uncontrolled, or controlled at set levels, and often aren’t uniform over the culture area.

1.7 Research Objectives

It is hypothesised that a system of microfabricated devices, for the development of processes involving the adherent culture of stem cells, will allow small-scale process development with reduced use of resources. Furthermore,

microfabricated systems offer advantages in the spatial and temporal control of process parameters, which may be useful in process development. Thus, such a system may help accelerate the development of processes culturing stem cells for both drug screening and regenerative medicine. An effective small-scale process development tool will require high levels of spatial and temporal control over a range of process parameters, and comparability with production-scale culture systems so that developed processes can be translated to these systems.

The research in this thesis aims to build on an existing prototype culture system, to develop a system that meets these needs. Central to the system will be a number of microfabricated culture devices. In order to be comparable with production scale systems, these devices should facilitate the use of traditional TC-PS culture surfaces and have directly accessible culture chambers to facilitate static seeding and cell recovery. The culture devices should integrate medium perfusion, through microfabricated channels, to achieve uniform shear stress and concentrations of soluble factors in the culture chambers. The culture device should also minimise the shear stress introduced by this medium perfusion. In addition the devices should have controllable and uniform concentrations of pericellular dissolved oxygen.

The system incorporating the culture devices should control key processing parameters. Control over the medium flow rate will affect both hydrodynamic shear and the concentrations of soluble factors in the culture chamber. Similarly, medium composition shuld be controlled to affect the concentration of soluble factors in the culture chamber. Finally, the culture system should incorporate monitoring by phase contrast microscopy. The entire system must be robust and easy to use with the ultimate goal being a system that could be produced and distributed to stem cell researchers for application in process development.

2. Investigation of a Prototype Microfabricated System for the Adherent Culture of Embryonic Stem Cells

The majority of work presented in this chapter has been previously published in Reichen & Macown *et al* (2012). Portions of the text in this chapter appear as previously published (particularly materials and methods). Material in this chapter not appearing in the above publication includes; the modelling of dissolved oxygen (sections 2.2.4 and 2.3.3), the seeding and culture of mouse embryonic stem cells (sections 2.2.5, 2.2.8, 2.2.9, 2.3.5, and 2.3.6), and analysis of the control and automation platform (section 2.3.8).

2.1 The Prototype Microfabricated System for the Adherent Culture of Embryonic Stem Cells

An autoclavable, microfabricated device for the adherent culture of embryonic stem cells (ESCs) was previously developed at University College London by Marcel Reichen (Reichen, 2012, Reichen et al., 2012). The prototype microfabricated culture device was designed with a re-sealable culture chamber to allow traditional static seeding in an otherwise fully assembled device. Additionally, the prototype device was designed to reversibly seal with a TC-PS microscope slide (or any other standard-sized microscope slide), allowing the use of standard culture substrates. Furthermore, a multiplexed automation and control platform was developed to house three of these prototype devices simultaneously, and control them through perfusion cultures for several days (Reichen et al., 2013).

The prototype culture system required evaluation to demonstrate its stem cell culture potential and to elucidate areas requiring improvement. To be an effective tool the system needs to be robust and easy to operate. The key design features needed evaluating to ensure they were fit for purpose, including the low shear perfusion system, the re-sealable lid and the reversible method of sealing. Critically, the ability to culture stem cells in the prototype device needed to be demonstrated. This included demonstrating that the prototype device can be effectively sterilised and seeded with cells as well as showing the expansion

of stem cells and maintenance of pluripotency when following standard expansion protocols.

2.2 Materials and Methods

2.2.1 Fabrication of the Culture Device

All parts and moulds were based on the designs of Marcel Reichen (Reichen, 2012). 3D designs were reproduced as parts in SolidWorks CAD (computer aided design) software (SolidWorks 2010, Dassault Systemes SolidWorks, UK). Technical drawings are shown in Appendix 1. Polycarbonate (PC) parts were fabricated from 3 mm and 5 mm sheets with a CNC micro-milling machine (M3400E, Folken Industries, USA) using 2-flute standard length end mills (Kyocera Micro Tools, USA). The G-code for the micro-milling machine was generated from the CAD files using MasterCam software (MasterCam X2, CNC Software, USA).

Structured poly(dimethylsiloxane) (PDMS) (Sylgard 184, Dow Corning, USA) parts were cast in moulds milled out of 5 mm thick PC, and 3 mm thick aluminium. The monomer and curing agent were mixed at a 10:1 ratio (by weight), degassed in a vacuum desiccator to remove bubbles, poured into moulds, and degassed a second time. The mould was covered with a flat sheet of polycarbonate, clamped between aluminium plates, and cured at 90°C for 2 hours. Once cooled, parts were removed from the moulds and any excess PDMS trimmed away with a scalpel.

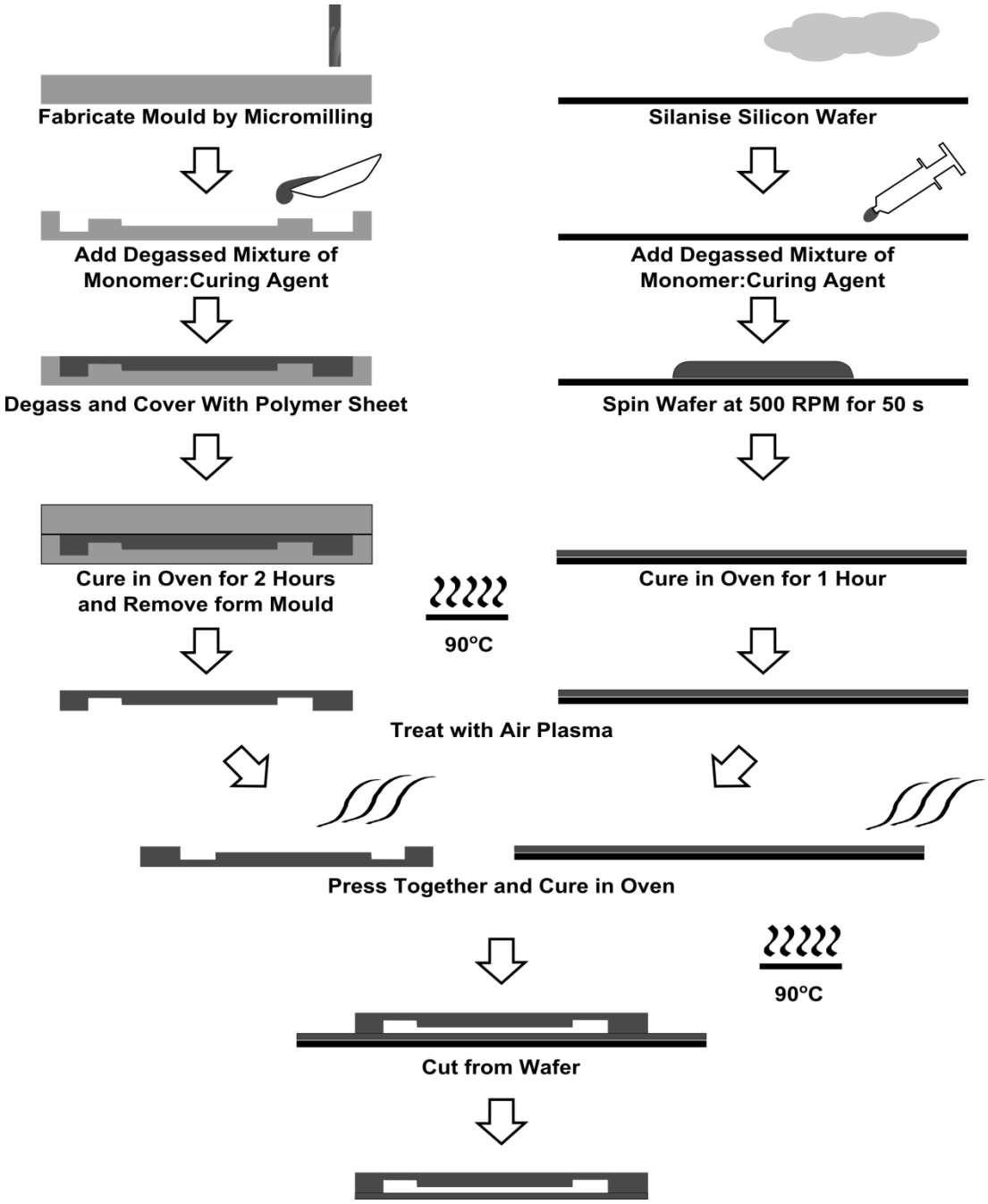

Figure 2.1 - Schematic of fabrication process for PDMS chip.

The fabrication of the PDMS chip involves casting a structured layer in a micro-milled mould, spin coating a thin spacer layer on a silicon wafer, and bonding the two together using air plasma.

PDMS 'spacer layers' were fabricated by spin-coating PDMS onto silicon wafers using a standard spin coater. (P6708D, Specialty Coating Systems, USA). A 4" silicon wafer (Prolog Semicor, Ukraine) was silanised by placing it in a vacuum desiccator with 200 μl of Trichloro(1H,1H,2H,2H-perfluorooctyl)silane (448931, Sigma-Aldrich, UK) for 2 hours. 5 ml of degassed PDMS monomer-curing agent mixture was transferred to the centre of the wafer using a syringe.

The wafer was spun at 500 RPM for 50 seconds and then cured at 90ºC for 1 hour. PDMS chips and spacer layers were bonded using air plasma (90 s, 30 W, 500 mTorr, PDC-002, Harrick Plasma, USA), and cured in an oven at 90ºC for 2 hours. Figure 2.1 shows a schematic of the fabrication steps.

2.2.2 Burst Pressure Measurements

To measure burst pressure a 10 ml plastic syringe (613-3931, VWR, UK) was connected to one interconnect bar via tubing and a 3-way valve (732-8103, Bio-Rad Laboratories, UK). Tubing connected to the other interconnect bar was blocked with a Luer lock plug. The third port of the 3-way valve was connected to a pressure sensor (40PC100G, Honeywell, USA) glued into a fitting (P-207, Upchurch Scientific, USA) with epoxy glue. A syringe drive was used to pump air into the device at 5 $ml.min^{-1}$ and the pressure was logged using LabVIEW software (LabVIEW 2011, National Instruments, USA) and a data acquisition card (USB-6229BNC, National Instruments, USA). The burst pressure was taken as the highest pressure recorded for a given experiment. A prototype device was assembled and disassembled 12 times. Each time the prototype device was assembled the burst pressure was recorded 3 times. Additionally, for the last 3 assemblies, single burst pressure measurements were made following iterations of lid removal and reinsertion. Measurements were made following 1-10, 20 and 30 iterations. Lid replacement burst pressures were normalised against the initial burst pressure before applying analysis of variance to investigate the relationship between burst pressure and lid replacement. All device components used for burst pressure experiments had previously been autoclaved.

2.2.3 Fluid Dynamic Modelling

Fluid flow through the PDMS chip and culture chamber was modelled. The Navier-Stokes equations were solved by using the finite element method (FEM) software package COMSOL Multiphysics 4.4 (COMSOL, Cambridge, UK). The bulk fluid was water at a temperature of 310K, with the viscosity (of water) modified to 7.8×10^{-4} Pa.s (Bacabac et al., 2005) to reflect the higher viscosity of cell culture media. Fully developed steady-state flow was assumed for the

laminar flow physics, with no-slip conditions at the boundaries. The pressure at the outlet was set to 0 Pa and the flow at the inlet was set to 300 µl.h^{-1}. Tetrahedral elements were employed to mesh the 3-D domains of the culture device. The mesh size was between 40 to 100 µm with a scaling factor of 3 in the z dimension resulting in 6.3×10^{6} elements. The model was solved with a built-in GMRES iterative solver.

Hydrodynamic shear stress at the culture surface was calculated from the simulated velocity profile using equation 2.1, where τ_h is the shear stress at a height h from the surface, μ the dynamic viscosity and γ the average shear rate from the FEM model.

$$\tau_h = \mu\gamma \tag{2.1}$$

To verify the calculated shear stress from the model, the analytical solution for the wall shear stress between infinite parallel plates was used (equation 2.2).

$$\tau_w = 6\mu\frac{Q}{h^2 w} \tag{2.2}$$

τ_w is the shear stress at the wall, *h* the height of the culture chamber, *w* the width of the culture chamber, μ the dynamic viscosity and *Q* the volumetric flow rate.

2.2.4 Dissolved Oxygen Modelling

The dissolved oxygen (DO) expected in the culture medium was calculated at different gaseous oxygen concentrations and cellular oxygen uptake rates (OURs) using the parameters shown in Table 2.1 (Macown et al., 2014).

Table 2.1 - Parameters used for dissolved oxygen modelling.

Parameter	Value/Formula	Units	Source
Solubility of O_2 in Media	9.04×10^{-7}	$mol.cm^{-3}.atm^{-1}$	(Nishikawa et al., 2008)
Diffusivity of O_2 in Media	2.00×10^{-5}	$cm^2.s^{-1}$	(Nishikawa et al., 2008)
Maximum O_2 Consumption During Growth Phase	2.80×10^{-17}	$mol.cell^{-1}s^{-1}$	Mouse ESCs at 20% and 40% O2, (Powers et al., 2008)
Minimum Cell Density	5.00×10^{4}	$cells.cm^{-2}$	Typical Seeding Density (mESC)
Confluent Cell Density	8.00×10^{5}	$cells.cm^{-2}$	Typical Confluent Density (mESC)

Fick's law (equation 2.3) was used to calculate DO concentrations in statically cultured flasks and culture wells. It was assumed the rate of change of OUR is low enough that DO concentrations could be approximated using steady state calculations. At steady state, the flux is equal to the oxygen uptake rate, which is the product of oxygen consumption per cell (*OC*) and cell density (*CD*). The equation can then be integrated across a layer of uniform material to give equation 2.4.

$$J = D\frac{\delta C}{\delta x} \tag{2.3}$$

$$C_2 = C_1 - \frac{OC \cdot CD \cdot \Delta x}{D} \tag{2.4}$$

where J is the flux in $mol.cm^{-2}s^{-1}$, D is the diffusion coefficient in cm^2s^{-1}, C is the concentration in $mol.cm^{-3}$ and x is the length of the diffusion path in cm. At the interface with atmosphere, C_1 is the saturation solubility of O_2 in the material.

The distribution of dissolved oxygen in the prototype device under perfusion conditions was modelled using the finite element method (FEM) software package COMSOL Multiphysics 4.4 (COMSOL, Cambridge, UK). The PDMS chip was previously built as a 3D model in COMSOL for fluid dynamic modelling with physics for laminar flow (section 2.2.3). For DO modelling, "transport of dilute species" physics were added to the model. The consumption of oxygen was modelled as a constant flux out through the culture surface with a magnitude equal to the OUR. All other surfaces were specified to have no flux.

The inflow of medium at the inlet had a dissolved oxygen concentration of 0.2 $mol.m^{-3}$, the saturation concentration at 37°C and 1.05 atm. Oxygen left the system at the outlet dissolved in the waste medium. The model was solved for two OURs, 1.40×10^{-8} and 2.24×10^{-7} $mol.m^{-2}s^{-1}$, representing mESCs at typical seeding and fully confluent cell densities respectively.

2.2.5 Sterilisation Study

Two PDMS chips and two polycarbonate lids were incubated for 17 hours at 37°C in Terrific Broth containing *E. Coli* XL10-Gold Kan® (Stratagene, UK). One of each type of part was then autoclaved at 121°C for 20 minutes. Following autoclave, each of the four parts were placed in separate shake flasks of sterile Terrific Broth and incubated on a shaker for 6 hours. A flask containing only media was also incubated as a negative control. After 6 hours the optical density of broth samples at 600 nm (OD600) were measured relative to the negative control. Terrific Broth agar plates were seeded with 100 µl of broth from each shake flask and incubated for 1 day at 37°C.

2.2.6 Mouse Embryonic Stem Cell Maintenance

E14Tg2a mouse embryonic stem cells (passage number <70, Stem Cell Sciences, Edinburgh, UK) were maintained in T-25 Nunclon® cell culture flasks (156367, Fisher Scientific, UK) and passaged 1:8 every three days. Prior to passaging flasks were coated with 0.1% gelatin (G1890, Sigma-Aldrich, UK) for 15 minutes at room temperature. To passage, medium was aspirated from a flask, the surface was washed with Dulbecco's phosphate buffer solution (DPBS) (D1408, Sigma-Aldrich, UK), and then the cells incubated with trypsin:EDTA (ethylenediaminetetraacetic acid) solution (T4049, Sigma-Aldrich, UK) for 3 minutes. The trypsin was quenched with culture medium and the cell suspension was centrifuged at 500 g for 3 minutes. The pellet was resuspended in culture medium consisting of Knock-Out Dulbecco's Modified Eagle Medium (10829-018) supplemented with 15% v/v Fetal Bovine Serum (26140-079), 1% v/v 100x Glutamax (35050-038), 1% v/v 100x non-essential amino-acids (11140-035), 0.1mM β-mercaptoethanol (31350-010, Life Technologies, UK) and 10 $ng.ml^{-1}$ Leukaemia Inhibitory Factor (130-095-779, Miltenyi Biotech, UK).

One eighth of the cell suspension was used to seed each new flask with a total volume of medium per flask of 7 ml. Flasks were incubated at 37°C and 5% CO_2 with medium exchanged two days after passage.

2.2.7 Ethics Statement

Primary mouse embryonic fibroblasts (MEFs) were derived from mouse embryos, which were harvested at day 12.5-13.5 of pregnancy (E12.5-13.5) from a naturally mated CD-1 female mouse. The pregnant female and the embryos were humanely sacrificed following Schedule 1 of the Animals (Scientific Procedures) Act 1986, for which specific ethical approval and licence are not required according to UK regulations.

2.2.8 Human Embryonic Stem Cell Maintenance

Cells of the Shef-3 hESC line (< passage 70), obtained from the UK Stem Cell Bank, were cultured on a layer of feeder cells consisting of inactivated MEFs (< passage 5). They were passaged every 3 days into T-25 Nunclon® cell culture flasks and cultivated in a humidified incubator at 37ºC with 5% CO_2.

MEF's were maintained in Dulbecco's Modified Eagle Medium (DMEM) (41965, Invitrogen, USA) supplemented with 10% (v/v) heat inactivated foetal bovine serum (FBS) (10270, Invitrogen, USA) and 1% (v/v) Non-Essential Amino Acids (NEAA) (11140, Invitrogen, USA). They were passaged every 3 days. To inactivate the MEFs the growth medium was replaced with 5-7 ml of normal MEF growth medium supplemented with 1 $mg.ml^{-1}$ of mitomycin C (M4287, Sigma-Aldrich, UK) and incubated for 2 hours at 37 ºC. After inactivation cells were washed three times with DPBS, detached by incubating with a trypsin:EDTA solution (T4049, Sigma-Aldrich, UK) for 3 minutes, quenched with normal MEF medium, centrifuged and re-suspended in MEF media. Cells were seeded, at a density of 9,200 cells cm^{-2}, into T-25 Nunclon® cell culture flasks that had been pre-coated with a 0.1% (w/v) in DPBS gelatine solution (G1890, Sigma-Aldrich, UK) for 10 minutes at room temperature.

hESCs were cultivated in KnockOut DMEM (10829, Invitrogen, USA) supplemented with 20% KnockOut Serum Replacement (10828, Invitrogen, USA), supplemented with 1 % 100x NEAA (11140, Invitrogen, USA), 2 mM L-Glutamine (21051, Invitrogen, USA), 0.1 mM β-mercaptoethanol (M3148, Sigma-Aldrich, UK) and 4 ng.ml^{-1} FGF2 (fibroblast growth factor 2) (4114-TC, R&D Systems, USA). For passaging, medium was aspirated and flasks were incubated with 1.5 ml of 0.025 mg.ml^{-1} collagenase solution (17104, Invitrogen, USA) for 5 minutes, before being replaced with fresh hESC medium. hESC colonies were then dissected into medium-sized colony fragments using pasteur pipettes and transferred into a new flask containing feeder cells prepared as outlined above.

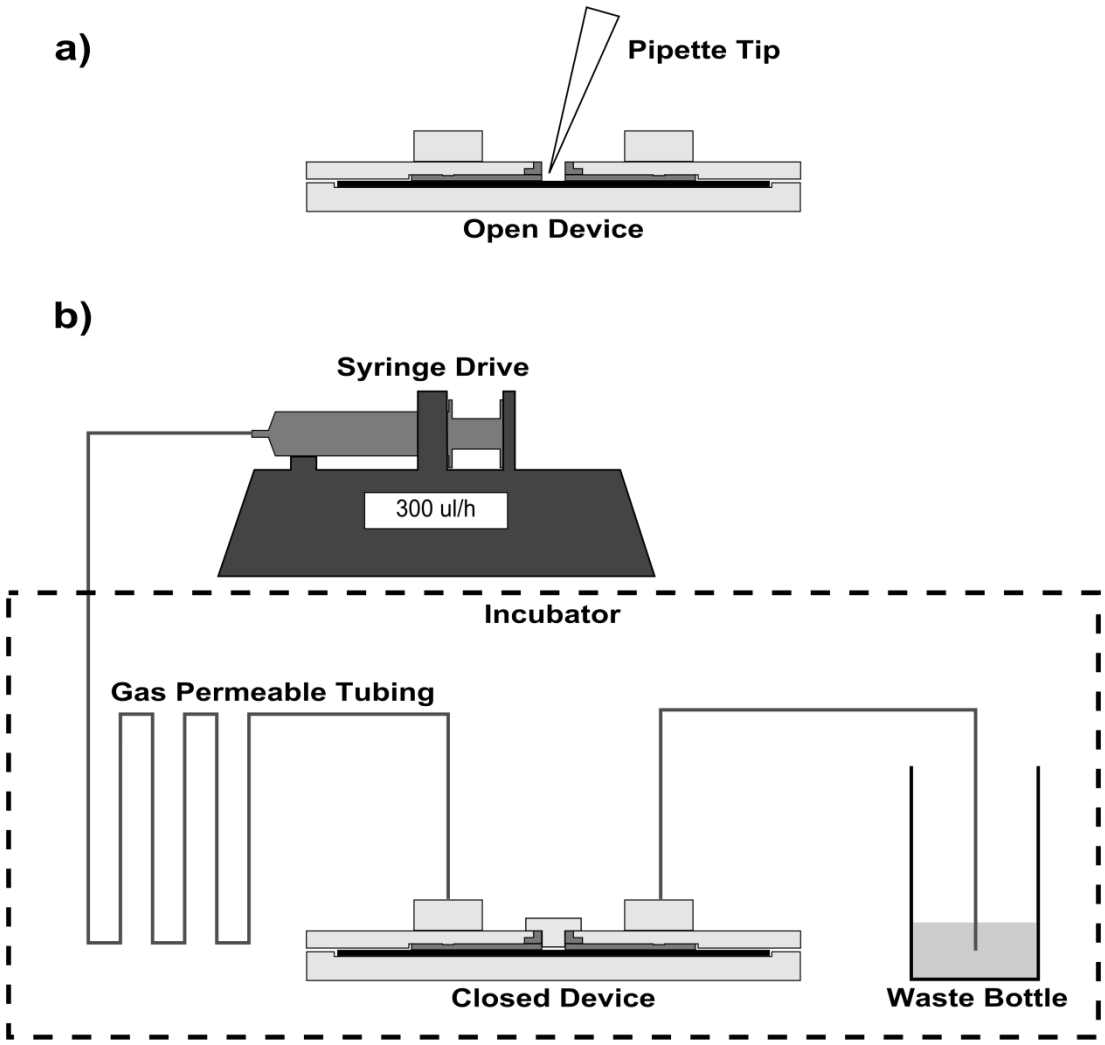

Figure 2.2 - Device setup for seeding and perfusion.

The device in open configuration [a], for coating of the culture surface and cell seeding by pipette, and the device in closed configuration setup for perfusion culture [b].

2.2.9 Seeding of Mouse Embryonic Stem Cells

Parts for six prototype culture devices were autoclaved and assembled with sterile Nunclon® TC-PS microscope slides (16004, Fischer Scientific, UK) in a class II biological safety cabinet. Lids were not included in the assembly as the experiments required only the open configuration (Figure 2.2[a]). The culture chambers were filled with 0.1% gelatine solution to ensure complete coverage of the culture surface. Similarly, the culture surfaces of six T-25 Nunclon® cell culture flasks were each covered with 0.1% gelatine solution. The gelatine was left for 15 minutes and removed before seeding.

Cells were harvested from a T-25 flask as per a normal passage. The concentration of resuspended cells was taken as the mean of two haemocytometer measurements and the concentration of the cell suspension was adjusted to between 3.5 10^4 and 11.5 10^4 cells.ml^{-1} by the addition of medium. The concentrations of the adjusted cell suspensions were checked with a haemocytometer. The cell suspensions were then used to seed the six T-25 flasks and six prepared prototype culture devices. The total volume of cell suspension seeded was 7.5 ml and 156 µl in the T-25 flasks and prototype devices respectively. The culture devices and flasks were then placed in an incubator at 37˚C with 5% CO_2. The prototype devices were incubated in a large glass petri dish (2175553, Schott, USA) to avoid contamination. The lid of the petri dish was propped open by small polycarbonate blocks to allow gas exchange with the incubator atmosphere.

Chips and flasks were removed from the incubator at set times. The media was aspirated and the culture surfaces were washed with DPBS. Attached cells were then detached with trypsin-EDTA and the resulting cell suspension collected. The concentration of cells in the aspirated medium and aspirated trypsin-EDTA were measured using a haemocytometer. Haemocytometer measurements were repeated and means taken.

2.2.10 Mouse Embryonic Stem Cell Culture

Parts for one prototype device were autoclaved and then assembled in a sterile manner in a class II biological safety cabinet using sterile Nunclon® TC-PS slides (16004, Fisher Scientific, UK). The culture surfaces of the prototype device and a T-25 culture flask were coated with 0.1% gelatin (G1890, Sigma-Aldrich, UK) for 15 minutes at room temperature. After removal of the gelatine, a suspension of E14 mouse embryonic stem cells (in standard mESC culture medium) was added by pipette to give a cell density of 4.9×10^4 cells.cm^{-2} and a medium height of 3 mm. The device (in the open configuration; Figure 2.2[a]) and flask were then incubated at 37°C and 5% CO_2 for four days. The prototype device was incubated in a large glass petri dish to avoid contamination. The lid of the petri dish was propped open by small polycarbonate blocks to allow gas exchange with the incubator atmosphere.

Medium was changed in both vessels every day and images were taken on an inverted fluorescence microscope (Ti-E, camera Fi-1, Nikon Instruments, UK). Images were then analysed with PHANTAST software (Jaccard et al., 2014a) to calculate the confluency of stem cells in each image. The settings of σ=3.5416, ε=0.0876, and a maximum halo removal ratio of 0.2812 were found using the built in parameter optimisation function. This optimisation maximised the F-value (an indicator of precision and accuracy where 1 represents perfect classification of pixels) to 0.9579 by testing different parameter sets against a set of manually classified pixels (selected from images of the flask and culture device over the four days). The remaining settings were, for halo processing, a minimum fill area of 25 pixels and removal of small objects setting of 400, and, for additional processing, removal of small objects bellow 100 pixels.

2.2.11 Human Embryonic Stem Cell Culture

Prior to each cell culture experiment, parts for one prototype culture device and all tubing and tools required for assembly were autoclaved at 121°C for 20 minutes. The culture device was then assembled with a sterile Nunclon® TC-PS slide (16004, Fisher Scientific, UK) in a class II biological safety cabinet. For substrate coating and cell seeding, the lid was removed (Figure 2.2[a]).

Laboratory pipettes with disposable 200 µl pipette tips were employed for all steps. The TC-PS culture surfaces of the prototype device and three single-well dishes (353653, BD Biosciences, USA; culture area 2.89 cm^2) were coated with 0.1% (w/v) gelatine in DPBS solution, and left to incubate at room temperature for 15 min. Then, each dish was seeded with ~45,000 inactivated MEFs (seeding density of ~15,600 cells cm^{-2}) in 1000 µl of MEF medium. The culture device was seeded with ~15,000 inactivated MEFs (~ 28,800 cells cm^{-2}) in 200 µl of MEF medium. (A higher cell density was chosen for the culture device to ensure a sufficient confluency.) The dishes and prototype culture device were transferred to an incubator (37 °C, 5% CO2). The culture device was placed in a large sterile glass Petri Dish to avoid contamination prior to insertion of the lid. 1 day later the MEF media was replaced with hESC media, dissected hESC colonies were seeded in the prototype device and the control dishes, and both were incubated (37 °C, 5% CO_2) for a further day.

After 1 day of static culture, the medium in the culture chamber was aspirated and the culture device closed with the re-sealable lid (Figure 2.2[b]). An autoclavable polyphenylsulfone tubing (R1230, Upchurch Scientific, USA), with Upchurch fittings (P207, Upchurch Scientific, USA) and a gas-permeable silastic tubing (R3607, Tygon, USA) connected a 20 ml syringe with the prototype culture device. The two types of tubing were attached to each other via Luer adapters (F331 and P659, Upchurch Scientific, USA). The gas permeable tubing was included to allow gas exchange between an incubator atmosphere and the medium, before it enters the culture chamber. The culture device was manually primed with culture medium using a syringe after which, the syringe was placed on a syringe drive (Model100, KD Scientific, USA) and culture medium perfused for 2 days at 300 $µl.h^{-1}$. Everything but the syringe pump was placed in an incubator to maintain the culture temperature and atmospheric composition (Figure 2.2[b]). Medium in the control dishes was exchanged every day.

2.2.12 Cell staining and imaging

Daily cell culture inspections and end-point assay imaging were performed with an inverted microscope (Ti-E, camera Fi-1, Nikon, UK). Cell staining in the culture device was performed in the open configuration. For apoptosis/necrosis staining, cells were washed once with DPBS then incubated for 5 min with Annexin V-FITC and propidium iodide (PI) each diluted 1:100 in binding buffer (K101-25, BioVision, USA).

For immunostaining, hESC colonies were fixed with 4% (v/v) paraformaldehyde (PFA) in DPBS for 20 minutes then washed three times. All washing was with DPBS supplemented with 10% (v/v) FBS to block non-specific binding. Cells to be stained for nuclear marker Oct-4 were permeabilised by incubating with 0.2% Triton X-100 for 15 min at room temperature before washing a further 3 times. Cells were incubated with primary monoclonal antibodies Oct-4 (SC-5279, Santa Cruz, USA) or SSEA-3 (ab109868, Abcam, UK), at a dilution of 1:200 in blocking solution, for one hour at room temperature. The cells were then washed three times and incubated with corresponding secondary antibodies that had excitation wavelengths of 488 nm (Oct-4, A11017, Invitrogen, USA and SSEA-3, A21212, Invitrogen, USA) for one hour at room temperature. Cells stained for Oct-4 were then washed three times and co-stained for Tra-1-81 by repeating the primary/secondary staining procedure above with a Tra-1-81 primary (ab16289, Abcam, UK) and a secondary with an excitation wavelength of 555 nm (A21426, Invitrogen, USA). Finally, the cells were washed with DPBS and stained with 4',6-diamidino-2-phenylindole (DAPI) (D1306, Invitrogen, Carlsbad, CA, USA). DAPI at a dilution of 1:200 was incubated with cells at room temperature for 10 minutes.

Stained cells were imaged with an inverted fluorescent microscope (Ti-E, camera Fi-1, Nikon, UK) using an LED excitation system (CoolLED pE-2, CoolLED, UK). Three experienced cell culture scientists (>3 years culturing adherent mammalian cells) counted cells staining positive for DAPI and Oct-4 in images of individual and partial colonies. Cells in images of three different colonies were counted in both the culture device and the control dish. The mean

counts across the three users were used to calculate the percentage of positive cells in each colony image.

2.3 Results and Discussion

2.3.1 Prototype Microfabricated Culture Device Design

The prototype microfabricated culture device (Figure 2.3) consists of a lid (PC), two interconnect bars (PC), top and bottom frames (PC), a gasket (PDMS), a microfluidic chip (PDMS), and a TC-PS slide (Reichen, 2012).

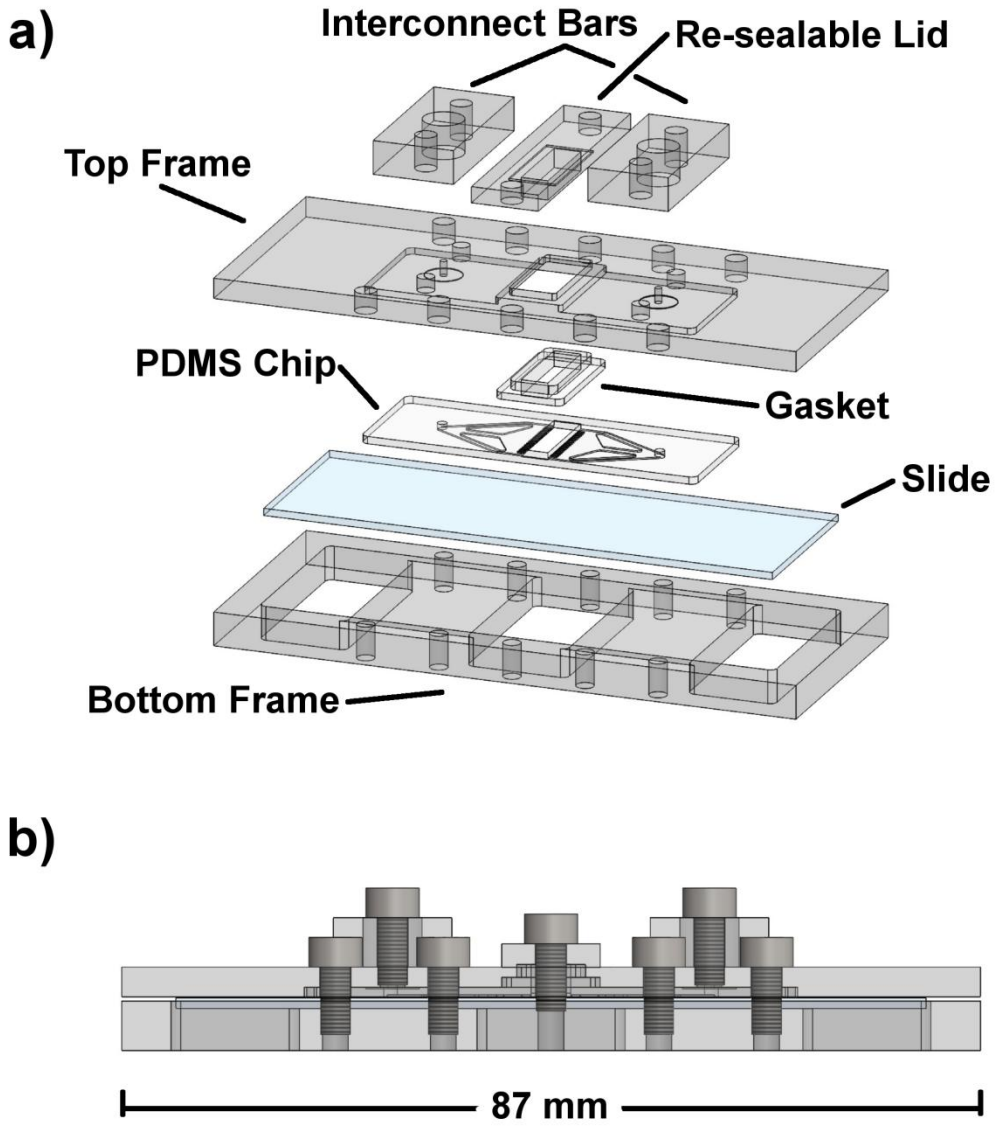

Figure 2.3 - Design of prototype microfabricated culture device.

Exploded view (a) and profile view (b) of the prototype device.

The top frame includes an opening to accommodate the lid as well as two recesses. The first recess positions the PDMS chip with respect to the top frame, and the second deeper recess accommodates the gasket. The top plate also has two 1 mm diameter bores as fluidic inlet and outlets. Centred on each bore is a boss that compresses the PDMS chip to form a seal. The bottom frame has the same outer dimensions as the top frame and a recess dimensioned to hold the TC-PS slide. An opening in the centre is designed to allow close proximity between objectives from an inverted microscope and the TC-PS slide for cell culture imaging. The bottom frame is also open at either end where it extends beyond the length of the PDMS chip.

The top and bottom frame are clamped together by ten M3 screws with five distributed evenly down each side of the frame. The central pair of screws also attaches the lid when in use. All the screws are tightened to 2 N.cm to form seals between the components by compression of the PDMS chip and gasket. While a larger number of screws ensure a more uniform distribution of compressive force, they also complicate assembly. This is particularly problematic when a device must be assembled in a sterile manner. The assembly is further complicated by requiring application of a precise torque to the screws. Care in both assembly and manufacture of parts is necessary to reliably deliver the correct torque. This reduced ease of use was noted and addressed in subsequent design improvements (section 3.3.3).

PDMS Chip

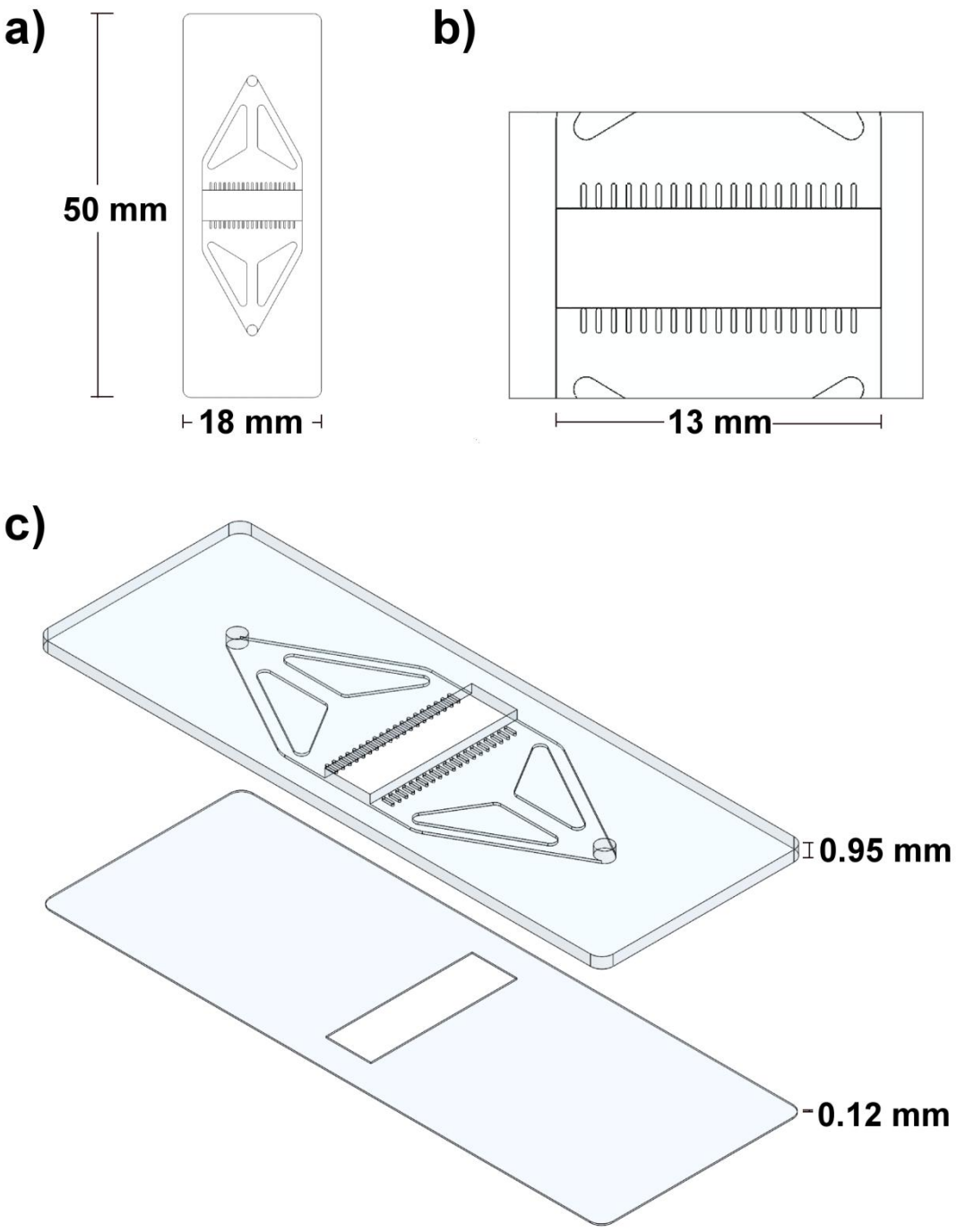

Figure 2.4 - Design of the prototype PDMS chip.

A top view of the PDMS chip [a], showing the flow channel structure, and a magnified view of the culture chamber area [b], showing the perfusion barrier layout. The chip is made of two layers (c); a structured layer containing the flow channels bonded to a spacer layer to elevate the channels above the culture surface.

The top layer of the prototype PDMS chip (Figure 2.4) contains the 200 µm deep flow channels connecting the inlet and outlet ports to the culture chamber (Reichen, 2012). The flow is expanded from a narrow inlet prior to the culture chamber and condensed back to a narrow outlet after the chamber by three merging channels. To promote flow uniformity across the chip, the top layer also includes flow equalisation barriers (or perfusion barriers) on each side of the culture chamber, each 200 µm wide and 1000 µm long (Figure 2.4[b]). The apertures between the barriers have rectangular cross-sections (400 µm × 200 µm). The identical flow resistance added by each aperture was intended to significantly outweigh the differences in the resistances of the different flow paths to the apertures. Therefore the relative variation in flow rate through the apertures would be minimal. The efficacy of perfusion barriers at distributing flow has been previously demonstrated (Petronis et al., 2006, Hung et al., 2005). However, these examples use a significantly larger ratio between the channel height prior to the apertures and the aperture height (and therefore a larger ratio between the flow resistances). The effectiveness of perfusion barriers in this design merited further investigation, which was carried out in chapter 3 (section 3.3.1).

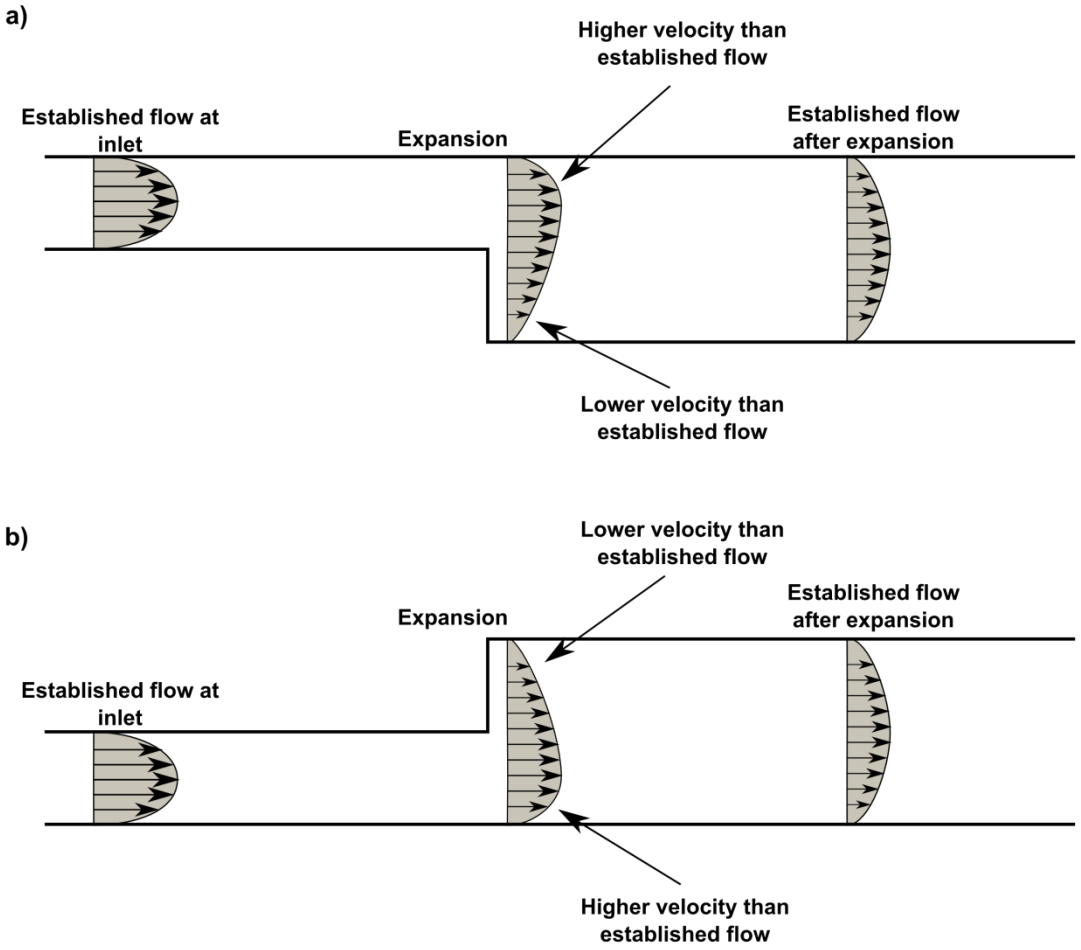

Figure 2.5 - The effect of inlet height on the velocity distribution immediately after expansion to the culture chamber.

Raising the inlet above the culture surface (a), rather than having the inlet adjacent to the culture surface (b), results in low fluid velocity and hydrodynamic shear stress at the culture surface. This is due to the non-symmetrical velocity profiles that occur as fluid transitions from established flow in the inlet to established flow in the culture chamber.

A more uniform distribution of flow results in more uniform concentrations of soluble factors perpendicular to the direction of flow. If medium travels across cells at the same speed, the same amount of soluble factors should be added and removed for each unit of distance travelled. Similarly, a more uniform flow distribution will result in more uniform shear stress, another important factor affecting cell growth and differentiation. In addition to striving for uniform shear effects, efforts have also been made to minimise them. The second (‘spacer’) layer of the chip elevates the first layer above the cell culture area by 120 µm (Figure 2.4[c]) to reduce shear stress. The shear experienced at the wall, in established flow between parallel plates, depends on only cross sectional area and flow rate (equation 2.2). However, immediately adjacent to expansions, the

position of the inlet has an effect (Figure 2.5). A greater elevation of the inlet above the culture surface reduces shear stress at that surface. The effectiveness of recessed culture chambers has been previously demonstrated in straight channels with grooves (Korin et al., 2009b), round wells (Figallo et al., 2007), and rectangular chambers (Petronis et al., 2006).

Culture Chamber

Both layers of the PDMS chip have a rectangular hole defining the culture chamber. The chamber is 13 mm wide and 4 mm in the direction of flow, giving a culture area of 0.52 cm^2 (between 96-well and 48-well plates). This is large enough to produce sufficient cells for immunostaining or qPCR (quantitative polymerase chain reaction) and may be sufficient for conventional flow cytometry (e.g. 4.2×10^5 cells based on an observed confluent cell density of ~8×10^5 with mESCs). The fabrication method can achieve a culture area of just 0.01 cm^2 but analysis of the cells cultured in this volume would be significantly more challenging. The design of the device limits the size of the culture chamber to the size of the PDMS chip, less the size of the inlet and outlet channels. The size of the chip is in turn limited to the size of a microscope slide.

The optimum culture area depends on the intended application, requiring knowledge of the required number of cells and the expected final cell density. Investigation of different culture processes or screening applications requires sufficient cells for statistically relevant analysis. As indicated previously the chosen culture area provides sufficient cell numbers for immunostaining and qPCR at typical cell densities ($0.05\text{-}1.00\times10^6$ $cells.cm^{-2}$). The expected dose sizes for medical applications range from 5×10^4 to 1×10^9 cells (Simaria et al., 2014, Mason and Dunnill, 2009). Hence, the slide limited system may be adaptable to production of very low dose personalised treatments if high efficiencies can be achieved. However, the majority of treatments are impractical to produce in a single layer system, or require removal of the size limitation of this design and/or significant scale-out to multiple parallel devices.

In addition to chamber size, the culture chamber length to width ratio must also be considered. When investigating the effects of specific process variables it is advantageous that these variables are uniform across the entire cell culture area. However, in long, narrow perfusion chambers, the consumption and secretion of soluble factors by cells near the inlet alter the conditions for the cells downstream (Titmarsh et al., 2012). This effect is exacerbated at lower flow rates as upstream cells have more time to alter medium before it reaches downstream cells. Consequently, when designing the culture area of the prototype device, the length dimension of the culture chamber was kept minimal. The resulting dimensions are distinctly different from other microfabricated devices for hESC culture (Yoshimitsu et al., 2014, Kamei et al., 2009, Korin et al., 2009a, Titmarsh et al., 2011, Villa-Diaz et al., 2009).

Re-sealable Lid

Previously Tkachenko *et al* (2009) presented a re-sealable system that requires seeding before assembly. In contrast, the prototype device includes a re-sealable lid enabling operation of the device in an ‘open’ configuration for cell seeding and recovery, and a ‘closed’ configuration for medium perfusion (Figure 2.2[a]). A similar system by Figallo *et al* (2007) limits the height of the culture chamber to the total thickness of the device. However in the prototype device, the lid is T-shaped with the upper ‘horizontal’ bar acting as a bed stop when the lid is pushed into the opening of the top frame. This defines the height of the culture chamber at 450 µm. The lid forms a press-fit with the PDMS gasket to seal the chamber. The dimensions of the inserted portion of the lid match the footprint of the culture chamber of the microfluidic PDMS chip.

In the closed configuration, the height of the culture chamber is defined by the re-sealable lid and the hard material of the lid does not deform during medium perfusion. In the open configuration, the culture chamber is directly accessible with laboratory pipettes, facilitating the pipette-based methods typically employed in laboratory-scale stem cell maintenance. These methods include static seeding, static cell recovery and immunostaining. A further advantage of the device is that, in open configuration, the depth of media in the culture

chamber is not limited to the height of the closed chamber. Thus, larger liquid volumes can be used during cell seeding, staining and recovery.

TC-PS Incorporation

Tissue-culture polystyrene TC-PS is the most widely employed culture surface in adherent stem cell biology (Berthier et al., 2012). TC-PS is used in tissue culture flasks, culture wells and larger systems such as Cell Factory™ systems (Thermo Scientific). Thus, use of TC-PS as a culture surface makes translation of results to other production scales more straightforward. However, integration of TC-PS with microfluidic devices is difficult, as TC-PS is not compatible with conventional air plasma or thermal bonding. Consequently, microfabricated devices for adherent cell culture make ubiquitous use of glass or PDMS culture surfaces (Young and Beebe, 2010), neither of which are commonly employed in regenerative medicine (Berthier et al., 2012). Introduction of novel growth surfaces to processing for medical applications, or accurate comparison of results with experiments using standard materials, would require extensive testing and validation.

In the prototype device, TC-PS is successfully integrated through use of compression seals between the PDMS components and smooth surfaces. Furthermore, the modular design of the device allows materials other than TC-PS to be integrated as long as they have a smooth, flat surface and the dimensions of a microscope slide; a common standard in microfluidics (van Heeren, 2012). This sealing system makes a number of materials immediately available for investigation. As a result, the prototype device could be employed to test growth surface candidates from microarray screening (Flaim et al., 2005), under the defined culture conditions obtainable in the device. This is analogous to the scale-up train in traditional biotechnology, where ‘hits’ from high-throughput screening plates are first investigated in shake flask cultures or small-scale bioreactors.

Interconnect bars

To facilitate rapid set-up of cell culture experiments and achieve leak-free long-term operation, an easy and robust interconnection with the macro-world is required (Fredrickson and Fan, 2004). The interconnect bars of the prototype device (Figure 2.3) are threaded to accept M6 Upchurch fittings and therefore permit simple connection with tubing for the provision and removal of media. The interconnect bars are interchangeable allowing the use of different fluidic connectors as required (e.g. ¼-28 threaded connectors). The interconnect bars are simple but attaching them (by two screws each) adds another step to assembly which is an inconvenience that could be avoided in future designs (as discussed in chapter 5). Further, it would be convenient to extensively reuse the interconnect bars but the threads tend to fail after just a few uses. This was addressed by different material choice in chapter 3.

Burst Pressure

The burst pressure of the prototype device was investigated to determine the robustness of the system and the multiple compression seals. The burst pressure is the maximum pressure that can be achieved before a rapid loss of pressure due to the failure of a component or seal. A positive burst pressure does not confirm that a system is leak free as any pathway for gradual fluid loss (such as extremely small channels or permeable material) that is available regardless of pressure will not necessarily be detected. The mean burst pressure of the prototype device is 59 kPa with a standard deviation of 18 kPa (n=36) and the lowest recorded burst pressure was 35 kPa. The mean standard deviation in burst pressure for the same assembly is 5% (standard deviation n=3, mean across 12 assemblies). Repeatedly achieving similar burst pressures without reassembly indicates the method of failure is reversible i.e. it is failure of a compression seal.

In comparison to the burst pressure, the pressure drop across the device at a flow rate of 500 $ml.h^{-1}$ is 20 kPa. This flow rate is three orders of magnitude higher than the intended maximum rate of medium perfusion. Therefore, the significant variation in the burst pressure may be acceptable as it remains

greater than the operating pressure. However, high variation between assemblies indicates that the compression based seals are highly sensitive to variations in manufacturing and/or assembly. Furthermore, variation in compression seal strength is most likely caused by similar variation in the level of compression which will also impact fluid flow. Based on this evidence, further investigation and design improvements were made to increase burst pressure reduce this variability (chapter 3).

Analysis of variance shows no statistically significant relationship between burst pressure and the number of times the lid is removed and reinserted for up to 30 repetitions (α=0.05, p=0.99, n=3). For a single assembly the variation in burst pressure is significantly lower than that between assemblies. The mean standard deviation between lid removals for a single assembly is 7% (n=12) relative to 31% between assemblies (n=12). Together, these results indicate that the re-sealable lid can be reliably used for repeated access to the culture chamber without significant impact on the performance of the device during perfusion. These results also indicate that the seal around the lid and the manner in which the lid is attached are not responsible for the high variation in burst pressure.

2.3.2 Modelling Velocity Fields and Hydrodynamic Shear

To evaluate the design of the prototype PDMS chip, the velocity fields and shear stress produced at a flow rate of 300 $\mu l.h^{-1}$ were calculated numerically and by finite element modelling. A flow rate of 300 $\mu l.h^{-1}$ corresponds to replacing 13.8 ml of media per day for each square centimetre of culture area, a rate 50 times higher than typical in hESC culture. It is therefore unlikely cells would ever be subjected to a higher shear stress during perfusion culture in the prototype device. The uniformity of the velocity field in the culture device was investigated at various heights above the culture surface (i.e. above the TC-PS slide).

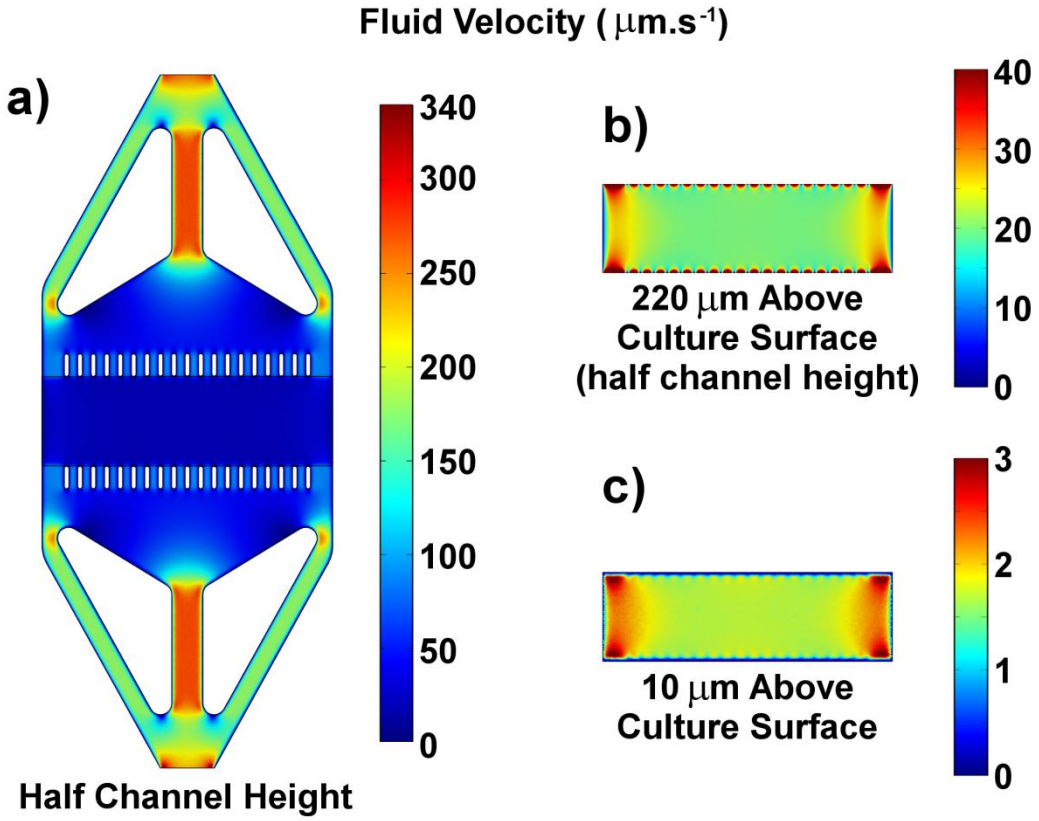

Figure 2.6 – Distribution of fluid velocity in the prototype PDMS chip.

The results of finite element modelling of media flow through the prototype PDMS chip at 300 $\mu l.h^{-1}$. The fluid velocity is shown at half the height of the flow channels (a), 220 μm above the culture surface (the same plane as half channel height) (b), and 10 μm above the culture surface (c).

Non-uniform growth patterns could be caused by spatial differences in shear stress or spatial differences in the exchange of soluble factors. The PDMS chip design produces a relatively even velocity field across the majority of the culture chamber (Figure 2.6). Consequently there should be minimal non-uniform cell growth patterns which can arise from variations in velocity fields (Aunins et al., 2003).

Previous reports indicate that shear stress is a critical parameter that can lead to cell dislodgement during perfusion of medium (Korin et al., 2006, Korin et al., 2009b). In the prototype device, finite element modelling predicts a mean hydrodynamic shear stress, 10 μm above the culture surface, of 1.33×10^{-4} Pa ± 0.37×10^{-4} Pa (standard deviation, based on a uniform grid of 4.7×10^{4} calculated points) at a flow rate of 300 $\mu l.h^{-1}$. The analytical solution for shear stress at the

culture surface is 1.48×10^{-4} Pa (assuming infinite parallel plates), which supports the result obtained through finite element modelling. The hydrodynamic shear stress of 1.33×10^{-4} Pa is three orders of magnitude below 1×10^{-1} Pa, the critical value previously reported for mESCs by Toh et al. (2011). Cell washout is therefore unlikely. Effects on gene expression have been reported at shear rates as low as 1.6×10^{-3} Pa (Toh and Voldman, 2011) and cannot be ruled out in the prototype device. However the very low shear stresses achievable in the prototype devices are expected to minimise induced changes in gene expression.

As previously discussed (section 2.3.1), low shear stress in the prototype device is primarily achieved through the large cross section of the culture chamber. The spacer layer of the PDMS chip also contributes by elevating the inlet and outlet channels 120 µm above the culture surface. This reduces the shear stress at the culture surface relative to an identical chamber height with no spacer layer. The effectiveness of recessed culture chambers has been previously demonstrated (Korin et al., 2009b, Figallo et al., 2007, Petronis et al., 2006). Since the thickness of the spacer layer is determined by spin-coating parameters, the elevation can easily be changed. This capacity to vary how far the culture surface is recessed could be utilised to investigate different shear stress levels at a fixed medium flow rate, or different flow rates with a fixed shear stress.

Higher velocity and culture plane shear stress are observed at the boundaries of the culture chamber (Figure 2.6). The large gap between the outermost perfusion barrier and the edge of the chamber has a lower resistance than the gaps between perfusion barriers resulting in a higher fluid velocity. This effect is deliberate and was included to remove air bubbles entrapped during closing or filling of the culture chamber. An alternative solution that does not affect flow uniformity was implemented in the next design (chapter 3) as uniformity of conditions is a key advantage of the microfabricated system.

The remaining heterogeneity in the culture plane velocity field stems from; low velocity areas adjacent to the perfusion barriers, low velocity caused by wall shear on either side of the chamber, and low velocities immediately adjacent to the expansion/contraction in fluid height. Wall shear is unavoidable and the fraction of the culture area affected is already reduced by the wide and short aspect ratio of the culture chamber. Furthermore, it is desirable to retain the difference in height between the channels and culture chamber as removing it would significantly increase either, cell shear stress, or medium hold up. Conversely, it is not clear from these results whether the perfusion barriers have a net positive effect on flow uniformity. Consequently, this was a target of further investigation (section 3.3.1).

2.3.3 Modelling of Dissolved Oxygen

Typically, in culture flasks and culture wells with direct medium/atmosphere interfaces, dissolved oxygen (DO) is not controlled, only the partial pressure of oxygen in the local atmosphere is kept constant. Under these conditions, the consumption of oxygen by cells creates a DO gradient, through the depth of medium, which drives oxygen transport by diffusion. Consequently, the DO experienced by cells (pericellular DO) will be lower than the saturation value and will reduce as the oxygen uptake rate (OUR) increases. Figure 2.7 shows how the pericellular DO varies through the duration of an open, static culture. Pericellular DO is shown for both a typical medium depth (3 mm), and with a medium depth equivalent to that found in the device in closed configuration (0.45 mm). The figure also shows pericellular DO for local atmospheres with both 21% gaseous oxygen (normoxic) and 2% gaseous oxygen (hypoxic) (1 atm pressure).

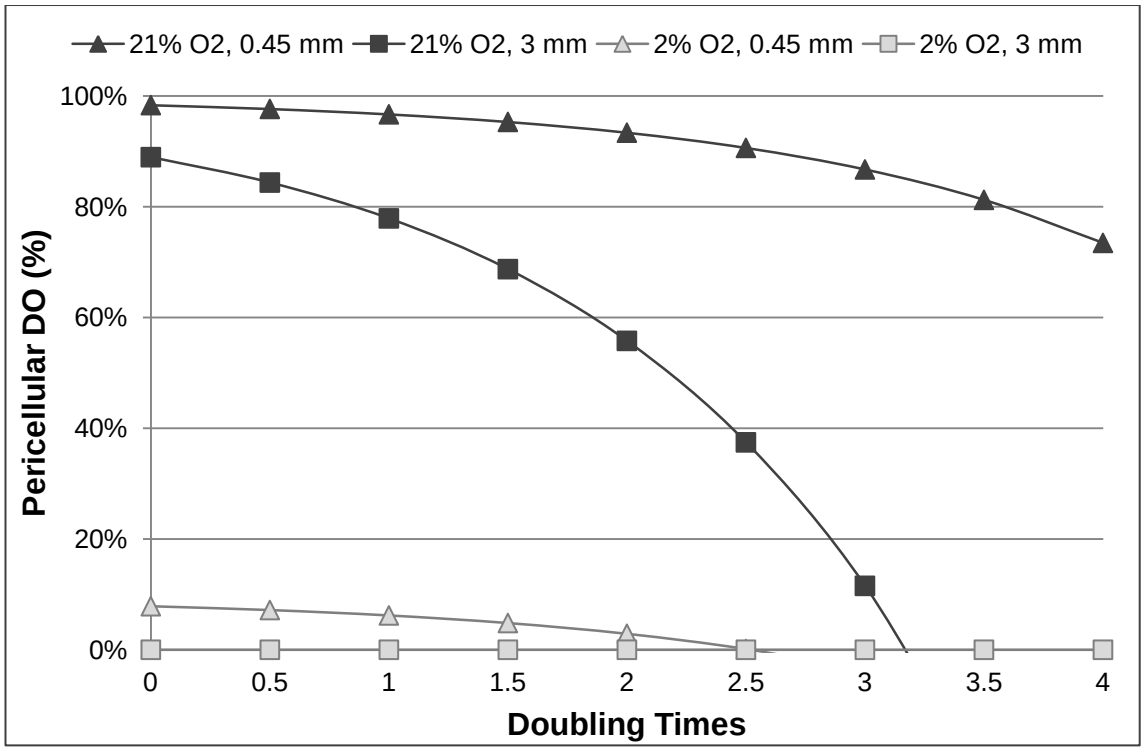

Figure 2.7 - Changes in pericellular dissolved oxygen through the duration of open, static culture.

The pericellular dissolved oxygen concentrations expected through the duration of open, static culture (calculated using Fick's law). Dissolved oxygen is shown as percentage of saturation with air (21% gaseous 0_2, 1 atm total pressure). The figure shows pericellular dissolved oxygen for a starting culture density of 5×10^4 cells.cm^{-2} with a constant oxygen consumption of 2.8×10^{-17} mol.s^{-1}cell^{-1}. Pericellular dissolved oxygen is shown for 2% and 21% concentrations of gaseous oxygen (total pressure of 1 atm) and 3 mm and 0.45 mm heights of medium overlay.

It is clear that, in a typical culture flask or well under normoxic conditions, there are significant changes in pericellular DO as the culture progresses from seeding to full confluency. The pericellular DO is expected to approach zero before the cells reach full confluency. Similarly, with hypoxic conditions, pericellular DO is expected to approach zero immediately after seeding. As pericellular DO approaches zero the OUR becomes limited by diffusion to 1.27×10^{-7} mol.m^{-2}.s^{-1}. Consequently, the oxygen consumption per cell will be increasingly limited as cell density increases. Figure 2.7 also shows the significant effect the height of medium has on pericellular DO. This is one reason why it is important to control the height of medium when culturing cells in open vessels.

The prototype culture device, in closed configuration, has no gas-medium interface. Once medium has entered the device the only source of additional

oxygen that could enter the medium is the PDMS parts. PDMS is oxygen permeable and oxygen's solubility in PDMS is over 8 times higher than the solubility in water (Sadrzadeh et al., 2010). However, the surface area of PDMS in contact with medium in the culture chamber (where dissolved oxygen is depleted) is low and confined to the edges of the culture area. Thus, the dissolved oxygen available to the cells is essentially limited to what is supplied by incoming medium. The medium is oxygenated by exposure to gaseous oxygen before entering the culture device. Thus, the rate of oxygen supplied can be controlled by adjusting medium flow rate and/or the partial pressure of gaseous oxygen the medium is exposed to.

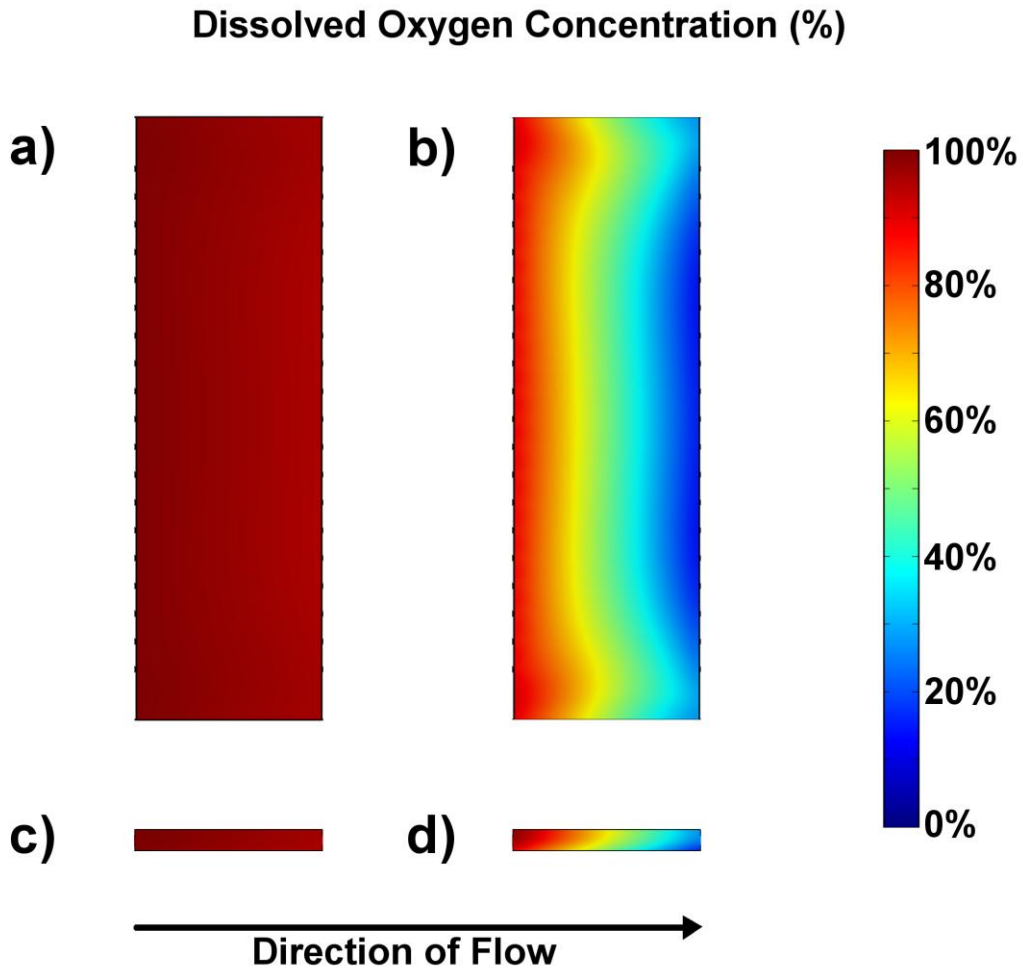

Figure 2.8 - Finite element modelling of dissolved oxygen in the prototype device during perfusion culture.
This figure shows the concentration of dissolved oxygen at the culture surface (a, b) and at a vertical slice through the centre of the chamber (c, d) during culture with medium perfused at 300 µl.h^{-1}. The concentration is shown at two different oxygen uptake rates; 0.14×10^{-7} mol.m^{-2}s^{-1} corresponding to a typical seeding cell density (a, c) and 2.240×10^{-7} mol.m^{-2}s^{-1} corresponding to a typical confluent cell density (b, d). Dissolved oxygen is shown as percentage of saturation at 1.05 atm (21% gaseous 0_2). Cross sections are shown at the same scale.

To investigate the pericellular DO expected in the closed and perfused prototype culture device, the transport of dissolved oxygen was added to the finite element model of fluid flow (section 2.3.2). Figure 2.8 shows the distribution of DO in the culture device at two different OURs that correspond to a typical seeding cell density and a typical confluent cell density. DO concentration is shown as a percentage of saturation with air at a pressure of 1.05 atm (0.20 mMol). At a typical seeding cell density (OUR = 0.14×10^{-7} $mol.m^{-2}s^{-1}$) the mean pericellular DO is 97% and the mean DO at the outlet is 96%. At high confluency (OUR = 2.240×10^{-7} $mol.m^{-2}s^{-1}$) the mean pericellular DO and outlet DO are 53% and 30% respectively.

At both high and low OURs the DO experienced by the cells is significantly higher than in a typical static flask (89% and 0% respectively, Figure 2.7). This shows that, with a flow rate of 300 $\mu l.h^{-1}$, oxygen is supplied more rapidly than is normally achieved by diffusion from a gas/medium interface. However, the rate at which oxygen is supplied is directly proportional to the flow rate. Therefore, changes in flow rate during or between experiments will significantly affect the pericellular DO. It would be advantageous to decouple oxygen supply from medium flow rate to allow independent control of this key parameter. This was achieved by the introduction of a gas permeable lid system in the next design (section 3.3.6).

It is clear from Figure 2.8 that, as the OUR increases, significant DO gradients develop across the culture chamber. At the OUR corresponding to high confluency, pericellular DO varies from 90% to 15% across the culture surface. With lower medium flow rates variation would be greater still. Such highly non-uniform concentrations prevent the investigation of specific parameter values to find optimum conditions. They may also result in spatial variations in growth rate and cell fate. As the device is designed to create a highly controlled culture environment this variability needed to be addressed and this, also, was achieved by the introduction of a gas permeable lid system (section 3.3.6). Further, the DO distribution demonstrates the importance of the culture

chamber dimensions. Concentration gradients across the length of the chamber will also occur with other (consumed or excreted) soluble factors such as glucose and signalling molecules. Therefore, the wide short chamber is necessary to minimise variation in concentrations while retaining low fluid velocity/shear stress.

2.3.4 Sterilisation by Autoclave

As the prototype device is designed for cell culture, it is essential that it can be sterilised. Autoclave is a simple and widely available sterilisation method which would allow the preparation of device parts in most cell culture laboratories. To investigate the effectiveness of sterilisation of prototype devices by autoclave, components were deliberately contaminated by incubating in *E. coli* broth prior to autoclave. The most complex PDMS component (chip) was used to ensure autoclaving could sterilise objects with small and complex geometries, as well as polycarbonate (PC) lids to investigate both materials (PC and PDMS) used in the device. Autoclaving effectively cleared all contamination from both parts as shown by subsequent incubation in sterile broth and plating of these broths after a day of incubation (Figure 2.9). The optical densities (OD600) of the broths relative to the negative control were 0.00 for the two autoclaved parts, and 1.16 and 1.55 for the PC and PDMS positive controls respectively. Effective sterilisation by autoclave was further supported by infection free multi-day cultures of mESCs and hESC colonies (sections 2.2.6 and 2.2.7). The reuse of parts sterilised by autoclave in these culture experiments also demonstrates that autoclaving does not detrimentally affect their function.

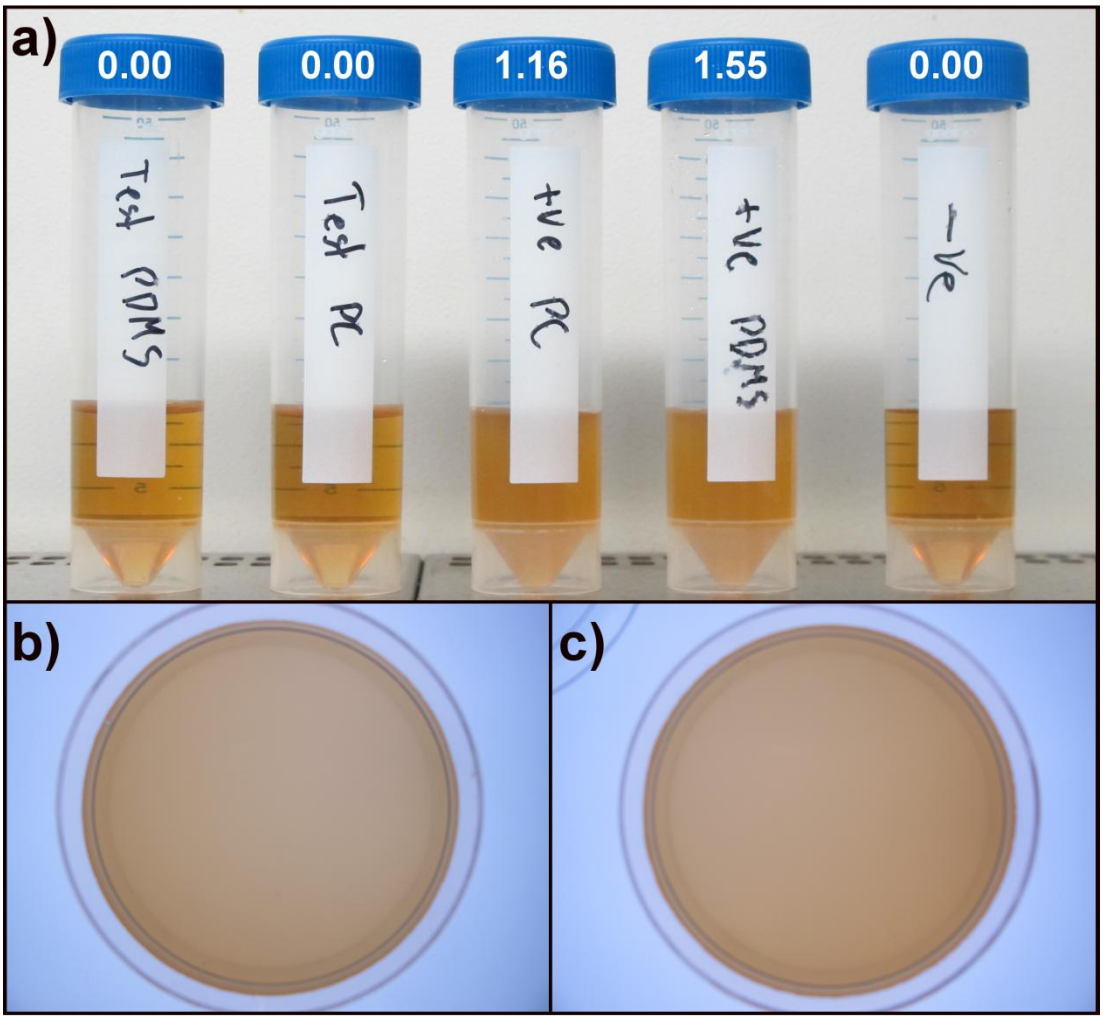

Figure 2.9 - Results of autoclave sterilisation of parts contaminated with *E.Coli*.

PDMS and polycarbonate parts deliberately contaminated with E.Coli were autoclaved to ensure autoclaving achieved sterilisation. Pane a) shows broth solutions after 1 day of incubation with autoclaved parts. From left to right the tubes are; autoclaved PDMS chip, autoclaved polycarbonate lid, positive control lid, positive control chip, negative control broth. Broth incubated with autoclaved parts remains clear, as does the negative control. The overlaid numbers indicate the measured optical density at 600 nm relative to the negative control. The two positive controls are cloudy with bacteria. Pane's b) and c) show agar plates made with the first two tubes after a further day of incubation. No colonies are visible on either plate unlike the positive controls which showed significant growth (not shown)

2.3.5 Seeding of Mouse Embryonic Stem Cells

Seeding cell density is a critical variable to both the expansion and differentiation of stem cell populations (Gage et al., 2013, Lu et al., 2009, Bitar et al., 2007). It is possible to dynamically seed systems by introducing cell suspension through channels. However, with dynamic seeding it is more difficult to control the number of cells and area in which they are seeded as cells are prone to settle in inlet and outlet channels. Additionally, dynamic seeding exposes the cells to shear stress which may influence cell fate or cause

damage. Dynamic seeding is particularly problematic for seeding clumps of cells, as is common practice with hESCs, as the clumps can be broken apart. Finally, weakly adhering cells like hESC colonies typically require long incubation times to achieve secure attachment (Oh et al., 2005). During this period, the static culture medium overlay provides the oxygen and nutrient demands of the cells. While this height is typically 2-3 mm in wells and flasks, the height of medium in closed microfluidic systems is typically very low and may be unable to support cells for the required period.

To overcome these issues, and allow more valid comparison with traditional well and flask systems, the culture device facilitates static seeding by pipette via the re-sealable culture chamber lid. Cells can be directly pipetted onto the culture surface using standard seeding protocols and, with the lid removed, up to a 3 mm height of medium can be used to sustain the cells during attachment. Cells should thus experience the same conditions during attachment as in standard flask culture. To investigate the seeding process and comparability with flask culture, measurements of attached and suspended cells were made at different time points after initial seeding. Mouse embryonic stem cells were used for this engineering study as they are more easily cultured reproducibly than human embryonic stem cells, particularly when seeding as a suspension of single cells. Seeding a suspension of single cells allows easier quantification of the cells deeded and the attached and unattached cells post-seeding. Mouse embryonic stem cells are from a similar *in vivo* environment to human embryonic stem cells and are therefore expected to be sufficiently representative of human embryonic stem cell behaviour for initial studies.

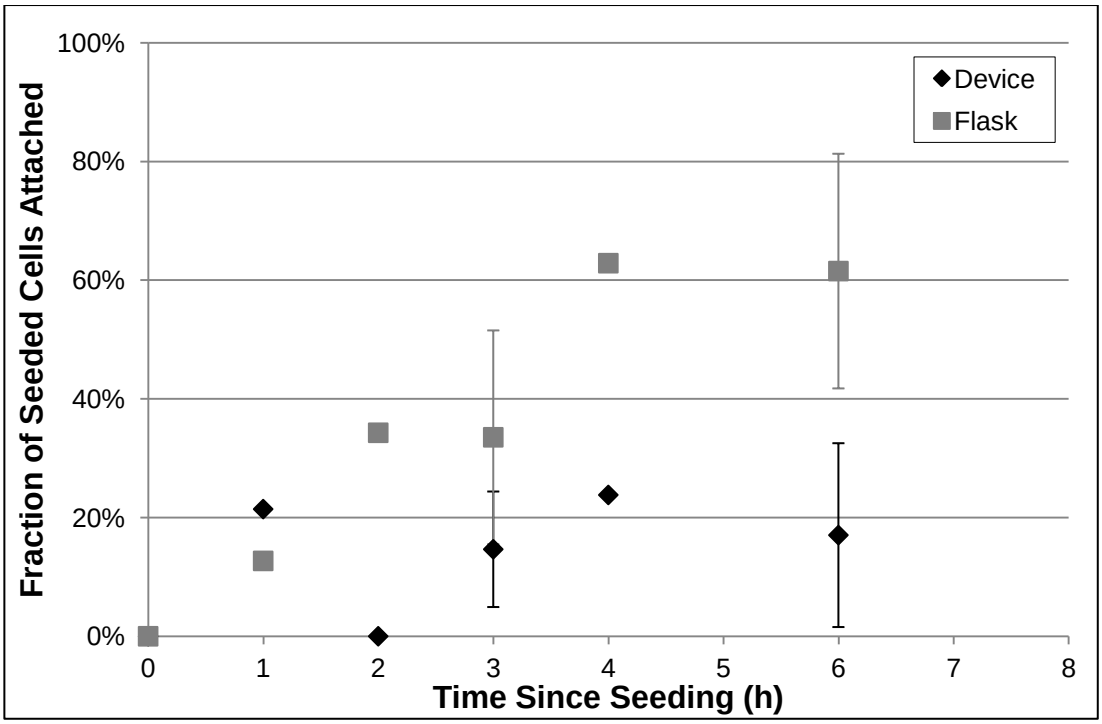

Figure 2.10 – Fraction of seeded cells attached to the culture surface over time.

Figure showing the fraction of seeded cells that were recovered from flasks and prototype devices, at various time points after seeding, using Trypsin. Points at 1, 2, and 4 hours are individual measurements while, at 3 and 6 hours, points are means of 10 measurements and error bars show the standard deviation between those 10 measurements.

Problems were encountered when trying to measure the number of attached cells by enzymatic detachment and subsequent counting. The number of cells collected in the aspirated trypsin showed high levels of variation (Figure 2.10). Visual inspection by inverted microscope showed some cells remaining on the surface after aspiration of trypsin. Subsequent experiments showed that up to 20% of cells left after aspiration of the initial medium could be removed when washing with DPBS in both flasks and culture devices. Further, in culture devices, a second trypsin treatment could remove up to 35% more cells than a single 6 minute incubation. Poor recovery is particularly problematic in the microfabricated culture devices due to the low cell density (so early after seeding) and small culture area.

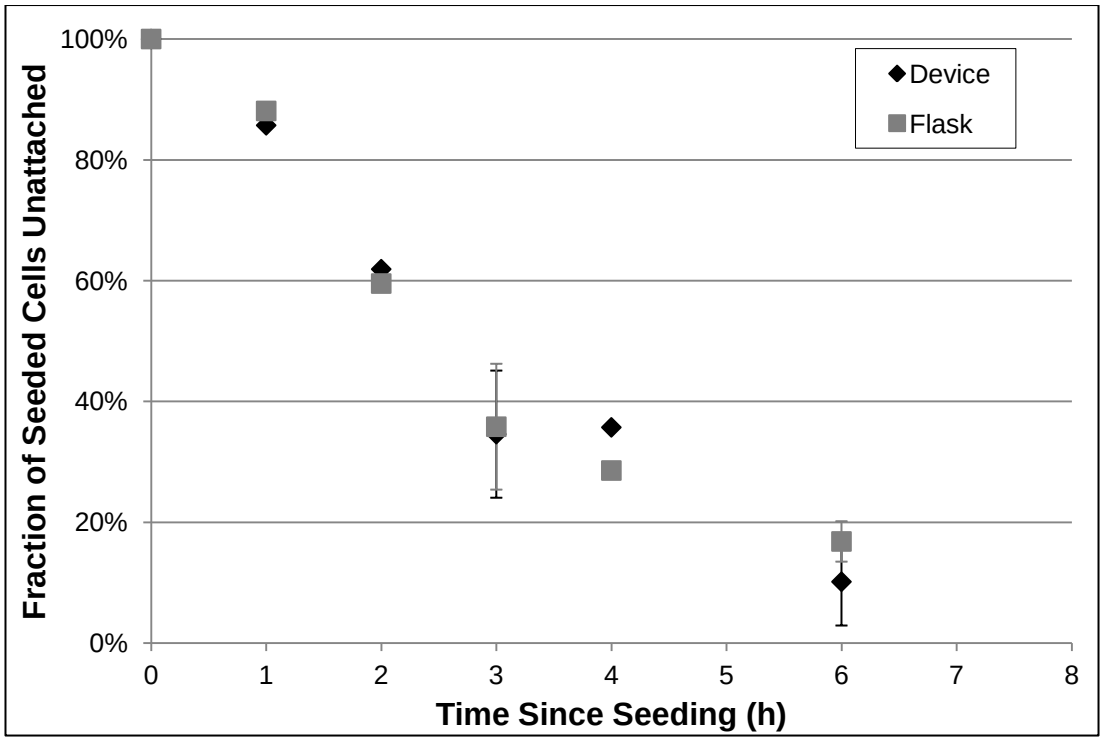

Figure 2.11 – Fraction of seeded cells that remain unattached over time.

Figure showing the fraction of seeded cells that were recovered in medium aspirated from flasks and prototype devices at various time points after seeding. Points at 1, 2, and 4 hours are individual measurements while, at 3 and 6 hours, points are means of 10 measurements and error bars show standard deviation.

Investigation of cells remaining unattached suggest that >80% of mESCs settled and attached within 6 hours (Figure 2.11). The unattached cells are those collected in the aspirated medium. The fraction of the originally seeded cells that remain unattached follow trends in the flasks and culture devices that are statistically indistinguishable. This suggests a similar seeding process occurs in both systems, as is expected. The experiments also show a high level of repeatability in the process. The standard deviations in the fraction of cells unattached after 6 hours were 3% and 7% in the flasks and prototype devices respectively (n=10, n=9). These results indicate that a standardised incubation period of 6 hours will result in consistent cell attachment. Consequently, this incubation period was adopted for subsequent experiments.

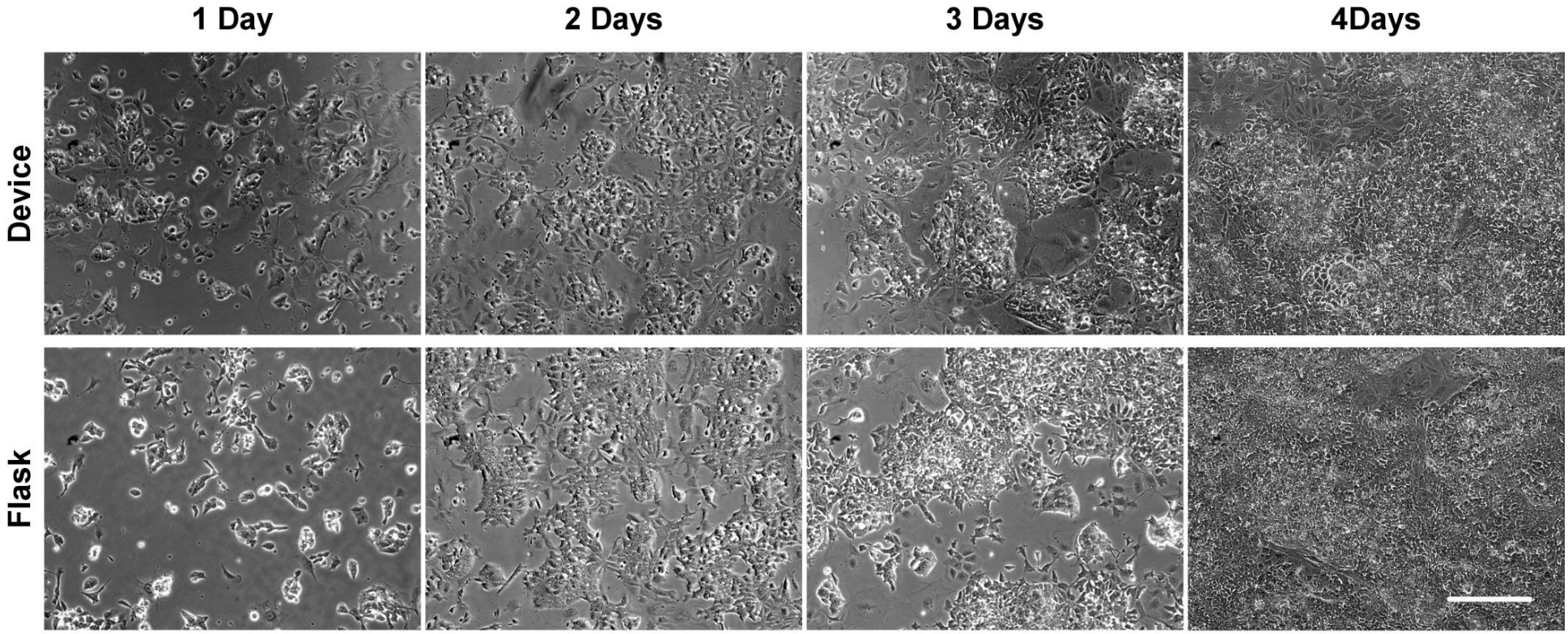

Figure 2.12 - Mouse ESCs cultured statically for 4 days.

Phase contrast images of E14 mESCs cultured statically for 4 days with daily medium exchange. Cells were grown in a prototype culture device and a T-25 culture flask. Images were taken with a 10× objective. Images were not taken in the same location at each time point. Scale bar represents 200 μm.

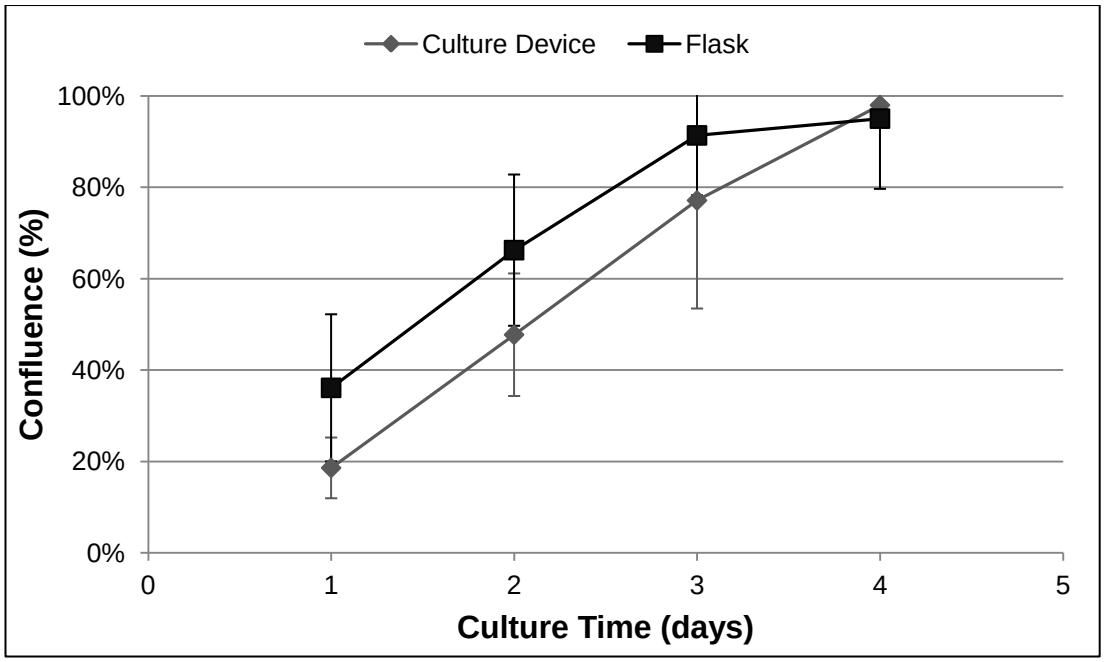

Figure 2.13 - Confluency over time of mESCs cultured statically.

The mean confluency of mESCs as calculated using PHANTAST image processing software (Jaccard et al., 2014a). A flask and prototype culture device were both seeded from the same cell suspension and cultured for 4 days with daily medium exchange and imaging. Error bars show the standard deviation between images (n≥9).

2.3.6 Culture of Mouse Embryonic Stem Cells

mESCs were cultured in the prototype culture device without perfusion as an initial investigation of its suitability as a culture system. Cells were also cultured in a T-25 culture flask to allow comparison of growth rates. Mouse embryonic stem cells were used for this engineering study as they are more easily cultured reproducibly than human embryonic stem cells and can be seeded as a suspension of single cells without a layer of feeder cells. As the purpose of these experiments is engineering characterisation of the device, the relative ease of reproducible culture is worth the lesser relevance of the mouse cell line. Mouse embryonic stem cells are from a similar *in vivo* environment to human embryonic stem cells and are therefore expected to be sufficiently representative of human embryonic stem cell behaviour for initial studies. Figure 2.12 shows images of cells in both systems at various time points during the culture. PHANTAST image analysis software was used to generate confluency values for each image. Confluency is indicative of cell number though it cannot be directly related due to small variations in the area occupied by individual

cells over the duration of a culture. Figure 2.13 plots the mean confluency of the two culture systems over time.

Results of the culture experiment support the suitability of culture device for the culture of stem cells as mESCs survived and proliferated for 4 days. The results also suggest that cells proliferate in the prototype device at similar rates to in flask culture when the only difference between the systems is the culture vessel. The number of images taken to represent the two systems was low so uncertainties were large. Further experimentation would be required to establish comparability between the systems but this was not performed as the culture device is only a prototype and was later developed further. It should be noted that the proliferation rate may change when medium is perfused as this changes the conditions experienced by the cells.

2.3.7 Co-culture of Human Embryonic Stem Cell Colonies

The potential of the prototype culture device to culture stem cells with perfused medium was evaluated by culturing feeder-attached hESC colonies. hESC were chosen for this study to be consistent with a preliminary experiment performed by Marcel Reichen. hESCs are more difficult to culture than other common model systems such as mouse embryonic stem cells and mouse embryonic fibroblasts. Additionally, co-culture techniques, which are inherently more complicated than monoculture, are common in stem cell research. Thus feeder-attached hESC culture is a more rigorous test than many other culture processes and successful feeder-attached hESC culture in the prototype device would indicate likely suitability for most other adherent cell cultures. Furthermore, hESCs are a clinically relevant cell type.

To test the suitability of the prototype device for hESC culture, open culture devices were seeded with inactivated MEF by pipette (Figure 2.2[a]). Single-well dishes were seeded in parallel to the culture devices to ensure the seeded cells proliferated and expressed pluripotency markers when following standard culture protocols. The following day hESC colonies were seeded onto the MEF layer and the device was incubated in open configuration for a further day. A

day after hESC seeding, the culture devices were closed and media was continuously perfused at 300 µl.h^{-1}, resulting in a residence time of approximately 5 min. The media was replaced once a day in the control dishes, in line with standard manual cell culture practice. During perfusion, medium equilibrated with the incubator gas partial pressures as it passed through gas permeable inlet tubing. This allowed dissolved gases to be supplied to the culture chamber via the incoming medium.

The above experiment was attempted 44 times (up to 4 attempts at a time in parallel). On 13 occasions (30% of attempts) the device clearly leaked. On a further 14 occasions (32% of attempts) the experiment failed due to the appearance and persistence of bubbles in the culture chamber. Where bubbles formed it is not clear whether this was a result of slow leaks, evaporation through PDMS components, outgassing of dissolved gases from the medium, or the wash through of bubbles present in tubing or inlet channels at the start of perfusion. However, the random occurance makes evaporation and outgassing less likely causes. The combined 62% failure rate indicates that the culture system is not robust. This clearly needed to be addressed before the device could be a useful culture system for research or production of cells. The cause was investigated further and a solution developed as presented in chapter 3.

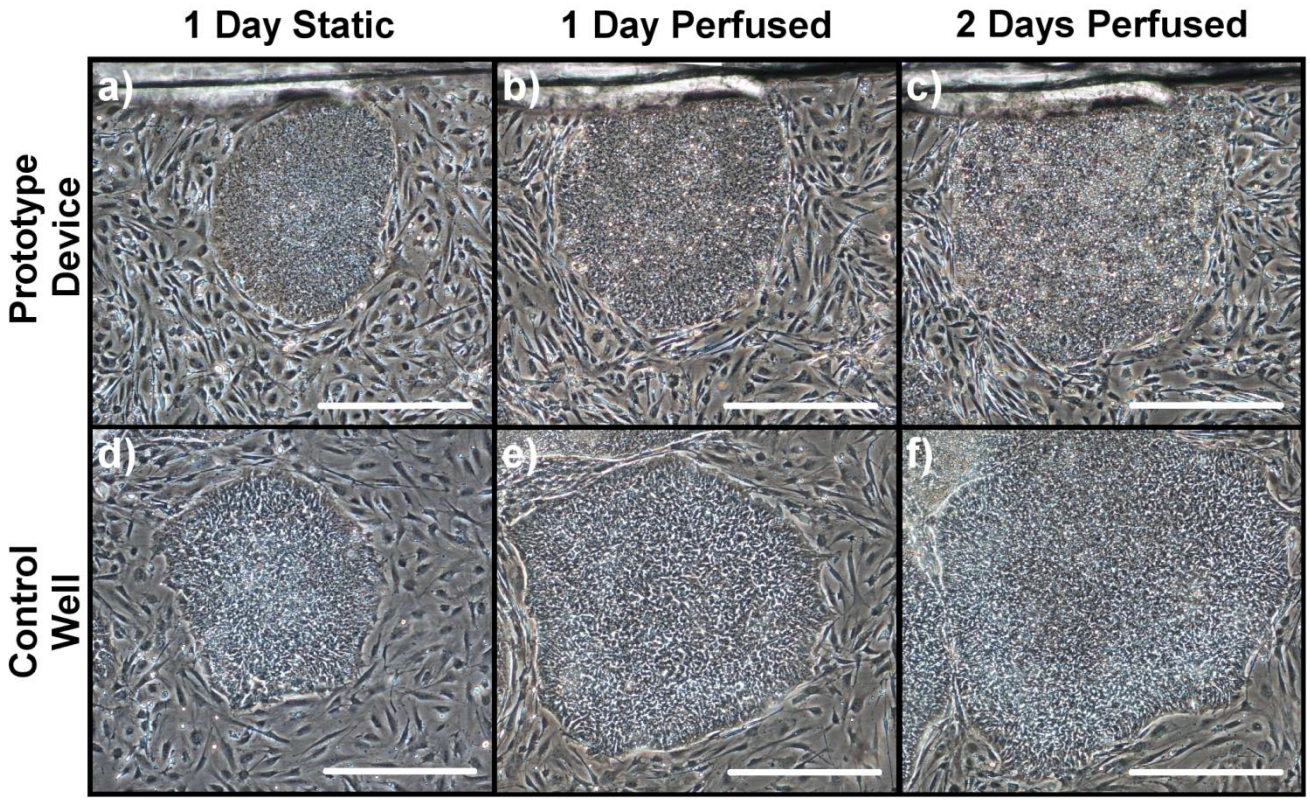

Figure 2.14 - hESC colonies in a prototype device and culture well imaged at intervals during a perfusion culture experiment.

Phase contrast microscope images of hESC colonies co-cultured on inactivated MEF feeder cells in a prototype culture device [a-c] and a single well culture dish [d-f]. For each system, the same colony is shown at each time point. Images were taken after 1 day of static culture (from hESC seeding) [a, d], 1 subsequent day of perfusion culture [b, e], and a further day of perfusion culture [c, f]. Images were taken with a 4× objective and the scale bars are 500 μm. (Reichen et al., 2012)

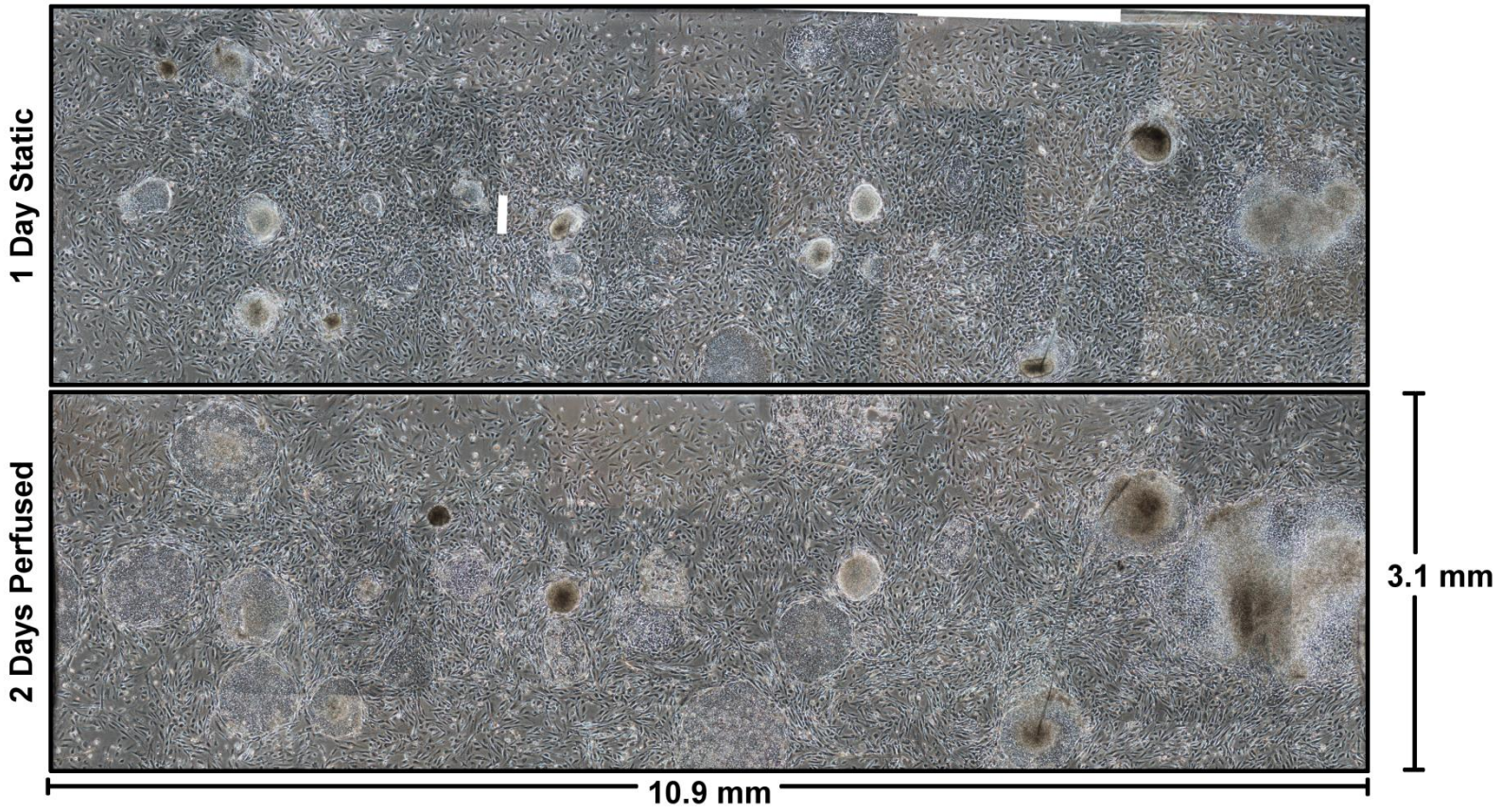

Figure 2.15 - Culture surface of a prototype device at the beginning and end of medium perfusion during the culture of hESC.

Stitched phase contrast microscopy images showing the majority of the culture surface of a device with hESC colonies co-cultured on inactivated MEF feeder cells. The cells are shown after 1 day of static culture (from hESC seeding) and after 2 subsequent days of culture with perfused medium.

In experiments where leaks and bubbles did not occur, the inactivated MEFs started to attach within 2 hours in both the prototype culture devices and in the control dishes. Within one day, the majority of cells had attached and spread in both systems. The majority of hESC colonies seeded onto the MEF layer also attached within one day. hESC colonies in the prototype devices maintained an undifferentiated morphology comparable to the colonies in the control dishes (Figure 2.14[a,d]). The successful seeding of both inactivated MEFs and hESC colonies utilising standard static seeding protocols demonstrate how the re-sealable lid facilitates static cell seeding.

After 1 day of perfusion culture, the cells within the colonies were small and tightly packed together; a characteristic morphology of undifferentiated hESCs (Figure 2.14[b,e]). After 2 days of continuous perfusion, hESC colonies maintained an undifferentiated morphology in both the prototype culture device and in the control dishes (Figure 2.14[c,f]). Figure 2.15 shows the most of the area of a culture chamber from the beginning to the end of perfusion. The majority of colonies expand over the 2 day period. Washout of hESC colonies was not observed, consistent with the results of shear stress modelling (section 2.2.2). Continued adherence and growth of the cells in these conditions is supported by both the low shear chip design and the use of traditional substrate.

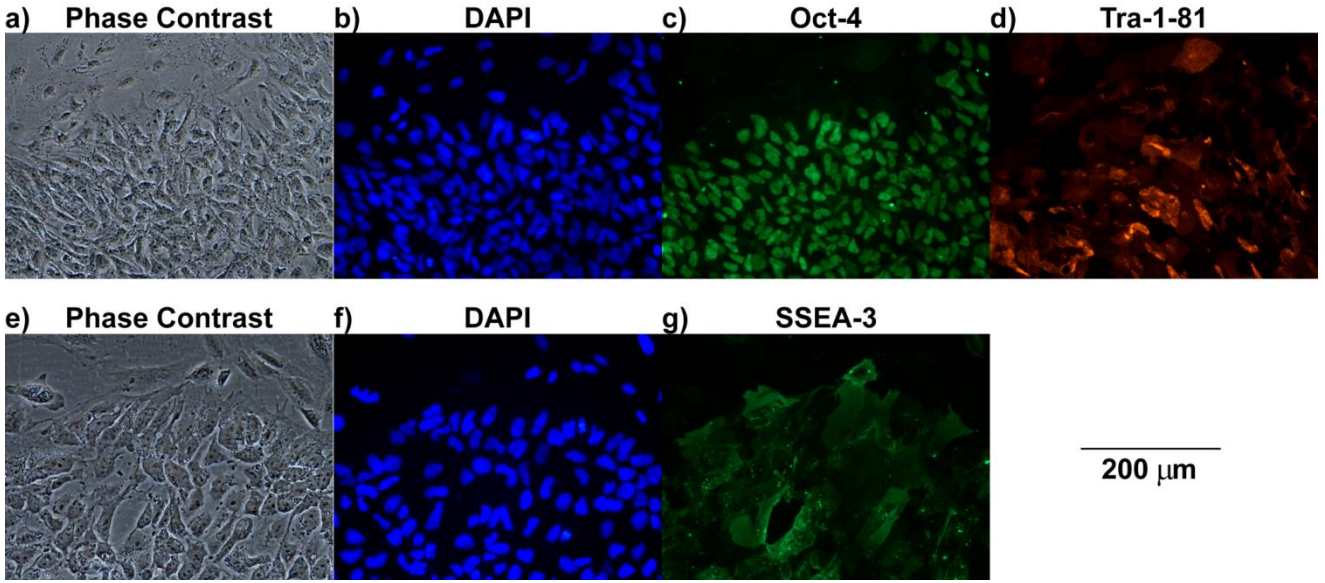

Figure 2.16 - hESC cells cultured in the prototype device with perfused medium then immunostained for pluripotency markers.

Images of human embryonic stem cells in the prototype device following 1 day of culture with static medium and 2 days of culture with perfused medium. DAPI staining shows the nucleus of all cells. Cells are positively stained for nuclear pluripotency marker Oct-4 [c], and surface pluripotency markers Tra-1-81 [d] and SSEA-3 [g]. Images were taken with a 20× objective. (Reichen et al., 2012)

Immunostaining was carried out to test for the expression of pluripotency markers Oct-4, Tra-1-81, and SSEA-3. The sequences of antibody incubation and washing were performed with the device in the open configuration (i.e. after removing the lid), further demonstrating the value of the re-sealable lid. The hESC colonies from one culture device were co-stained for Oct-4 and Tra-1-81, and the cells from a second device were stained for SSEA-3 (both devices were also co-stained with DAPI). As can be seen in Figure 2.16, the hESC colonies stained positively for Oct-4 [c], Tra-1-81 [d] and SSEA-3 [g] with the correct localisation (nuclear, surface and surface respectively). These antigens are all expressed in pluripotent hESCs but not after early stage differentiation. The percentage of cells staining positive for Oct-4, in images of individual colonies, was 91% in the culture device and 94% in the control well with standard deviations of 2% and 5% respectively (n = 3 colonies, ~1,500 cells total).

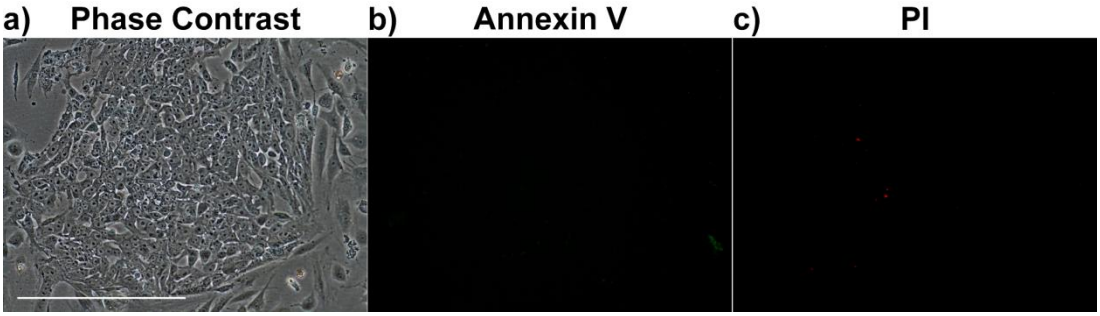

Figure 2.17 - Viability staining of hESCs after culture in a prototype device with perfused medium.

Images of hESC cells in a prototype device stained for viability after 1 day of static culture and 2 days of culture with perfused medium. The cells visible in the phase contrast image [a] are negative for apoptosis marker Annexin V (green) [b] and necrosis marker PI (red) [c]. Images were taken with a 20x objective. Scale bar is 200 μm.

In a repeat experiment, a culture device and a control dish were stained with Annexin V and propidium iodide to detect apoptotic and necrotic cells. The numbers of cells staining positive were very low (Figure 2.17). These positive staining results for viability and pluripotency, in combination with the morphology observations, are evidence supporting the expansion of viable, undifferentiated hESC colonies through one day of static culture and two days of continuous medium perfusion. These results cannot be directly compared with the control wells due to multiple differences between the systems including

feeder cell density, medium exchange rate, and availability of oxygen. However, they demonstrate the suitability of the microfabricated device as a culture system for hESCs.

2.3.8 Control and Automation Platform

A prototype control and automation platform was previously developed to house three prototype culture devices and to control them during perfusion culture experiments (Reichen, 2012). The platform consists of two modules; a medium handling module and a microscope module to house the devices (Figure 2.17). The platform is controlled by custom LabVIEW software (National Instruments, UK) via a data acquisition card (DAQ). The platform is designed to control medium flow rate, medium source, and medium temperature. It also allows acquisition of images with a microscope mounted camera. In this section the platform was assessed for strengths to be retained and weaknesses to be addressed in the improved platform presented in chapter 3.

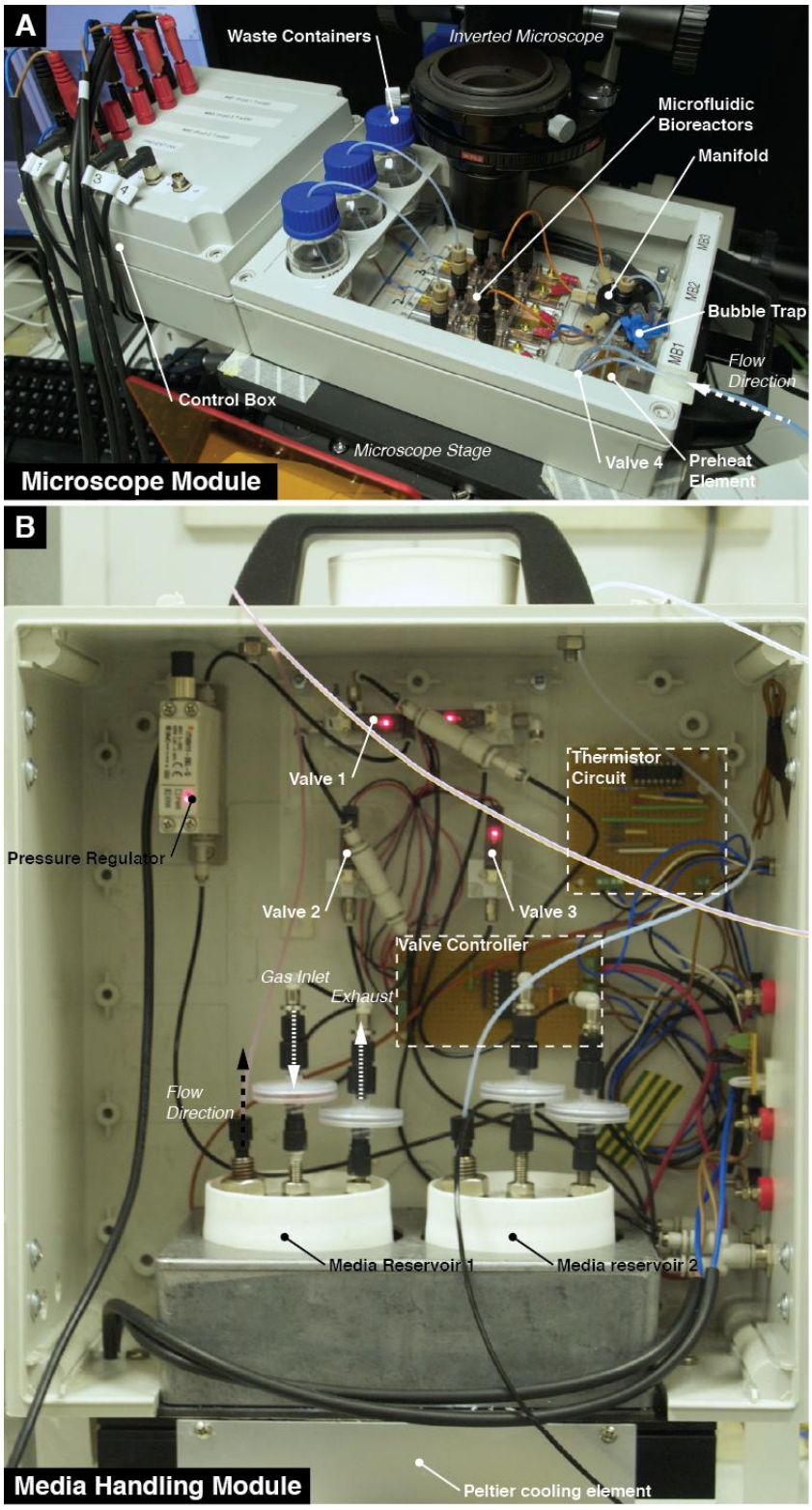

Figure 2.18 – Prototype control and automation platform.

Photographs of the prototype control and automation platform reproduced with permission (Reichen, 2012). The platform consists of two modules; a microscope module to house the devices [a] and a medium handling module [b].

Medium Perfusion

The medium supply module houses two custom made medium reservoirs (Figure 2.18[b]). Medium is pumped from these reservoirs by displacement with a pressurised gas mixture. The flow rate of the medium is controlled by an electronic pressure regulator via the LabVIEW software. When the pressure is reduced an exhaust port on the lid of the reservoir allows rapid reduction in reservoir pressure. Three way valves allow the user to choose between two medium reservoirs. Both medium reservoirs are situated in a cooled water bath to reduce thermal degradation of components.

The pressure driven pumping system was demonstrated to deliver more rapid changes in flow rate than syringe driven flow (Reichen et al., 2013) (Reichen, 2012). Sparging pressurised gas into the medium reservoirs also introduces dissolved oxygen and carbon dioxide to the medium. However, high downstream flow resistance will cause back flow of medium when pressure is reduced. Also, larger volumes of gas in the reservoirs may reduce the speed at which flow rate can be increased (depending on the maximum flow rate of gas). Furthermore, the system could make use of a variety of cheap and standardised commercially available reservoirs such as Schott bottles.

The pumping system assumes a constant pressure resistance is generated by the tubing and culture devices. However, as the collected volumes in the waste reservoirs increase over the duration of an experiment, the back pressure will also increase. Furthermore, the burst pressure results indicate that the flow resistance of the devices are also likely to be variable. In addition to affecting the overall flow rate, this will also affect the distribution of flow between the devices. The flow is split between the three devices by a four port junction and it is assumed they will have equal flow resistances and hence equal flow rates. But results show some variation in the flow rate through three parallel devices (Reichen et al., 2013) (Reichen, 2012). Moreover, the flow meter used to make these measurements introduces an additional resistance to that flow path which may have reduced the flow through that path while the measurement was being

made. These issues were all considered in designing the fluidics for the improved platform (section 3.3.7).

Temperature Control

The medium reservoirs are situated in a waterbath cooled by a peltier element. The device housing “microscope module” contains a preheat unit which uses a thin film resistor to heat medium before it enters the culture devices. Immediately after the preheat is a bubble trap to capture gases evolved as a result of the temperature rise. The culture chamber is maintained at 37°C by heating the microscope slide. To achieve this, a glass microscope slide coated with a thin layer of indium tin oxide is used. Passing a current through the resistive coating generates heat which is conducted through the slide. These systems were demonstrated to maintain medium at the desired temperature (Reichen et al., 2013) (Reichen, 2012).

The major limitation of the heating system is the requirement for a glass microscope slide. A unique selling point of the culture device is its ability to incorporate multiple substrates including TC-PS. This is also the driving factor for use of pressure based seals. Removal of this unique selling point reduces the value of the whole design. An alternative solution was developed in chapter 4 (section 4.3.3). In addition, the bubble trap has a fixed capacity which is relatively low and can only be refreshed by manually opening a valve and allowing medium to force out the trapped gas. A solution with a higher or automatically refreshed capacity would be beneficial and the latter was introduced in the next design (section 3.3.7).

Microscopy

The module housing the devices (Figure 2.18[a]) is designed to sit on the stage of a microscope to allow the capture of phase contrast images throughout a culture experiment. Phase contrast images provide useful information on cell morphology and confluency (Matsuoka et al., 2014). Therefore, the regular capture of such images would greatly increase the information output of any

culture experiment. However, automated image acquisition can only be performed at a single position. Any changes to the image position or settings (such as magnification) must be performed manually. Further, the window in the microscope stage does not cover the culture area of all three chambers. Hence, the entire module must be moved if all three chambers are to be imaged. With such manual manipulation it is not possible to return to an identical imaging position. If phase contrast imaging is to be a key monitoring system of the platform it should be fully automated. This was achieved in the improved design by use of a motorised microscope (section 3.3.7).

Software and Connectivity

The platform draws power from eight separate DC power supplies. These power supplies deliver different voltages ranging from 5 V to 24 V. Similarly eight separate 4-pin connectors are required to connect to the DAQ for communication with a computer. The large number of external connections complicates setup of the platform and occupies a lot of physical space. Further the requirement for multiple power supplies adds unnecessary expense. The connectivity of the improved platform was simplified and a single power supply used (section 3.3.7).

The platform is controlled by a computer using a virtual instrument created with LabVIEW software. This virtual instrument was developed in parallel with the control and automation platform and became unwieldy and cluttered with redundant functions. While functional when setup correctly this code is complicated to use. There is also redundant code including code for the control of alternative pumping solutions and code for measurement of DO, by fluorescent lifetime measurements, using equipment that was never integrated with the prototype device. The software was streamlined and the user interface simplified in the new design to allow use by researchers not proficient in LabVIEW coding. The software incorporates a control file which allows the automated time dependent adjustment of set points for the temperature control loops, valve positions, and regulator pressure. There is also facility to override pre-programmed set points if required.

2.4 Conclusions

As demonstrated in this chapter, the prototype microfabricated culture device, developed by Marcel Reichen, shows considerable promise as a system for the perfusion culture of adherent stem cells. The short wide culture chamber reduces variation in the soluble environment caused by cellular consumption and excretion. In addition, the design of the PDMS chip delivers relatively uniform fluid velocities across the width of the chip and a low level of hydrodynamic shear. Hence, the culture device delivers a highly uniform soluble environment allowing precise control of conditions.

The device's resealable lid allows direct access to the culture chamber at any point during the culture process. Furthermore, the removal and insertion of the lid does not significantly affect the burst pressure of the device. Direct access facilitates static seeding, manual cell recovery, and immunostaining as typically practised in culture wells and flasks. Similarly, the device facilitates multiple culture surfaces including the TC-PS typically employed in culture flasks, wells, and larger scale systems. These features are advantageous as they allow translation of processes and results between the device and other culture systems.

The device is readily sterilised by autoclave, a process commonly available to cell culture laboratories. The majority of mESC cells seeded in the device attach within 6 hours allowing the prompt initiation of medium perfusion. Furthermore, the rate of attachment is the same in the culture device as in a culture flask. Likewise, in open configuration, and under static conditions, the device delivers a similar mESC growth rate to a culture flask. These results indicate the suitability of the device for conventional static cell culture. They also support the ability to translate processes and results between the two systems.

The device was used to co-culture hESC colonies on inactivated MEF feeder cells with continuously perfused medium. The hESC colonies attach and expand over the course of perfusion culture. Furthermore, the cells remain viable and continue to express pluripotency markers. These results show the

suitability of the device for perfusion culture of stem cells. They also demonstrate the low shear environment, the integration of a TC-PS culture surface, the facility to statically seed cells (including cell aggregates), and the ability to assemble and operate the device in a sterile manner.

Finally, a prototype control and automation platform has also been developed to capitalise on the added control and functionality of the microfabricated device. The platform houses three culture devices on an inverted microscope. The platform delivers control over medium temperature at different points, as well as medium flow rate. It also allows switching between two medium reservoirs and image acquisition for a single field of view.

However, while promising, the prototype device and platform required further investigation and improvement before they could be widely applied to stem cell processes. The prototype device, platform, and control software needed to be made simpler and easier to use (Sackmann et al., 2014). The prototype device, while functional, is difficult to assemble due to the large number of parts and the sensitivity to screw torque. Similarly, the platform required fewer connections for data and power. Finally, the software needed to be streamlined and a better user interface developed. These changes are important to allow use of the system by the widest possible audience.

The device also needed to be made more robust. If it cannot be used reliably it will not be adopted by the stem cell sector. The interconnect bars needed to be made more reusable by better material choice. However, more pressing is the high occurrence of leaks and bubbles in culture experiments. These issues were likely linked to the large variation observed in the burst pressure. Evidence suggested this variation stems from a lack of consistency in the pressure based seals formed with the PDMS chip. The cause of this inconsistency needed to be found and addressed.

Modelling results presented in this chapter suggested the uniformity of both fluid velocity and dissolved oxygen could be increased. The fluid velocity is made less uniform across the culture chamber by dead zones behind perfusion barriers and high velocities between them. The necessity of these perfusion barriers required investigation along with alternative methods of flow distribution. The variation in fluid velocity across the chip also causes variation in DO. In addition, DO varies in the direction of flow as oxygen is depleted from medium when it passes over cells. The device needed a more uniform delivery of oxygen that is independent of medium flow rate.

Finally, the control and automation platform required a number of key improvements. Most importantly, a new solution to heat the culture chamber was required. The solution used in the prototype platform requires the use of a glass slide, which removes one of the key advantages of the culture device. Another major improvement needed is the automation of microscopy, allowing regular and repeated imaging of multiple fields of view. Finally, medium handling needed to be improved to ensure equal flow through multiple devices and minimise the occurrence of backflow. All these areas for further investigation and improvement were addressed and the results are presented in the following chapters.

3. Design Improvements to the Microfabricated Culture System

The majority of work presented in this chapter has been previously published in Macown *et al* (2014). Portions of the text in this chapter appear as previously published (particularly materials and methods). Some of the improvements to the monitoring and fluid control do not appear in the above publiction.

3.1 Summary of the Prototype Microfabricated Culture System and Required Improvements

Investigation showed the prototype adherent stem cell culture system developed by Marcel Reichen (Reichen, 2012, Reichen et al., 2012) had multiple beneficial design features making it a promising tool for stem cell process development (section 2.3.1). The design of the prototype chip and culture chamber achieved a higher degree of uniformity in the soluble microenvironment than typical in other microfluidic culture devices. It also minimised hydrodynamic shear stress at the culture plane. The resealable lid allowed static seeding and cell recovery and an interchangeable culture surface allowed the use of TC-PS (tissue culture polystyrene). These features enable translation of processes from traditional flask and dish culture.

The seeding and maintenance of mouse embryonic stem cells (mESCs) in the culture device was demonstrated under static culture conditions (sections 2.3.5-6). Furthermore, the maintenance of human embryonic stem cells (hESCs) co-cultured on inactivated mouse embryonic fibroblast feeders (MEFs) was demonstrated with continuous perfusion of medium by a syringe drive (section 2.3.7). These results supported the devices suitability for the culture of adherent stem cells. They also provided evidence of some relation between device and flask culture. Finally, a system was established to house multiple culture devices, control medium flow and temperature, and facilitate monitoring by phase contrast microscopy (section 2.3.8).

Yet the prototype culture system required further improvement in three key areas. Firstly, both the fluid velocity and dissolved oxygen in the culture chamber could be made more uniform. The fluid velocity in the prototype device was higher at the edges due to larger gaps in the perfusion barriers (section 2.3.2). The necessity and effectiveness of the perfusion barriers also merited further investigation as there was evidence they decreased rather than increased flow uniformity. Modelling also indicated dissolved oxygen would become highly heterogeneous at high cell confluency (section 2.3.2). Therefore an improved method of oxygen delivery is required.

Secondly, the device and surrounding system needed to be made more robust and simpler to use. A highly variable burst pressure indicated the prototype device design was not robust (section 2.3.1). Furthermore, the mode of failure and low variability resulting from lid removal imply that the issue is with the seal between the PDMS (poly(dimethylsiloxane)) chip and the microscope slide. The interconnect bars could also be made more robust by a material change. In addition, the prototype device is complicated to assemble in a sterile manner and would benefit from simplification. Similarly the control and automation platform merits simplification.

Finally, improvements to the prototype control and automation system are required. The system facilitates monitoring by phase contrast microscopy but is limited as it requires manual adjustment to the field of view. The fluid control system should be upgraded to ensure equal flows through parallel devices, prevent bubble formation, prevent backflow, and allow more rapid medium switching. Last of all, an alternative on chip heating solution is needed that allows continued use of TC-PS culture surfaces. This chapter will address improvements to the uniformity of the culture environment (sections 3.3.1 and 3.3.6), the robustness and ease of use of the system (sections 3.3.2-5), monitoring (section 3.3.7), and the fluidic control systems (section 3.3.7). An alternative heating solution will be addressed in chapter 4 (section 4.3.3).

3.2 Materials and Methods

3.2.1 Fabrication of Parts

Polycarbonate and PDMS parts were fabricated as previously (section 2.2.1). Briefly, polycarbonate parts were machined directly using a micro-milling machine, structured PDMS parts were cast in moulds fabricated by micro-milling, and the spacer layer of the PDMS chip was made by spin coating PDMS on a silicon wafer before being bonded to the cast element of the chip using air plasma. The aluminium interconnect bars were fabricated from 6 mm aluminium sheet (grade 6082) by micro-milling. The top plate, bottom plate, and brackets of the new device holder were manufactured by Finetech Engineering Limited (Hatfield, UK). The parts were fabricated from anodised aluminium following technical drawings produced in SolidWorks (Dassault Systemes, UK). The clamps and bottom frames, used as an interim solution with the prototype design (section 3.3.3), were manufactured from 6082 grade aluminium by Proto Labs Ltd (Halesfield, UK). SolidWorks drawings of all parts are shown in Appendix 2.

3.2.2 Fluid Dynamic Modelling

As in section 2.2.3, the flow of medium through different chip designs was analyzed by finite element analysis using COMSOL Multiphysics. The fluidic networks were built as 3D models using SolidWorks and imported as the geometry for the COMSOL models. The fluid material was defined as water with the dynamic viscosity adjusted to 7.8×10^{-4} Pa.s. A fully developed steady-state flow with no slip condition at the boundaries was assumed. The inlet boundary conditions were set to an average velocity calculated from the flow rate (300 $\mu l.h^{-1}$), and at the outlet boundary conditions were set as zero pressure. The geometry was divided into a free tetrahedral mesh with maximum and minimum element sizes of 40.6 µm and 0.05 µm respectively resulting in 1.4×10^{7} elements for the most complex chip design investigated. The models were solved using COMSOL's GMRES iterative solver. Hydrodynamic shear stress at the culture surface was calculated from the simulated velocity profile using equation 2.1.

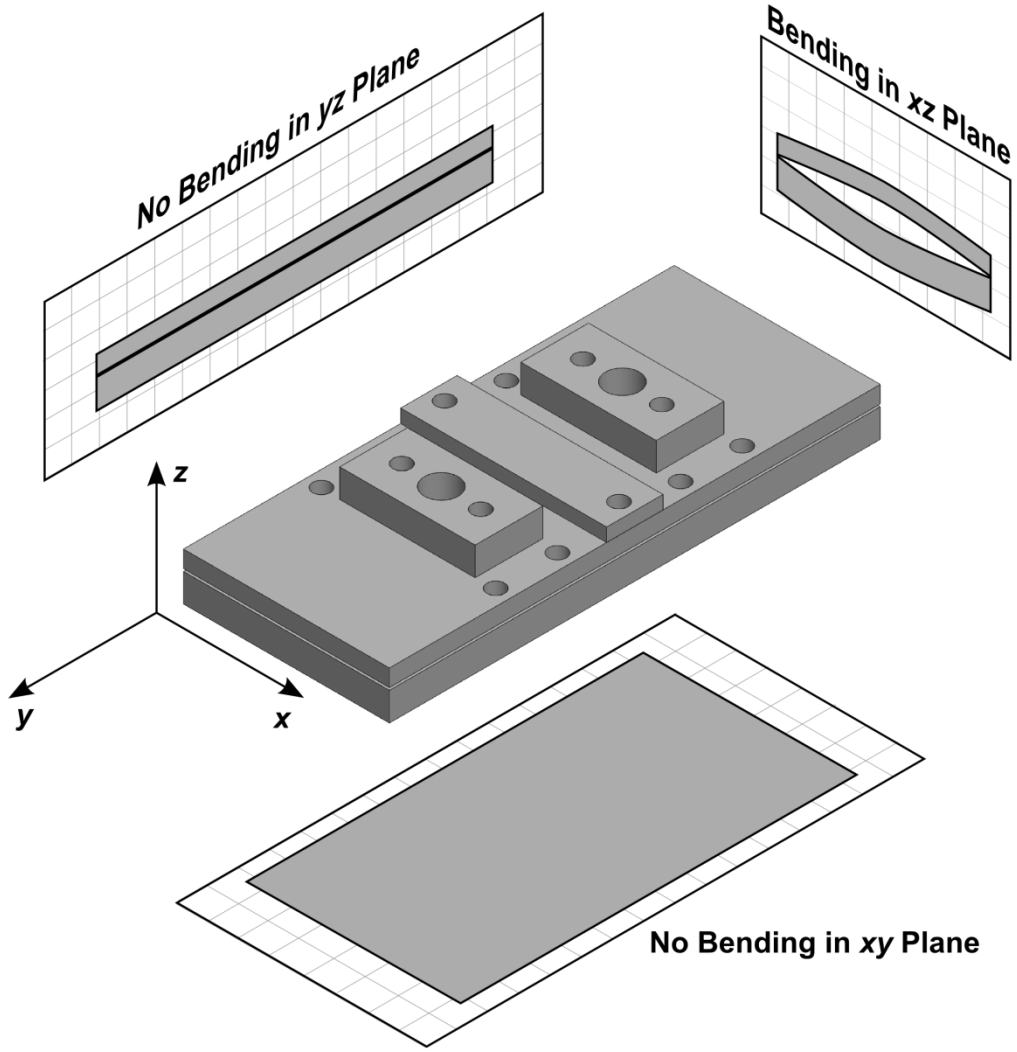

Figure 3.1 - Planes and axes for bending analysis.

To simplify bending analysis it is assumed there is no bending in the *xy* and *yz* planes.

3.2.3 Bending Analysis

A number of assumptions were made in order to approximate the bending of rigid device components. Firstly, the problem was treated as a bending beam problem rather than a bending plate problem. This simplification was made to allow simpler and more rapid investigation of potential bending effects. Secondly, the bending was simplified to a 2D problem by assuming no bending in the *xy* and *yz* planes; the *y* axis being parallel to a line from the inlet to the outlet and the *z* axis normal to the culture surface (see Figure 3.1). In Marcel Reichen's prototype design, the screw forces are distributed evenly along the length of the chip so bending in the *yz* plane is likely to be negligible. With the new design the clamping points of the aluminium holder are fewer and distributed non-symmetrically relative to the PDMS chip. However, bending in the *yz* plane is still likely to be negligible as the relevant second moments of inertia of the aluminium parts are high relative to those relevant to bending in the *xz* plane. As there are no forces applied in the *x* and *y* directions bending in the *xy* plane would not be expected.

Finally, when calculating second moments of inertia, cross sections were simplified to be symmetrical and some smaller features were ignored (Appendix 3). This simplification to symmetry was necessary as symmetry is a key assumption of the calculation method used. For the prototype design the cross sections were already symmetrical but for the new design the recesses were shifted off centre. Because height of cross section is much more significant than breadth the effects of the simplification should be low. The smaller features that were ignored are small holes whose cross section would have little impact on the second moment of inertia.

The second moments of inertia for each cross section were calculated using the formula for a rectangle (Equation 3.1) and parallel axis theorem (Equation 3.2). The second moment of inertia of a rectangle about its centre is given be the equation

$$I_z = \frac{H^3 B}{12} \qquad (3.1)$$

where H is the height (*z* dimension) and B is the breadth (y dimension). The second moment of inertia of the same rectangle about an off centre axis *n* can be calculated using parallel axis theorem;

$$I_n = I_{centroid} + A \cdot d^2_{n-centroid} \quad (3.2)$$

Where A is the cross sectional area and d is the distance between the centre and the neutral axis. The second moment of inertia of complex cross sections can be calculated as the sum of the moments of their components. See Appendix 3 for the calculated second moments of inertia for each cross section.

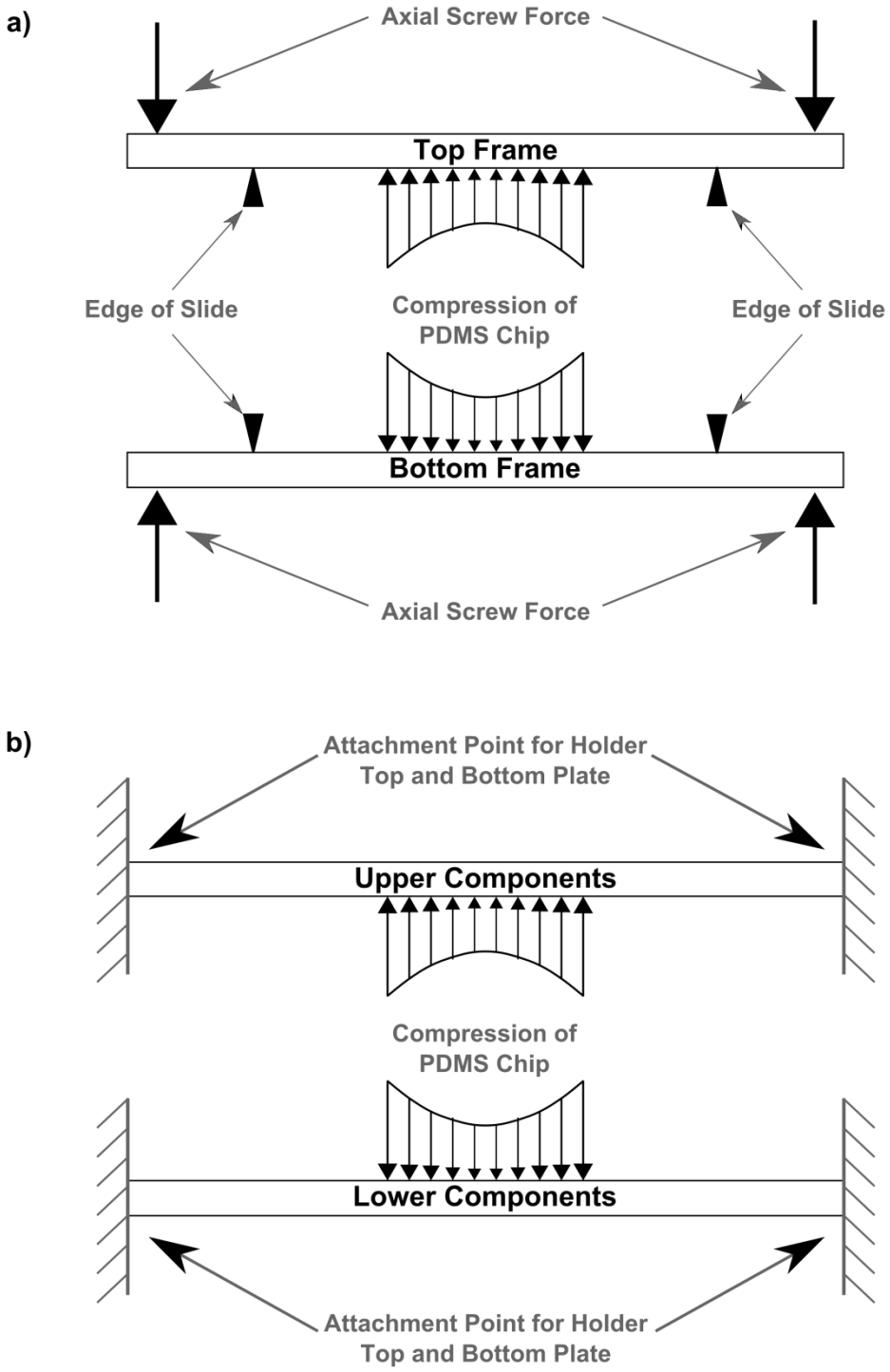

Figure 3.2 - Beam approximations of device components for bending calculations.

To approximate the bending of device components they were treated as beams. For the prototype device the components are approximated as beams bent about pivots at the edge of the slide by axial screw force and the PDMS chip's resistance to compression [a]. For the new device design the components are approximated as beams fixed at both ends but deformed by the PDMS chip's resistance to compression [b]. The resistance to compression reduces towards the centre of the beam where bending reduces the compressive strain.

The Conjugate Beam Method was applied to calculate the angle and displacement of the components above and below the PDMS chip. Displacement was calculated at 50 µm intervals across the width of the device using Microsoft Excel. The prototype device was modelled as beams supported by two pivots at the edges of the slide (Figure 3.2[a]). Screw torques as low as 0.4 N.cm provide enough force that the top frame contacts and pivots about the slide edges. One section of the new design was modelled as beams fixed at both ends (Figure 3.2[b]). The elastic moduli used for Aluminium, Polycarbonate, TC-PS, and PDMS were 7×10^{10} Pa, 2.3×10^{9} Pa, 3.0×10^{9} Pa, and 1.82×10^{6} Pa (Schneider et al., 2008) respectively. The resultant force from compression of the PDMS chip was integrated numerically using the rectangle rule with a step distance of 50 µm. The axial force delivered by a screw was calculated using equation 3.3;

$$F = \frac{2\tau}{p/\pi - \mu \cdot d} \qquad (3.3)$$

where F is the axial force, τ is the torque, p is the thread pitch (5×10^{-4} m), μ is the friction factor (assumed 0.5), and d is the pitch diameter (2.675×10^{-3} m).

3.2.4 Burst Pressure Measurements

Burst pressure of the new device was measured in the same manner as for the prototype device in section 2.2.2. Briefly, a 10 ml glass syringe (81660, Essex Scientific Laboratory Supplies, Benfleet, UK) connected to a syringe pump was used to pump air into a device at 7 $ml.min^{-1}$. The outlet to the device was blocked ¼-28 plug fitting. The pressure was measured by a sensor connected to a three way junction on the inlet tubing. The highest recorded pressure was taken as the burst pressure. The burst pressure was recorded three times for each of three unique sets of parts assembled in the three slots of the new device holder (total of 9 measurements). All device components used in the measurements had been previously autoclaved.

3.2.5 Dissolved Oxygen

The distribution of dissolved oxygen (DO) was modelled in COMSOL by adding a transport of dilute species model to an existing fluid flow model. The new chip design with a tree-like structure of channels and perfusion barriers was used (Figure 3.3[d]). Cellular oxygen consumption was modelled as a constant flux through the culture surface. All other boundaries were set to zero flux. The parameters used for DO modelling are shown in Table 3.1. The diffusivity of oxygen in medium was set to 2×10^{-9} m^2s^{-1}. The incoming media had an oxygen concentration of 0.2 $mol.m^{-2}$, the air saturation concentration at 37°C and 1.05 atm.

Table 3.1 - Parameters used in dissolved oxygen modelling with gas permeable lid.

Parameter	Value/Formula	Units	Source
Solubility of O_2 in Media	9.04×10^{-7}	$mol.cm^{-3}.atm^{-1}$	(Nishikawa et al., 2008)
Diffusivity of O_2 in Media	2.00×10^{-5}	$cm^2.s^{-1}$	(Nishikawa et al., 2008)
Solubility of O_2 in PDMS	7.92×10^{-6}	$mol.cm^{-3}.atm^{-1}$	(Merkel et al., 2000)
Diffusivity of O_2 in PDMS	3.40×10^{-5}	$cm^2.s^{-1}$	(Merkel et al., 2000)
Maximum O_2 Consumption During Growth Phase	2.80×10^{-17}	$mol.cell^{-1}$	Mouse ESCs at 20% and 40% O2, (Powers et al., 2008)
Minimum Cell Density	5.00×10^{4}	$cells.cm^{-2}$	Typical Seeding Density (mESC)
Confluent Cell Density	8.00×10^{5}	$cells.cm^{-2}$	Typical Confluent Density (mESC)

The distribution of dissolved oxygen was modelled for the prototype (all polycarbonate) lid design as well as for the new gas-permeable lid system with both open and closed polycarbonate elements (Figure 3.13). To model the gas-permeable lid system a 4.12 mm layer of PDMS was added above the culture chamber with a swept mesh. As there is no facility in the software to allow for the different solubility of oxygen in PDMS the concentration and diffusivity values were adjusted. The diffusivity of oxygen in PDMS was set to 3.02×10^{-8} m^2s^{-1}; the diffusivity in PDMS adjusted by the ratio of solubility in PDMS to solubility in medium (Table 3.1). When modelling the gas-permeable lid system with a closed PC element, no flux was allowed through the upper surface of the

PDMS. When modelling the gas-permeable lid system with an open PC element, the upper surface of the PDMS layer was given a constant defined DO of 0.2 $mol.m^{-2}$; the solubility in medium in equilibrium with air at 1.05 atm and 37°C.

The model was solved with a segregated solver with both segregations using COMSOL's GMRES iterative solver. The model was solved for two oxygen uptake rates; 1.40×10^{-8} and 2.24×10^{-7} $mol.m^{-2}s^{-1}$. These rates reflect a low and high confluency of mouse ESCs respectively. As an additional model, the low oxygen uptake rate was modelled with the concentration at the top surface of the PDMS set to 0.19 $mol.m^{-2}$; the air saturation concentration of medium at atmospheric pressure. Mean DO at the culture surface was calculated from a uniform grid of points with a step size of 10 μm.

3.3 Results and Discussion

3.3.1 PDMS Chip Design and Flow Modelling

As discussed in sections 2.3.1 and 2.3.2, the final prototype chip of Marcel Reichen (2012) was designed with the inlet and outlet channels expanding to three channels to distribute the flow (Figure 3.3[a]). Immediately either side of the culture chamber are perfusion barriers intended to deliver a highly uniform fluid velocity across the culture chamber. This concept relies on the fluid resistance of the channels between the barriers being significantly higher than the fluid resistance in the larger channels. However, where this concept has been previously employed the channels between the barriers are substantially less deep than the main channels (Petronis et al., 2006, Hung et al., 2005). Furthermore, fluid dynamic modelling of the prototype chip suggests the perfusion barriers may decrease flow uniformity (Section 2.3.2).

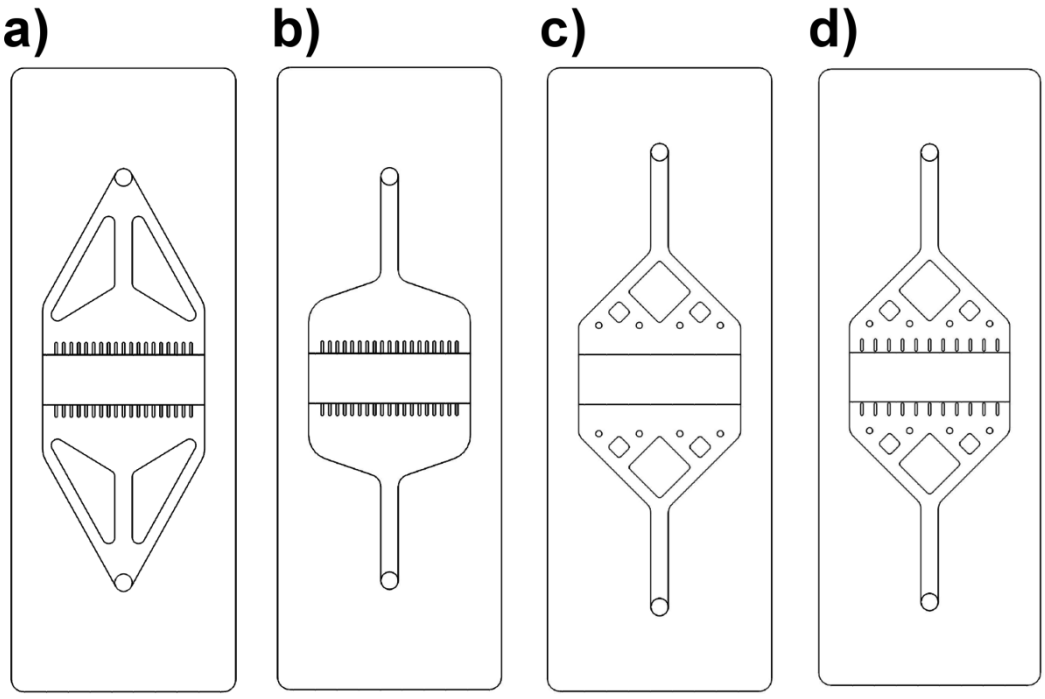

Figure 3.3 - Four chip designs investigated for flow distribution.

Four different designs of PDMS chip were investigated using COMSOL modelling; the design from Marcel Reichen's prototype device [a], Marcel Reichen's penultimate design [b], and a new design with a tree-like network of channels with [c] and without [d] perfusion barriers.

To investigate the effectiveness of the perfusion barriers and alternative methods of flow distribution, fluid flow was modelled in three further chip designs. The first was the penultimate design of Marcel Reichen (2012). This

design does not use multiple channels to distribute flow but does employ perfusion barriers (Figure 3.3[b]). The other two designs were new and based on a tetrahedral tree-like structure of channels (Figure 3.3[c,d]) (Saias et al., 2011). The tree-like structure expands from a single channel to eight evenly spaced channels. The path from the inlet to the end of each of the eight channels is equal in length and should thus have equal flow resistance. The difference between the two designs is the inclusion or exclusion of perfusion barriers. Where the barriers are included a larger gap is no longer included between the chamber wall and outermost barrier. The barriers remain 200 μm across but the gap between them increases from 400 μm to 900 μm.

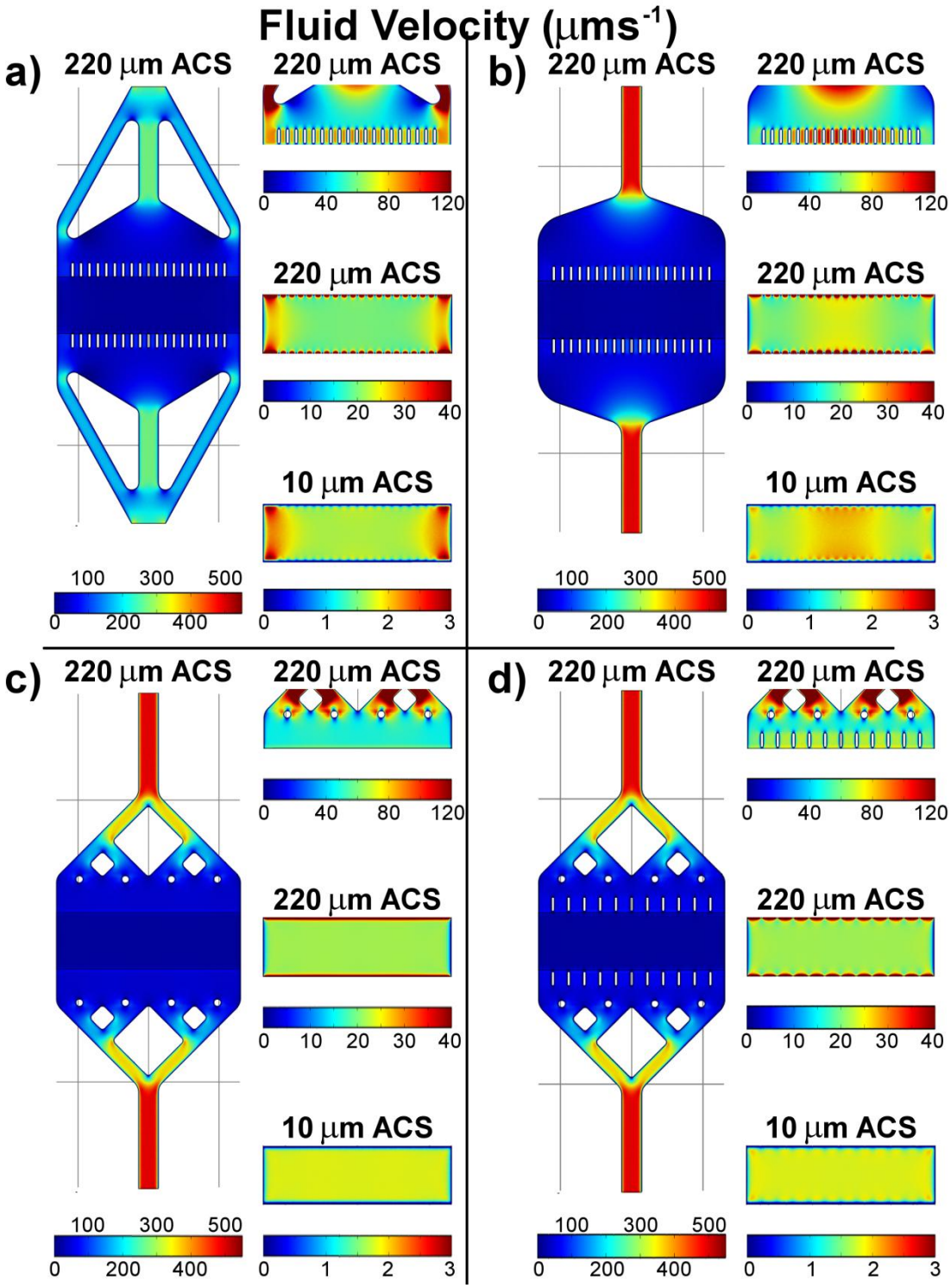

Figure -3.4 – Finite element modelling of fluid velocity for four designs of PDMS chip.

The results of COMSOL modelling showing fluid velocity for a flow rate of 300 μl.h^{-1}. Four designs were modelled; Marcel Reichen's prototype design [a] and penultimate design [b], and new designs with tree-like networks of channels with [d] and without [c] perfusion barriers. For each design the velocity profile of the whole ship is shown 220 μm above the culture surface (ACS). Also shown is the region prior to the chamber with a narrower colour scale, the culture chamber with a narrower colour scale, and the culture chamber 10 μm ACS.

Figure 3.4 shows the velocity distribution in the four different chip designs. It is clear from Figure 3.4[b] that, where the flow is not expanded by channels, the

perfusion barriers are ineffective at eliminating non uniform flow. Evidently the resistance of the channels between the gaps is not sufficiently greater than the resistance in the main channel. This could be addressed by reducing the width and height of the channels between the barriers. However, this would significantly increase the flow resistance of the device. A high flow resistance is not desirable as it necessitates a higher burst pressure. Also, if the chip has a higher flow resistance it is harder to ensure equal flow between parallel devices (see section 3.3.7). Therefore it is desirable to achieve uniform flow through the method of expansion so that the intended effect of the perfusion barriers is not needed.

Figure 3.4[c] and 3.4[d] show that with a tree-like structure of channels perfusion barriers are unnecessary and, in-fact, reduce the uniformity of flow. High velocities in the centre of the gaps and dead zones behind the barriers result in less uniform fluid velocities at the edges of the culture chamber. Comparing the regions prior to the culture chamber, it is also evident that the tree-like channel structure is more effective at distributing flow than Reichen's designs. This demonstrates the effectiveness of the tree-like structure's multiple paths with equal path length. The mean shear stresses 10 μm above the culture plane are within 2.4% of each other, being 0.131 mPa, 0.131 mPa, 0.128 mPa, and 0.128 mPa for the four designs respectively.

In theory, the tree-like chip design without perfusion barriers gives the most uniform flow distribution. However, in practice PDMS chips without perfusion barriers are less effective. Without the support of perfusion barriers the thin, elastomeric spacer layer and, to a lesser extent, the channel containing layer deform towards each other. This results in the majority of flow being directed along the edges of the culture chamber. Hence, the perfusion barriers play a vital structural role in PDMS chips. Accordingly, the tree-like structure with perfusion barriers was adopted as the new chip design. The inlet and outlet were also moved further apart to allow more space between the interconnect bars. The thickness of the top layer of the chip was increased from 0.95 mm, to 1 mm to increase compressive force relative to channel deformation, and the overall chip length was kept the same.

3.3.2 Bending Analysis of Prototype Device

Burst pressure analysis of the prototype stem cell culture device showed significant variation between different assemblies of the same parts (section 2.3.2). There was also a high failure rate in the attempted perfusion culture experiments due to leaking (section 2.3.7). Clearly, this needs to be addressed before the culture device can be considered a useful tool for stem cell process design. Low variation between multiple measurements of the same assembly indicates that the variability originates from a reversible compression seal. Furthermore, similar measurements of burst pressure after lid removal and reinsertion show that the seal in question is unlikely to be between the PDMS gasket and polycarbonate lid. Variation of a compression seal is likely correlated with variation in the extent of compression. If the PDMS chip undergoes variable compression this is likely to translate into variations in flow distribution and flow resistance.

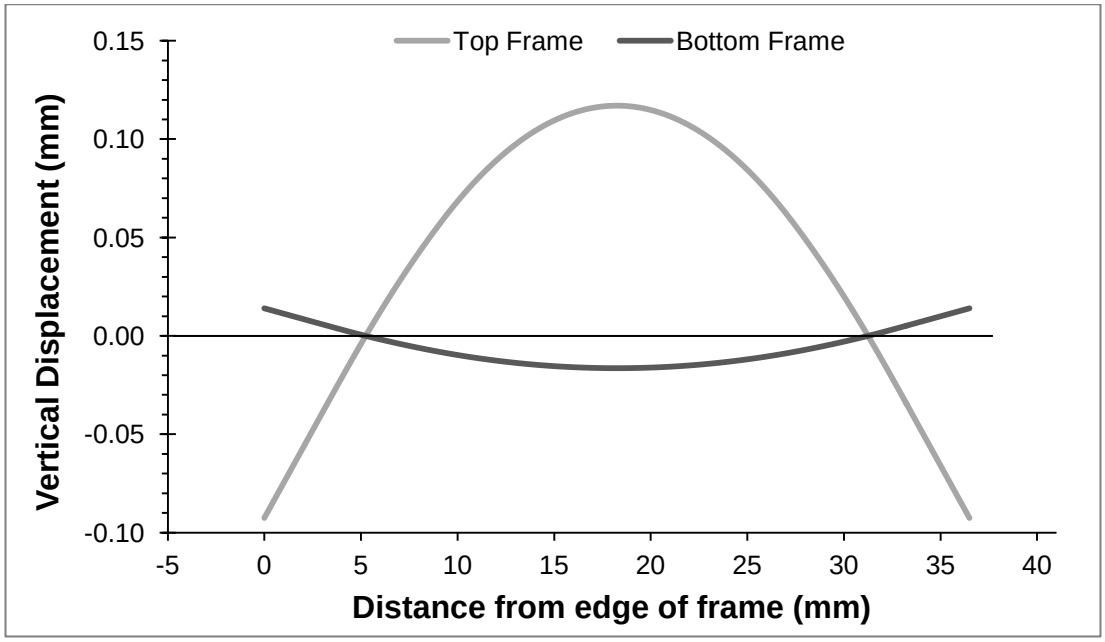

Figure 3.5 - Displacement of top and bottom frames of prototype device through bending.

Axial screw force causes the top and bottom frames of the prototype device to bend about two pivots at the edges of the TC-PS slide. Here the displacement is approximated by the conjugate beam method for an applied screw torque of 2 N.cm. The displacement of the two components is relative to zero at the two points where the top frame contacts the edge of the slide.

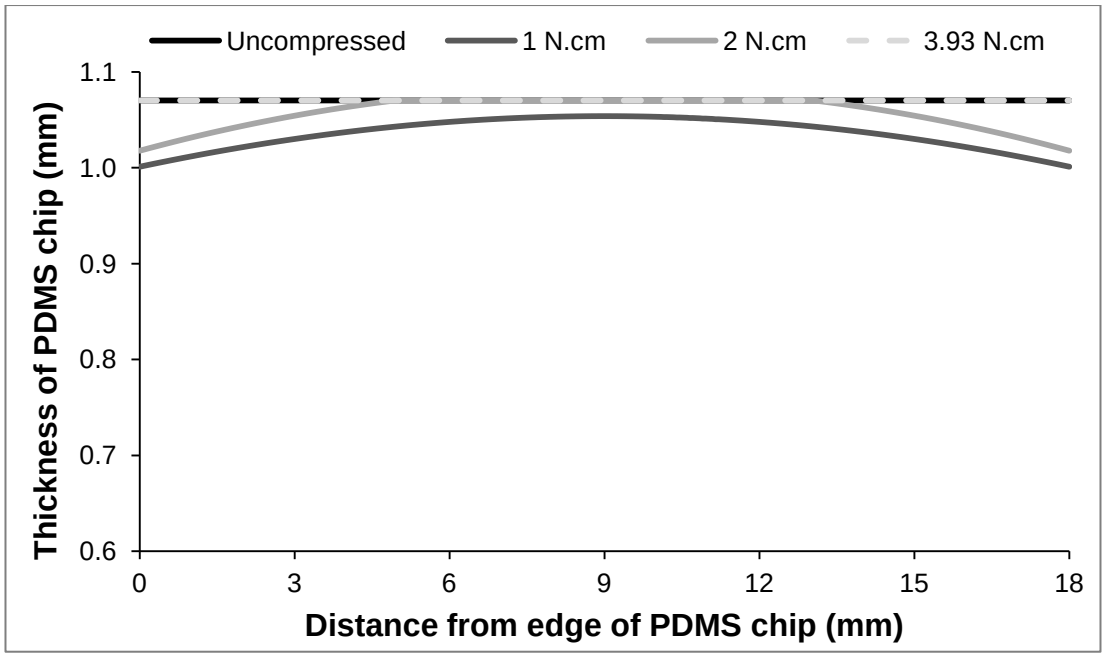

Figures 3.6 - Thickness of PDMS chip compressed by prototype frames at different screw torques.

Axial screw force causes the top and bottom frames of the prototype device to bend. The resulting displacement affects the compression of the PDMS chip. This figure approximates the thickness of the PDMS chip for different applied screw torques (and hence axial screw force). The model assumes compressive force is directly proportional to vertical strain.

A simplified model was used to investigate the bending and compression achieved in the prototype culture device. The approximate bending of the rigid slide and frames were calculated using the Conjugate Beam Method. In order to investigate sensitivity to axial screw force, the bending of the frames was calculated at three different screw torques. The model assumes an arbitrary coefficient of friction for the screws of 0.5 though this varies depending on thread materials, cleanliness, and quality. The model also assumes the device is in the closed configuration i.e. the screws attaching the lid have been inserted and tightened. Figure 3.5 shows the bending profiles across the width of the top and bottom fames with 2 N.cm of screw torque. Figure 3.6 shows the profile of the compressed PDMS chip at all three torques investigated.

It is evident that there is a trade off between the compressive force at the edges and the middle of the chip. There will therefore be an optimum where the best profile of compressive force is achieved. However, small increases in axial screw force bend the frame to the extent that there is a gap rather than compression along the centreline of the chip (see Torque = 2 N.cm, Figure 3.6).

This gap will result in leaking. At higher forces the frames will bend to the extent that the PDMS chip is not compressed at all (see Torque = 3.93 N.cm, Figure 3.6). Conversely, lower axial forces will result in the minimum bending of the frames and the most uniform compression of the chip. The price of this uniform compression is that the compressive force will be very low. This may also result in leaking. In addition, it is difficult to deliver very low axial screw force and small thread or material imperfections will have a very significant impact in relative to such low forces.

Between these two extremes of axial force the varying compression profile will result in varying burst pressure as encountered in the investigations in the previous chapter (section 2.3.2). The uneven compression profile will also result in a non-uniform profile through the culture chamber contra to the efforts made designing the PDMS chip. Attempts are made to always deliver the same axial screw force by using a high precision torque screw-driver. However, as mentioned above, axial force does not only depend on torque but is also sensitive to the thread materials, quality and cleanliness. Small imperfections or contaminating material can significantly impact the axial force delivered. Furthermore, the total axial force depends on whether the device is in the closed configuration (10 screws) or open configuration (8 screws).

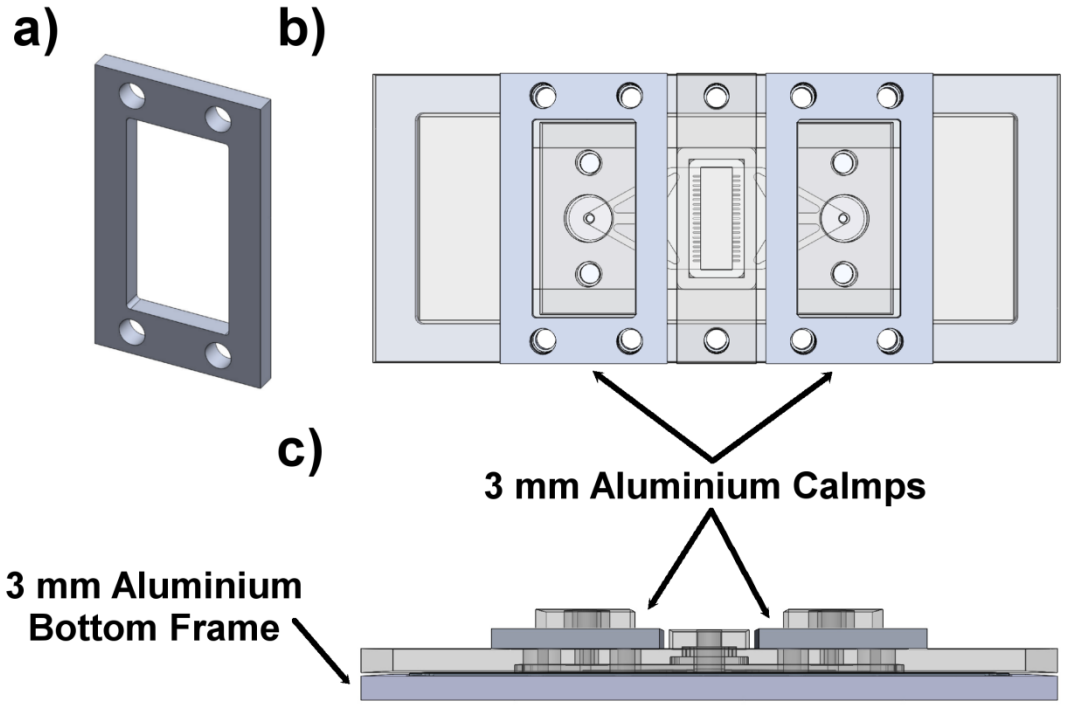

Figure 3.7 - Interim strengthening of prototype frame.
As an interim solution to strengthen the prototype frame, 3 mm aluminium clamps [a] were added above the top frame and surrounding the interconnect bars [b, c]. The bottom fame was also changed from 5 mm polycarbonate to 3 mm aluminium [c].

A clamping solution should be sought that delivers a reliable profile of compressive force impartial to small variations in screw torque, thread quality and thread sensitivity. The profile of compressive force should also be uniform in order to maintain a uniform flow profile. This was addressed in the next section (section 3.3.3). As an interim solution a device was trialled with reinforced frames. The bottom frame was changed from 5 mm polycarbonate to 3 mm aluminium. The top frame was supported by two rectangular clamps made from 3 mm aluminium (Figure 3.7). Observations suggested this reinforced device was less prone to leaking. This supports the hypothesis that frame bending is responsible for the high failure rate of the prototype device.

3.3.3 Improved Design of Culture Device

As discussed above, to achieve robust compressive seals, a clamping solution is required that delivers a reliable and uniform profile of compressive force to the PDMS chip. The solution should not be sensitive to small variations in screw torque, thread quality and thread sensitivity. In addition, the device needs to be

made easier to assemble and use in a sterile environment. Moreover, the reusable components of the device, including the interconnect bars, should be made more robust. Finally, to improve the monitoring capabilities of the prototype system we integrated it with a motorised microscope stage. To this end, it should be possible to position the culture chambers of the maximum number of devices within the area of a motorised stage that can be imaged.

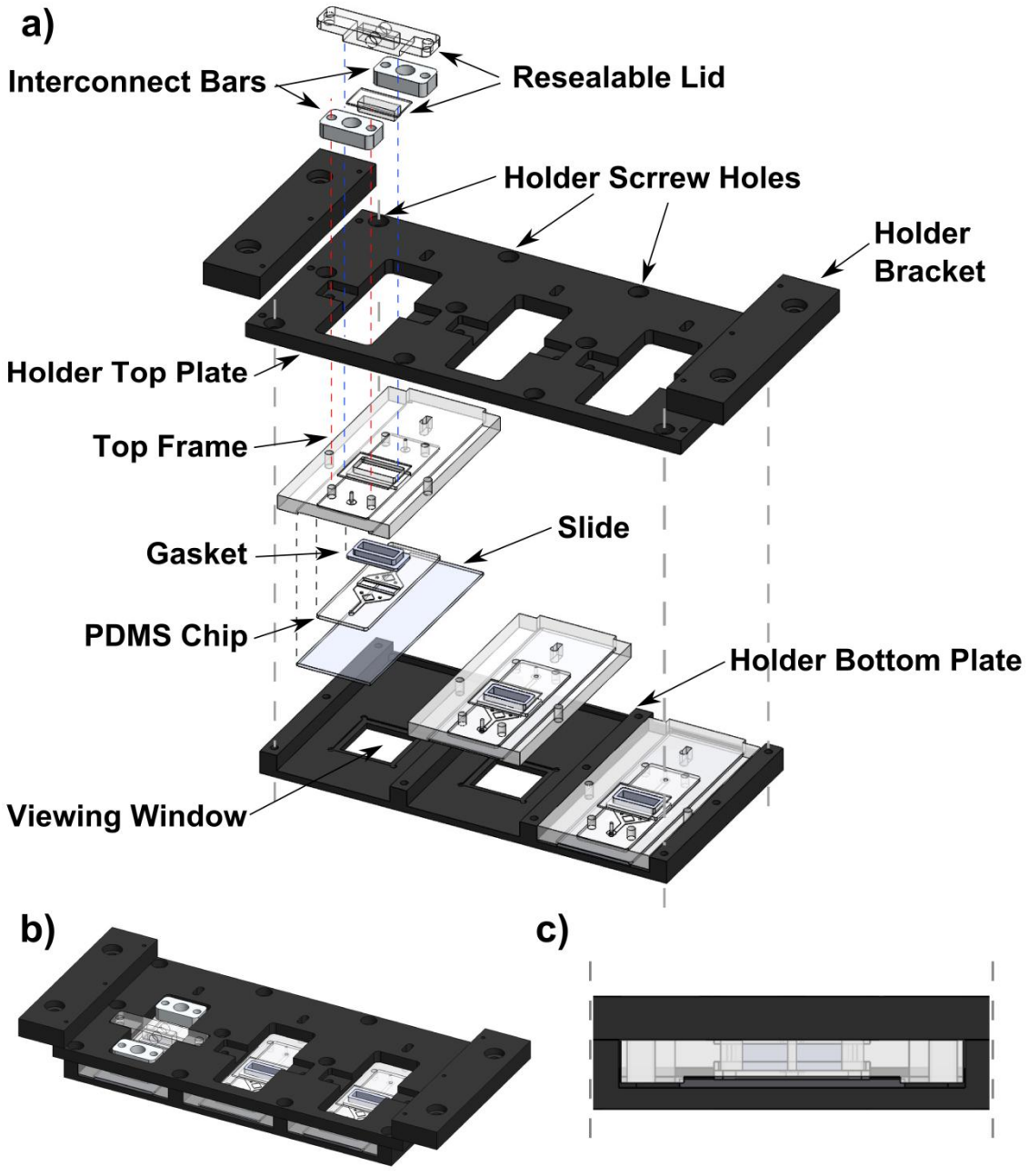

Figure 3.8 - Improved culture device design.
An exploded view [a] of the new culture device design showing the components of the holder and individual culture devices (screws are not included). Also shown is an assembled view [b] with the lid and interconnects included only for the left most culture device. A front view of the central compartment [c] shows the top frame, flat against the top plate of the holder, and the slide, flat against the bottom plate of the holder, with the PDMS chip compressed between them.

An improved culture device was designed and fabricated to address all the above concerns (Figure 3.8). Up to three individual culture devices are housed in a holder comprised of a top plate, a bottom plate and two brackets. The top and bottom plates are connected by four rows of three screws. Individual bottom frames have been eliminated and microscope slides are now recessed into the top frames which have been thickened to 5 mm. An assembly of top frame, gasket, chip and slide is inserted into each of the three slots in the holder with the screws loosened. The screws are then tightened to a high torque (as high as possible by hand) using a standard hex screwdriver.

Compression of the PDMS chips is delivered by the top and bottom plates of the holder. As the screws are tightened to a high torque the height of the slots is defined as the depth to which they were milled. The top and bottom plates are made from anodised aluminium with the intention that they not bend significantly in response to the compressive force. This is investigated in the following section (section 3.3.4). The strength and corrosion resistance of anodised aluminium also make the parts more robust than if they were made from polycarbonate. Similarly, the holder brackets and interconnect bars are robust due to the choice of materials (anodised aluminium and 6 mm grade 6082 aluminium respectively). The thickness of aluminium below each device was originally 0.7 mm to allow close proximity of microscope objectives. However, the aluminium distorted during tooling and the finished piece was too flexible. The use of extra long working distance objectives permitted the thickness of the component to be increased to 2.45 mm.

The holder and devices were designed so that six culture chambers (2 holders each with 3 devices) could be imaged on a Nikon Ti-E motorised microscope. The dimensions of a holder bottom frame are 144 mm by 78 mm such that two can fit in the opening of the motorised stage (115 mm by 157 mm). The brackets suspend the holders from a 5 mm PC sheet laid on top of the stage. Positioning the devices below the top of the stage moves them into the focusable range of the microscope as specimens are typically positioned slightly

inset to the stage rather than elevated (by the holder bottom) above it. To conform to the holder dimensions the top frame was shortened to be the same length as the slide (77 mm). The top frame was also widened to 40 mm for easier handling as it is not possible to narrow them enough to fit four devices side by side within the area that can be imaged. Finally, the chip and gasket recesses and hole for lid insertion were offset from the centre of the top frame so that the culture chambers would be within the area that can be imaged by the microscope.

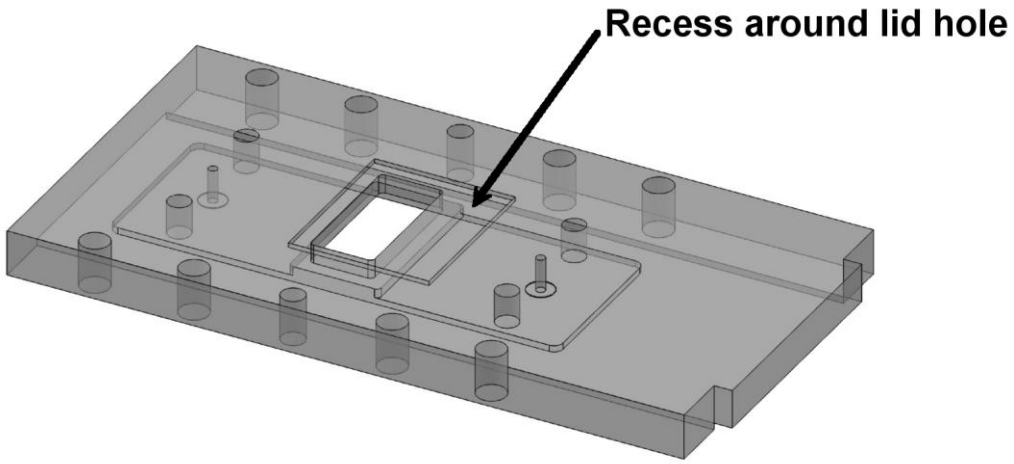

Figure 3.9 - Top frame showing the recess around the lid hole.

An image showing the 0.5 mm deep recess around the hole into which the resealable lid is inserted. The recess is included to contain medium displaced by insertion of the lid.

The culture device is now significantly easier to assemble and use: The number of screws that must be done up to seal three devices has been reduced from 24 to 12. Furthermore, these screws can be left in position, and must merely be tightened and loosened. Also the screws do not need to be tightened to a precise and low torque but can simply be tightened as much as possible using a standard hex-head torque screwdriver. Furthermore, the elimination of the bottom frame reduces the number of parts per device. A shallow recess has been added to the top of the top frame surrounding the lid hole (Figure 3.9). This recess is designed to contain media overflowing from the culture chamber limiting the area that it can contact and making it easier to aspirate. Finally, there is a recess around the viewing windows in the bottom plate of the holder.

These windows were included to give the option of inserting a cover slip to improve the thermal insulation of the culture chambers.

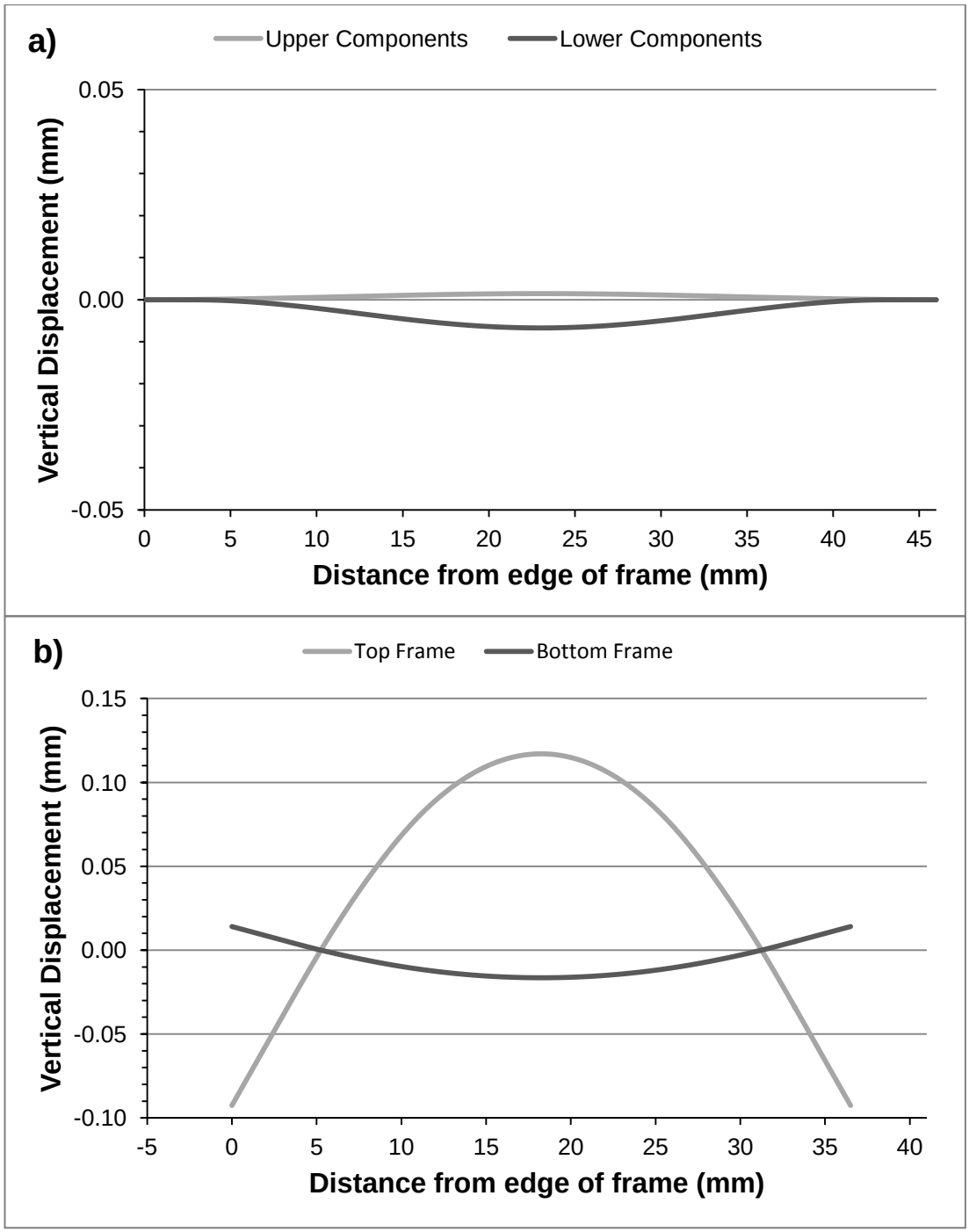

Figure 3.10 - Displacement of components due to bending in the new device design compared to the prototype design.

In the new device design, compressive force causes the upper (top plate and top frame) and lower (bottom plate and slide) components of the prototype device to bend apart between fixed points.

These fixed points occur where the top and bottom plates of the holder are screwed together. Here the displacement of these components across one slot in the new device is approximated by the conjugate beam method [a]. The displacement is set to zero at the fixed points on either side. For comparison the displacement of the prototype device is shown [b] for an applied screw torque of 2 N.cm, as calculated in reported in section 3.3.2.

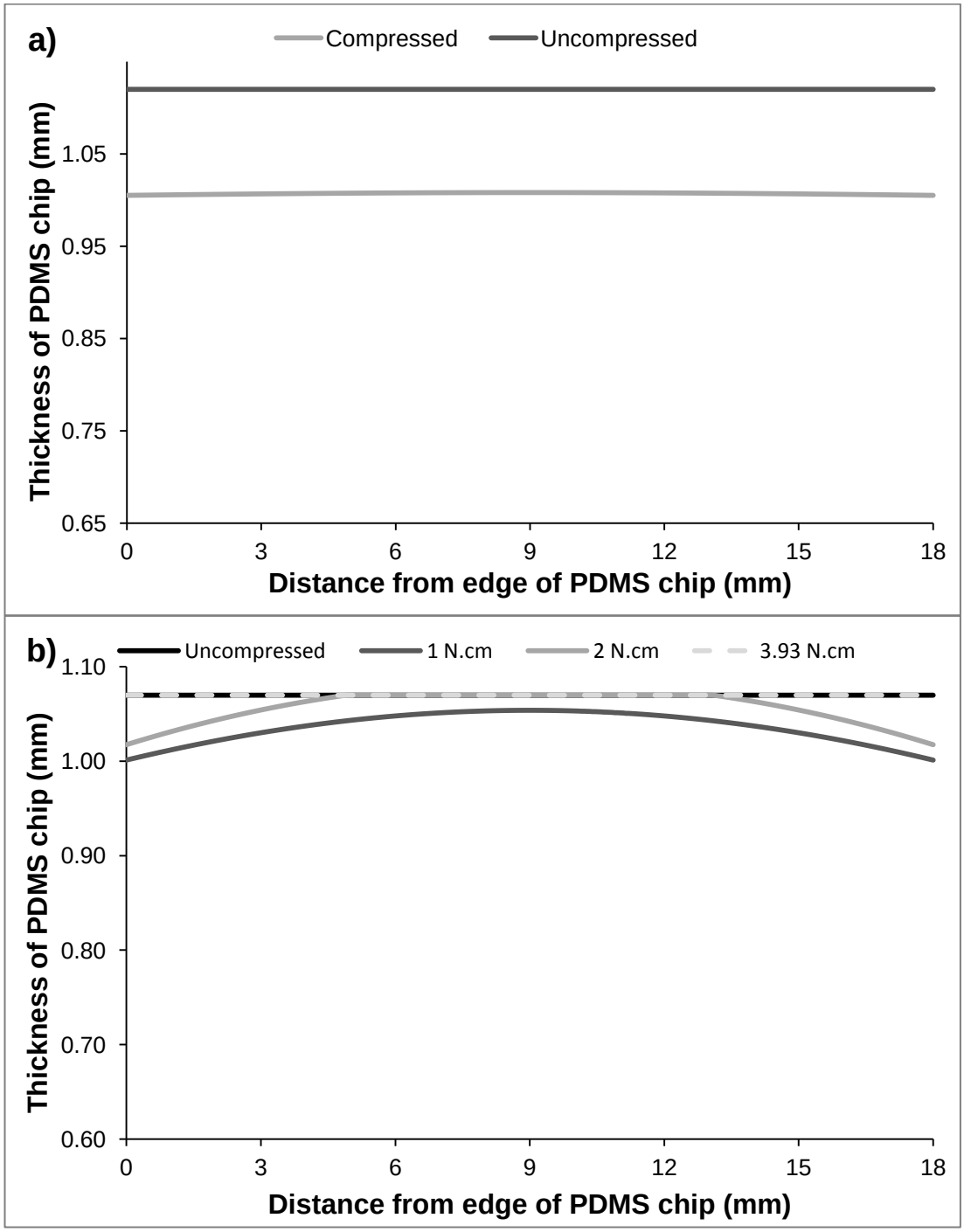

Figure 3.11 - Compression across the width of the PDMS chip for the new device design and the prototype design.

In the new and prototype culture devices the PDMS chip is compressed between the top frame and slide. The bending of components due to vertical forces affects the compression of the PDMS chip. This figure approximates the thickness of the PDMS chip in the new device [a] and in the prototype device for different applied screw torques [b].

3.3.4 Bending Analysis of New Devices

The bending of top and bottom plates of the new chip holder were modelled in the same manner as for the prototype design (section 3.3.2) and the results compared. Figure 3.10 compares the bending of the components on either side of the PDMS chip. It is evident that significantly less bending occurs with the new holder system than with the prototype design. Figure 3.11 compares the compression profiles of the PDMS chips. The maximum combined displacement of the upper and lower components in the new device design is 8.2 μm. This compares with 130 μm for the prototype device design with an applied torque of 2 N.cm. As a result of the lower deformation and thicker PDMS chip, the minimum compressive strain is 9.98% (112 μm of compression) in the new device. There was no compression predicted at the centre of the prototype design but instead 13.4 μm of additional space.

The compression profile delivered by the new device holder is also highly uniform. Compressive strain ranges from 9.98% (112 μm of compression) to 10.27% (115 μm of compression) rather than the 0% to 4.9% (52 μm of compression) achieved in the prototype device. The level of compression can also be specified by the thickness of the parts i.e. reducing the recess depths in the top frame will increase compression. Furthermore, the model indicates the minimum screw torque required to achieve this compression is 1.48 N.cm (assuming a coefficient of friction of 0.5), while a manual screwdriver can easily achieve hundreds of N.cm. Therefore, the new design delivers the required reliable and uniform compression with low sensitivity to minor variations in screw torque or friction factor.

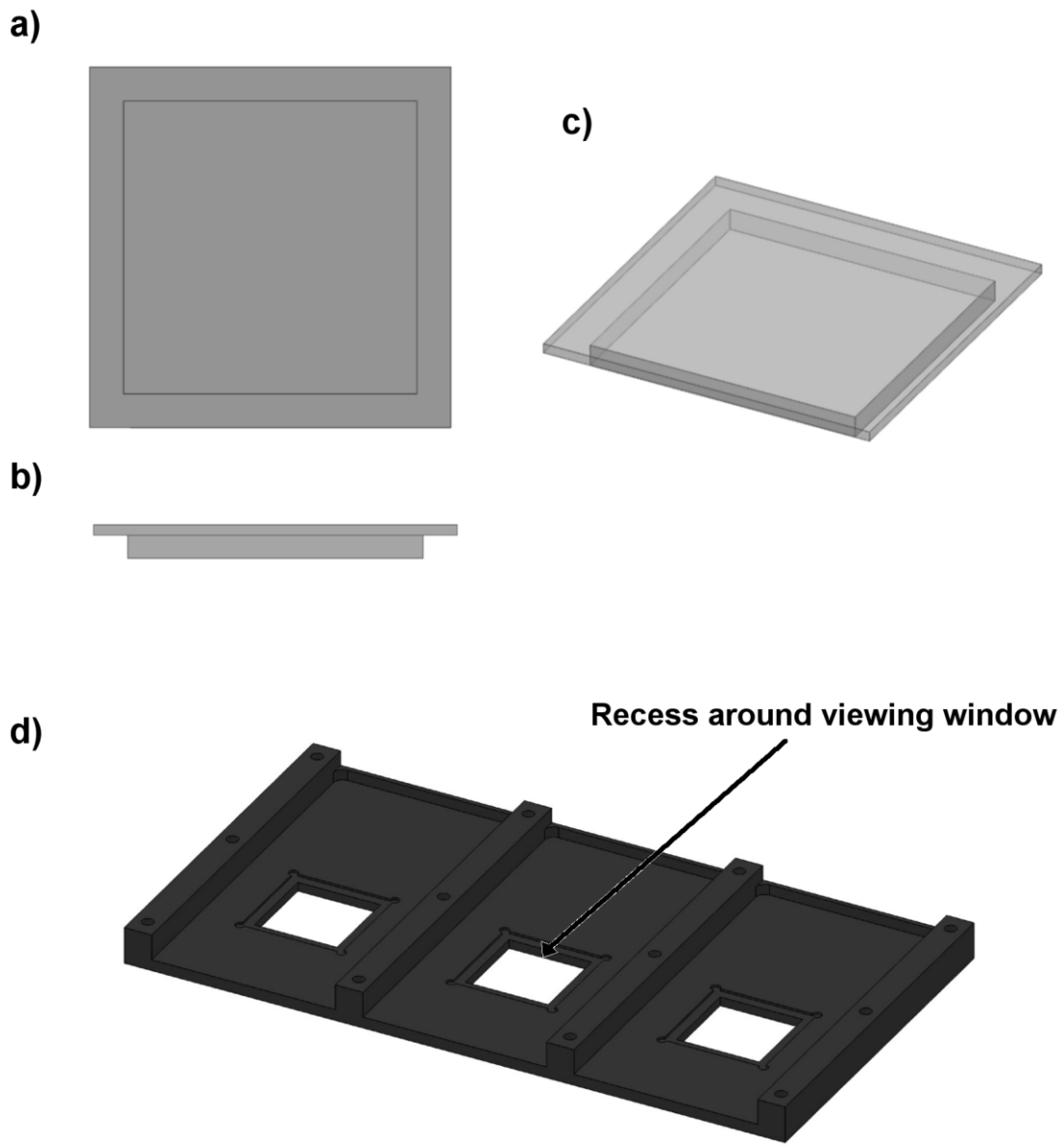

Figure 3.12 - Figure showing 'window filler' and the recess into which it sits.

Top [a], side [b], and 3D [c] views of the polycarbonate window filler which is inserted into the viewing window and surrounding recess [d].

3.3.5 Burst Pressure Measurements of New Devices

The new device design was tested with pumped water to verify that the rigidity of the new holder has a positive effect on sealing. Initial investigations found that the new device regularly leaked from between the top frame and TC-PS slide. It was hypothesised that the portion of slide above the viewing window was bending resulting in leaking around the culture chamber. To reinforce this area a piece of polycarbonate was inserted in the viewing window, suspended from the recess surrounding it (Figure 3.12). The polycarbonate is 2 mm thick and protrudes 125 µm above the top surface of the bottom plate to increase compression around the culture chamber. With this addition leaking was no longer observed. Polycarbonate was used as it is transparent to visible light, tolerant of autoclave, and easy to mill. However, polycarbonate is not transparent to the UV light used with some fluorescent stains so glass may be a more appropriate choice in future work.

With the polycarbonate piece in place, burst pressure measurements were carried out as for the prototype device (section 2.3.1). The mean burst pressure of the new device is 370 ± 120 kPa (standard deviation n=9), a significant increase compared with the 59 ± 18 kPa of Marcel Reichen's prototype design. The standard deviation has also increased significantly though it remains a similar fraction of the mean. Two standard deviations below the mean (370-2×120 = 130 kPa), the burst pressure still remains well in excess of the previous mean. Furthermore, the lowest burst pressure recorded with the new design was 250 kPa. These results confirm that the manner in which compression is delivered by the new design has significantly improved the robustness of the culture devices. The increased burst pressure permits the application of higher back pressures with reduced risk of leaks occurring. This is important for the redesigning of the external fluidics (see section 3.3.7).

When the burst pressure is exceeded, loss of pressure occurs by reversible failure of a compression seal rather than permanent damage to a component. This is evidenced by repeatability of the burst pressure with the same parts. The mean standard deviation with the same assembly of parts is 10 kPa (standard

deviation of 3 measurements, mean for 3 assemblies). Consequently, it is not possible to damage reusable parts by exceeding the burst pressure. The high variation in the burst pressure measurements remains linked to variation in one or more of the reversible seals; between chip and slide, chip and top frame, top frame and fluidic connector, chip and gasket, and/or gasket and lid. In turn, this variation could stem from variation in assembly technique or variation in manufactured parts. The new design should prevent assembly technique affecting seals involving the PDMS chip. However, there is still potential for variation in the force applied when attaching the lid and fluidic connectors. Parts will remain subject to significant manufacturing variation as long as they are manufactured individually and can only be minimized by the care and precision of the manufacturer. Upon achieving fine manufacturing tolerances this design is likely to achieve very well defined burst pressures with small standard deviations.

3.3.6 A Gas Permeable Lid System

Design of Lid System

Modelling of dissolved oxygen (DO) in the prototype device under perfusion conditions showed that significant gradients in pericellular DO would be expected at oxygen uptake rates (OURs) corresponding to high cell confluency (Figure 2.7). In a static device with the medium volume of a closed culture chamber but without the gas impermeable polycarbonate lid, pericellular DO is uniform and much higher than in typical flask or well culture (Figure 2.6). This is due to the shorter distance that oxygen must diffuse through medium from the gas medium interface. However, when the lid is inserted oxygen can only be supplied with the incoming medium. In addition to causing gradients at high confluency, this limitation also makes dissolved oxygen highly dependent on medium flow rate. DO gradients and a dependence on flow rate are both detrimental to the control offered by the culture device.

Dissolved oxygen is key to cell growth as well as being a determining factor in stem cell fate. For a process development tool to test a single set of conditions, gradients in pericellular DO must be kept to a minimum. It is also important to

be able to control pericellular dissolved oxygen over time. With oxygen only supplied via incoming medium, control can only be achieved through adjustment of flow rate or the partial pressure of oxygen the incoming medium is exposed to. The extent to which the partial pressure of oxygen at the inlet can be adjusted is limited. If incoming medium is equilibrated with the atmosphere in an incubator (as in section 2.2.11) the total pressure is limited to atmospheric. Alternatively, if medium is equilibrated with gas in the inlet bottle (see section 3.3.7) the total pressure will impact the medium flow rate. Using medium flow rate to control pericellular DO is not ideal as flow rate also affects shear stress and the concentration of other soluble factors.

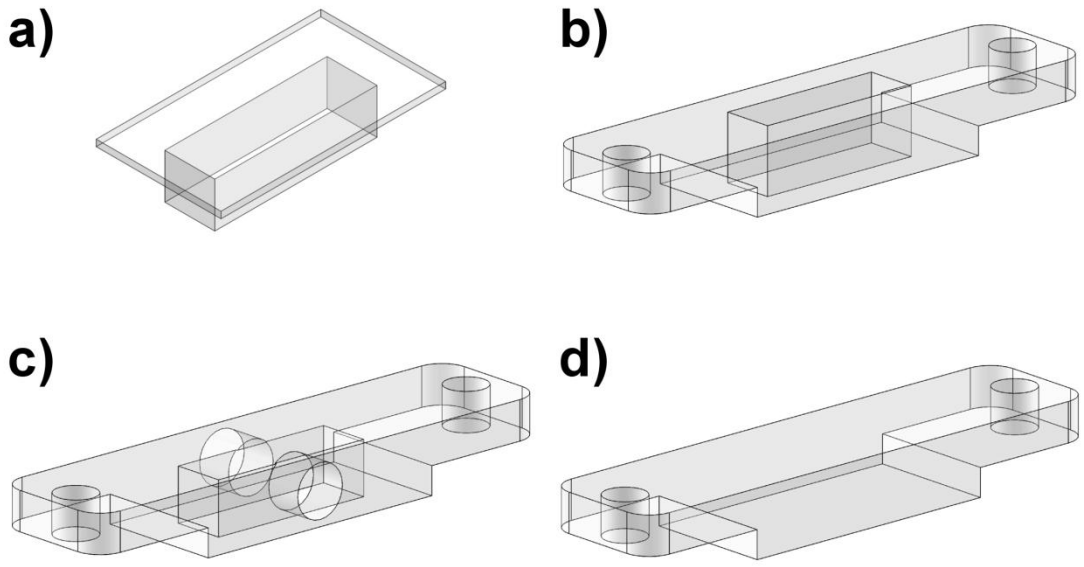

Figure 3.13 - Components of gas permeable resealable lid system.

The new gas permeable resealable lid system consists of two components. The first component is a PDMS piece inserted into the lid well [a]. This component is gas permeable and defines the height of the culture chamber. The second polycarbonate component secures the PDMS component in place and has three variations. The first is open to atmosphere for gas exchange [b], the second has a cavity above the culture chamber and ports to connect an external gas supply [c], and the third is solid polycarbonate to prevent gas exchange [d].

New gas permeable lids were designed to address these issues (Figure 3.13). A permeable PDMS component inserts through the gasket to seal the chamber (Figure 3.13[a]). As with the previous lid design, the PDMS component is T-shaped and defines the height of the culture chamber. The PDMS component is

held in place by a polycarbonate (PC) component. The PC component has a cavity with the same footprint as the culture chamber. The cavity can either go all the way through the part (Figure 3.13[b]), so that oxygen is supplied from the external atmosphere, or can be connected to a gas inlet and outlet (Figure 3.13[c]). There is also the option to retain a gas impermeable lid by removing the cavity all together (Figure 3.13[d]).

Gas permeable lids add a second route of oxygen supply. If this is the major source of dissolved oxygen then gradients will be greatly reduced as oxygen is supplied evenly across the culture area. Introducing oxygen through the lid also takes advantage of the short diffusion distance through medium in the microfabricated culture device. The PDMS lid adds a second diffusive resistance to oxygen transfer but PDMS has a much higher permeability than medium due to a similar diffusivity and much larger solubility (Table 3.1).

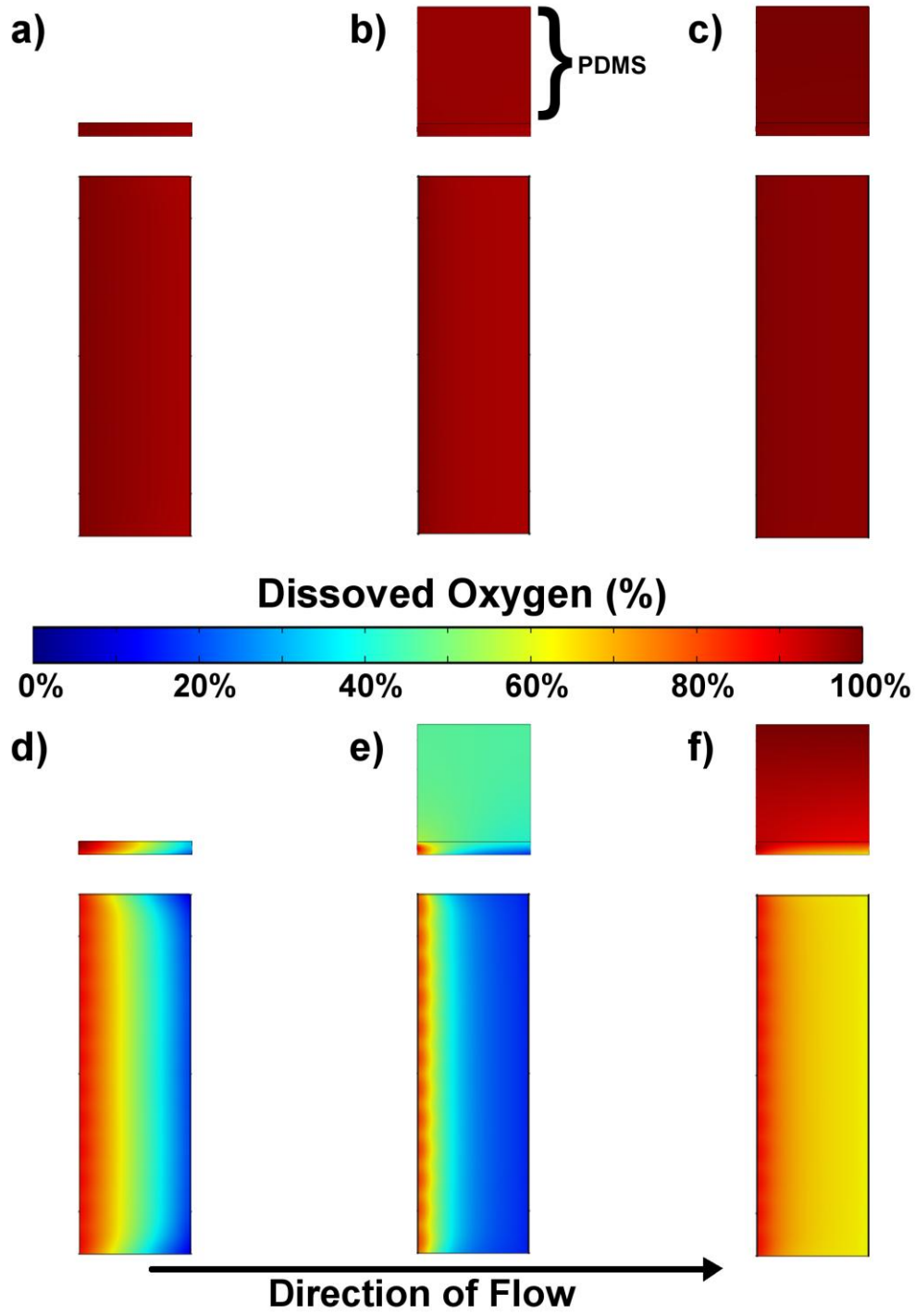

Figure 3.14 - Dissolved oxygen distribution at different oxygen uptake rates and with different lid systems.

Dissolved oxygen distribution is shown for two different oxygen uptake rates; 1.4×10^{-8} $mol.m^{-2}s^{-1}$ corresponding to cells at seeding [a-c], and 2.24×10^{-7} $mol.m^{-2}s^{-1}$ corresponding to cells at high confluency [d-f]. Three different lid systems are shown; [a, d] the entirely polycarbonate lid of Marcel Reichen's prototype device, and the new gas permeable lid system with [b, e] a closed polycarbonate component and [c, f] an open polycarbonate component. Shown for each combination are a vertical slice through the centreline of the culture chamber (top) and a horizontal slice at the culture surface (bottom). Dissolved oxygen is shown as percentage of saturation at 1.05 atm (21% 0_2).

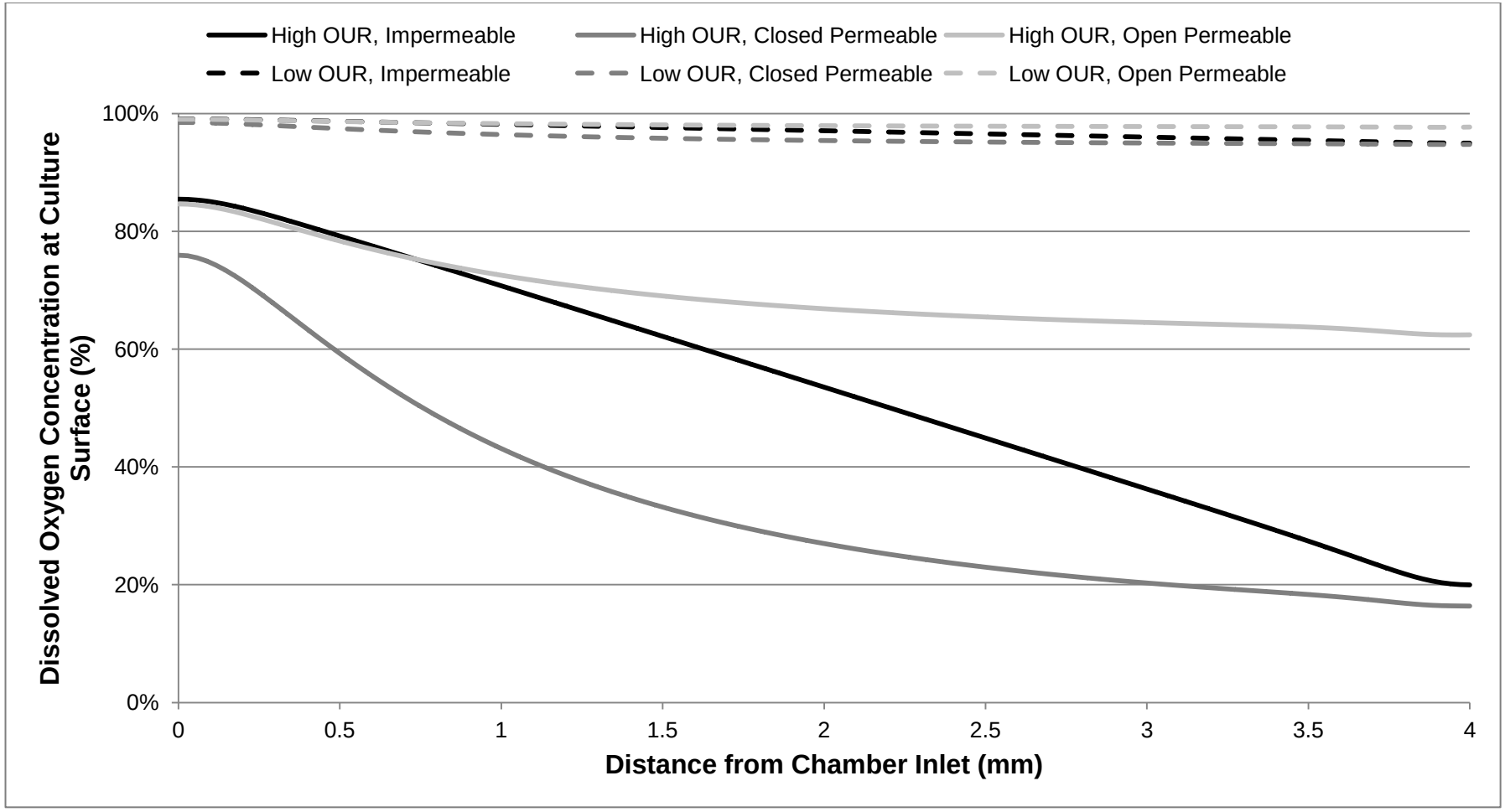

Figure 3.15 - Centreline dissolved oxygen at culture surface for different oxygen uptake rates and lid systems.

The dissolved oxygen concentration along a centreline of the culture chamber at the culture surface. Dissolved oxygen distribution is shown for two different oxygen uptake rates (OURs); 1.4×10^{-8} mol.m^{-2}s^{-1} corresponding to cells at seeding, and 2.24×10^{-7} mol.m^{-2}s^{-1} corresponding to cells at high confluency. Three different lid systems are shown; the impermeable entirely PC lid of Marcel Reichen's prototype device, and the new gas permeable lid system with a closed polycarbonate component and an open polycarbonate component. Dissolved oxygen is shown as percentage of saturation at 1.05 atm (21% 0_2).

Modelling of Dissolved Oxygen with Gas Permeable Lid

Modelling was used to investigate dissolved oxygen in microfabricated culture devices under different conditions. Devices were modelled with an entirely PC lid, as in Marcel Reichen's prototype design, and with the new gas permeable lid system using closed (Figure 3.13[d]) and open (Figure 3.13[b,c]) PC components. As in section 2.3.3 oxygen uptake rates (OURs) were chosen to represent the upper and lower limits of what would be expected during mESC culture; 1.40×10^{-8} $mol.m^{-2}s^{-1}$ to represent immediately after seeding and 2.24×10^{-7} $mol.m^{-2}s^{-1}$ to represent a highly confluent culture. The inlet DO was set to 0.20 mM, the saturation concentration at 1.05 atm (21% O_2 37°C), as positive pressure is required to pump the medium. The concentration at the top of the permeable lid was set also set to 0.2 mM at both OURs, as well as 0.19 mM at the higher OUR to investigate the effect lower pressure (1 atm) above the PDMS lid. The resulting distributions of DO are shown in Figures 3.14 and 3.15. Dissolved oxygen is shown as percentage of saturation at 1.05 atm (21% 0_2).

At both OURs the mean concentration and the uniformity of DO at the culture surface are lowest with an entirely PC lid (Figure 3.14 [a,d] & Figure 3.15) and highest with the gas permeable lid system using an open (Figure 3.13 [b or c]) PC component (Figure 3.14 [c,f] & Figure 3.15). The mean culture surface DOs at low and high OURs are 97% ± 1% and 53% ± 20% (± 1 standard deviation) respectively, for an entirely PC lid, and 98.1% ± 0.4% and 69% ± 6% respectively, for the gas permeable lid system with an open PC component. The mean DO is higher in the gas permeable lid system, as oxygen passes through the highly permeable PDMS to replace oxygen consumed from the medium by the cells. A gradient must exist as the driving force for this mass transfer. This gradient is higher at higher OURs resulting in lower mean DO concentrations in the medium.

With an entirely PC lid the only source of oxygen is the medium which, arriving from one side of the culture surface, causes a gradient across the length of the culture surface (Figure 3.15); the cells closest to the inlet experience a

pericellular DO near the concentration of the incoming medium but the pericellular DO then reduces along the length of the chamber as oxygen is consumed by the cells. The gas permeable lid system with an open PC component introduces oxygen from above the culture surface, reducing the gradient by replacing some of the consumed oxygen. Using the gas permeable lid system with an open PC component, pericellular DO reduces from near the inlet DO towards the pericellular DO achieved in static conditions (which can be calculated from Ficks Law; see below).

The gradient across the length of the chamber will be reduced further if the DO concentration in the incoming medium is reduced. The gradient will most rapidly reach the equilibrium that exists under static conditions if the DO concentration at the inlet is equal to the mean DO in the culture chamber under static conditions. Gradients will also reduce further as the medium flow rate is reduced and the lid becomes responsible for a greater portion of the supplied oxygen. At a flow rate of zero no gradient should exist across the length of the chamber and the DO across the whole culture surface can be calculated using Fick's law, as in chapter 2 (sections 2.2.4 and 2.3.3).

In a static system, at the same pressure used in the finite element models, a gas permeable lid system with an open PC component delivers culture surface DOs of 97% and 59% at the low and high OURs respectively. These correspond to the asymptotes on Figure 3.15. Due to its high permeability the PDMS is responsible for just 38% of the difference between the pericellular DO concentration and 100% DO concentration despite creating 90% of the diffusion distance. For the same reason, reductions in PDMS thickness have a less significant impact on culture surface DO than reductions in the medium height. For example, halving the thickness of the PDMS lid component only increases pericellular DO by 13% at the highest OUR.

When using the gas permeable lid system with a closed PC component (Figure 3.14[b,e] & Figure 3.15) the DO at the culture surface is more uniform and the mean value (96% ± 1% at low OUR and 34% ± 18% at high OUR) is lower than

the DO with an entirely PC lid (Figure 3.14[a,d] & Figure 3.15). While no oxygen is supplied through the PDMS lid, its high permeability facilitates more rapid transfer of oxygen along the length of the chip than the combination of medium flow and diffusion through the medium. At the inlet to the chamber the high DO of incoming medium drives oxygen into the PDMS reducing culture surface DO in that area relative to an entirely PC lid. The oxygen is then transported through the PDMS towards the chamber outlet where it is driven back into the now depleted medium. The oxygen returned to the medium near the outlet reduces the decrease in culture surface DO along the length of the chip. Consequently, the culture surface DO is lower on average than with an entirely PC lid, but more uniform.

When using the gas permeable lid system with an open PC component, and the oxygen pressure above the gas permeable lid is lower than the pressure in equilibrium with incoming medium, oxygen is rapidly transferred from the incoming medium to the PDMS lid. The asymptote that the pericellular dissolved oxygen approaches is also reduced. This results in a steeper gradient in culture pericellular DO and a lower average value. Where the inlet pressure is 1.05 atm (21% O_2) and the pressure above the lid is 1.00 atm (21% O_2), the mean culture surface DO is reduced to 66% ± 7% for the higher OUR (compared to 69% ± 6%). Therefore, it may be advantageous to use a polycarbonate lid component connected to a controlled gas supply (Figure 3.13[c]) (the inlet gas supply or a secondary gas supply) to achieve higher and more uniform pericellualar dissolved oygen

The gas permeable lid system with open PC components can clearly be employed to deliver higher and more uniform pericellular DO. However, achieving a specific target and maximising uniformity requires careful manipulation of the partial pressure of oxygen both at the inlet and in the head space of the PC lid component. The inlet pressure strongly affects the pericellular DO concentration experienced by cells nearest the inlet. It is best manipulated to have a inlet DO concentration slightly above the target pericellular concentration. The partial pressure in the lid head space should then be manipulated to achieve the desired pericellular DO across the

remainder of the culture surface. Such manipulations could be based either on model predictions or feedback from an oxygen sensor (Super, 2014).

3.3.7 Improvements to Monitoring and Fluid Control

Microscopy

The design of both the prototype culture device and the new culture device facilitate the monitoring of cell culture by phase contrast microscopy. Moreover, acquisition of phase contrast images was automated by the prototype control and automation platform. However, automated acquisition was only possible for a single field of view and microscope objective. To expand the automated imaging capabilities the new culture device design is compatible with a motorised microscope stage (MEC56110, Nikon Instruments, UK). This motorised microscope stage delivers accurate and precise *x* and *y* positioning allowing the automated time-lapse imaging of multiple *xy* co-ordinates. Furthermore the motorised stage was purchased as part of a fully motorised microscope (Nikon Ti-E, Nikon Instruments, UK). This microscope included a motorised *z*-drive, an digital microscope camera (Fi-1), and an LED based fluorescent excitation system (CoolLED pE-2, CoolLED, UK).

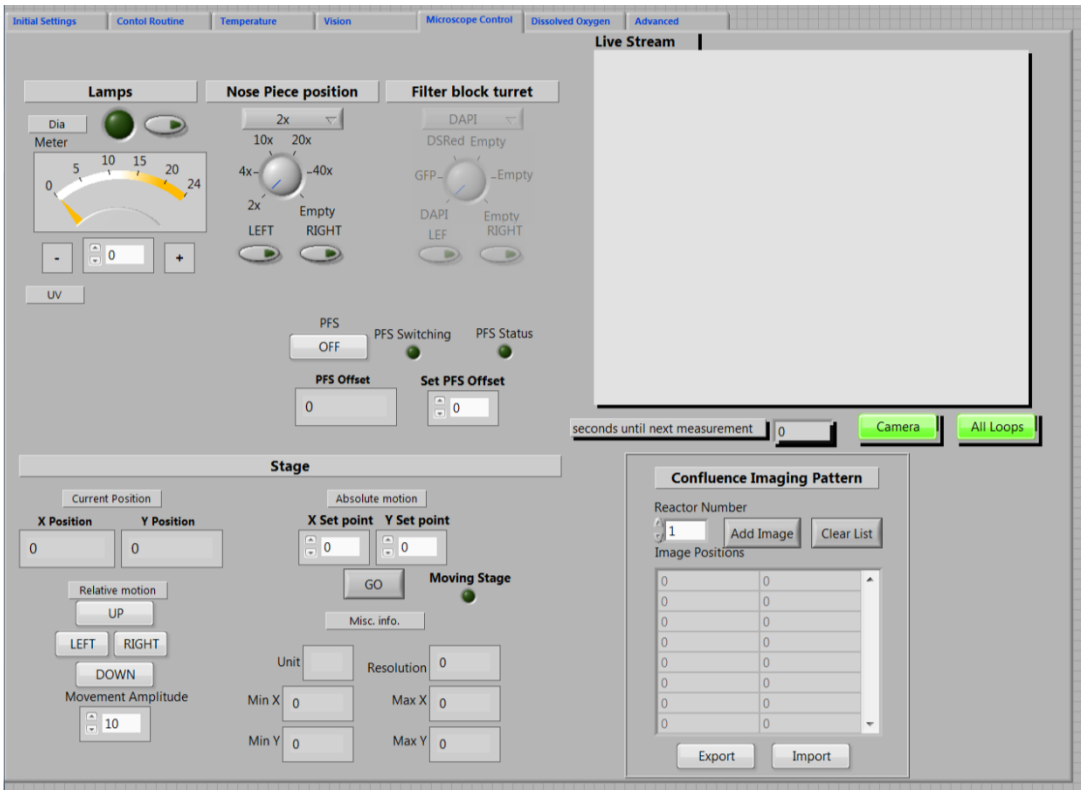

Figure 3.16 - Microscope control screen of LabVIEW VI.

The screen of the LabVIEW VI used to control the microscope. On the top left are controls to adjust lighting, nose piece position and fluorescent filter. On the bottom left are controls to adjust the motorised *xy* stage. On the bottom right is a list to which image positions and setting can be added. On the top right is the feed from the microscope camera which is displayed in all control screens.

The motorised microscope system is connected to a computer by USB. The digital microscope camera and fluorescent excitation system are connected by separate USB cables. Control of the microscope and camera were integrated into the LabVIEW (National Instruments, UK) VI used for the prototype control and automation system. This programming was done in conjunction with Nicolas Jaccard. The microscope control screen of the LabVIEW VI (Figure 3.16) allows control of the lamp, the nose piece position, the filter turret position, and the motorised *xy* stage. The *xy* stage can be stepped relatively by a specified increment or moved to an absolute position. Once a set of imaging parameters are optimised they can be stored in a list to be cycled through automatically.

The vision screen of the LabVIEW VI displays a live feed from the digital microscope camera that could be switched on and off at will. There are also

buttons to perform an auto-white operation to adjust the colour balance and to immediately commence imaging each parameter set in the list recorded on the microscope control screen. Camera settings including exposure mode and image size can be set at the start of an experiment in the settings screen as can a frequency for automated image acquisition. The VI programming of the microscope and camera allow the regular, automated, time-lapse imaging of multiple fields of view (up to the entire culture area) with the option to use multiple microscope objectives. This greatly expands the quantity of phase contrast microscopy data that can be captured from each culture experiment with the microfabricated culture device.

While the motorised microscope provides a powerful monitoring solution for the microfabricated culture device it presents a number of draw backs. In order to carry out the automated time-lapse imaging facilitated by the microscope the culture device must either be left in position on the stage or removed and replaced with extreme positional accuracy for each imaging time point. The later is impractical but maintaining the device in position on the stage throughout the culture is possible. This does however require an on-microscope method for temperature and atmospheric control. Atmospheric control should be possible through the gas permeable lid designs discussed in this chapter. The prototype control and automation platform delivers temperature control by directly heating the slide but this is only compatible with glass microscope slides. An alternate heating solution is proposed in chapter 4 but an interim solution is the use of a cage incubator (Okolab, Italy). With or without a cage incubator, the size and expense of the microscope system relative to the 1-6 devices it can support means it is not a practical solution for wide scale use.

Fluidics

The fluidics of the prototype control and automation platform were modified for a new design of control and automation platform. The custom medium reservoirs were replaced with pressure resistant, amber SCHOTT bottles coupled with 2-port lids (SCOT1094367 & 554-3000, VWR, UK). SCHOTT bottles are commercially available allowing users to more easily replace and customise

reservoirs. The amber glass also provides additional light protection, high resistance to autoclave, and a reduced risk of contamination with leachables relative to plastic. A length of 0.8 mm ID PEEK tubing with a male Luer connector on the end is inserted through each port to the bottom of the bottle. One length of tubing introduces pressurised gas mixture which bubbles through the medium to the head space and forces medium to flow out of the other length of tubing.

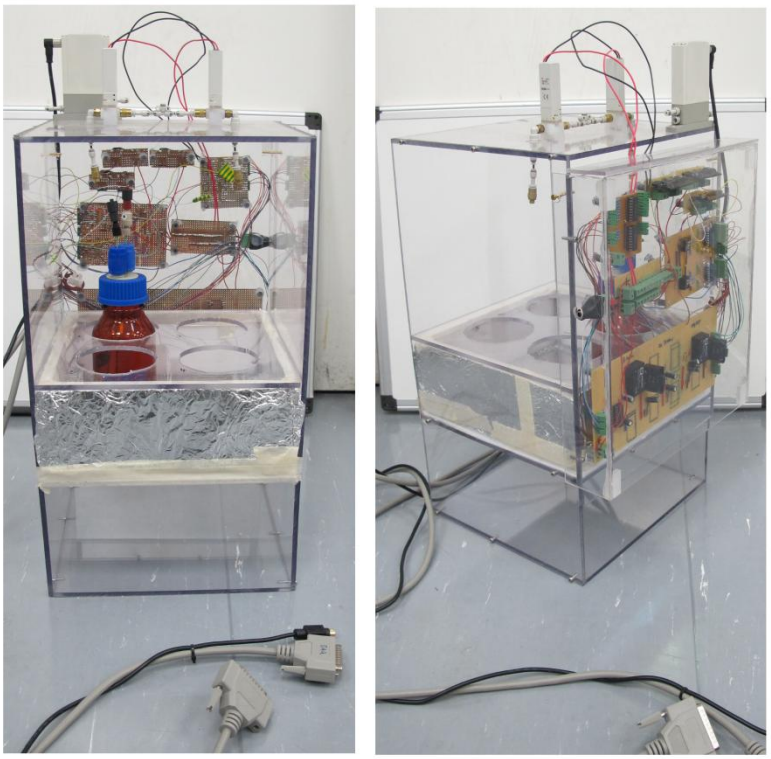

Figure 3.17 - Media storage and cooling unit of new control and automation platform.

The unit of the new control and automation platform that houses the medium bottles. Up to four medium bottles are housed in a water bath. The water bath is elevated to leave room for a peltier cooling system. On top of the unit are valves and regulators for gas control. On the back are the circuit boards for valve switching and temperature control. Two leads connect the unit to a data acquisition card and one lead connects to a unit housing the culture devices and medium switching valves.

A unit constructed from polycarbonate houses up to four medium bottles in a water bath that can be used to maintain medium at a low temperature to reduce the thermal degradation of medium components. The base of the water bath is polycarbonate with a hole in the centre covered by a 1.2 mm aluminium sheet to allow cooling through attachment of a peltier cooling system (designed for CP-061, TE Technology, USA). Alternately, the water bath can be kept cool by the addition of ice. The base and walls of the water bath are insulated with 4 mm of calcium-magnesium silicate sheeting (724-8906, RS components, UK) to reduce the required cooling load. The unit containing the water bath also includes all the circuit boards (Appendix 4) required for fluidic and thermal control as well as the valves and regulators used to control gas flow (Figure 3.17). These components were kept off the microscope stage to avoid clutter and respect the load limits of motorised stages.

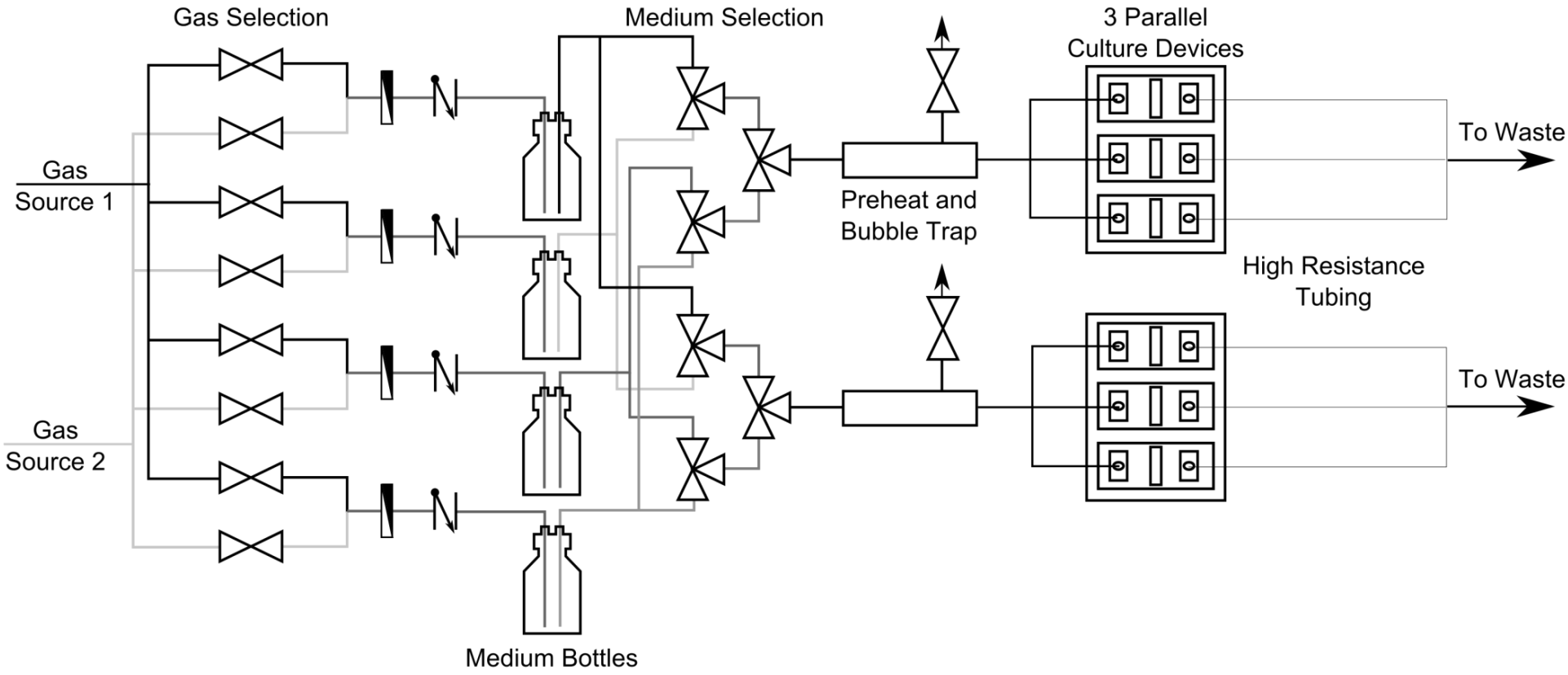

Figure 3.18 - Design of fluidics for new control and automation platform.

A schematic design of the fluidics for a new control and automation platform. Either or both of two gas sources can drive medium from any combination of four medium bottles. Which bottle supplied each set of three devices is dictated by six 3-way valves. Medium passes through a preheat and bubble trap which includes a purge outlet. Heated medium is split to the three parallel devices then flows through equal lengths of high resistance tubing before merging to a single waste stream.

The new control and automation platform is designed for two sets of three culture devices run in parallel, with a choice of four medium supplies and two gas supplies (Figure 3.18). To test the design, sufficient components were installed to control one set of three culture devices run in parallel, with a choice of two medium supplies and single gas supply. Each gas supply is connected to an electronic pressure regulator (ITV0011-2BL, Pneu-Store, UK) that controls the pressure between 0 and 1 bar using a 0-5 V signal. The output of the regulator is split into four lines each going to an on/off valve (LVM10R3Y-6A1-1-Q, Pneu-Store, UK) which is, in turn, connected to each of the four medium bottles. The on/off valves are used to control which gas (where there are two available) is delivered to which bottle. The same gas can be delivered to up to four bottles or different bottles can be pressurised by different gas mixtures. (The gas leaving the regulator could be connected to gas permeable lids before returning to be split to the four on off valves.) Immediately prior to each bottle are a 0.22 μm filter for sterility and a check valve to prevent media flowing in reverse when gas pressure is reduced.

Medium flows from the bottles to a small second unit mounted on the microscope stage. For each set of three parallel devices a combination of three 3-way valves (LFRA1230110H, The Lee Company, UK) are used to select the source of medium. The selected medium then passes through a combined preheat and bubble trap unit (technical drawings in Appendix 2). Up to the preheat/bubble trap unit all tubing is 0.03” ID PEEK. The preheat and bubble trap unit consists of three layers of PDMS clamped between aluminium plates. Medium passes through a 50 mm long channel (0.5×0.2 mm) to the bottom of a circular chamber (2 mm D, 3 mm h) and then on from the bottom of the chamber to the outlet.

Heat is introduced by a flexible heating circuit (HK5160R157L12B, Minco, France) in response to readings from a thermistor (B57863S103F40, Farnell, UK) positioned near the outlet. The heating circuit is positioned between the bottom two PDMS layers (0.12 mm below the below channel). Any bubbles in the medium at the end of the channel will rise to the top of the circular chamber. The top of the circular chamber is connected to an on/off valve that can be used

to regularly purge trapped gas. This valve can also be used to purge the fluidics up to this point. This capability facilitates more rapid switching of medium source. As the purge is very near the culture devices dead volume is minimised.

After the preheat and bubble trap unit the ID is reduced to 0.01” to reduce dead volume. The medium is split into three streams connected to the three parallel culture devices. A single 10 cm length of tubing is split into three 6 cm lengths giving a dead volume of approximately 5 µl per device. The outlet of each device is connected to a 50 cm length of 0.004” ID PEEK tubing. These lengths of tubing are included to add an equal and high resistance to each of the three flow paths to achieve equal flow regardless of small variations in the resistance of the culture devices. The resistances of each of the three lengths of tubing are 156, 155, and 157 $TPa.s.m^{-3}$ respectively (recorded pumping medium at 6 $ml.h^{-1}$). In comparison the resistances of three different culture devices were 1.58, 1.67, and 1.14 $TPa.s.m^{-3}$ (recorded pumping medium at 60 $ml.h^{-1}$). The difference between the upper and lower resistances of the chips is 37% of the mean but when coupled to the high resistance tubing the variation is reduced to ≤1%.

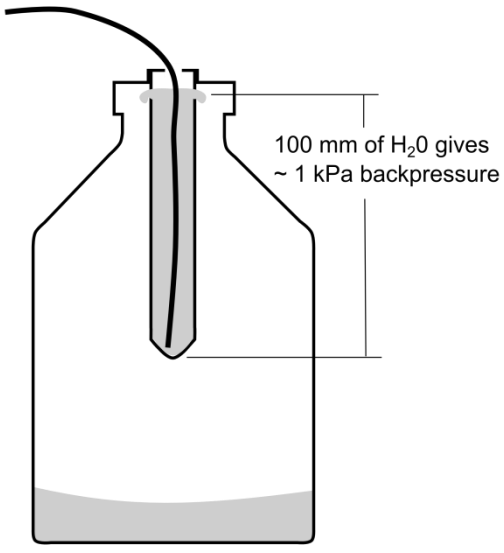

Figure 3.19 - Waste bottle with regulated back pressure.

Waste medium flows into the bottom of a 15 ml Falcon tube suspended in a SCHOTT bottle. Medium overflows from the Falcon tube though holes at the top and into the SCHOTT bottle. This maintains a constant height of medium at the tubing outlet.

Finally, the three outlets are connected to a single length of 0.03” ID tubing connected to a waste reservoir. The waste reservoir was designed to maintain a constant back pressure. A small back pressure means that even under low or no flow conditions a pressure is maintained on the culture chamber driving out gas bubbles and replacing evaporating medium. The waste reservoir consists of a 15 ml Falcon tube suspended in the lid of a SCHOTT bottle (Figure 3.19). Tubing enters the falcon tube via a small hole in the lid. Four 3 mm holes in the tube just below the lid allow liquid to overflow into the SCHOTT bottle. The Falcon tube is initially filled with sterile water which is then displaced by the waste medium resulting in a constant height of liquid at the tubing outlet. This arrangement maintains a back pressure of approximately 1 kPa.

Software and Connectivity

An issue with the prototype control and automation platform was the complexity of both the software and the connectivity. The prototype platform required 16 cables to be connected; 8 power supplies and 8 signal cables. For the new platform the number of connections was reduced to a single power connection, one connection between the main unit and the stage-top unit, and two connections between the main unit and the data acquisition card (DAQ) (NI USB-6221, National Instruments, UK). All valves, regulators, heaters and thermistors were powered by a single 112W 12V DC power supply (L52BR, Maplin, UK) connected to the main platform unit by a simple cylindrical connector. A DB-25 serial cable transmits power and signals between the stage-top unit and the main unit. A DB-25 serial cable and a PS/2 cable transmit signals and power between the main unit and DAQ. There are not only fewer cables to connect in the new platform but the connections are faster to make (push fit). Because there is only one power supply less physical space is occupied and there is less opportunity to make a wrong connection. To compensate for the reduced number of power supplies the DC voltage is stepped up or down for certain components via the circuit boards on the main unit.

The LabVIEW VI for the prototype platform had a number of redundant sections of code. Code for measurement of DO by fluorescent lifetime measurements and code for the control of different pumping solutions were removed for the new platform. In its place, code was added to control the motorised microscope and microscope camera as discussed above. Code was also added to allow use of a PreSens dissolved oxygen probe (PreSens, Germany) with the fibre mounted to the microscope nosepiece. This was done to support the research of Alexandre Super (Super, 2014) to measure pericellular dissolved oxygen in a culture device. Efforts were made to reduce the settings that need adjusting for each experiment. Typically, a user must select the camera settings (exposure mode, exposure, gain, image resolution) and automated image acquisition settings (off/on, period, save location). The DAQ input and output lines no longer require adjustment. These software changes increase functionality of the software while simplifying operation.

3.4 Conclusions

New designs of microfabricated culture device and control and automation platform have been developed based on Marcel Reichen's prototype designs. The new designs build on key features of the prototype designs that deliver well-controlled, uniform culture conditions and processes that can be translated to/from traditional culture systems:

- The use of reversible compression seals to facilitate the use of various culture substrates and the inclusion of a resealable lid for direct access to the culture chamber.
- The short wide culture chamber design with raised inlet and outlets that delivers low shear perfusion with more uniform concentrations of soluble factors.
- A proven capacity to culture embryonic stem cells and evidence of comparability with traditional culture systems.
- Gas driven perfusion with automated medium switching.
- Monitoring by phase contrast microscopy.

The new design strengthens the culture device concept in a number of key areas.

Firstly, a new design of PDMS chip with tree-like channel structures achieves more uniform expansion of perfused medium than the prototype design. Uniform expansion of medium is vital as modelling shows that the perfusion barriers are ineffective at increasing uniformity. In fact, perfusion barriers decrease uniformity through the creation of dead zones and high velocity zones. However, perfusion barriers play a key structural role maintaining separation between the two flexible layers of the PDMS chip.

Secondly, bending analysis of the prototype device implied the bending of frames is responsible for a high frequency of leaking, a highly variable burst pressure, and a high sensitivity to screw torque. A new device design, including a holder to house up to three devices, minimises bending. The decrease in bending increases the burst pressure from 59 ± 18 kPa to 370 ± 120 kPa though the variation remains high. The new design no longer encounters leaks at typical operating pressures and is not sensitive to the screw torque used for clamping.

The elimination of the sensitivity to screw torque also makes the new design easier to use. Ease of use is also increased by reducing the number of parts per device (by eliminating the bottom plate) and the number of clamping screws (from 30 to 12 for three devices). The reusable parts of the new system have been made more robust. This is achieved through use of aluminium for the holder and interconnects, and thicker polycarbonate for the top frame which is also subject to less bending stress.

A newly designed gas permeable lid system allows oxygen to be supplied to cells without the perfusion of medium. The rate of oxygen supply can therefore be controlled independent from shear stress and the concentration of other soluble factors (albeit not fully decoupled). Higher pericellular dissolved oxygen

concentrations can be achieved than with the previous impermeable lid system. The pericellular dissolved oxygen is also more uniform, even when oxygen is not supplied through the lid, due to the high permeability of PDMS. While the new lid system improves control, careful manipulation of the partial pressure of oxygen is required to deliver the most uniform and consistent pericellular dissolved oxygen possible.

The new designs of culture device and control and automation platform increase the extent of data that can be obtained by phase contrast microscopy. Up to two sets of three parallel culture devices can be positioned on a motorised microscope stage. This allows time lapse imaging of the entirety of all six culture areas. Use of a fully motorised microscope facilitates the use of different magnifications and lighting conditions. A fully motorised inverted microscope is a powerful and useful tool for analysis of culture in microfabricated culture devices but is not suitable for wide-scale use.

The new platform now incorporates commercially available medium reservoirs to make user customisation easier. The fluidics have also been expanded to allow selection from up to two gas supplies and four medium reservoirs to supply 1-2 sets of 3 parallel culture devices. An automated purge valve attached to the bubble trap allows regular removal of trapped gas and more rapid switching of medium supply. High resistance tubing is employed to increase the uniformity of flow through parallel devices. Finally, a waste collection system has been designed that delivers a constant back pressure to reduce bubble formation.

The control and automation platform still consists of two units but the number of components on the stage-top unit has been reduced to minimise weight. The number of power supplies required has been reduced to one. Similarly, the number of connections between the two units and the data acquisition card has been reduced to three. These changes make the platform simpler to operate and reduce space requirements. The control software is also simpler to operate than it was in the previous platform, and all redundant code has been removed.

The new designs retain the strengths of the prototype designs while improving control, monitoring, robustness, and ease of use. While none of the changes would be expected to make the system less suitable for cell culture, the capacity for cell culture must be revalidated. It would also be beneficial to investigate any significant differences in culture outcome due to the design changes to the PDMS chip and the lid system. Finally, a new heating system for device culture chambers is still needed that allows continued use of TC-PS as a culture surface.

4. Evaluation of the Improved Microfabricated Culture System

4.1 Review of the Prototype and Improved Culture Systems

A prototype microfabricated adherent culture device was introduced in chapter 2. The device facilitates low-shear perfusion of medium through a short, wide culture chamber, providing good control over soluble factor concentrations. A resealable lid allows static seeding of cells directly onto the culture surface, which can be tissue culture polystyrene or any other smooth flat material. Mouse embryonic stem cells appear to attach at similar rates in the prototype culture device and a T-25 culture flask. Mouse embryonic stem cells also appear to expand at a similar rate under static culture conditions, with the resealable lid not included. Furthermore, the prototype culture device was shown suitable for the perfusion culture of human embryonic stem cells co-cultured on inactivated mouse embryonic fibroblasts. Colonies expand over two days of perfusion culture and continue to stain positive for pluripotency markers.

Chapter 2 also introduced a control and automation platform to house the device. Medium can be perfused form one of two chilled reservoirs, through a preheat unit, to up to three prototype culture devices. The devices themselves can also be heated though this requires use of a glass culture substrate. The platform is designed to be used with an inverted microscope, which can be used to monitor cultured cells using phase contrast microscopy.

The designs of both the culture device and the control and automation platform were improved upon in chapter 3. The structure of the channels in the PDMS chip (through which the medium is perfused) was changed to improve the uniformity of the fluid velocity field when the chip is uncompressed. Consequently, uniformity of shear stress and soluble factor concentrations should also improve. Uniformity of pericellular dissolved oxygen was further improved by introducing a gas permeable lid design. Design changes made to the packaging of the culture device improve robustness by reducing the bending of rigid components. The design changes significantly increase burst pressure,

and the reduced bending should increase the uniformity of fluid flow. Furthermore, the new device design, which includes an aluminium holder, is easier to assemble; sealing devices in a biological safety cabinet setting requires the tightening of fewer screws, and to less specific screw torques.

The aluminium holder fits in the stage of a motorised microscope, expanding monitoring capabilities to include time-lapse imaging of whole culture chambers and the use of multiple objectives. Up to two sets of three culture devices can be imaged in this way. These devices can be controlled and monitored by the improved control and automation platform. The improved platform is designed to use two pressurised gas mixtures to perfuse medium from a choice of four medium reservoirs. The fluidics of the improved platform achieve more equal flow through parallel devices and maintain a back pressure to reduce bubble formation. The whole platform, including the control software, has been made simpler to assemble and operate.

4.1.1 Next Steps

Following the implementation of these design changes, the next step is to demonstrate that the microfabricated culture system remains able to culture embryonic stem cells. The changes made are not expected to make the device unsuitable for stem cell culture, but validation of this assumption is required. Furthermore, it would be useful to investigate whether the design changes significantly affect culture outcomes. In particular, the changes to the PDMS chip and the introduction of the gas permeable lid may result in more uniform culture outcomes across the chip, corresponding to the increased uniformity of culture conditions. The higher pericellular DO, resulting from the additional oxygen supplied through the gas permeable lid, may also affect culture outcomes.

Once a culture system design is finalised, equivalence will need to be established with traditional adherent culture systems. This will validate results generated with the system and support the translation of protocols to and from the microfabricated system. The first step of this process is establishing identical starting points in both the microfabricated and traditional culture

systems. The rate of seeding in the prototype culture device was investigated in chapter 2 by counting the cells that remained unattached. By this method the rate of attachment appears to be the same as the rate in a T-25 culture flask. With techniques to automatically measure confluency now available (Jaccard et al., 2014a), this work needs to be extended to show that the confluency after seeding is equal in both systems.

Finally, a new solution is needed to heat the culture chambers of the microfabricated culture devices. The prototype control and automation platform achieved this using Indium-Tin-Oxide coated glass slides. This solution was rejected for the improved platform as it removes the substrate flexibility that is a key advantage of the microfabricated culture device. As an interim solution, the improved platform can be housed within a cage incubator to maintain the culture chamber temperature. However, a more compact, direct and cost efficient heating solution would be preferred if the microfabricated culture system is to become widely used.

4.2 Materials and Methods

E14Tg2a mouse embryonic stem cells were maintained as previously (section 2.2.6). Likewise, culture system parts were manufactured as previously (sections 2.2.1 and 3.2.1).

4.2.1 Seeding of Mouse Embryonic Stem Cells

Prior to each experiment, the aluminium holder and parts for three microfabricated culture devices (top frames, PDMS chips, and gaskets) were cleaned with reverse osmosis water, autoclaved at 121°C for 20 minutes, and placed in a drying oven over night. The microfabricated devices were assembled with sterile Nunclon® TC-PS microscope slides (16004, Fisher Scientific, UK) inside a biological safety cabinet and inserted into the aluminium holder. The 12 screws of the aluminium holder were then tightened to seal the three devices. The culture chambers of the devices were filled with 0.1% gelatine solution (156 µl), as were three T-25 Nunclon® cell culture flasks (2 ml) (156367, Fisher Scientific, UK). The gelatine solution was left for 15 minutes and removed before seeding.

Cells were harvested from a T-25 flask as per a normal passage. The resuspended cells were analysed twice with a haemocytometer and used to prepare a cell suspension of the desired concentration and volume. The cell suspensions were analysed again with a haemocytometer. The cell suspension was then used to seed the three culture devices (156 µl) and three flasks (7.5 ml). A 200 µl pipette tip was used to seed the microfabricated device and a 10 ml sterological pipette was used to seed the flasks. In both cases the pipette tip was placed in a specific corner of the culture surface (top left in the microfabricated devices and bottom left in the flasks). Flat pieces of sterilised polycarbonate were placed loosely on top of the culture chambers of the microfabricated culture devices to protect them from contamination.

Experiments 1-7

For the first seven experiments, the microfabricated culture devices and T-flasks were immediately transported to an incubator. The culture vessels were incubated for 6 hours at 37°C and 5% CO_2. Following incubation the vessels were transported back to the biological safety cabinet and the medium was exchanged. During the exchange, the pipette tip was placed in the same corner of the culture surface as for seeding. An excess of medium (200 µl) was replaced in the microfabricated culture devices and the sterile polycarbonate cover was replaced to eliminate meniscus effect for imaging. The vessels were then transported to an inverted microscope (Ti-E, camera Fi-1, Nikon, UK) and 20 random phase contrast images were taken of each vessel using a 10× objective.

Experiment 8

For the eighth experiment, all culture vessels were imaged prior to incubation. As the flasks were placed into the incubator, they were held with one corner down and swirled gently to mix the cell suspension then immediately laid flat on the incubator shelf. Following the 6 hour incubation the vessels were imaged again prior to the medium exchange and then for a third time after the medium exchange. At all imaging time points, 20 random phase contrast images were taken of each vessel using a 10× objective.

Experiments 9-14

For the last six experiments, the culture vessels were only imaged after the medium exchange, as was done in the first seven experiments. However, the flasks were mixed immediately before laying them flat in the incubator, as was done in the eighth experiment.

Seeding Experiment Image Analysis

Images from the seeding experiments were analysed with PHANTAST software (Jaccard et al., 2014a) to calculate the confluency of stem cells in each image.

The previously optimised settings (section 2.2.10) of σ=3.54, ε=0.0876, and a maximum halo removal ratio of 0.281 were used. The remaining settings were; for halo processing, a minimum fill area of 25 pixels and removal of small objects setting of 400, and for additional processing, removal of small objects bellow 100 pixels.

4.2.2 Perfusion Culture of Mouse Embryonic Stem Cells

These culture experiments used different combinations of open and closed PC lid components, and prototype and improved PDMS chips. Special top frames were manufactured to accommodate the prototype PDMS chip in the aluminium holder of the improved culture system. These top frames had the inlet and outlet holes, and interconnect attachment points, 4 mm closer together to match the prototype chip. The special top frames were otherwise the same as the standard top frames (see appendix 2 for full dimensions).

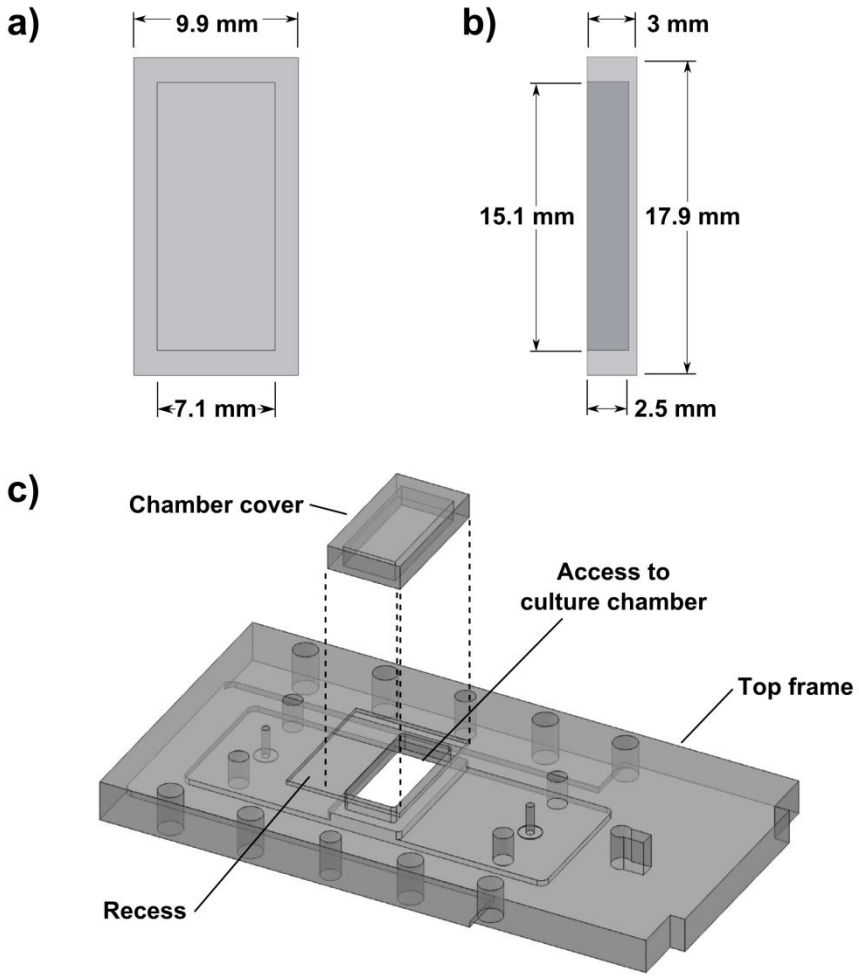

Figure 4.1 - Chamber cover for seeding period.

Bottom [a] and side [b] views of the polycarbonate cover used to protect against contamination during seeding. The outer dimensions fit inside the recess around the lid hole [c] while the dimensions of the cavity are slightly larger than the dimensions of the lid gasket.

Prior to each experiment, the aluminium holder and parts for three microfabricated culture devices (top frames, PDMS chips, gaskets, interconnect bars, and PDMS and PC lid components) were cleaned with reverse osmosis water, autoclaved at 121°C for 20 minutes, and placed in a drying oven over night. Also cleaned and autoclaved, were covers to protect the culture chambers from contamination during seeding (Figure 4.1) and the medium bottle, waste bottle and tubing of the improved control and automation platform (section 3.3.7). The valving and temperature control systems of the improved platform were not used.

The microfabricated culture devices were assembled in open configuration, using sterile Nunclon® TC-PS microscope slides (16004, Fisher Scientific, UK), inside a biological safety cabinet. The devices were then inserted into the aluminium holder and the 12 screws of the aluminium holder were tightened to seal the three devices. The culture chambers of the devices were filled with 0.1% gelatine solution (156 µl). The gelatine solution was left for 15 minutes and removed before seeding.

Cells were harvested from a T-25 flask as per a normal passage. The resuspended cells were analysed twice with a haemocytometer and used to prepare a cell suspension of approximately 2.5×10^5 cells.ml^{-1}. The cell suspensions were analysed again with a haemocytometer. The cell suspension was then used to seed the three culture devices (156 µl) using a 200 µl pipette tip. The pipette tip was placed in the top left corner of the culture surfaces. After seeding, sterilised polycarbonate covers were placed loosely on top of the culture chambers of the microfabricated culture devices to protect them from contamination. The holder was then transferred to an incubator and incubated statically for 6 hours at 37°C and 5% gaseous CO_2.

The perfusion system was prepared during the static incubation. A sterile 0.22 µm syringe filter was attached to the gas inlet of the medium bottle. The medium bottle was filled with 100-120 ml of mESC culture medium and transferred to the cage incubator surrounding the motorised microscope. The

Sensirion flow meter (SLG64-0075, Sensirion AG, Staefa, Switzerland), used in all but the first experiment, was sterilised by flushing with 80% ethanol, leaving filled with ethanol for 30 minutes, and then flushing with autoclaved reverse osmosis water. Finally, the inlet and outlet tubing were assembled and flushed with mESC culture medium. The flow meter was positioned in the inlet tubing upstream from where the combined inlet split into three streams.

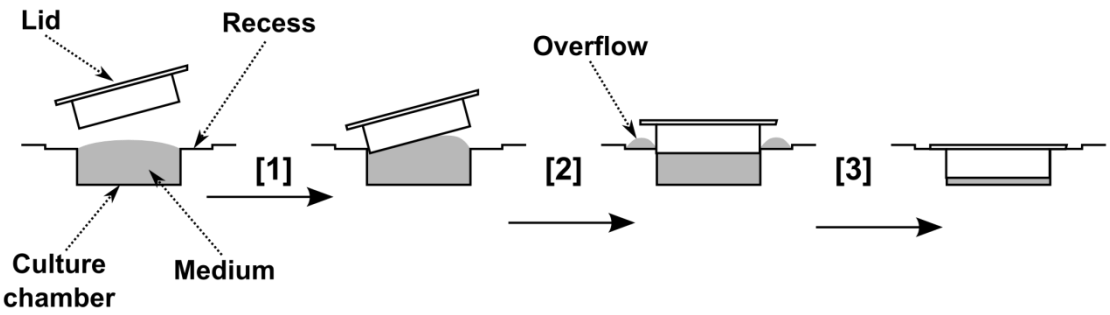

Figure 4.2 - Schematic of lid insertion process.

A schematic showing the insertion of the PDMS component of the gas permeable lid system. First one edge of the lid is partially inserted with the lid at an angle [1]. Then the angle is slowly reduced to inset the other edge without entrapping any air [2]. Finally, the whole lid is slowly pressed down until the top layer is flush with the top of the gasket [3].

Following 6 hours of static incubation, the aluminium holder was returned to the biological safety cabinet and the polycarbonate covers removed. The medium was gently aspirated from the culture chambers and new medium was inserted through both the inlet and outlet ports in order to prime the channels. The final volume of medium in the culture chambers was sufficient that the surface protruded above the top of the gasket. The PDMS lid components were inserted using sterile tweezers (Figure 4.2): First, one side of the lid was inserted slightly [1], before slowly bringing down the other side to avoid entrapping any air bubbles [2]. Once the whole lid was partially inserted it was gently pressed the rest of the way [3]. Medium forced from the chamber was aspirated with a pipette. Finally, the PC lid components were screwed down on top of the PDMS components.

Following lid insertion, the inlet and outlet tubing was connected to the culture devices. This was done after lid insertion in order to provide low resistance flow

paths by which medium could be forced from the chamber during lid insertion. The holder, complete with tubing, was then transported to the microscope and connected to the medium bottle. In all but the first experiment, the flow meter was connected to the computer and the logging and control software was initiated. Pressure was manually increased until the flow rate was near the set point, before setting this pressure as the pressure bias and initiating the PI flow controller. For the first experiment the pressure was left manually controlled to a pressure expected to give the target flow rate (2.24 V from previous resistance measurements; section 3.3.5 and 3.3.7).

With medium perfusion and the control software initiated, the holder was screwed in place on the microscope stage and the image positions entered. Image positions were added in a grid pattern with a fixed step between images that ensured overlap. The cells were then cultured with continuously perfused medium for up to 92 hours. Phase contrast images were taken every 2 hours using a 10× objective. At the end of this period perfusion was stopped, inlet and outlet tubing disconnected, and the holder transported back to the biological safety cabinet for immunostaining of the cells.

Culture Experiment Image Analysis

Phase contrast microscopy images were analysed with software developed by Nicolas Jaccard (Jaccard et al., 2014b, Reichen et al., 2012): At each time point, all the image positions of a culture chamber were stitched into single images showing the whole culture chamber. Each stitched image was then analysed to detect cells and determine confluency. The image analysis software uses a random forest machine learning algorithm (Breiman, 2001) to classify pixels as either cell or background. The classifications are based on local histograms of Basic Image Features (BIFs) computed at different scales. Computation of BIFs consists of classifying each pixel of an image according to local symmetries and structures, for example radially symmetric blobs or lines (Griffin et al., 2009). The machine learning software had been trained on a set of phase contrast microscopy images of E14 mESCs achieving a mean F-score (i.e. overlap between the algorithm output and manual annotations by human

experts) of 0.92. The software also splits each image into a 36×10 grid of smaller images (350×350 μm) and outputs the confluency of each grid square to allow the determination of spatial variation in confluency and growth rate.

The output of the image processing software was used to generate growth curves showing confluency over time. Confluency is not perfectly proportional to cell number, as cell area can change through an experiment. However, confluency provides a reasonable estimate of cell number throughout monolayer growth (Jaccard et al., 2014a). Instantaneous specific growth rates were generated from the confluency curves using an average of the forward, backward and central differences (equation 4.1);

$$SGR_n = \frac{1}{3}\left(\frac{ln(C_{n+1}/C_n)}{t_{n+1} - t_n} + \frac{ln(C_n/C_{n-1})}{t_n - t_{n-1}} + \frac{ln(C_{n+1}/C_{n-1})}{t_{n+1} - t_{n-1}} \right) \quad (4.1)$$

Where SGR_n is the specific growth rate, t_n is the time, and C_n the confluency at point n. Relative specific growth rates were also calculated for each device in each experiment. This was done by taking the mean specific growth rate of all the devices in an experiment away from the individual specific growth rates for each device.

The average growth rate of each grid element was calculated over two periods; 12-26 and 26-40 hours after the start of perfusion. These calculations used the following equation;

$$GrowthRate_{1-2} = \frac{ln(C_2/C_1)}{t_2 - t_1} \quad (4.2)$$

Where C_1 and t_1 are the concentration and time at the start of the period, and C_2 and t_2 are the concentration and time at the end of the period.

Relative growth rates for each grid element were then calculated by subtracting from the growth rate of each grid element, the mean growth rate across the entirety of all three culture chambers in that experiment.

4.2.3 Cell Staining

Cells from the triplicate perfusion culture experiments were stained for pluripotency markers. After halting perfusion culture, the aluminium holder was returned to a biological safety cabinet for immunostaining. With all tubing disconnected, the PC lid components were unscrewed and removed. The PDMS lid components were then carefully removed using tweezers. mESC cells were fixed with 4% (v/v) paraformaldehyde (PFA) in DPBS for 20 minutes then washed three times. All washing was with DPBS supplemented with 10% (v/v) FBS to block non-specific binding. Fixed cells were permeabilised by incubating with 0.2% Triton X-100 for 15 min at room temperature before washing a further 3 times.

Permeabilised cells were incubated with primary monoclonal antibodies Oct-4 (ab19857), Nanog (ab80892), or Sox-2 (ab97959, Abcam, UK) at a dilution of 1:200 in 10% FBS, for one hour at room temperature. The cells were then washed three times and incubated with a corresponding secondary antibody, which had a excitation wavelengths of 488 nm (A-11008, Invitrogen, USA), at a dilution of 1:200 in 10% FBS, for one hour at room temperature.

Cells in the second and third experiment were then washed three times and co-stained for SSEA-1. Co-staining involved repeating the primary/secondary staining procedure above, with an SSEA-1 primary antibody (ab16285, Abcam, UK) and a secondary that had an excitation wavelength of 555 nm (A-21422, Invitrogen, USA). For the second experiment both the primary and secondary antibody were diluted 1:200 in 10% FBS. For the third experiment the primary antibody was diluted 1:10 following information from supplier.

Finally, the cells in all three experiments were washed with DPBS and stained with 4',6-diamidino-2-phenylindole (DAPI) (D1306, Invitrogen, Carlsbad, CA, USA). DAPI at a dilution of 1:200 was incubated with cells at room temperature for 10 minutes. Stained cells were imaged with an inverted fluorescent microscope (Ti-E, camera Fi-1, Nikon, UK) using an LED excitation system (CoolLED pE-2, CoolLED, UK). For the second and third experiments devices

were removed from the aluminium holder for fluorescent imaging. Care was taken not to move the PDMS chips relative to the TC-PS slides, as this would disrupt the culture surface.

4.3 Results and Discussion

Mouse embryonic stem cells were used for the engineering studies in this chapter as they are more easily cultured reproducibly than human embryonic stem cells and can be seeded as a suspension of single cells without a layer of feeder cells. As the purpose of these studies is engineering characterisation of the device, the relative ease of reproducible culture is worth the lesser relevance of the mouse cell line. Mouse embryonic stem cells are from a similar in vivo environment to human embryonic stem cells and are therefore expected to be sufficiently representative of human embryonic stem cell behaviour for engineering characterisation and preliminary studies.

4.3.1 Seeding of Mouse Embryonic Stem Cells

The rate at which seeded cells attach in the prototype microfabricated culture device was compared to the rate in T-25 culture flasks, in section 2.3.5. The number of adherent cells proved difficult to measure, particularly in the microfabricated culture device, due to inefficient detachment of cells. However, the decrease in unattached cells proved easier to measure and is the same in the both culture systems. Following improvements to the culture device, and the development of software to accurately and consistently measure the confluency of attached cells (Jaccard et al., 2014a), this work is now extended to compare the confluency of attached cells after seeding. Previous work indicated that over 90% of seeded cells attach within 6 hours of seeding (Figure 2.10). This was the incubation time chosen to allow cell attachment in future experiments.

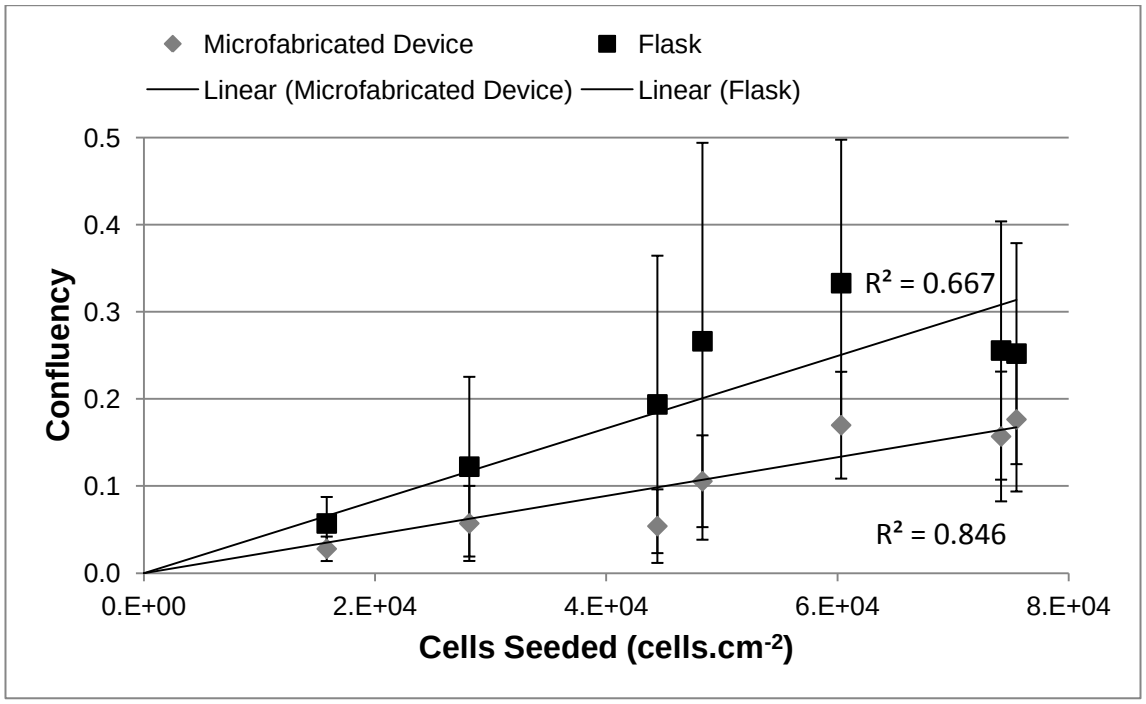

Figure 4.3 - The results of initial experiments to investigate post-seeding confluency as a function of seeding cell density.

The average confluency of culture flasks and improved culture devices after 6 hours of incubation and a medium exchange. The confluency was investigated for different densities of seeded cells, with the same cell suspension used to seed 3 flasks and 3 culture devices. Error bars show the standard deviation of all images of the same vessel type seeded from the same suspension (n=60). Displayed on the figure are linear trend lines through the origin and their respective R^2 values.

Seeding was investigated at a range of seeded cell densities. This was done in order to search for a relationship between the two systems that is independent of the seeding density. Following the six hour incubation, culture medium was exchanged to remove unattached cells. Images of the culture vessels were then taken and analysed to determine confluency. Initial experiments indicated that the post-seeding confluency is lower in microfabricated culture devices than in T-25 flasks (Figure 4.3). However, the expected linear trend between seeded cells and flask confluency is not apparent in this data ($R^2 = 0.667$).

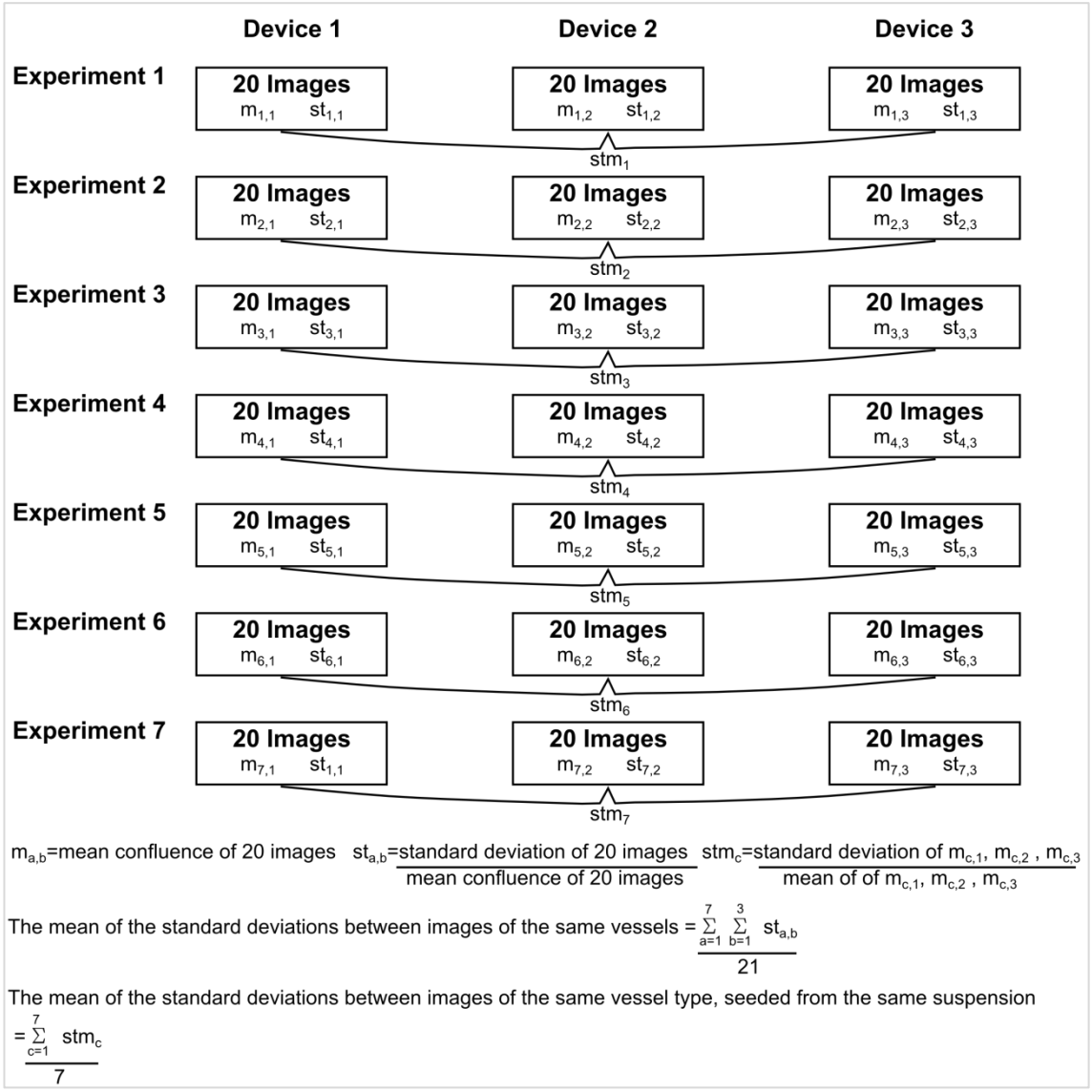

Figure 4.4 - Illustration of mean and standard deviation calculations made following seeding experiments.

This figure illustrates the calculations made following the seeding experiments. 20 images are taken of each vessel (flask or microfabricated culture device) in each experiment. The images are processed with PHANTAST software to get confluence figures. Means [$m_{a,b}$] and standard deviations [$st_{a,b}$] are calculated for each set of 20 images. The mean of these standard deviations, across all flasks or devices, and in all experiments, is the mean of the standard deviations between images of the same vessels. This indicates the average uniformity of cell distribution. The standard deviations between the mean confluencies of the three similar vessels in each experiment are also taken [stm_c]. The mean of these values across all experiments is the mean of the standard deviations between images of the same vessel type, seeded from the same suspension. This value indicates how repeatably a culture system can be seeded from the same suspension and, consequently, the variation in average starting confluence between vessels in a culture experiment.

Moreover, there is significant variation both between the mean confluency of vessels seeded from the same cell suspension, and between the individual confluency measurements made at different locations within these vessels. The mean of the standard deviations between images of a specific culture vessel is 65%, for culture flasks, and 51%, for microfabricated devices (Figure 4.4). The mean of the standard deviations, between the confluencies of vessels of the same type, seeded from the same cell suspension, are lower at 12%, for culture flasks, and 18%, for microfabricated devices (Figure 4.4). A higher variation is expected between microfabricated culture devices as their small volumes make them more susceptible to non-uniform cell suspensions.

There are a number of possible reasons why the confluency might be lower in microfabricated culture devices than in flasks. A greater percentage of cells may be lost during pipetting due to the different surface area to volume ratios of different sized pipettes. Alternatively, cells may be forced into the channels of the microfabricated device. These three possibilities would result in fewer cells being in suspension above the culture surface at the start of the 6 hour incubation. Reduced confluency may also be caused by increased cell death over the 6 hour incubation or by wash-out of cells during the medium exchange due to shear near the pipette tip.

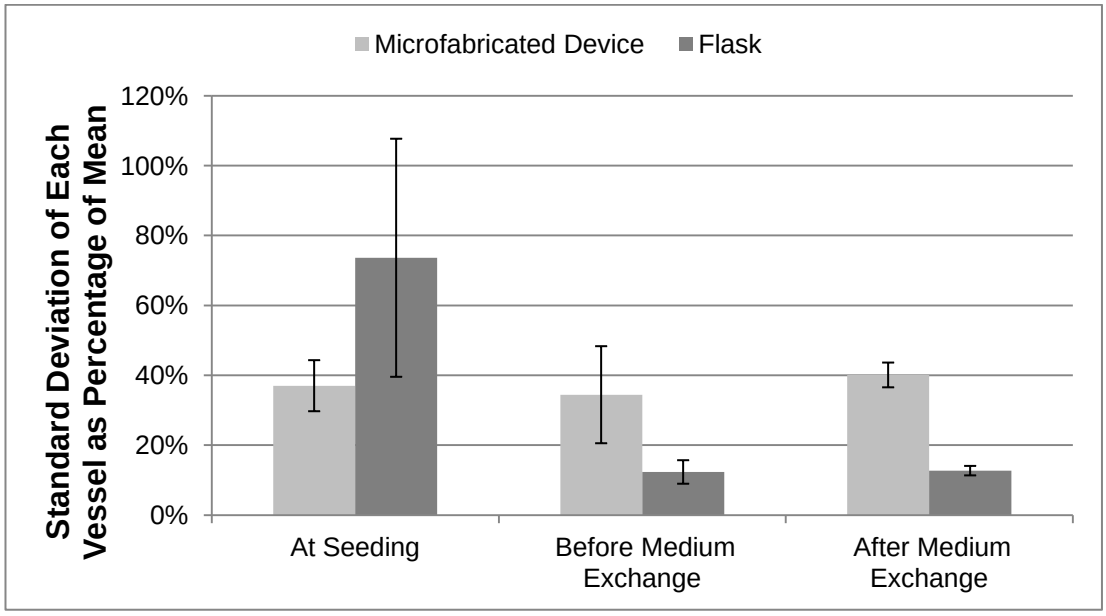

Figure 4.5 - Variability between images of the same culture vessel during seeding experiment 8.

The figure shows the standard deviation in image confluency (n=20), for individual culture vessels, as a fraction of the mean confluency for those culture vessels. The mean of three vessels' standard deviations is shown, with error bars showing the standard deviation between vessels. Variation is shown immediately after seeding, 6 hours later immediately before medium exchange (following redistribution of cells in flasks), and immediately after medium exchange.

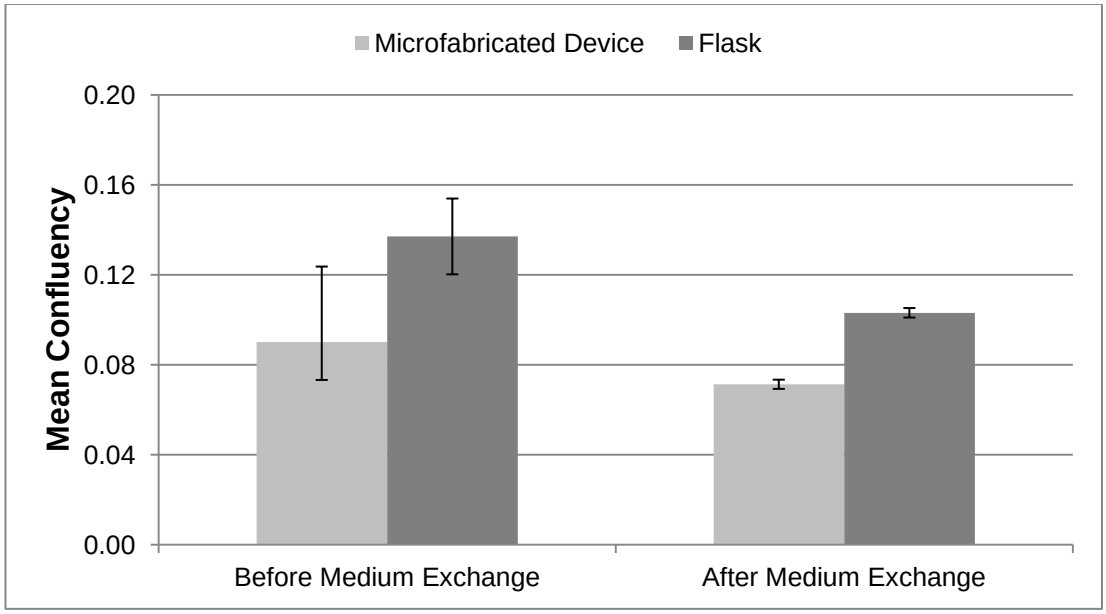

Figure 4.6 - Changes in mean confluency due to post-seeding medium exchange in seeding experiment 8.

The figure shows the mean confluency of vessels before and after the medium exchange that takes place 6 hours after seeding. Error bars show standard deviation between vessels (n=3).

To narrow this range of possibilities, an experiment was carried out where the culture vessels were imaged immediately after seeding as well as prior to medium exchange. When imaging the cells immediately after seeding, it was noted that cells were concentrated in the middle of the flasks. The mean of the standard deviations between images of the same flask was 74% of the mean confluencies for those flasks (Figures 4.4 and 4.5). The cells were redistributed immediately prior to incubation by holding the flask with one corner down (to achieve a high volume to surface area ratio) and gently swirling (to achieve a uniform suspension), then immediately laying the flask flat on the incubator shelf.

Cells in microfabricated devices appeared to be present in slightly higher density near the edges of the culture chamber. The mean of the standard deviations between images of a culture device is 37% (Figures 4.4 and 4.5).

This is possibly due to fluid flow during the filling of the culture chamber; fluid flows rapidly away from the pipette tip towards the chamber edges and forms a meniscus. The image processing software appeared to struggle when classifying cells immediately after seeding. This is due to the significantly different morphology of unattached cells, and the fact that not all cells had settled into the focal plane. However, while the mean values are not accurate, the image to image variation remains indicative of variation in cell density.

Immediately prior to medium exchange the cells in the flask were more uniformly distributed (Figure 4.5) (the mean of the standard deviations between images of a specific culture flask is 12%), showing the effectiveness of the redistribution method. As expected, the mean of the standard deviations in the microfabricated devices remained similar (34%) (Figure 4.5). Following the medium exchange, the mean confluencies in the microfabricated devices and in the flasks were 7% and 10% respectively (Figure 4.6). These results were much closer than previously recorded, and suggest that the very low uniformity of cell distribution in the flasks was having a significant effect on the calculated means.

The final mean confluency of the flasks is 75% of the mean confluency before the medium exchange, and the mean standard deviation remains similar (the mean of the standard deviations between images of a specific culture flask is 13%) (Figures 4.5 and 4.6). The final mean confluency of the culture devices is 79% of the confluency before the medium exchange, and the mean of the standard deviations is higher at 40% (Figures 4.5 and 4.6). This suggests that the medium exchange removes a lower fraction of cells in the microfabricated culture device but that cells are removed less uniformly. The reduced fraction of cells removed may be due to the steep fluid velocity gradients caused by the close proximity of the chamber walls. The low velocity areas near the chamber walls may protect more loosely adhering cells. Similarly, more cells are removed in the high velocity area immediately adjacent to the pipette tip. As these high and low velocity areas are also significant fractions of the culture area, this would also explain the decrease in uniformity. The larger culture area of the flasks results in shallower velocity gradients, and the low velocity areas

near the walls and high velocity area near the tip are much smaller fractions of the culture area.

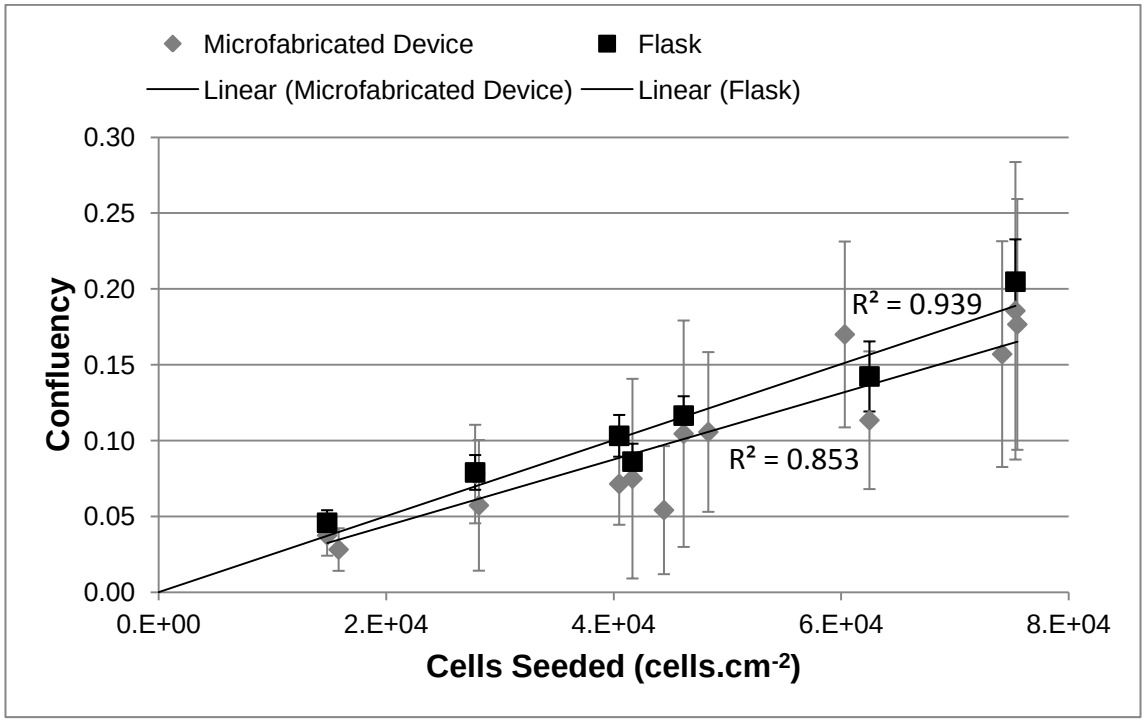

Figure 4.7 - The results of experiments, using an improved methodology, to investigate post-seeding confluency as a function of seeding cell density.

The average confluencies of culture flasks and improved culture devices after 6 hours of incubation and a medium exchange. The confluencies were investigated for different densities of seeded cells, with the same cell suspension used to seed 3 flasks and 3 culture devices. Error bars show the standard deviation of all images of the same vessel type seeded from the same suspension (n=60 images). Displayed on the figure are linear trend lines through the origin and their respective R^2 values.

The same range of seeding densities was investigated again, using the technique outlined above to distribute cells more uniformly in the flasks. Figure 4.7 shows the results of these experiments as well as the microfabricated device results from the previous experiments. Results with the improved method show that a specific density of seeded cells will result in a similar confluency of attached cells, in both culture systems, following the 6 hour incubation period. Furthermore, there is a more linear relationship (R^2 = 0.939 compared to previous value of 0.667) visible between the density of cells seeded and the confluency of attached cells in the flask (Figure 4.7). The mean of the standard deviations in confluency between images of the same flask is reduced to 14% (Figure 4.4), and the mean of the standard deviations, between

the mean confluencies of flasks seeded from the same cell suspension, is reduced to 6% (Figure 4.4). The additional experiments with the microfabricated culture device have minimal effect on their standard deviations, which are 47% and 17% respectively.

The results show that seeding the same density of mouse embryonic stem cells, in a microfabricated culture device and in a T-25 culture flask, will result in a similar confluency of attached cells after a 6 hour incubation period. Therefore, this parameter can be maintained when translating processes between the two systems. This result also implies that significant quantities of cells are not forced into the channels of the microfabricated culture device and that the device does not have a significant impact on the attachment process or cell viability over this period. This supports the microfabricated culture devices suitability for adherent cell culture. Figure 4.7 also shows that the mean confluency achieved with a particular density of seeded cells is repeatable. It is therefore possible for repeat experiments to start at the same mean confluency making them more comparable.

The significant difference in results, resulting from the change in methodology to better distribute cells, highlights the high levels of variability that can be introduced in manually operated culture systems. Care must be taken to minimise such variations, as they may lead to similar variations in culture outcome throughout the culture vessel. It is not obvious how the uniformity of seeding can be increased in the microfabricated culture devices. The low volume of the chamber makes mixing in the chamber ineffective, as the near proximity of the chamber walls creates high velocity gradients. If the lack of uniformity persists beyond the early stages of culture, then a new seeding technique may need to be developed to minimise variation within the device.

4.3.2 Perfusion Culture of Mouse Embryonic Stem Cells

Initial Experiment

To demonstrate a continued capacity of the improved microfabricated devices to culture ESCs, they were used to expand mouse ESCs with continuously perfused medium. Furthermore, to investigate the effects of specific design changes, three different device configurations were used; with either the prototype or improved PDMS chip (Figure 3.3[a,d]) used in combination with either the open or closed PC component of the new gas permeable lid system (Figure 3.11[b,d]). For the first experiment, the three combinations were; the improved chip with the open PC lid component, the improved chip with the closed PC lid component, and the prototype chip with the closed PC lid component. The experiment utilised the monitoring, gas driven perfusion, and outlet fluidics (capillaries and back pressure regulating waste bottle) of the improved control and automation platform, but not the valves and temperature control systems, which were still under construction. As previously, the target flow rate in each reactor was 300 $\mu l.h^{-1}$, to check for cell retention and survival at extreme flow rates (a factor of 50 higher than a typical medium exchange rate in flask culture).

The improved culture devices with the aluminium holder are much simpler to assemble in a sterile manner than the prototype culture devices (testimony of multiple users within the department). Assembly can also be achieved with a simple hex screwdriver or hex key, rather than a precision torque screwdriver. Time savings are estimated at approximately 60%, or 40 minutes, relative to assembling 3 prototype devices. The assembly of the fluidics remains more challenging, due to the number of connectors that must be tightened and the relatively low flexibility of PEEK tubing. This is an area that would benefit from further improvement. As expected from previous experiments (sections 2.3.5 and 4.3.1), the majority of cells attach to the culture surface after 6 hours of static incubation, allowing medium to be exchanged and perfusion to be initiated.

In the initial experiment, it was observed that too much medium had accumulated in the waste bottle after 16 hours of perfusion culture. This indicated the required pressure was significantly lower than expected from pressure measurements using water and a syringe pump. The voltage to the gas pressure regulator was lowered from 2.24 V to 1 V in an effort to achieve a closer flow rate to the target. After a further 24 hours of culture the medium volume in the waste bottle had not risen significantly and the regulator voltage was increased to 1.5 V. In spite of the variable flow rate, cells were retained, and survived and proliferated. Devices two and three surpass 90% confluence after less than 48 hours of perfusion culture (Figure 4.8). The uneven illumination caused by the open PC lid component of device one over expose some images affecting image processing. Auto-exposure was used for subsequent experiments to avoid this issue. Culture with perfused medium was continued for 92 hours but the cells were not stained due to the variable and unmeasured flow rate.

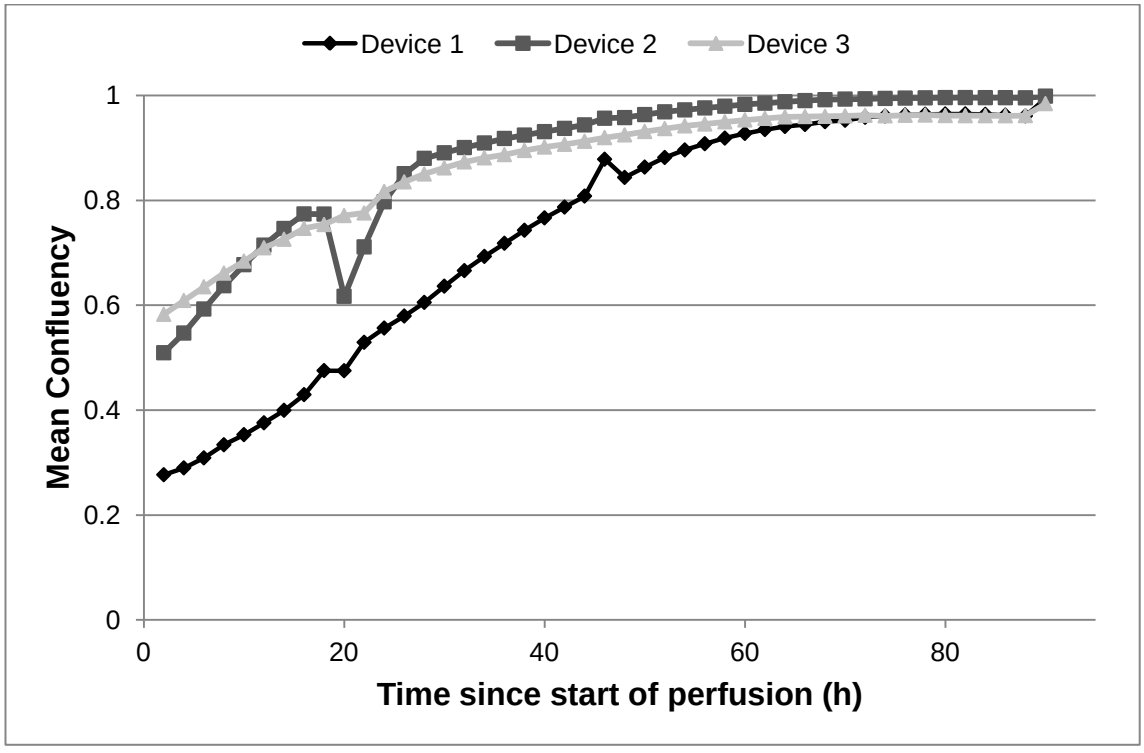

Figure 4.8 – Confluence curves for each device in the initial perfusion culture experiment.

Following 6 hours of static culture to allow seeded cells to settle and adhere, medium was perfused through the three culture devices for 92 hours with a target combined flow rate of 900 $\mu l.h^{-1}$. The confluence of all three device configurations is shown over the duration of medium perfusion. Device 1 used the improved PDMS chip with the open PC lid component. Device 2 used the improved PDMS chip with the closed PC lid component. Device 3 used the prototype PDMS chip with the closed PC lid component.

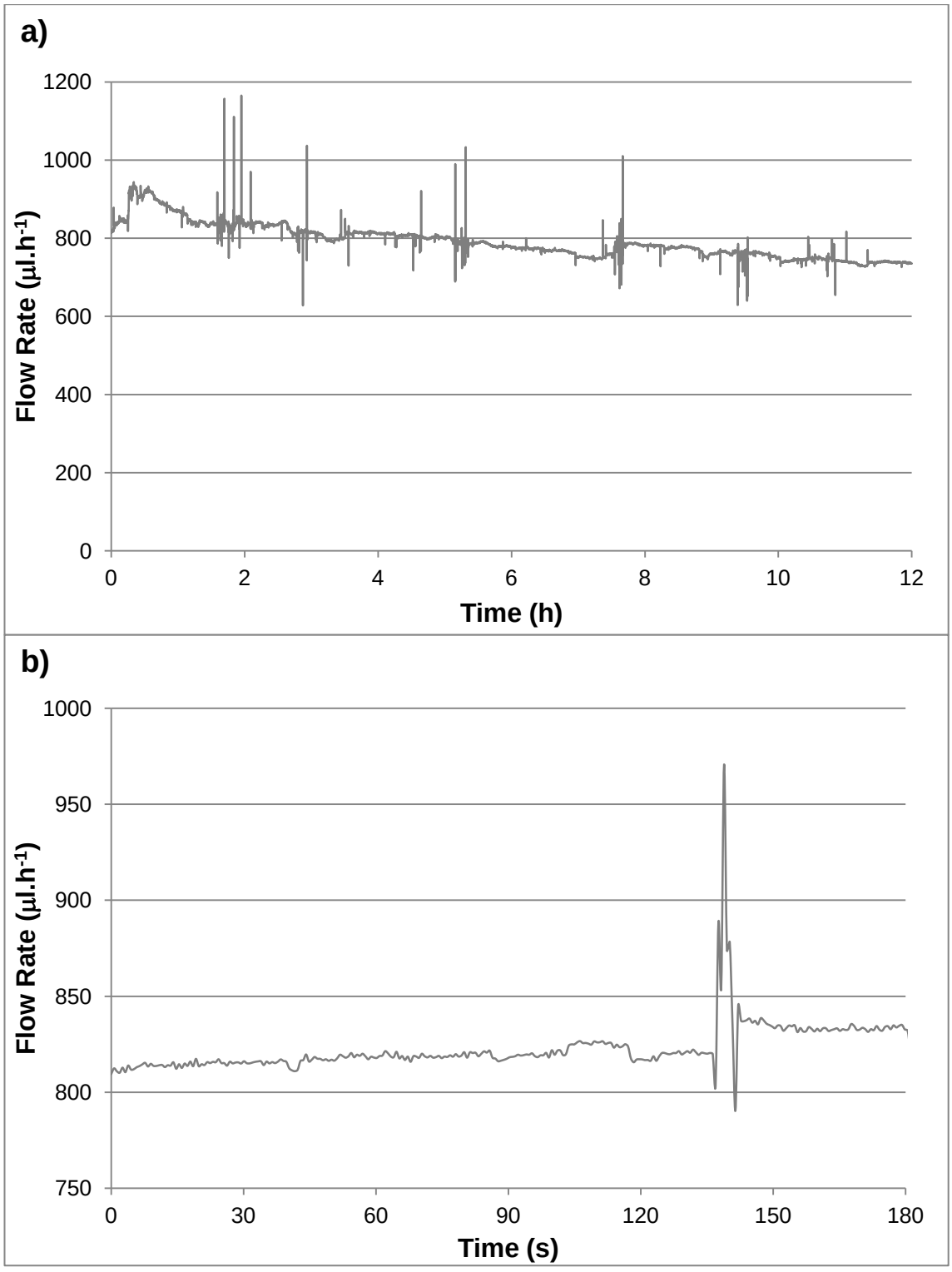

Figure 4.9 - Flow rate at the combined inlet of three culture devices with a constant pressure regulator voltage.

Graphs showing the flow rate measured at the combined inlet of three culture devices, with a constant pressure regulator voltage of 1.2 V. Graph [a] shows a 12 hour period of culture, with points every 6.4 seconds, while pane [b] shows the first 180 seconds of that same period with points every 0.64 seconds.

A repeat experiment, with a flow sensor included at the inlet, indicated that the flow resistance of the culture system is highly variable during a culture

experiment. Figure 4.9 shows the variation in flow rate, while applying the same driving gas pressure, over different time scales. The reason for the variation in flow rate is unclear. The precision of the pressure regulator is the most likely source of the small variations seen in the flow measurements (Figure 4.9[b]). More uniform flow may be achievable with a higher quality regulator.

Spikes in flow rate (Figure 4.9[a,b]) are most likely due to either small bubbles passing through the flow sensor or temporary flow obstructions, such as detached cells in the capillaries or bubbles anywhere in the flow path. Detached cells in the capillaries could be avoided if the capillaries were moved upstream of the culture chamber. However, the back pressure at the outlet would need to be increased to force out bubbles formed as pressure drops along the capillaries. Bubble formation appears minimal in the current configuration, and may be reduced further with the introduction of the combined preheat and bubble trap unit (section 3.3.7).

The gradual increase in flow resistance, over the long term (Figure 4.9[a]), may be caused by fouling of the capillaries by medium components. Fouling is difficult to avoid but, if the length of the capillaries could be reduced, the effects of fouling may be minimised. Reducing the length of the capillaries would be possible if the flow resistance of different culture devices was more consistent. This consistency could potentially be achievable by using a single device design mass produced by a technique such as injection moulding or hot embossing (as discussed in chapter 5).

Integration of Flow Control

To compensate for the changing flow resistance of the system, proportional-integral flow rate control was added to the LabVIEW VI that had been developed as part of the improved control and automation platform. Derivative control was not used as it is not appropriate for systems with noise. The VI allows regulator pressure to be adjusted by the proportional-integral routine, in order to maintain the combined flow rate of the three devices at a setpoint. A ‘bias’ setting is included to set the initial regulator pressure, while a

'deadband' setting prevents excessive controller action. The frequency of measurements and the number of measurements averaged per control action can be adjusted to reduce measurement noise. The proportional and integral control terms can also be easily adjusted through the user interface. The proportional integral routine used the following algorithm;

$$Regulator\,Voltage = Bias + Kp \times \left(error + \int_0^t \frac{error}{Ti}\, dt \right) \qquad (4.3)$$

Where *Kp* is the proportional term, *Ti* is the integral term, and *error* is equal to the current flow rate subtracted from the flow rate setpoint. If the controller output exceeds the upper or lower limit of the regulator (0-5 V), the integrated error term is adjusted to compensate. When the flow rate falls within the deadband, the bias is adjusted to the current regulator voltage and the integrated error term is set to zero. No further control action takes place until the flow rate moves outside the deadband.

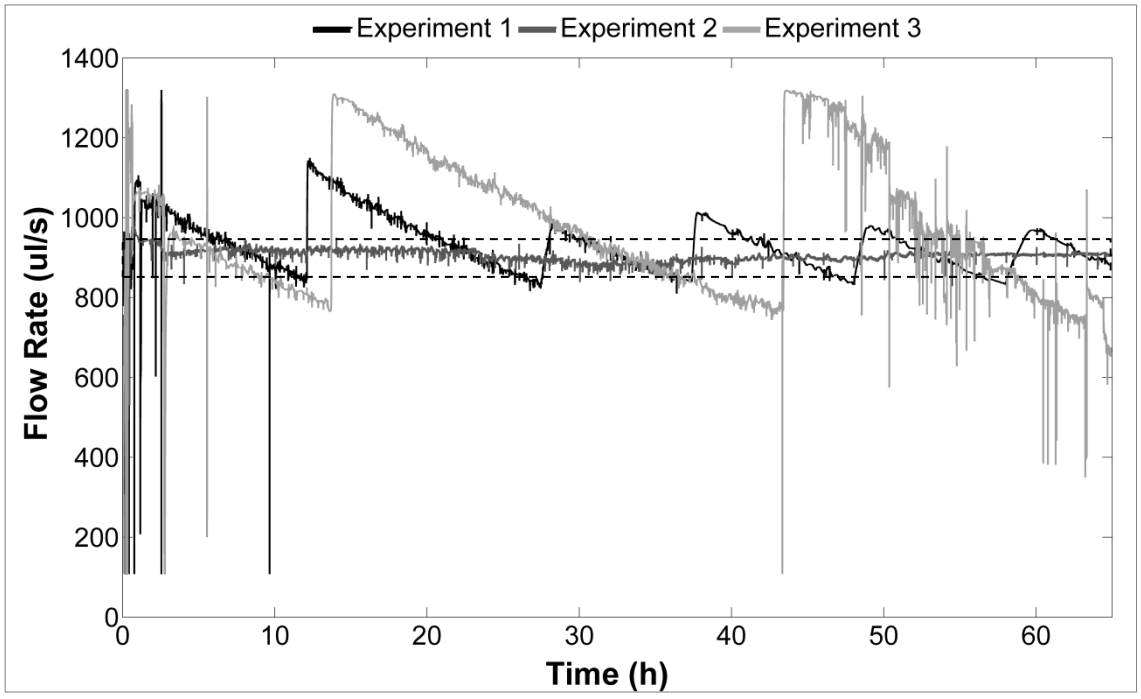

Figure 4.10 - Measured flow rate, at the combined inlet for three culture devices, over the duration of three perfusion culture experiments.

This figure shows measurements of the medium flow rate, taken every 0.2 seconds, over the duration of three perfusion experiments. The flow rate is measured at the combined inlet of three parallel culture devices. The flow rate is shown for three perfusion culture experiments all of which had a flow rate setpoint of 900 µl.h^{-1}. The dashed lines show the upper and lower limits of the dead band.

The proportional-integral flow rate control routine was used for three subsequent culture experiments. The set point for all three experiments was 900 $\mu l.h^{-1}$, with a dead band of ± 45 $\mu l.h^{-1}$, a sampling rate of 5 Hz, and 20 points averaged per controller action. The values of *Kp* and *Ti* were changed between experiments in an attempt to optimise flow rate stability. They were 0.35 $mV.h.\mu l^{-1}$ and 30 s in experiment 1, 0.25 $mV.h.\mu l^{-1}$ and 200 s in experiment 2, and 0.35 $mV.h.\mu l^{-1}$ and 200 s in experiment 3. Figure 4.10 shows the recorded flow rates for the three experiments. The second experiment had the most consistent flow rate but this may be due to the initial flow rate rather than the values of *Kp* and *Ti*.

It is challenging to implement an effective flow routine due to the differing response times of positive and negative control actions. Increases in regulator voltage have a relatively rapid effect, as the driving pressure can be increased in a matter of seconds. Conversely, decreases in regulator voltage have a very slow effect, as pressure is relieved by the gradual flow of medium. This disparity is seen in the rapid rises and slow decays of flow rate in experiments one and three (Figure 4.10): As the initial flow rates (1090 $\mu l.h^{-1}$ and 1060 $\mu l.h^{-1}$ 60 minutes after the start of perfusion for experiments one and three respectively) are higher than the upper limit of the deadband, and the response to reducing regulator voltage is slow, the regulator voltage reduces too far before the flow rate drops into the deadband. Therefore, when the flow rate enters the deadband the controller bias is set to the now very low controller output. Consequently, the pressure continues to drop below the setpoint and the system then over reacts causing the flow rate to spike above set point again. This did not occur in the second experiment, where the initial flow rate was very close to the set point (947 $\mu l.h^{-1}$ 60 minutes after the start of perfusion).

Logically, the *Kp* value could be decreased, to reduce the magnitude of the initial controller response, and the *Ti* value could be significantly increased, to reduce the rate at which the integrated error increases the magnitude of the control action. This would reduce oscillation at the cost of slower recovery from disturbances. Alternatively, different *Kp* and *Ti* values could be used for positive and negative error values to allow for the non-symmetrical control action. These

options were considered and are listed here for completeness. However, the challenge of this non-symmetrical control action will be overcome by the valve system of the improved control and automation platform. The improved platform includes a normally closed valve, attached to the bubble trap, which can be opened to rapidly relieve pressure. Accordingly, none of the listed changes may be necessary.

Triplicate Culture Experiments

The three experiments with flow control used different combinations of parts to the initial experiment. The three combinations were; the prototype chip with the open PC lid, the prototype chip with the closed PC lid, and the improved chip with the closed PC lid component. This allowed separate investigation of the open PC lid component and the improved PDMS chip, both of which were expected to improve uniformity relative to a closed PC lid and prototype PDMS chip. As previously, the seeded cells were allowed to attach over a 6 hour static incubation before changing the medium and beginning perfusion. The cells were cultured for a further 65 hours with phase contrast images taken every two hours. At the end of this period the phase contrast images were analysed using image processing software developed by Nicolas Jaccard (Jaccard et al., 2014b, Reichen et al., 2012). The cells were fixed and stained for pluripotency markers.

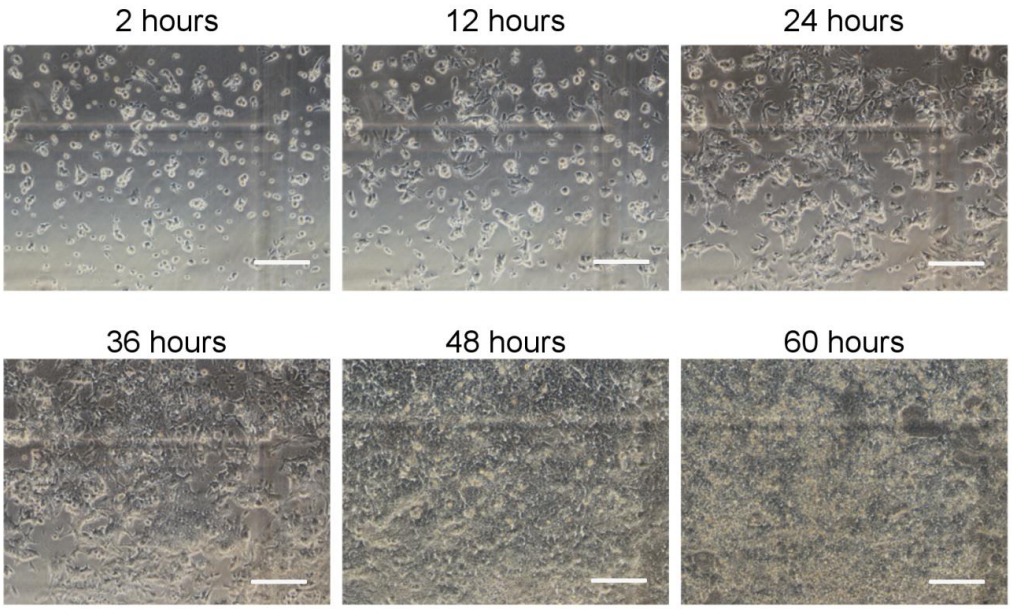

Figure 4.11 - Representative phase contrast microscope images of cells in culture device 1 throughout the course of the first culture experiment.

Representative phase contrast microscope images are shown for device 1 in the first of three repeat perfusion culture experiments. Device 1 included a gas permeable lid system with an open PC element and the prototype PDMS chip. Images are shown at 12 hour intervals after the start of perfusion as well as the first set of images taken at the 2 h mark. Images were taken with a 10× objective and the scale bars are 200 μm.

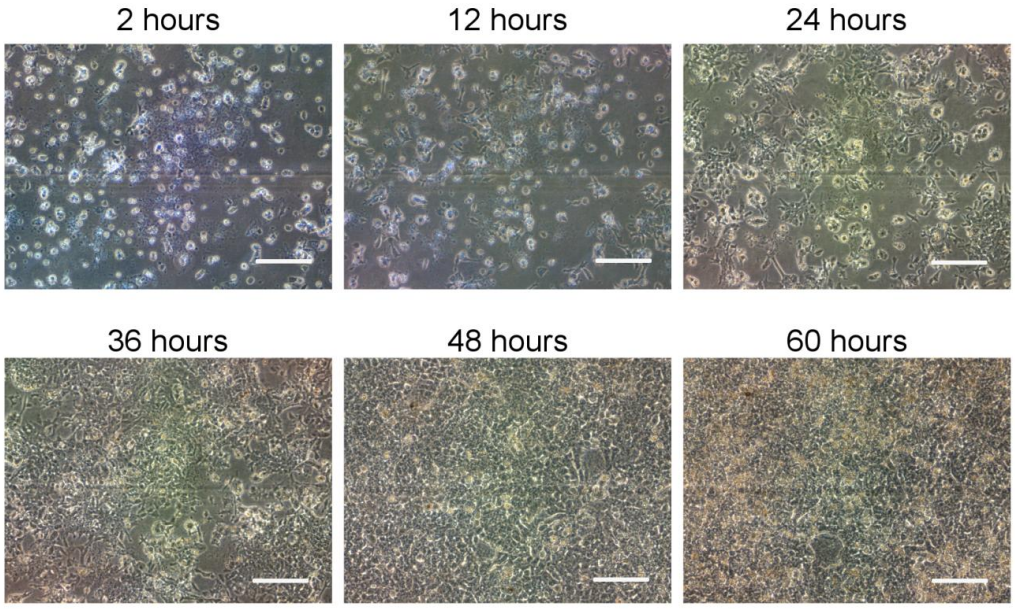

Figure 4.12 - Representative phase contrast microscope images of cells in culture device 2 throughout the course of the first culture experiment.

Representative phase contrast microscope images are shown for device 2 in the first of three repeat perfusion culture experiments. Device 2 included a gas permeable lid system with a closed PC element and the prototype PDMS chip. Images are shown at 12 hour intervals after the start of perfusion as well as the first set of images taken at the 2 h mark. Images were taken with a 10× objective and the scale bars are 200 μm.

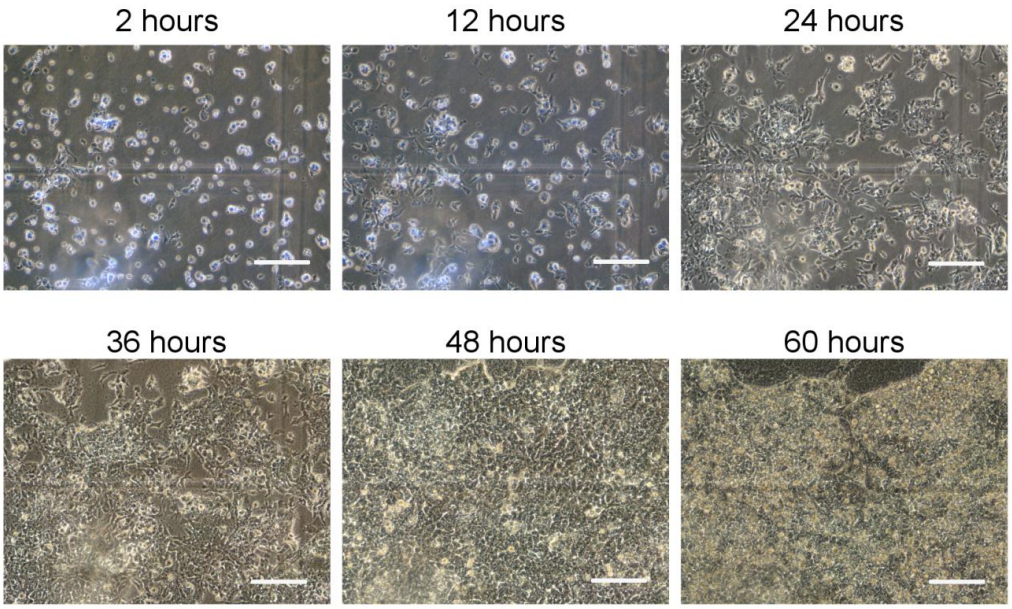

Figure 4.13 - Representative phase contrast microscope images of cells in culture device 3 throughout the course of the first culture experiment.

Representative phase contrast microscope images are shown for device 3 in the first of three repeat perfusion culture experiments. Device 3 included a gas permeable lid system with a closed PC element and the improved PDMS chip. Images are shown at 12 hour intervals after the start of perfusion as well as the first set of images taken at the 2 h mark. Images were taken with a 10× objective and the scale bars are 200 μm.

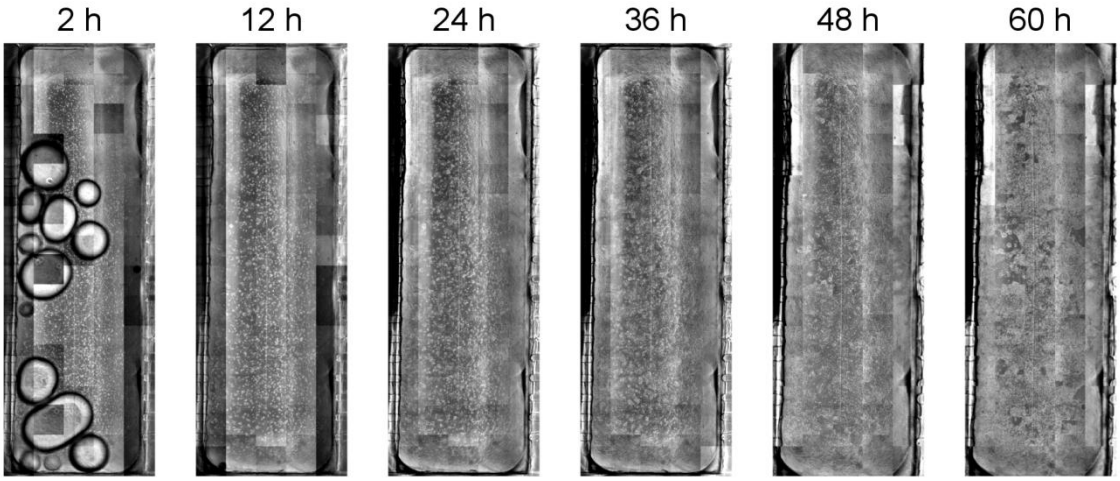

Figure 4.14 - Stitched images of the whole culture chamber of culture device 1 throughout the course of the first culture experiment.

Images of the whole culture chamber of culture device 1 stitched together from individual phase contrast microscope images are shown for the first of three repeat perfusion culture experiments. Device 1 included a gas permeable lid system with an open PC element and the prototype PDMS chip. Images are shown at 12 hour intervals after the start of perfusion as well as the first set of images taken at the 2 h mark. Individual images were taken with a 10× objective. The direction of flow is left to right.

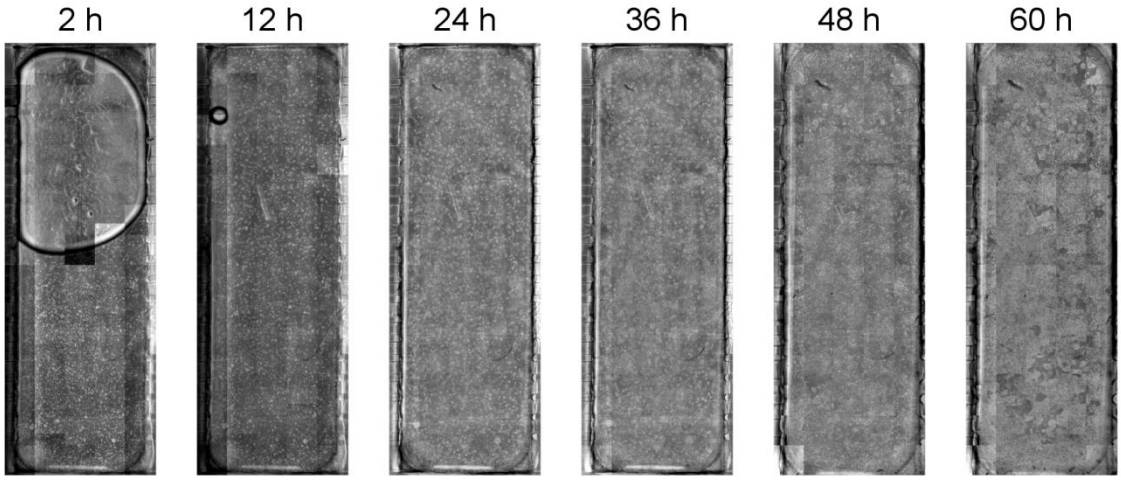

Figure 4.15 - Stitched images of the whole culture chamber of culture device 2 throughout the course of the first culture experiment.

Images of the whole culture chamber of culture device 2 stitched together from individual phase contrast microscope images are shown for the first of three repeat perfusion culture experiments. Device 2 included a gas permeable lid system with a closed PC element and the prototype PDMS chip. Images are shown at 12 hour intervals after the start of perfusion as well as the first set of images taken at the 2 h mark. Individual images were taken with a 10× objective. The direction of flow is left to right.

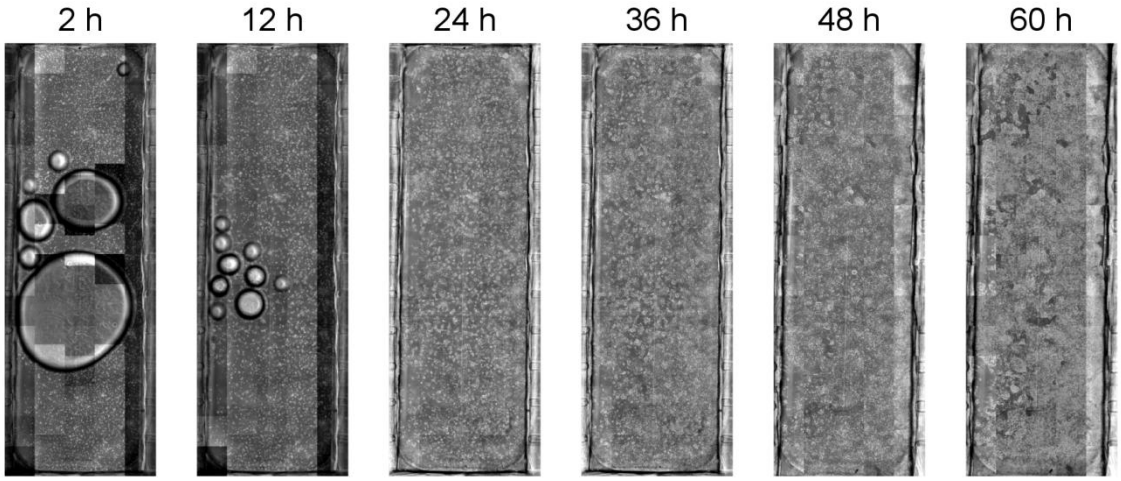

Figure 4.16 - Stitched images of the whole culture chamber of culture device 3 throughout the course of the first culture experiment.

Images of the whole culture chamber of culture device 3 stitched together from individual phase contrast microscope images are shown for the first of three repeat perfusion culture experiments. Device 3 included a gas permeable lid system with a closed PC element and the improved PDMS chip. Images are shown at 12 hour intervals after the start of perfusion as well as the first set of images taken at the 2 h mark. Individual images were taken with a 10× objective. The direction of flow is left to right.

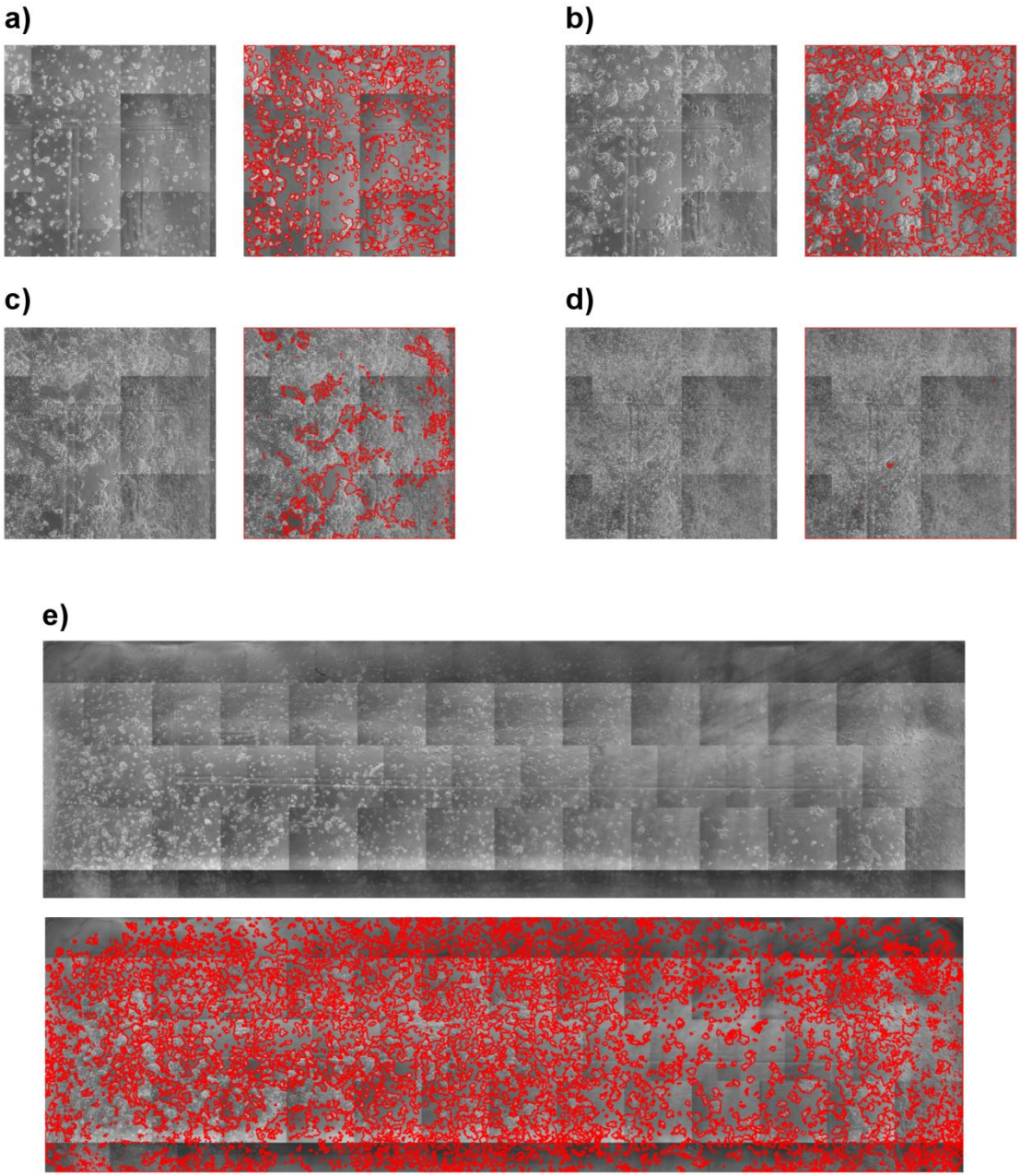

Figure 4.17 - Examples of pixel classification by image processing software.

Raw images side-by-side with images showing (in red) the border between pixels classified as cells and pixels classified as background. The first four images [a-d] show single elements (350×350 μm) of the 36×10 grid at 2 [a], 12 [b], 22 [c], and 32 [d] hours after the start of medium perfusion. The final pair of images [e] shows the entire culture chamber 12 hours after the start of medium perfusion. All images are from the first device (open PC lid component and prototype PDMS chip) in the third experiment.

Figures 4.11 - 4.13 show representative phase contrast microscope images from the three culture devices, in the first experiment, at 12 hour intervals. Images were taken using a 10× objective. For each culture device, one chosen image position is shown at each time point. Likewise, Figures 4.14 – 4.16 show the entire culture chamber of each device at 12 hour intervals. These images

have been stitched together from multiple microscope images taken using a 10× objective. A few gaps were present in images of the second experiment. Due to overly rapid entry of the imaging positions, the same position was imaged twice and the next position was skipped. Finally, Figure 4.17 shows examples of image processing outputs.

Figures 4.11 - 4.16 show the expansion of mESCs over the duration of the culture experiment, through full confluency, into multilayer culture. mESC are typically cultured statically in T-flasks for 72 hours between passages. However, the culture devices reach full confluency well before the completion of culture (6 hours static and 65 hours perfused). This shows that the constant replenishment of nutrients and removal of secreted molecules achieved in perfusion culture significantly increases the growth rate of mESCs. This increased average growth rate with more frequent (continuous) medium exchange is consistent with static culture experiments in 6-well plates (Jaccard et al., 2014a). Finally, Figure 4.17 shows that the image processing software accurately classifies the majority of pixels as cell or background. The generated confluency measurements can therefore be used to further analyse cell growth.

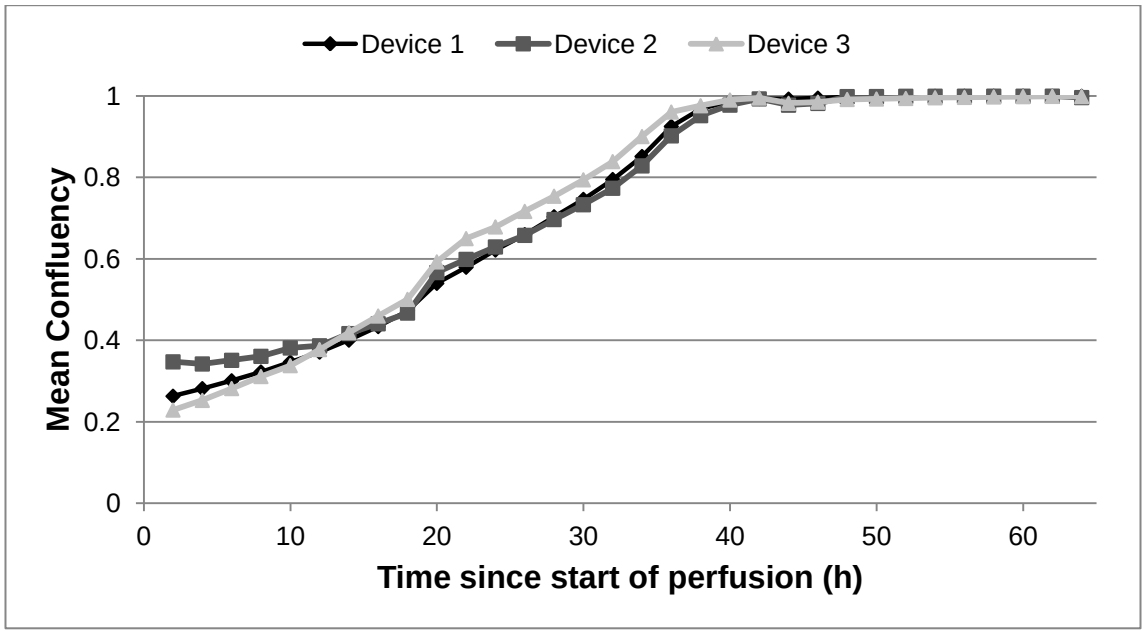

Figure 4.18 - Mean culture surface confluency of each culture device through the first of three perfusion experiments.

The mean confluency of the entire culture surface is plotted against time for each device in the first of three repeat perfusion culture experiments. Device 1 included a gas permeable lid system with an open PC element while the other two devices included closed PC components. Device 3 included the improved PDMS chip while the other two devices included the prototype PDMS chip.

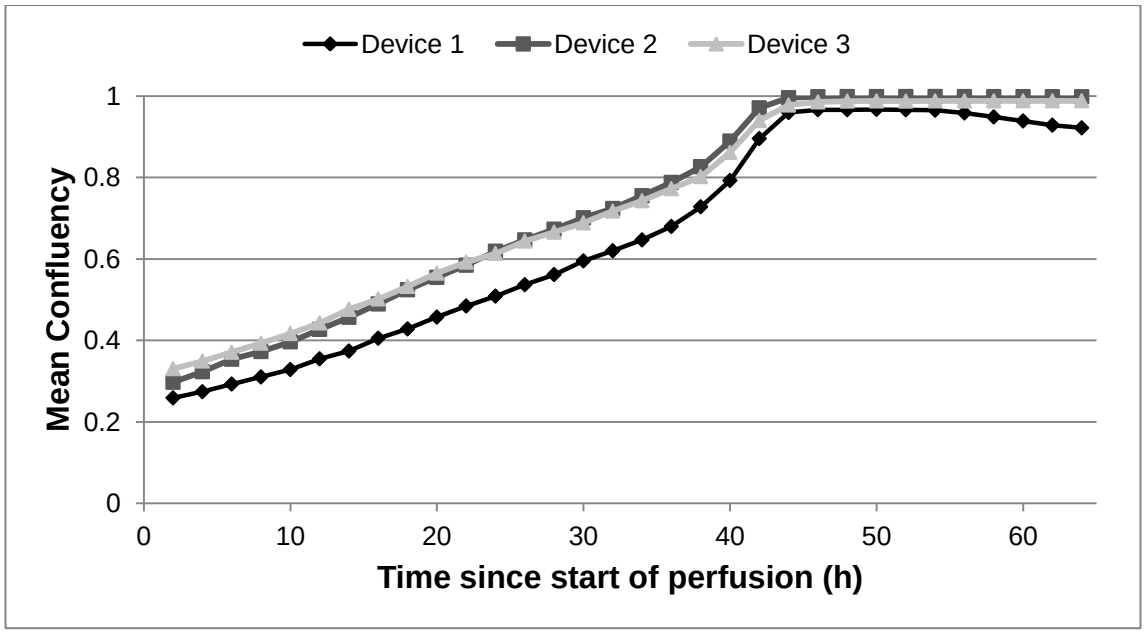

Figure 4.19 - Mean culture surface confluency of each culture device through the second of three perfusion experiments.

The mean confluency of the entire culture surface is plotted against time for each device in the second of three repeat perfusion culture experiments. Device 1 included a gas permeable lid system with an open PC element while the other two devices included closed PC components. Device 3 included the improved PDMS chip while the other two devices included the prototype PDMS chip.

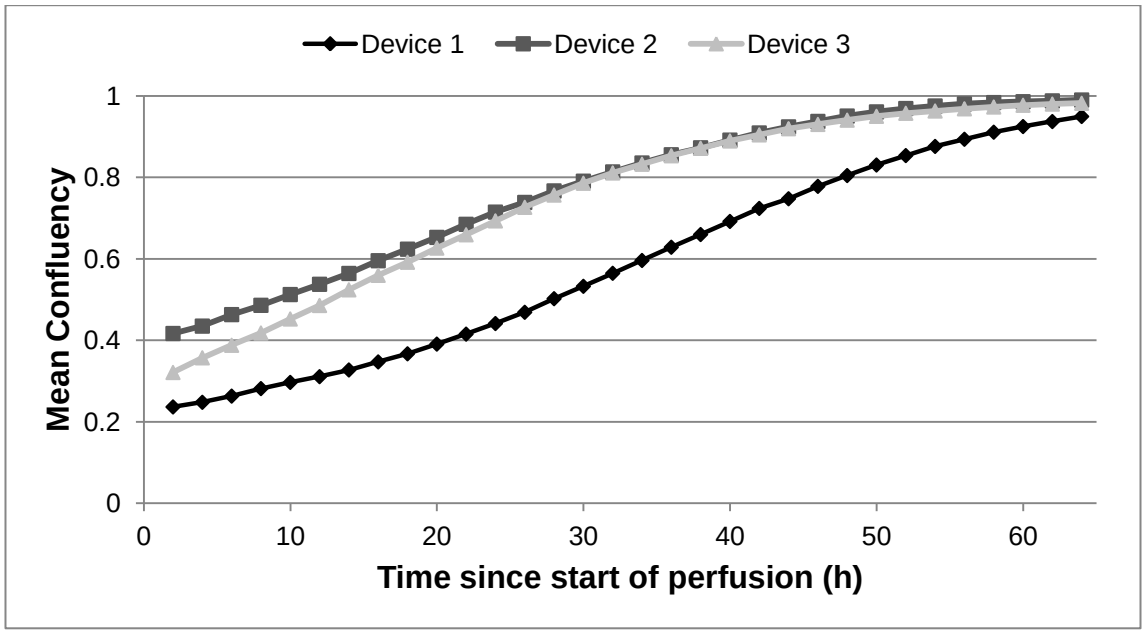

Figure 4.20 - Mean culture surface confluency of each culture device through the third of three perfusion experiments.

The mean confluency of the entire culture surface is plotted against time for each device in the third of three repeat perfusion culture experiments. Device 1 included a gas permeable lid system with an open PC element while the other two devices included closed PC components. Device 3 included the improved PDMS chip while the other two devices included the prototype PDMS chip.

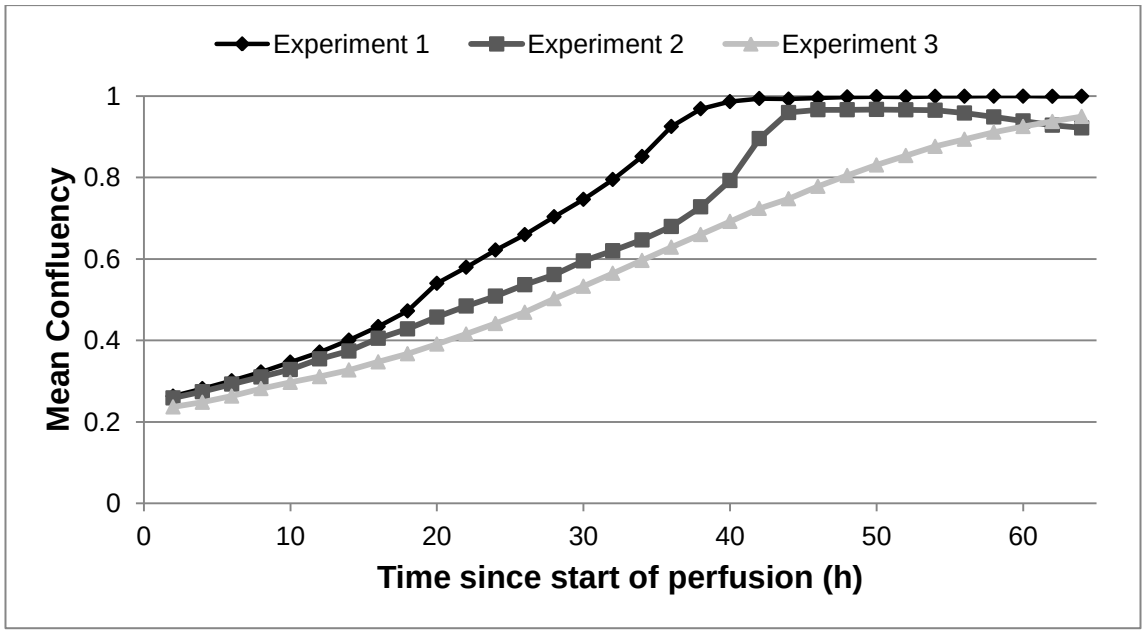

Figure 4.21 - Mean culture surface confluency of culture device 1 through all three perfusion experiments.

The mean confluency of the entire culture surface is plotted against time for device 1 in each of three repeat perfusion culture experiments. Device 1 included a gas permeable lid system with an open PC element and the prototype PDMS chip.

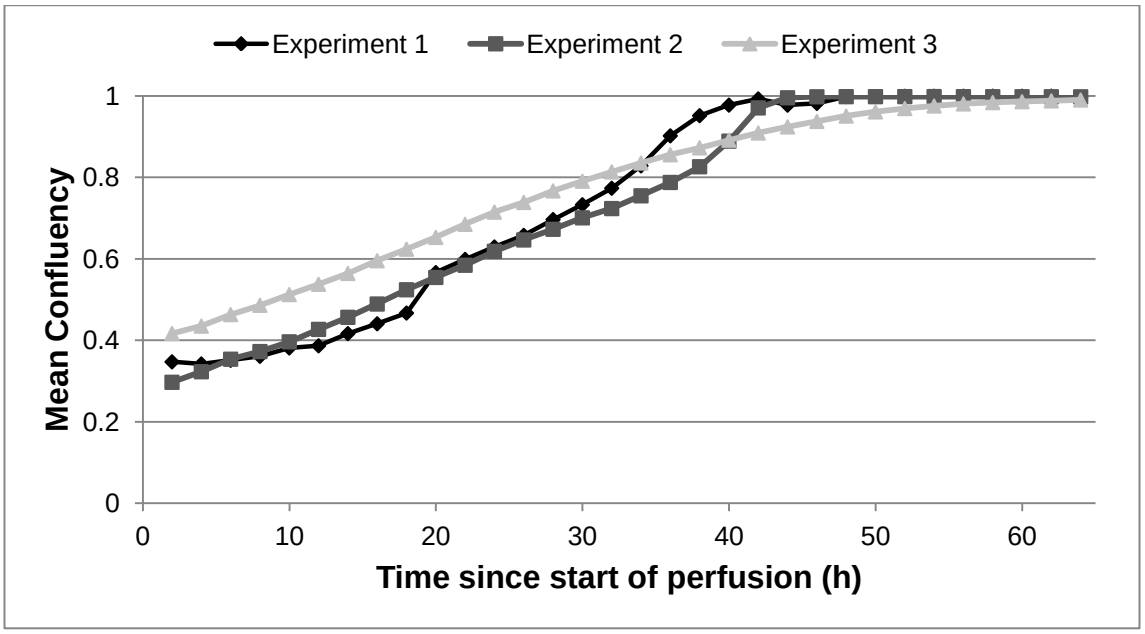

Figure 4.22 - Mean culture surface confluency of culture device 2 through all three perfusion experiments.

The mean confluency of the entire culture surface is plotted against time for device 2 in each of three repeat perfusion culture experiments. Device 2 included a gas permeable lid system with a closed PC element and the prototype PDMS chip.

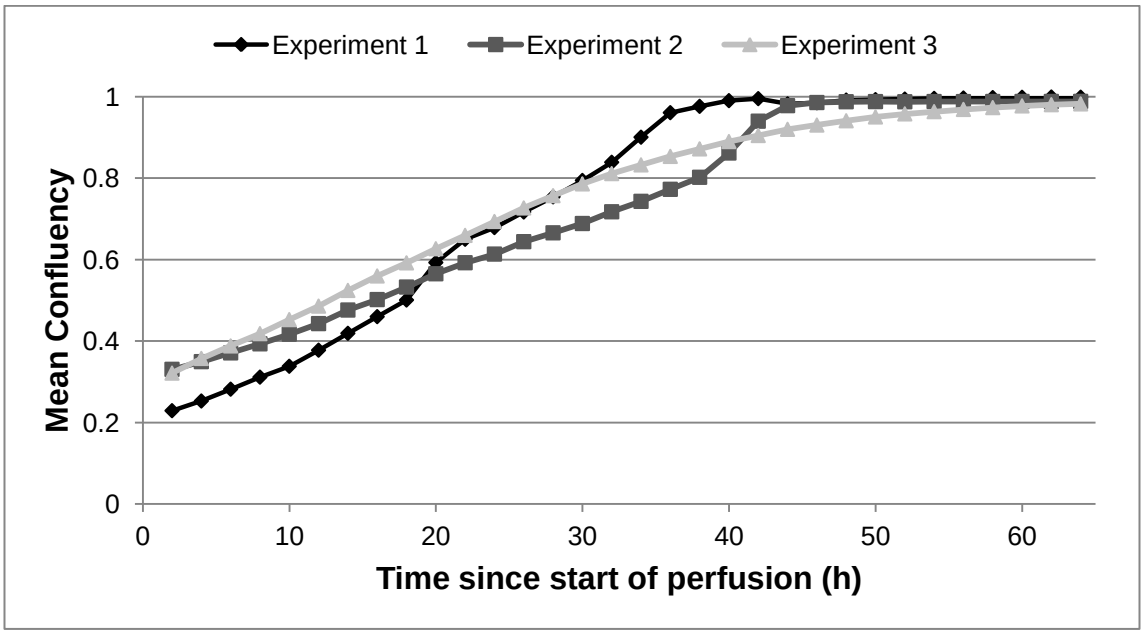

Figure 4.23 - Mean culture surface confluency of culture device 3 through all three perfusion experiments.

The mean confluency of the entire culture surface is plotted against time for device 3 in each of three repeat perfusion culture experiments. Device 3 included a gas permeable lid system with a closed PC element and the improved PDMS chip.

Repeatability

Figures 4.18, 4.19, and 4.20 show the confluency curves, for all three combinations of components, for each experiment respectively. Figures 4.21, 4.22, and 4.23 show the confluency curves, for all three experiments, for each combination of components respectively. Three measurements were calculated from this data as indicators of reproducibility; the confluency at 2 hours (C_2), the time taken to reach a confluency of 0.5 ($T_{0.5}$), and the time taken to reach a confluency of 0.8 ($T_{0.8}$). Confluency at 2 hours indicates the reproducibility of the seeding, lid insertion and initialisation of perfusion. Time to 0.8 is an indicator of reproducibility in average monolayer growth rate. A confluency value of 0.8 is used rather than 1, as cells in some areas may begin multilayer growth prior to other areas reaching full confluency. Time to 0.5 indicates reproducibility in how specific growth rate varies between early and late phase monolayer growth.

The mean C_2 values across all three devices in an experiment are 0.28 ± 0.06, 0.30 ± 0.04, and 0.32 ± 0.09 for the three experiments respectively (Standard deviation, n=3 devices). The standard deviation between the three experiments is 0.02 or 8% of the mean value (n=3 experiments). The mean of the standard deviations between the three devices in each experiment is higher at 21%, close to the variation seen in the seeding experiments in section 4.3.1 (17%).

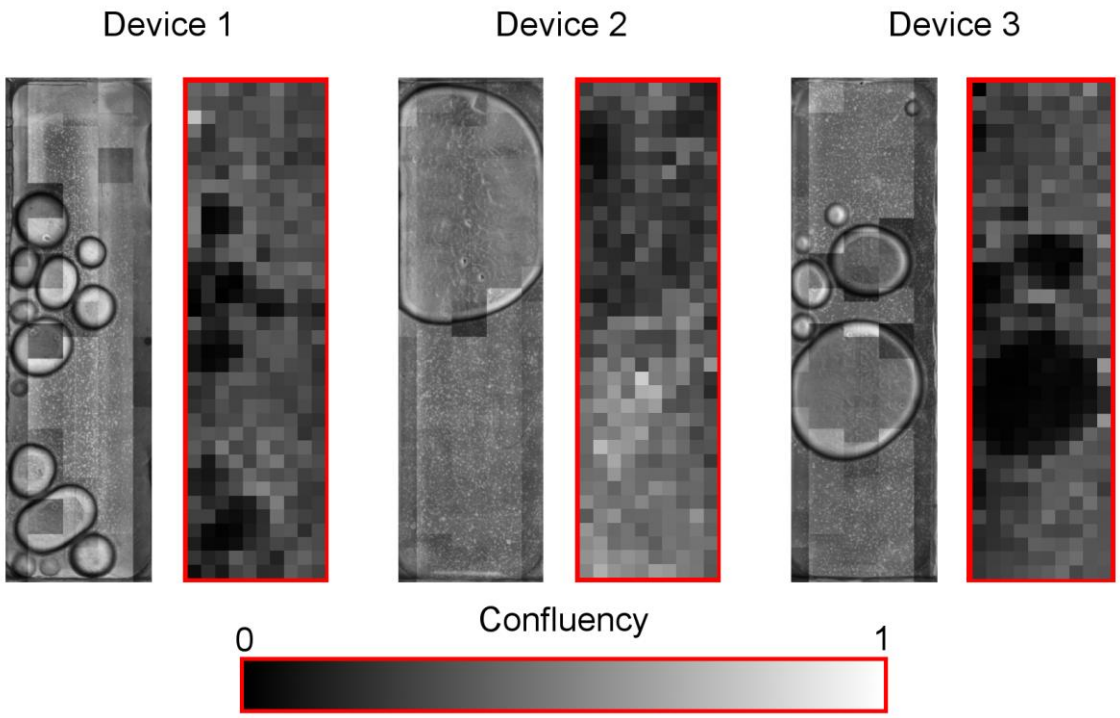

Figure 4.24 – The effect of bubbles on image analysis of early time points.

Stitched phase contrast images, of the three devices in the first experiment, next to grids showing the spatial distribution of confluency based on image analysis. Images were taken 2 h after the start of medium perfusion. Dark low confluency areas on the grids correspond to the bubbles in the culture chamber.

The C_2 values indicate a reasonably repeatable process of seeding, lid insertion, and initialisation of perfusion. However, the C_2 results are affected by bubbles that are present in the chamber at this early stage of perfusion. Bubbles can be trapped during the connection and insertion of parts or originate from incompletely primed channels in the PDMS chip. These bubbles are detected by the image processing software as areas of lower confluency, as seen in Figure 4.24. It takes up to 12 h for bubbles to be completely forced from the culture chamber in some devices. Therefore, confluency data prior to the 12 h point will not be as accurate as data after the 12 h point.

The mean $T_{0.8}$ values are 31 ± 1 h, 37 ± 2 h, and 35 ± 9 h for the three experiments respectively (averaged across the three devices in each experiment). The standard deviation between the three experiments is 3 h. This indicates a variation in average monolayer growth rate, between experiments, of just 9%. The mean of the standard deviations between devices in the same experiment is slightly higher at 12%. The mean $T_{0.5}$ values are 17 ± 1 h, 17 ± 4

h, and 15 ± 9 h for the three experiments respectively (averaged across the three devices in each experiment). The standard deviation between the three experiments is 1 h or 7%. This low variation indicates that a greater fraction of the variation in $T_{0.8}$ comes from late stage monolayer growth than comes from early stage monolayer growth. The mean of the standard deviations in $T_{0.5}$ between devices in the same experiment is 31%.

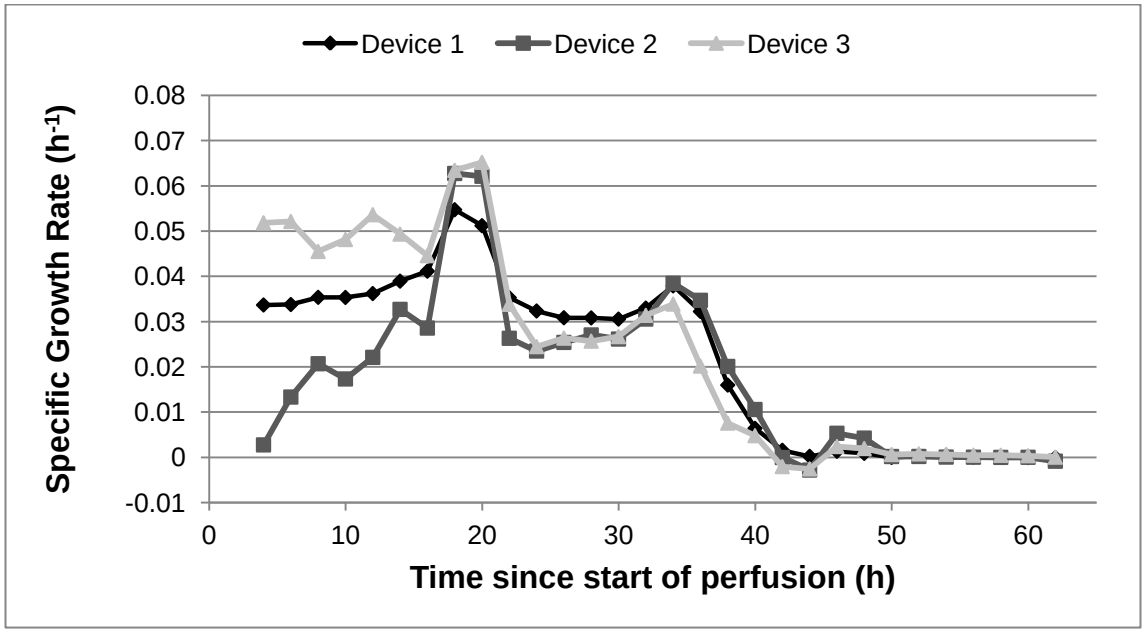

Figure 4.25 - Specific growth rate of each culture device through the first of three perfusion experiments.

The specific growth rate is plotted against time for each device in the first of three repeat perfusion culture experiments. Device 1 included a gas permeable lid system with an open PC element while the other two devices included closed PC components. Device 3 included the improved PDMS chip while the other two devices included the prototype PDMS chip.

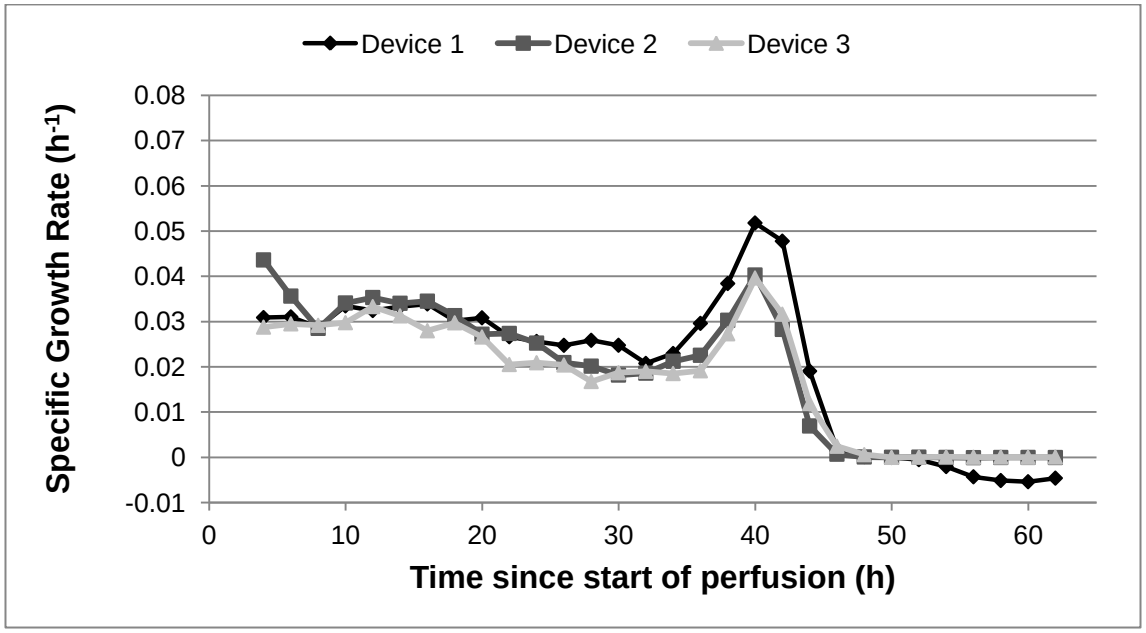

Figure 4.26 - Specific growth rate of each culture device through the second of three perfusion experiments.

The specific growth rate is plotted against time for each device in the second of three repeat perfusion culture experiments. Device 1 included a gas permeable lid system with an open PC element while the other two devices included closed PC components. Device 3 included the improved PDMS chip while the other two devices included the prototype PDMS chip.

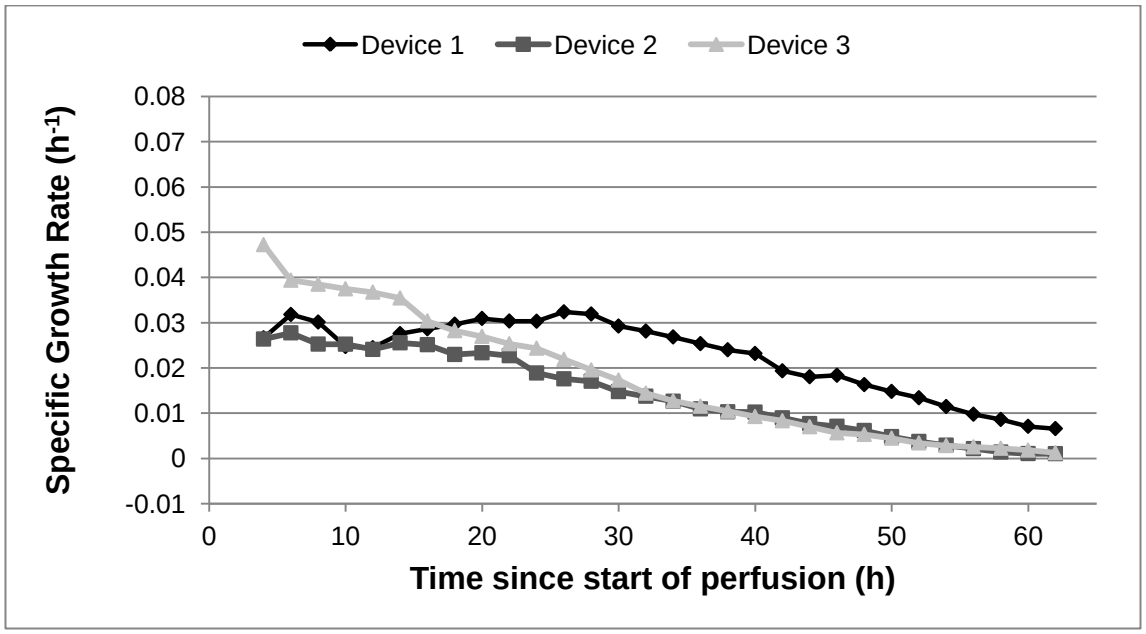

Figure 4.27 - Specific growth rate of each culture device through the third of three perfusion experiments.

The specific growth rate is plotted against time for each device in the third of three repeat perfusion culture experiments. Device 1 included a gas permeable lid system with an open PC element while the other two devices included closed PC components. Device 3 included the improved PDMS chip while the other two devices included the prototype PDMS chip.

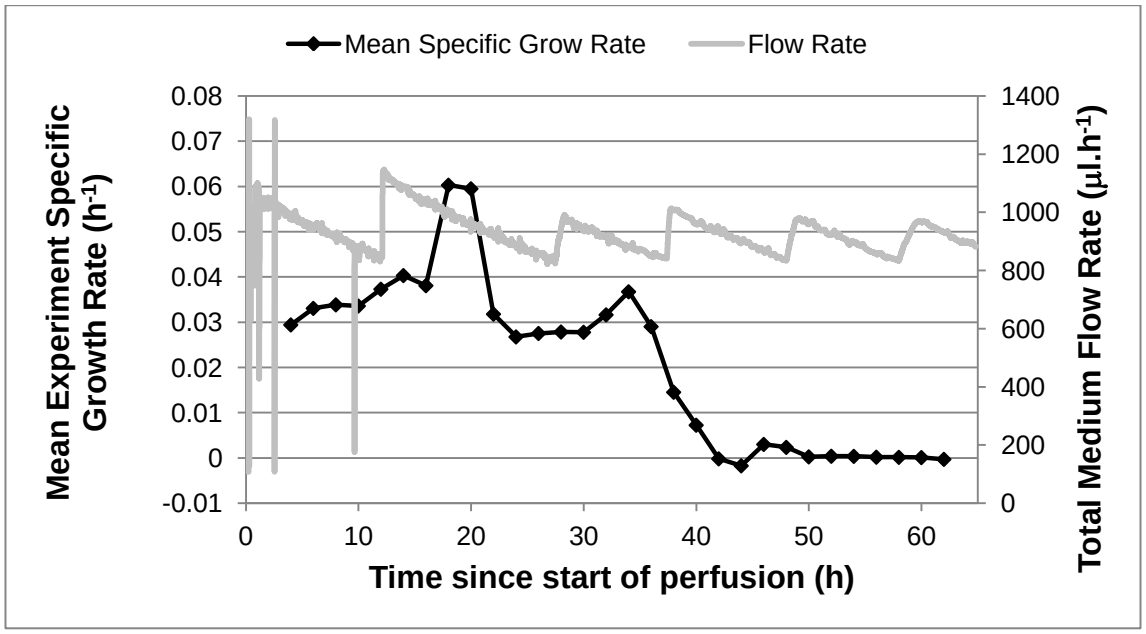

Figure 4.28 - The mean specific growth rate for the first of three perfusion culture experiments plotted alongside the recorded total flow rate.

Plotted on the left axis is the mean specific growth rate of all three devices in the first of three repeat perfusion culture experiments. Plotted on the right axis is the total medium flow rate measured at the combined inlet of the three devices. The flow rate was measured every 0.2 s and then every 40 points were averaged.

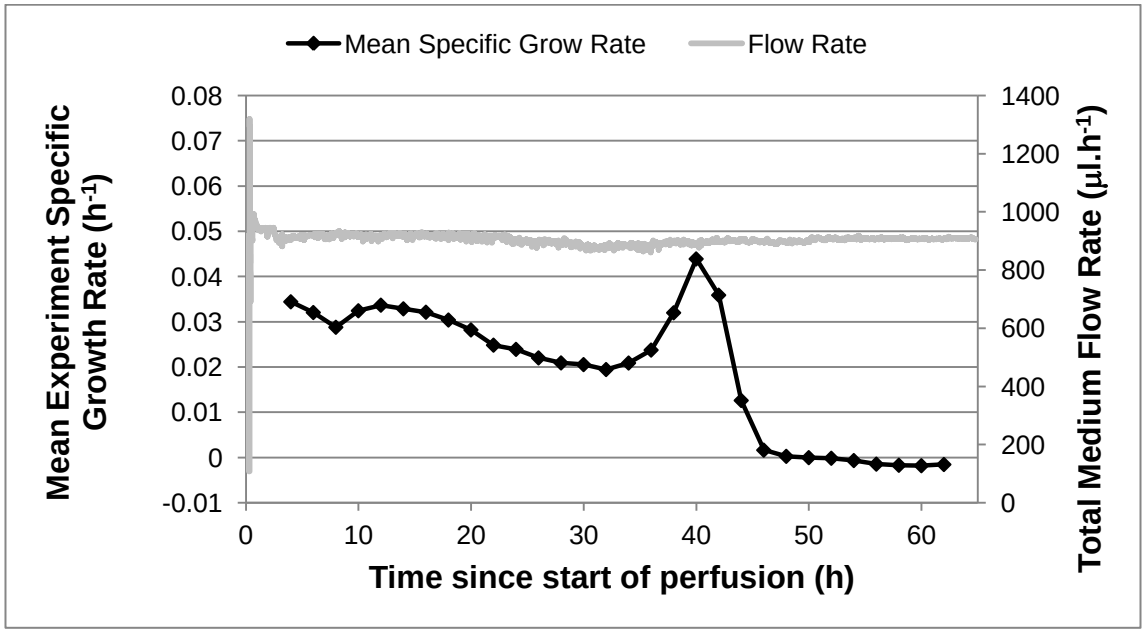

Figure 4.29 - The mean specific growth rate for the second of three perfusion culture experiments plotted alongside the recorded total flow rate.

Plotted on the left axis is the mean specific growth rate of all three devices in the second of three repeat perfusion culture experiments. Plotted on the right axis is the total medium flow rate measured at the combined inlet of the three devices. The flow rate was measured every 0.2 s and then every 40 points were averaged.

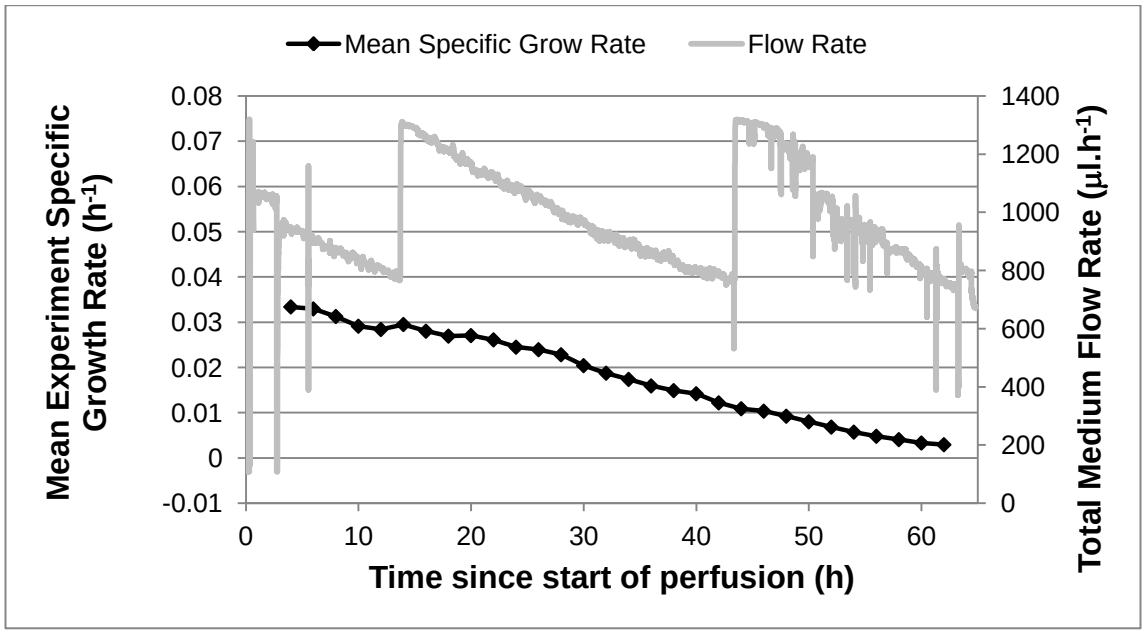

Figure 4.30 - The mean specific growth rate for the third of three perfusion culture experiments plotted alongside the recorded total flow rate.

Plotted on the left axis is the mean specific growth rate of all three devices in the third of three repeat perfusion culture experiments. Plotted on the right axis is the total medium flow rate measured at the combined inlet of the three devices. The flow rate was measured every 0.2 s and then every 40 points were averaged.

It is clear, from Figures 4.18 – 4.23, that variations between experiments have more effect on the shape of the confluency curves than variations in the components used in the devices (PDMS chip design and PC lid component). This is clearer still when considering the specific growth rate (Figures 4.25-4.27). Peaks and troughs in the specific growth rate occur at the same time for all three devices in each experiment. However, these peaks and troughs do not occur at consistent times or confluency points across experiments. It is also clear, from Figures 4.28 - 4.30, that the variations are not correlated with the changes in total medium flow rate. The reasons behind these peaks and troughs in the specific growth rate remain unclear.

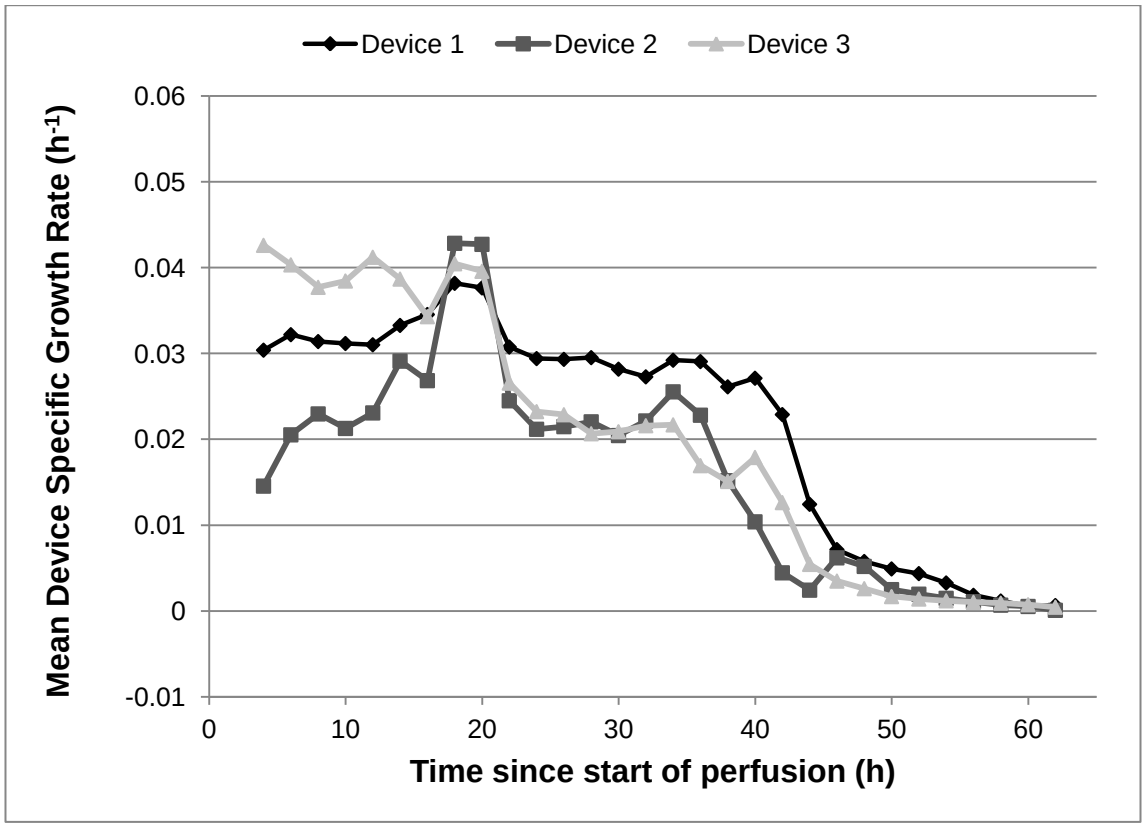

Figure 4.31 – Mean specific growth rates of each culture device across all three perfusion experiments.

The mean specific growth rate is plotted against time, for each device, across all three repeat perfusion culture experiments. Device 1 included a gas permeable lid system with an open PC element while the other two devices included closed PC components. Device 3 included the improved PDMS chip while the other two devices included the prototype PDMS chip.

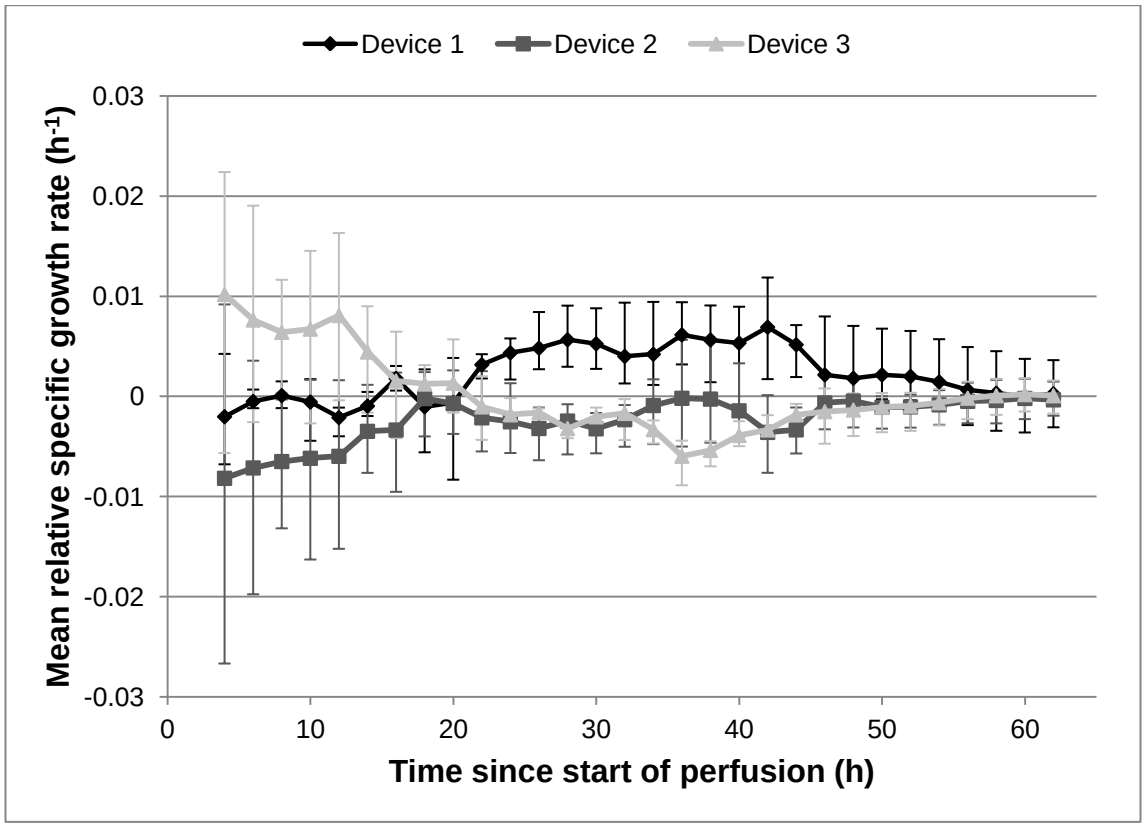

Figure 4.32 - Mean relative specific growth rates of each culture device, across all three perfusion experiments, plotted against culture time.

For each device, in each experiment, the mean specific growth rate of all devices in that experiment, was subtracted from the individual device's specific growth rate to give a relative specific growth rate. For each device, a mean was taken of these relative specific growth rates across the three repeat experiments. The error bars show the maximum and minimum relative specific growth rates for each device at each time point. Device 1 included a gas permeable lid system with an open PC element while the other two devices included closed PC components. Device 3 included the improved PDMS chip while the other two devices included the prototype PDMS chip.

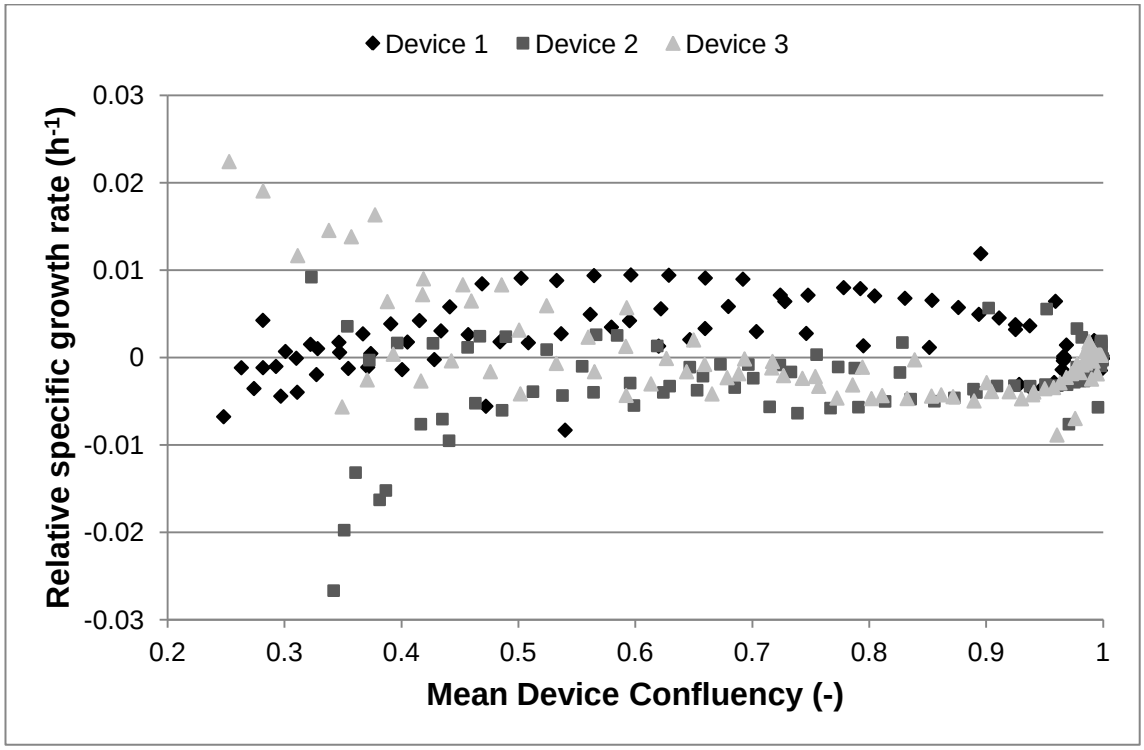

Figure 4.33 - Mean relative specific growth rates of each culture device, across all three perfusion experiments, plotted against mean device confluency.

For each device, in each experiment, the mean specific growth rate of all devices in that experiment, was subtracted from the individual device's specific growth rate to give a relative specific growth rate. For each device, across the three repeat experiments, these relative specific growth rates were plotted against the mean confluency of the culture surface. Device 1 included a gas permeable lid system with an open PC element while the other two devices included closed PC components. Device 3 included the improved PDMS chip while the other two devices included the prototype PDMS chip.

Effect of Different Components

While significant variation exists between experiments, the specific growth rate is also affected by the different components used in the three devices. This is indicated by the mean standard deviations in $T_{0.5}$ (31%) and $T_{0.8}$ (12%) between different devices in the same experiment. Variation is also somewhat evident in Figure 4.31 where the mean specific growth rate across all three experiments is plotted for each device. While the major trends are similar for all three devices there are also variations about these trends. These variations can be made clearer by removing the features specific to experiments. Figure 4.32 shows the mean relative specific growth rates of each device (the mean difference between, the specific growth rate of a device, and the mean specific growth rate of devices in that experiment). Relative specific growth rates are also plotted against mean device confluency in Figure 4.33. As any temporal variations consistent across all devices in an experiment have been removed, remaining trends are most likely caused by the changing cell density.

The results (Figures 4.32 and 4.33) suggest that the third device (improved PDMS chip and closed PC lid component) promotes growth in the early stages of culture (the first 16 hours, or up to a confluency of ~0.45). The first device (prototype PDMS chip and open PC lid component) shows the second highest early growth and the highest specific growth rate from 16 hours, or confluency of ~0.45, to 56 hours, or confluency of ~0.95. The specific growth rate of the second device (prototype PDMS chip and closed PC lid component) is lower than the first device for the first 18 hours, or up to a confluency of ~0.5, after which the relative specific growth rates of the two devices are comparable. After 56 hours (confluency of ~0.95), the specific growth rates of all three devices converge and no observable differences remain.

Increased growth using the gas permeable lid system, with an open, rather than closed, PC component (Device 1), is consistent with expectations. A previous investigation by Powers *et al* (2008) found that gaseous oxygen concentrations of less than 20% reduced the specific growth rate of mESCs grown statically in T-25 culture flasks. The open PC lid component has an increasing effect on the

pericellular DO concentration as confluency increases (section 3.3.6) This effect appears to outweigh the early advantage of the improved PDMS chip partway through monolayer culture (16 hours, confluency ~0.35). The key advantage of the improved PDMS chip over the prototype PDMS chip, is the increased uniformity of flow (section 3.3.1). This may improve specific growth rate in early culture through increased provision of nutrients/removal of waste to/from the central areas of the culture chamber and/or reduced shear at the edges of the chamber.

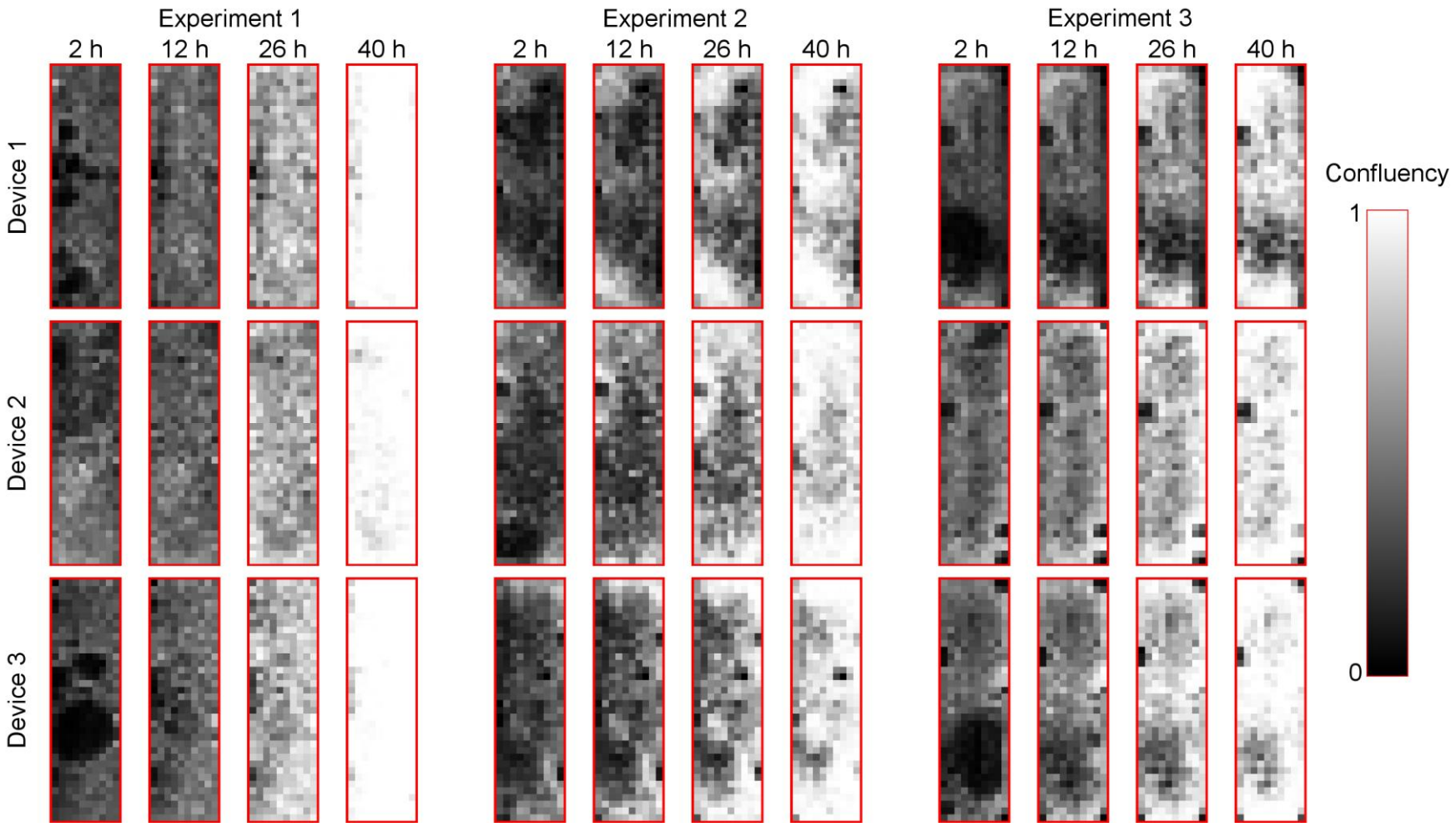

Figure 4.34 - Spatial distribution of confluency, in each culture device, during monolayer growth.

36×10 grids showing the spatial distribution of confluency, in each culture device, during monolayer culture. For each device, the confluency distribution is shown 2, 12, 26, and 40 hours after the start of medium perfusion. Medium flows left to right.

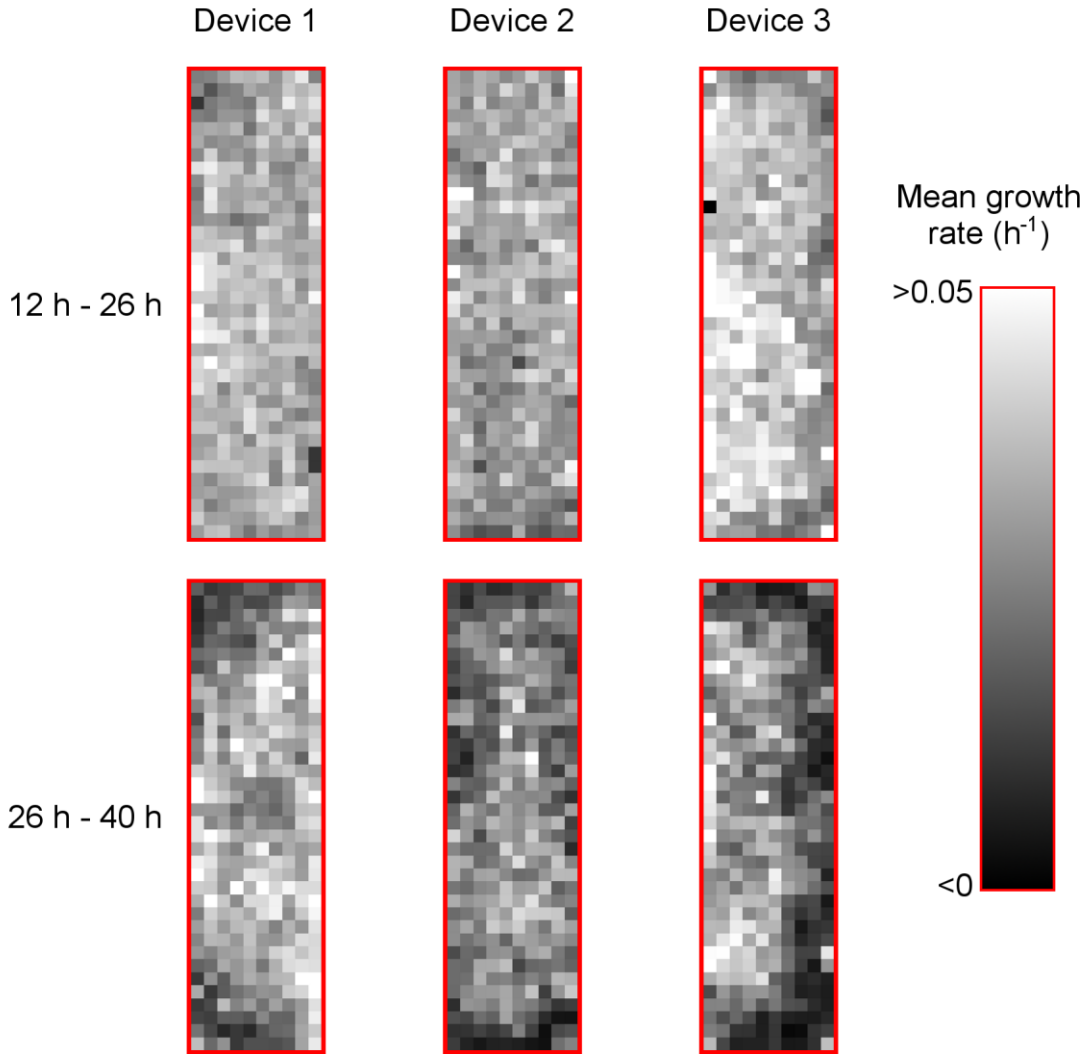

Figure 4.35 - Mean spatial distribution of growth rate for different device configurations.

36×10 grids showing the mean spatial distribution of growth rate for each device configuration. The growth rates are shown for the periods from 12 to 26 h and 26 to 40 h after the start of medium perfusion. Medium flows from left to right. Device 1 included a gas permeable lid system with an open PC element while the other two devices included closed PC components. Device 3 included the improved PDMS chip while the other two devices included the prototype PDMS chip.

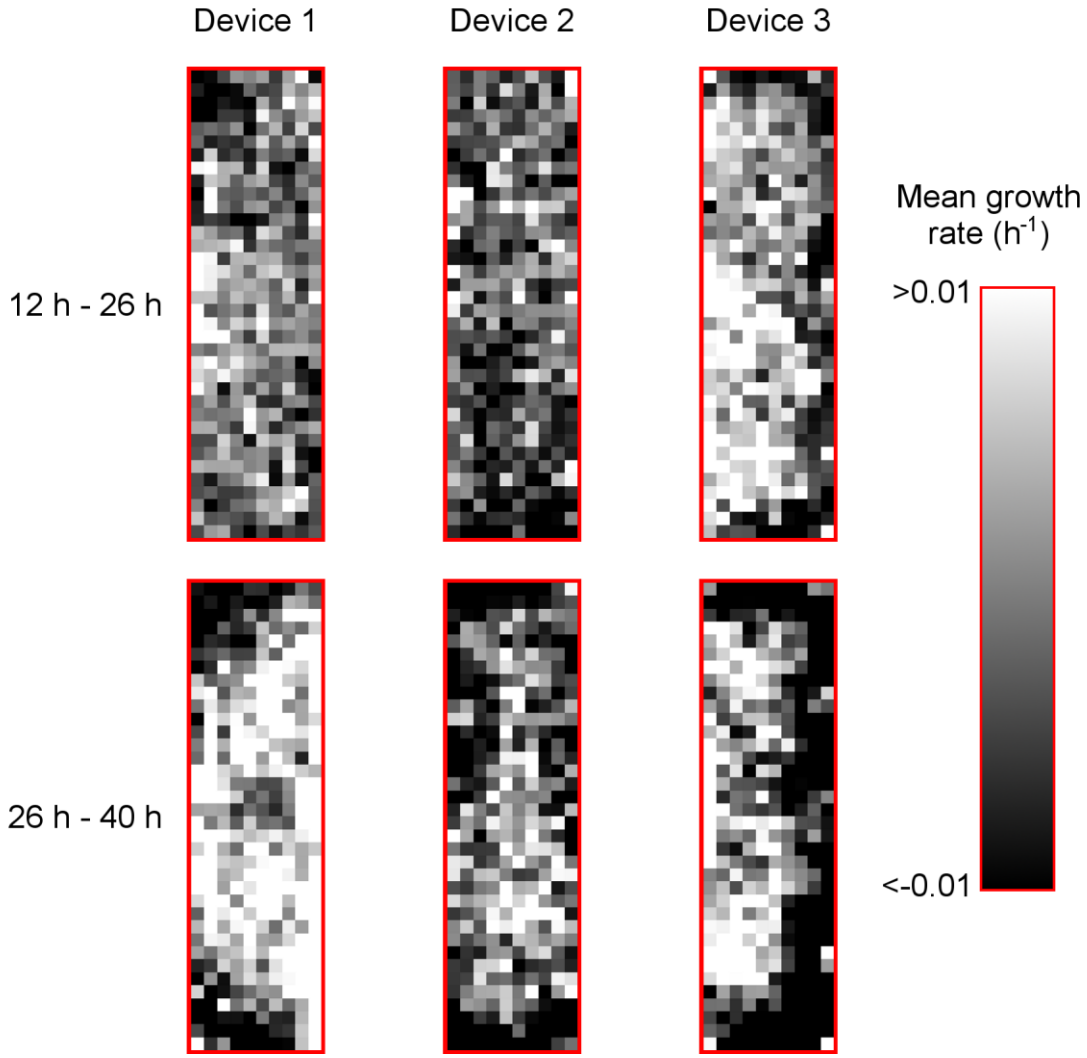

Figure 4.36 - Mean spatial distribution of relative growth rate for different device configurations.

36×10 grids showing the mean spatial distribution of growth rate, relative to the mean experimental growth rate, for each device configuration. The relative growth rate of a single grid element is calculated by subtracting from the growth rate of that element the mean growth rate (over the same period) for all devices in that experiment. A mean is then taken of the relative growth rates of that grid position, in that device configuration, across the three repeat experiments. The relative growth rates are shown for the periods from 12 to 26 h and 26 to 40 h after the start of medium perfusion. Medium flows left to right. Device 1 included a gas permeable lid system with an open PC element while the other two devices included closed PC components. Device 3 included the improved PDMS chip while the other two devices included the prototype PDMS chip.

Figure 4.34 shows the spatial distribution of confluency in the three different device configurations, in all three experiments, at four different time points. As with the mean confluency curves, there are no clear differences in the spatial distribution of confluency between different device configurations. However, the mean spatial distributions of growth rate for each device show some evidence of configuration based differences (Figure 4.35). These differences are clearer when looking at whether growth rates are above or below the mean experimental growth rate (Figure 4.36). To visualise this, the mean experimental growth rate (over the same period) is subtracted from each growth rate distribution, and the range represented by the intensity gradient is reduced so that growth rates significantly above the mean are white, growth rates significantly below the mean are black, and growth rates near the mean are shades of grey. The growth rates were investigated between 12 h and 40 h to avoid the effects of both bubbles (<12 h), and space limitations at confluencies near 1 (>40 h). This range was split in half to allow comparison of mid and late monolayer culture.

The observed patterns in growth rate (Figure 4.36) for the different configurations are consistent with the expectations for oxygen controlled growth. The first device configuration achieves higher downstream growth than the second and third configurations. Its open PC lid component replenishes more of the oxygen consumed form the medium by upstream cells. The third device configuration achieves lower growth in the downstream corners of the culture chamber. Its improved PDMS chip delivers reduced flow rate at the chamber edges as part of the overall increase in flow uniformity. Both patterns are more exaggerated during the later stages of monolayer culture when higher cell densities result in lower pericellular dissolved oxygen.

The mean standard deviations in the spatial distribution of growth rate are 35%, 38%, and 44%, between 12 and 26 hours, and 57%, 63%, and 80%, between 26 and 40 hours, for the three different configurations respectively (standard deviation n=370, mean n=3). As expected for a system with oxygen controlled growth, the first device configuration, with the open PC lid component and the prototype PDMS chip, achieves the most uniform growth rate over both periods.

This is due to the open PC lid element and permeable membrane supplying a more uniform DO across the top surface of the culture chamber, which translates to a more uniform pericellular DO.

However, contrary to expectations, the third device configuration, with the closed PC lid component and the improved PDMS chip, achieves the least uniform growth rate over both periods investigated. This implies that the slightly below average velocities at the chamber edges (caused by wall shear) have a more negative effect on growth rate uniformity than the significantly above average velocities present with the prototype chip. This supports the theory that, under these experimental conditions, a rapidly consumed or secreted factor (most likely DO) has more effect on growth rate than hydrodynamic shear.

The mean and spatially distributed confluency data provides evidence that mESC growth is significantly affected by pericellular DO when medium is perfused through a culture device at 300 $\mu l.h^{-1}$. Consequently, use of the gas permeable lid system with an open PC component increases the uniformity of growth in mid to late monolayer culture. Furthermore, use of this lid configuration with a normoxic atmosphere increases the growth rate during mid to late monolayer culture. Under these conditions, the hydrodynamic shear rate does not appear to significantly affect growth rate in mid to late monolayer culture. As a result the improved PDMS chip has a negative effect on growth rate uniformity. At lower medium flow rates these effects, of both the gas permeable lid system and the PDMS chip design, are expected to become more exaggerated. Thus, experiments at lower flow rates could be employed to more conclusively confirm these design based effects.

Bubbles in the culture chamber prevent a similar understanding of early monolayer culture. Improvements in design, or assembly and priming techniques, may overcome this limitation. It is also not clear from this data, what effect parameters such as DO, shear rate, and the concentration of soluble factors have on cell fate. A quantitative assessment of pluripotency markers (e.g. qPCR) would allow the investigation of overall affects on cell fate.

Investigation of effects on spatial distribution would require the use of a spatially resolved assessment of marker expression, such as laser scanning cytometry. These are all areas for future investigation.

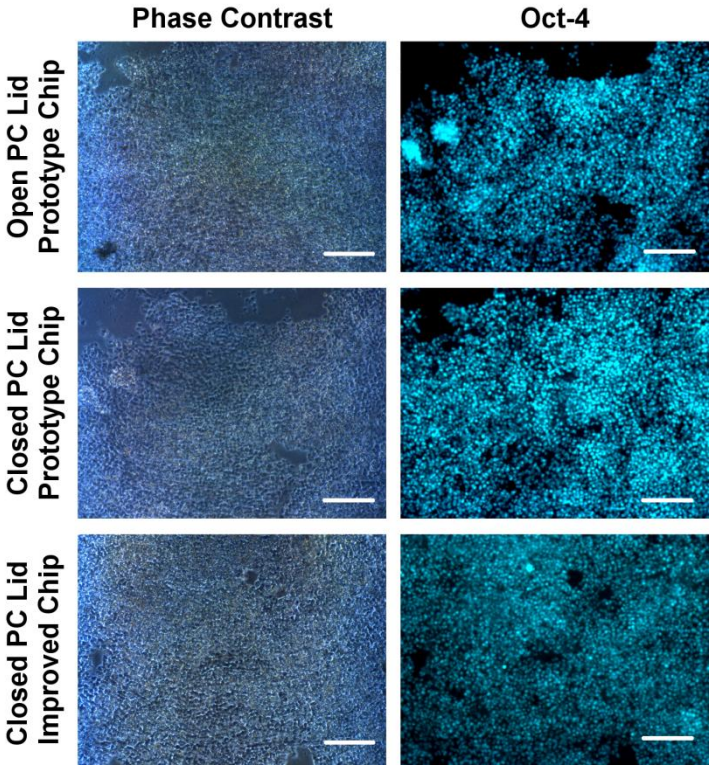

Figure 4.37 – Mouse embryonic stem cells cultured in the improved microfabricated culture devices and stained for the pluripotency marker Oct-4.

Microscope images of mESCs cultured in the three different microfabricated culture devices; a device with an open PC lid component and a prototype PDMS chip, a device with a closed PC lid component and a prototype PDMS chip, and a device with a closed PC lid component and an improved PDMS chip. Phase contrast references are compared with fluorescent microscopy images after the cells were stained for the nuclear pluripotency marker Oct-4. Images were taken with a 10× objective and the scale bars represent 200 μm.

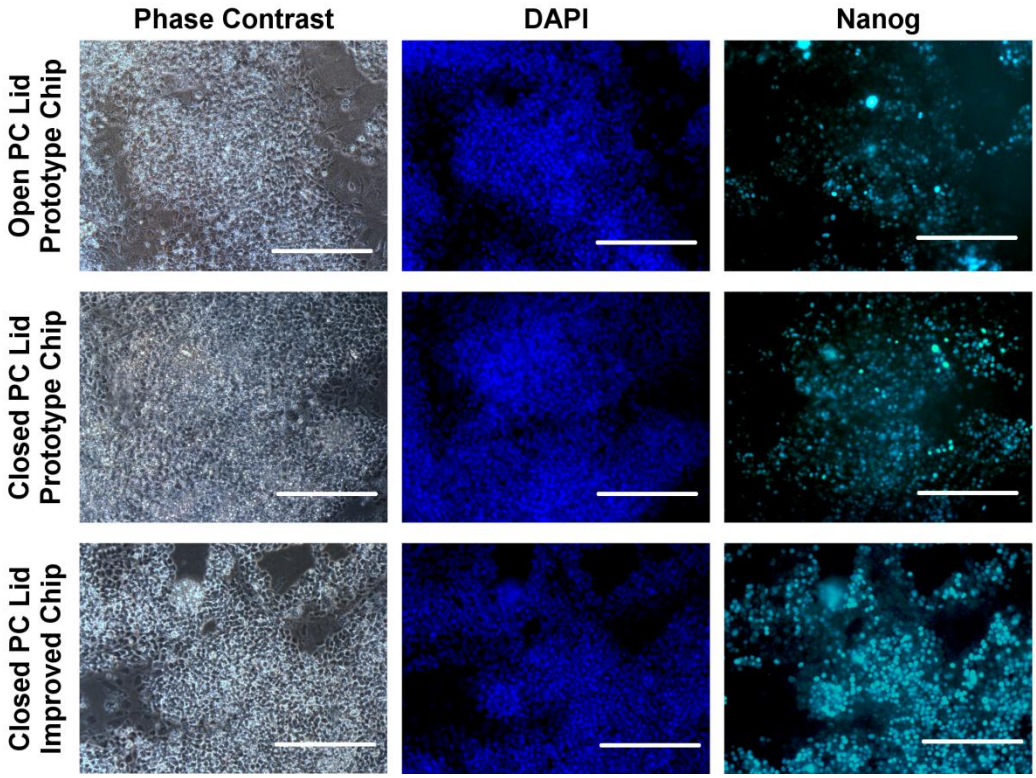

Figure 4.38 - Mouse embryonic stem cells cultured in the improved microfabricated culture devices and stained for the pluripotency marker Nanog.

Microscope images of mESCs cultured in the three different microfabricated culture devices; a device with an open PC lid component and a prototype PDMS chip, a device with a closed PC lid component and a prototype PDMS chip, and a device with a closed PC lid component and an improved PDMS chip. Phase contrast references are compared with fluorescent microscopy images after the cells were stained for the nuclear marker DAPI and the nuclear pluripotency marker Nanog. Images were taken with a 20× objective and the scale bars represent 200 μm.

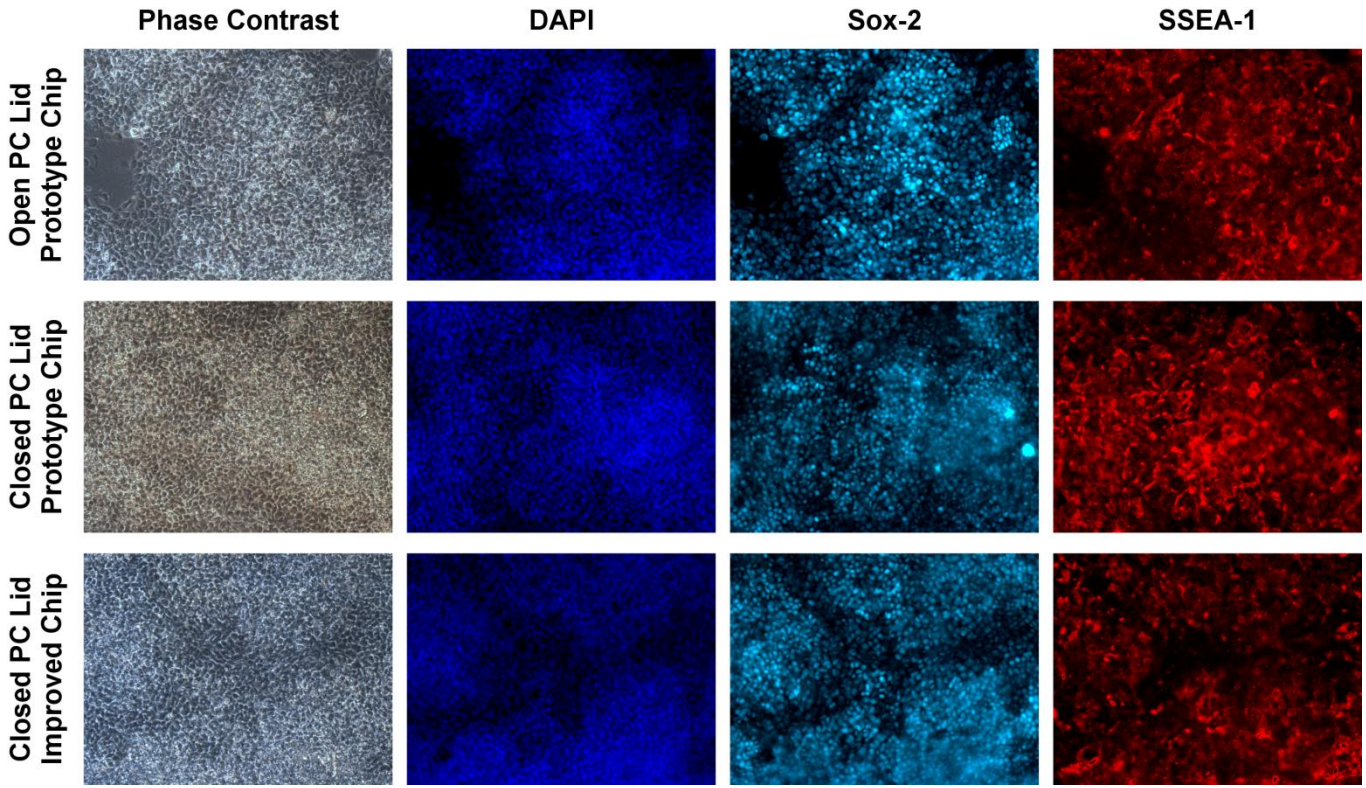

Figure 4.39 - Mouse embryonic stem cells cultured in the improved microfabricated culture devices and stained for the pluripotency markers Sox-2 and SSEA-1.

Microscope images of mESCs cultured in the three different microfabricated culture devices; a device with an open PC lid component and a prototype PDMS chip, a device with a closed PC lid component and a prototype PDMS chip, and a device with a closed PC lid component and an improved PDMS chip. Phase contrast references are compared with fluorescent microscopy images after the cells were stained for the nuclear marker DAPI, the nuclear pluripotency marker Sox-2, and the surface expressed pluripotency marker SSEA-1. Images were taken with a 20× objective and the scale bars represent 200 μm.

Pluripotency Markers

For each culture experiment, all three culture devices were stained in the same way. The first experiment was stained for Oct-4 as well as staining with the nuclear stain DAPI. The second experiment was stained for Nanog and SSEA-1 as well as staining with the nuclear stain DAPI. The third experiment was stained for Sox-2 and SSEA-1 as well as staining with the nuclear stain DAPI. No DAPI signal could be obtained for the first experiment. It was later established that the PC component filling the viewing window of the aluminium holder (Figure 3.12) blocks the excitation wavelength of the DAPI stain. For experiments 2 and 3 the culture devices were removed from the aluminium holder for staining. In the future, the material of the window filler should be changed to one that transmits this wavelength e.g. polystyrene or glass. The SSEA-1 signal for the second experiment was very weak due to use of insufficient primary antibody. This was corrected for the third experiment.

Figures 4.37, 4.38, and 4.39 show the staining results for the 9 different culture devices. Oct-4, Nanog, and Sox-2 are nuclear markers and match the nuclear stain DAPI, while SSEA-1 is a surface marker. The majority of cells in every culture device stain positive for the four pluripotency markers. This evidence supports the maintenance of pluripotency (section 1.1.2). In turn, the maintenance of pluripotency during expansion supports the continued suitability of the culture device for stem cell culture.

4.3.3 Culture Chamber Heating Solution

Following the improvements made to the control and automation platform in chapter 3, control of the temperature in the culture chamber remained an outstanding issue. In the prototype platform, the culture chamber was heated by applying a voltage across an ITO coating on the bottom of a glass microscope slide (section 2.3.8). However, this solution limited the culture surface to glass, negating the design efforts to allow the use of TC-PS and other flat materials. Furthermore, any heating solution integrated into the disposable device components (i.e. the microscope slide or PDMS chip) will complicate and

increase the expense of producing those components. This is a significant disadvantage for single use components.

Following the improvements to the platform in chapter 3 (section 3.3.7), heat was provided to the culture chambers via a cage incubator. This was the method used for the culture experiments in this chapter. The cage incubator has the advantage of being entirely separate from the culture system. Therefore, it complicates neither the production of parts nor the assembly of the culture system. Furthermore, as the incoming medium and all external surfaces of the culture system are heated to 37°C by the incubator environment, no temperature gradients exist within the culture devices. Not only does this result in a completely uniform temperature in the culture chamber, it eliminates the need for an integrated temperature sensor to control the heating input.

Unfortunately, in order to enclose the culture system and imaging system, the cage incubator must be much larger than the holder and three culture devices, making it space inefficient. The cage incubator is also inconvenient as it interferes with installation of the culture system on the microscope. Furthermore, it would be useful if the heating could be operated throughout manual handling exercises, such as cell seeding. This would avoid the temperature shifts that occur when moving between an incubator and biological safety cabinet (Veraitch et al., 2008, Jaccard et al., 2014a).

An alternative to the two heating solutions discussed above, is to integrate heating with the reusable components of the culture system. As these components are used for multiple culture experiments, the additional expense and complexity of integrating heating is less of a disadvantage. This solution will also avoid limitations on the culture substrate material, allowing the use of TC-PS as intended. However, unlike the cage incubator solution, this solution requires an integrated temperature sensor to control heat input. It will also result in temperature gradients between the heat sources and external surfaces of the culture system. These gradients must be accounted for when relating the measured temperature to the temperature at the culture surface.

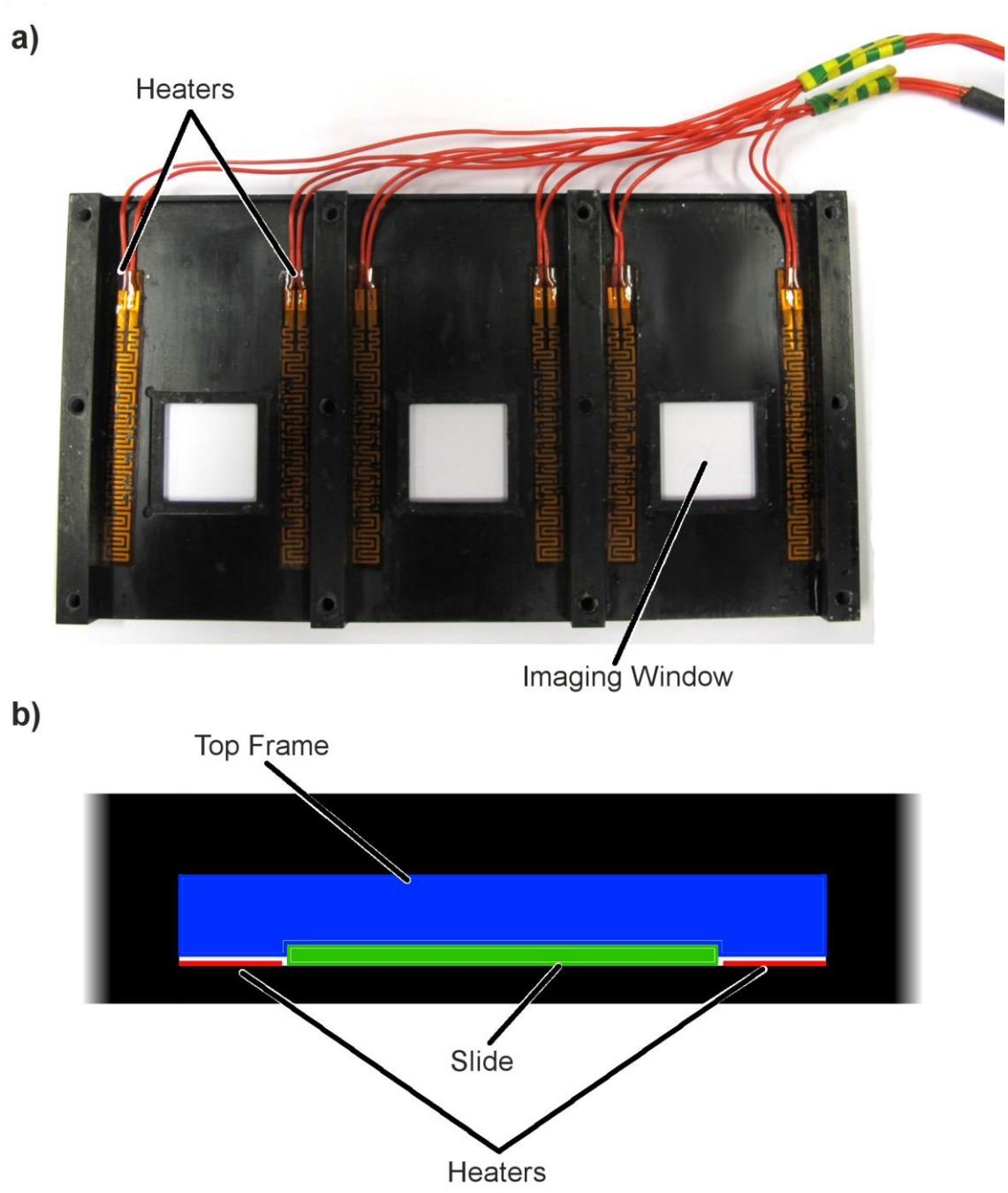

Figure 4.40 - Positioning of flexible heating circuits for culture chamber temperature control.

A photograph [a] showing six flexible polyamide heating circuits in place on the bottom plate of the aluminium holder. The circuits are affixed with thermally conductive adhesive. A schematic front view of a single device [b] shows how the heating circuits fit in an existing gap between the bottom plate of the holder and the top frame of the device.

To implement this heating solution, heaters were placed either side of the TC-PS slides in order to provide heat symmetrically, and as near as possible to the culture chamber without interfering with the light path for imaging. Flexible, polyamide heating circuits (6× HK5571R40.0L12B, Minco, France) were used so as to fit in the existing space between the bottom plate and top frame (Figure 4.40). The heating circuits were fixed to the bottom plate with thermally conductive adhesive, and the negative and positive lead wires were bundled into single pin connectors. This design has minimal impact on the space requirements, ease of assembly, and ease of operation of the culture system.

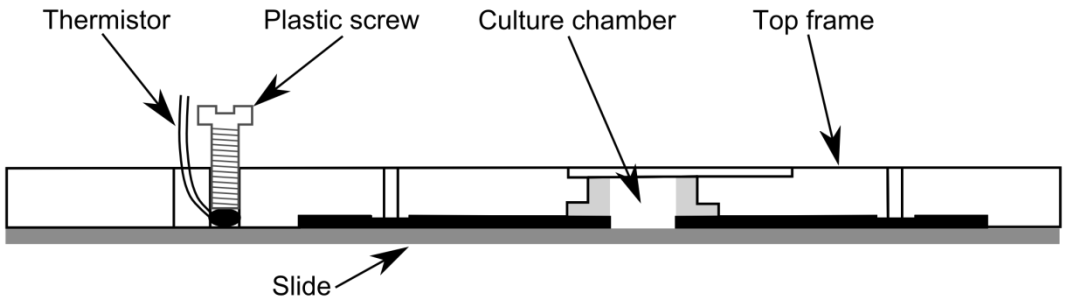

Figure 4.41 - Cross-section view showing thermistor position.

A thermistor is required to provide feedback to the controller, which adjusts the heater output to control the temperature of the culture chamber. The thermistor is held against the top surface of the microscope slide by a plastic screw. It is offset from the culture chamber to an area beyond the limits of the PDMS chip.

As with the prototype platform (section 2.3.8), the temperature of the culture chamber can be controlled by using pulse width modulation, which varies the fraction of time the heaters are active over a short cycle time. The pulse width modulation can be adjusted in response to temperature measurements from a thermistor that is in contact with the top surface of the microscope slide but offset from the culture chamber (Figure 4.41). The heating solution was tested using a manually switched 12 V laboratory power supply (IPS-2303, RS, UK) and a thermistor connected to a multimeter (Fluke 179 True RMS DMM with 80BK Temperature Probe, Fluke, UK). Heating was applied to the aluminium holder assembled with 3 improved culture devices, but without fluidics connected to the devices, as the low flow rate of preheated medium will not significantly impact chamber heating.

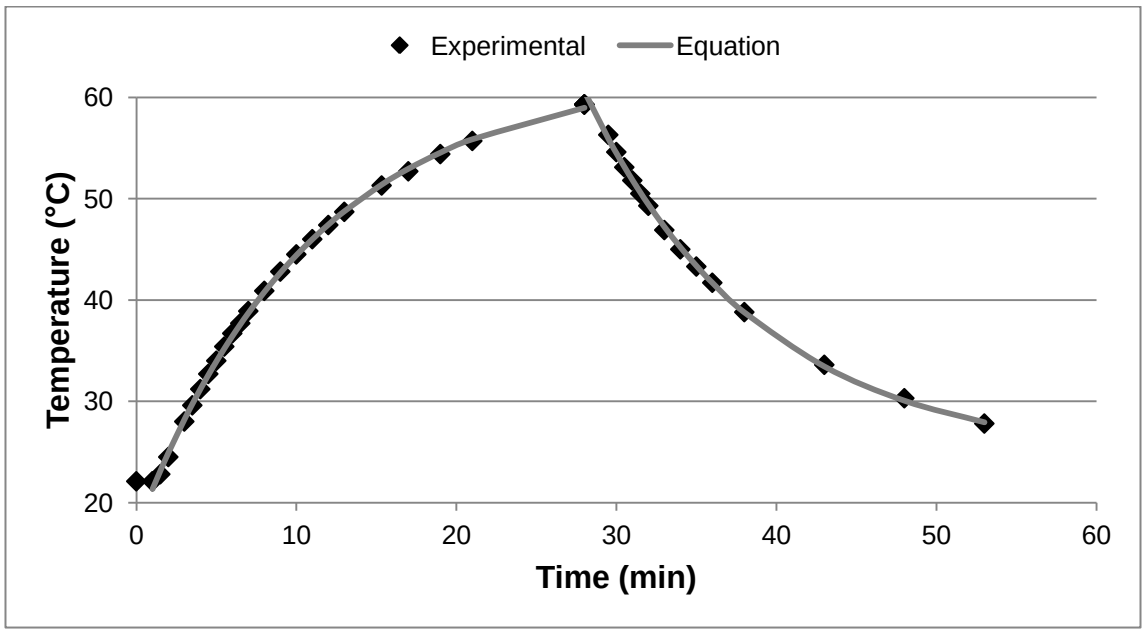

Figure 4.42 - Measured and predicted temperature change during heating and cooling.

The temperature measured by the thermistor is shown over periods of heating (100% power) and cooling (0% power). Also shown are the temperatures predicted by equation 4.5, with the terms of the equation optimised to fit the experimental data.

Upon application of 12 V across the heating circuits, the temperature measured by the thermistor immediately began to rise. Temperature rose, at a decreasing rate, for 27 minutes before the power supply was switched off allowing the system to cool down (Figure 4.42). Assuming uniform temperature throughout the aluminium holder and the culture devices, the temperature rise and fall can be modelled by the following energy balance (equation 4.4);

$$\frac{dT}{dt} = \frac{P}{m \cdot C_P} - \frac{hA\left[T(t) - T_R\right]}{m \cdot C_P} \qquad (4.4)$$

Where *T* is the temperature, *P* is the applied heater power, *m* is the mass, *Cp* is the average heat capacity, *hA* is the sum of the products of heat loss coefficients area for the external surfaces, and T_R is room temperature. This first order differential equation can be integrated to give equation 4.5;

$$T(t) = \frac{P + T_R hA}{hA} + C_1 \cdot exp\left(-\frac{hA \cdot t}{m \cdot C_P}\right) \qquad (4.5)$$

Microsoft Excel's solver add-in was used to minimise the sum of squares difference between the equation and experimental results by adjusting the three terms $\frac{P + T_R hA}{hA}$, C_1, and $-\frac{hA}{m \cdot C_P}$ (Figure 4.42).

From the optimised values and the known power input (21.6 W), room temperature (22.1°C), and weight (0.344 kg), the calculated C_p is 1.02 $kJ.kg^{-1}K^{-1.}$ This value falls between the values for the constituent materials (Aluminium 0.91 $kJ.kg^{-1}K^{-1}$, Polycarbonate 1.2-1.3 $kJ.kg^{-1}K^{-1}$, PDMS 1.5 $kJ.kg^{-1}K^{-1}$). The calculated value of *hA* is 0.54 $J.K^{-1}s^{-1}$. Based on these values the maximum temperature achievable in a 20°C room is 60°C.

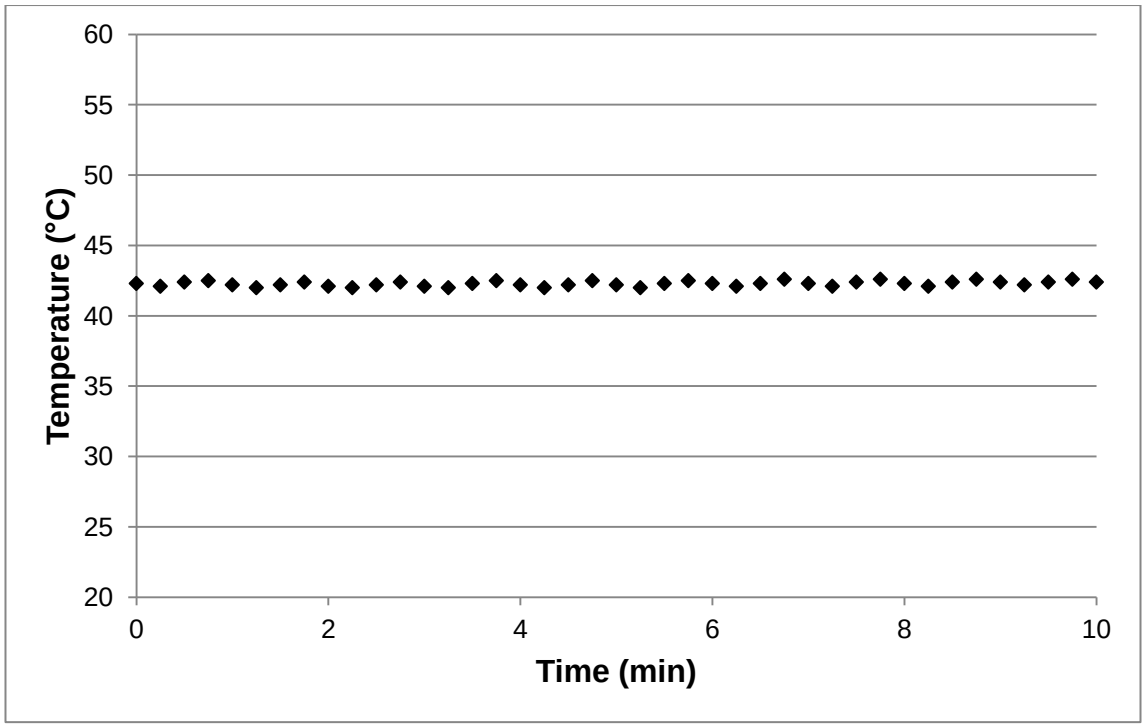

Figure 4.43 - Stability of measured temperature with constant average power output.

The figure shows temperature measurements made by the thermistor every 15 second over a 10 minute period. During this period the heaters were switched between 0% and 100% power ever 30 seconds i.e. a heater duty of 50% and a cycle time of 60 seconds.

The temperature of the culture chamber will be less than the measured temperature due to gradients between the heat sources and external surfaces of the system. To investigate this, the temperature was held constant by alternating the voltage on and off for 30 second periods (average power of 10.8 W). Figure 4.43 shows the temperature measured by the thermistor, under these conditions, over a 10 minute period. The average temperature is 42.3°C, which is in agreement with the temperature predicted by equation 4.4 (setting *dT/dt* to 0). The variation in temperature is minimal, and will be reduced further by increasing the frequency of the voltage switching.

After 20 minutes of alternating voltage on and off, the thermistor was moved to the culture chamber and pressed against the centre of the culture surface. The chamber was open to allow this but full of water. The temperature was measured twice, 5 minutes apart, reading 33.0°C on both occasions. The thermistor was then returned to its original position and showed that the temperature remained ~42.3°C. At room temperature (22.1°C) the temperature at the two points would be the same. Extrapolating linearly from these two

points, the set point for temperature control should be 49.7°C to give a chamber temperature of 37°C. This will require pulse width modulation with power applied 74% of the cycle length. The heating solution described can reach this temperature from room temperature in less than 15 minutes.

4.4 Conclusions

In chapter 3 improvements were made to the design of the microfabricated culture system. In this chapter the effects of those improvements were evaluated by investigating the seeding and perfusion culture of mESCs. Initial experiments showed large variations in the post-seeding confluence when a uniform cell suspension was not achieved immediately prior to incubation. It is relatively easy to achieve this uniform cell suspension in tissue culture flasks but not in microfabricated culture chambers due to the low volume. The low volume also contributes to greater variation between devices. Despite these issues, the average post-seeding confluency is the same for tissue culture flasks and the microfabricated culture devices. Therefore, experiments in these two systems can be conducted with the same starting point for the sake of comparability.

Initial culture experiments showed that the improved culture system is easier to assemble. However, the flow resistance of the system is variable over the course of multi-day perfusion culture experiments. Feedback control over medium flow rate was implemented but the control parameters used were not optimal for the system used. The planned inclusion of a purge valve to regularly relieve pressure should make optimisation of these parameters easier.

With flow control in place, a culture experiment was repeated three times, with three different device configurations in each experiment. Confluency monitoring by phase contrast microscopy shows 7% variation, between experiments, in the time taken to reach a confluency of 0.5, and 9% confluency in the time taken to reach a confluency of 0.8. While this indicates reasonable repeatability,

confluency curves also show clear variations between experiments. The reasons for these experiment to experiment variations are unclear and require further investigation. All the cultures reach full confluency well before 72 h of total culture time; the typical passage period of statically cultured cells. This suggests that culture in the microfabricated devices, with medium perfused at 300 $\mu l.h^{-1}$, increases the average growth rate relative to typical static culture.

Differences between the configurations of microfabricated device can be seen in both the overall growth rates, and the spatial distribution of growth rates. There is weak evidence that the introduction of a gas permeable lid (with an open polycarbonate element) increases the magnitude and uniformity of growth rate, particularly late in monolayer culture. Likewise there is weak evidence that the improved PDMS chip decreases the magnitude and uniformity of growth rate. These observations are consistent with pericellular dissolved oxygen being the most limiting factor in the expansion of the cells. However, the evidence of these design induced differences is weak due to the extent experiment to experiment variability. Furthermore, it was not possible to draw conclusions on the first 12 hours of culture due to the presence of bubbles in some culture devices.

Finally, a new method of temperature control for the culture chambers was investigated. A heating system was developed that is independent of disposable parts, allowing the use varied culture substrates including TC-PS. Flexible heating circuits were affixed to the bottom plate of the aluminium holder near the TC-PS microscope slide. These heaters can heat the culture chamber well above the standard set point of 37C. Temperature control can be achieved by pulse width modulation in response to measurements from a thermistor near the culture chamber. The system does not overly complicate the assembly or operation of the culture devices, and could be operated while conducting manual operations such as cell seeding. The chief limitations of the new heating system are, that thermal gradients exist in the culture system, and that, consequently, monitoring of a site offset from the culture chamber, and relation of that position to the culture chamber, is required.

In its current state the microfabricated adherent culture system has improved reliability, ease of use, comparability with traditional culture systems, and control over process parameters that should make it a useful tool for process development.

5. Potential Commercial Adaptations of the Microfabricated Culture system

Thus far, the microfabricated culture system has been developed as a prototype process development system. This chapter discusses how it might be adapted into a commercial system; firstly for process development and then for small scale production.

5.1 A Commercial Process Development System

As a prototype, the microfabricated culture system has been designed around the use of commercially available parts wherever possible. Custom parts have only been used where they directly impact the intended function of the device e.g. the PDMS chip, the aluminium holder, and the lid system. For a commercial system greater use of custom parts becomes a viable option. This is particularly true of disposable parts as mass production lends itself to different manufacturing techniques. The requirements of a commercial system and opportunities presented by the use of custom parts can be considered for the different system components; the online monitoring, the culture device, the fluidics, and environmental control.

Monitoring

First, consider the monitoring. As discussed in section 3.3.7, the cost of the fully motorised inverted fluorescent microscope (>£60,000) is very high relative to the 6 microfabricated culture devices it can continually monitor. Similarly, the space requirements are very large relative to those of the culture devices. Ideally, a commercial system would make use of a smaller and cheaper monitoring solution. However, phase contrast microscope images remain a preferred option due to their non-invasive nature and the wealth of information they provide (Matsuoka et al., 2014, Jaccard et al., 2014a). Other non-invasive methods, such as electrical cell-substrate impedance sensing, quartz crystal microscopy, and optical waveguide lightmode spectroscopy, require the integration of sensors or electrodes (Hug, 2003, Arndt et al., 2004, Hong et al.,

2011), which alter the cell culture surface and make them less appropriate for use with disposable parts.

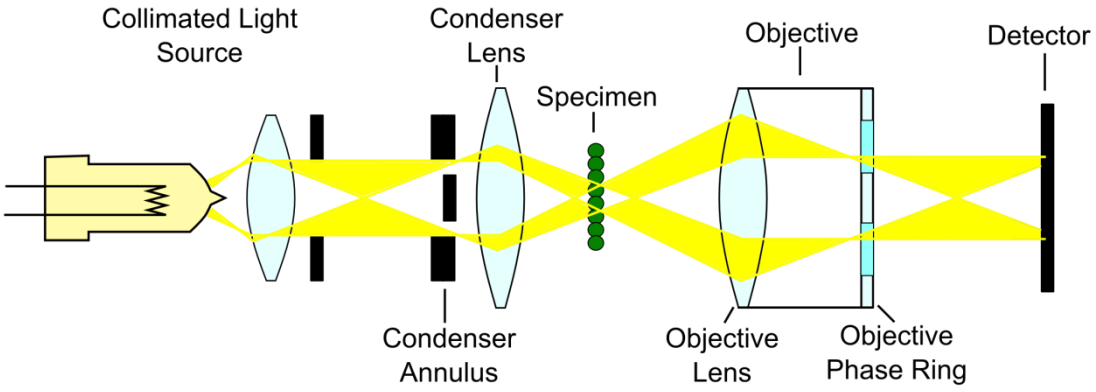

Figure 5.1 - Optical train for phase contrast microscopy.

A schematic of the optical train required for phase contrast microscopy including; the source of collimated light, the condenser annulus, the condenser lens, a specimen to be imaged, a phase contrast objective containing an objective lens and phase ring, and a detector such as a CCD camera.

Monitoring with phase contrast microscope images does not require all the functionalities of an inverted fluorescent microscope, and removing redundant components will reduce the cost. Neither the fluorescent light source nor the filter turret is required. Similarly, the nosepiece turret may not be required as, to date, only the 10× objective has been utilised. Finally, it is not necessary to have eyepieces in addition to the microscope camera. Phase contrast monitoring does require a camera and a single phase contrast objective as well as the collimated light source, condenser lens and condenser annulus (Figure 5.1).

Monitoring also requires the ability to move the culture chambers relative to the optics while keeping the cells in focus. When using the improved control and automation platform, this was achieved by manually setting the *x, y* and *z* positions, for each individual image, at the start of the experiments. The temperature control of the cage incubator was relied on to prevent thermal drift over the duration of the experiment. This method was effective but time consuming and would not be practical for larger numbers of culture chambers or experiments done without the cage incubator.

There are a number of different options to automatically adjust focus between images. Different microscope manufacturers offer solutions to automatically adjust for physical and temporal focal drift (Nikon's Perfect Focus System, Leica's Adaptive Focus Control, Olympus' IX3-ZDC module, and Carl Zeiss' Definite Focus). These systems rely on the interaction of infrared light at the interface between a culture vessel and the liquid it contains, to track those interfaces and automatically adjust for changes in height. Alternatively, software approaches can adjust focus based on analysis of images at different focal positions. However, such systems are computationally expensive and inherently less reliable, as they rely on a computer's interpretation of which image is most in focus.

Finally, while it is necessary to move the culture devices relative to the optics, either the optics or the culture device can be moved to achieve this. If a commercial system integrates custom optics these could be motorised to move rather than moving the culture devices on a stage. This may allow the imaging of culture chambers across a larger area making, the imaging system more cost and space effective.

A promising alternative microscopy method to scan large areas is digital holographic microscopy (Kim, 2010, Mann et al., 2005). Digital holographic microscopy uses interference patterns to image a specimen through its entire depth without moving it in the vertical direction (Colomb et al., 2010). This allows the generation of both phase contrast equivalent images and 3D topographies. The additional information provided by 3D topographies can be used to detect morphological differences (Rappaz et al., 2014, Pavillon et al., 2012) increasing the power of microscopy as a monitoring tool. Amongst other methods, digital holographic microscopy can be achieved with as little as one lens, a laser light source (both stationary), and a commercial scanner as a detector (Shimobaba et al., 2013). However, the reconstruction of images from interference patterns and selection of the correct focal plane is computationally expensive.

Culture Device

Regardless of the chosen microscopy method and its limitations, fitting more culture chambers in the area that can be imaged will increase the cost and space effectiveness of the system. The areas of the microfabricated culture devices presented in the previous chapters are more than 50 times the area of the culture chamber. This size was dictated by both the size of the microscope slide used to provide a culture surface, and the area occupied by the fluidic connections and the channels used to expand and contract the fluid flow. For a commercialised system, custom parts can be used to overcome both of these limitations.

The prototype and improved microfabricated culture devices utilise the microscope slide format as a commercially available source of flat, sterile TC-PS. For a commercialised system, custom disposable TC-PS components could be mass produced by hot embossing or injection moulding. Doing so would have multiple advantages: Firstly, the size of a culture device would no longer be limited to larger than a microscope slide. Similarly, the culture chamber would no longer be limited to smaller than a microscope slide. Furthermore, the TC-PS component could have complex 3D geometries including the recessed culture chamber and the inlet and outlet channels currently included in the PDMS chip. This would eliminate the need for some parts and, consequently, reduce the number of reversible seals required. Finally, mass production methods should significantly increase the reproducibility of dimensions and therefore flow resistances and burst pressures.

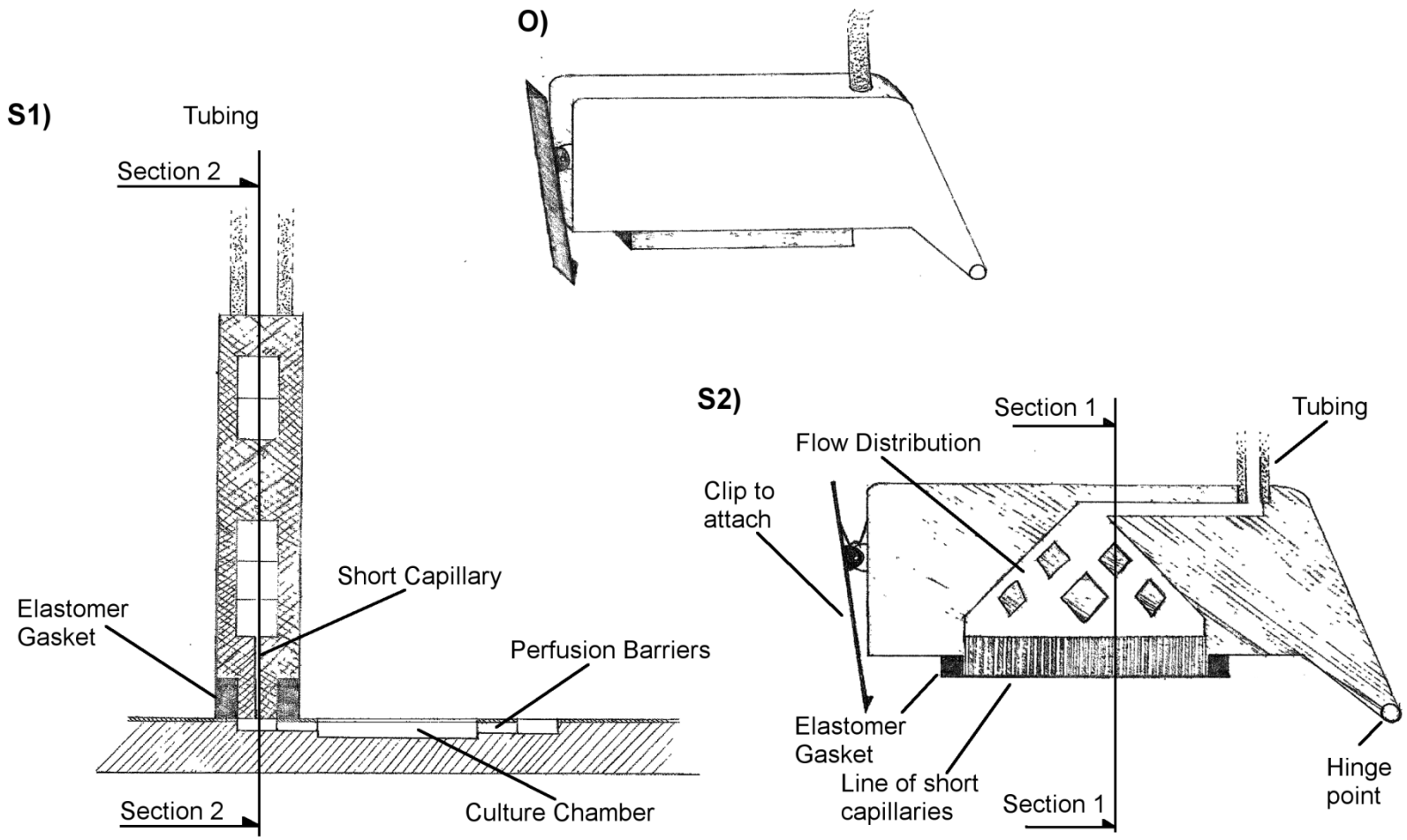

Figure 5.2 - Commercial connector concept.

Orthographic [O] and section views [S1,S2] of a concept for a commercial connector. Section 1 [S1] shows the connector in-situ on a TC-PS component. Flow is distributed in the connector rather than the TC-PS component. A line of short capillaries, as seen in section 2 [S2], will both distribute flow and provide a significant resistance. The connector is anchored at one end by a hinge and at the other by a clip, both of which attach to the structure under the TC-PS component.

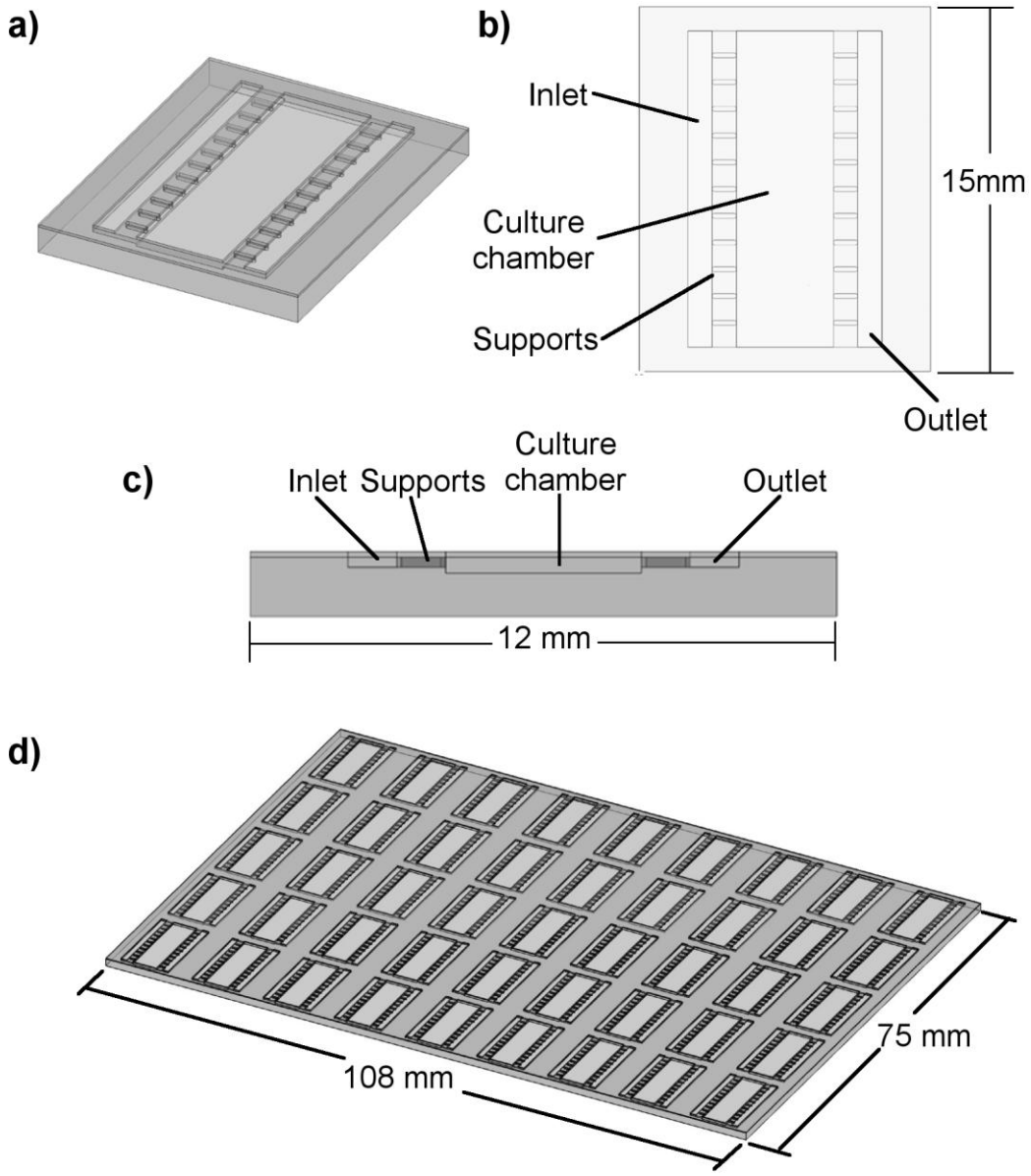

Figure 5.3 - Concept for a mass produced TC-PS component.

A concept for a mass produced TC-PS component to be used in a commercial system. 3D [a], plan [b], and side [c] views show a single culture chamber that has a significantly reduced footprint, as it relies on the connectors to distribute flow. The component is comprised of two elements: a lower element with recessed inlet and outlets, a deeper recessed culture chamber, and supports for the thin top element. The top element has rectangular holes corresponding to the inlet, outlet and culture chamber. These two elements could be bonded prior to surface treatment and sterilisation. The final image [d] shows how a 9×5 array of these culture chambers can fit in the area that can be imaged on the motorised microscope.

Another area where mass production could alter the culture device is the fluidic connections and the distribution of flow. The prototype and improved culture devices were designed to utilise simple and widely available connectors. Fluid flow was then expanded and contracted within the culture device by channels in the PDMS chip. A commercial system could make use of custom connectors to connect external fluidics to the culture device. These custom connectors could be the width of the culture chamber and include the flow distribution function in a vertical orientation (Figure 5.2). Such connections would eliminate the space requirements of the flow channels in the PDMS chip. Combined with the mass production of structured TC-PS components, this could reduce the area of a single culture device to 12×15 mm (Figure 5.3) allowing 45 culture chambers within the travel (110×75 mm) of the motorised microscope stage (rather than the current 6).

Fluidics

With the decreased variability in resistance offered by mass produced parts, less additional fluidic resistance will be required to ensure equal flow distribution between parallel devices. A significant back pressure would still be desirable to prevent the build up of gas in the culture chamber. However, if this could be largely achieved by pressurising the waste bottle, then the pressure resistance of the downstream fluidics could still be reduced. Eliminating the long capillaries of the improved culture system would reduce the impact of fouling and small flow obstructions resulting in more consistent conditions.

Simple sterilisation of custom fluidics would be a challenge in a commercial system. It is unlikely that the entire fluidic path could be autoclaved or sterilised by steam in place. The improved control and automation platform required chemical sterilisation of the flow meter, and this method may be required for all non-disposable parts in a commercial system. If chemical sterilisation (e.g. NaOH and Ethanol) is the preferred method, care must be taken in the selection of construction materials to ensure compatibility.

For a commercial process development tool, the ability to vary process parameters between individual culture chambers remains important. Therefore, the availability of multiple switchable medium reservoirs per set of parallel chambers should be retained (as seen in section 3.3.7). To this end, Schott bottles remain a useful standard that is reusable and available in a variety of sizes. To maximise versatility and economy of space it would be useful if inactive bottles could be switched for new ones during an experiment. This would require sterile connection changes, which are becoming common in disposable biotech systems. It should also be possible to pump medium form different reservoirs at different rates. This would require an electronic pressure regulator and flow meter for each set of parallel chambers (Figure 5.4).

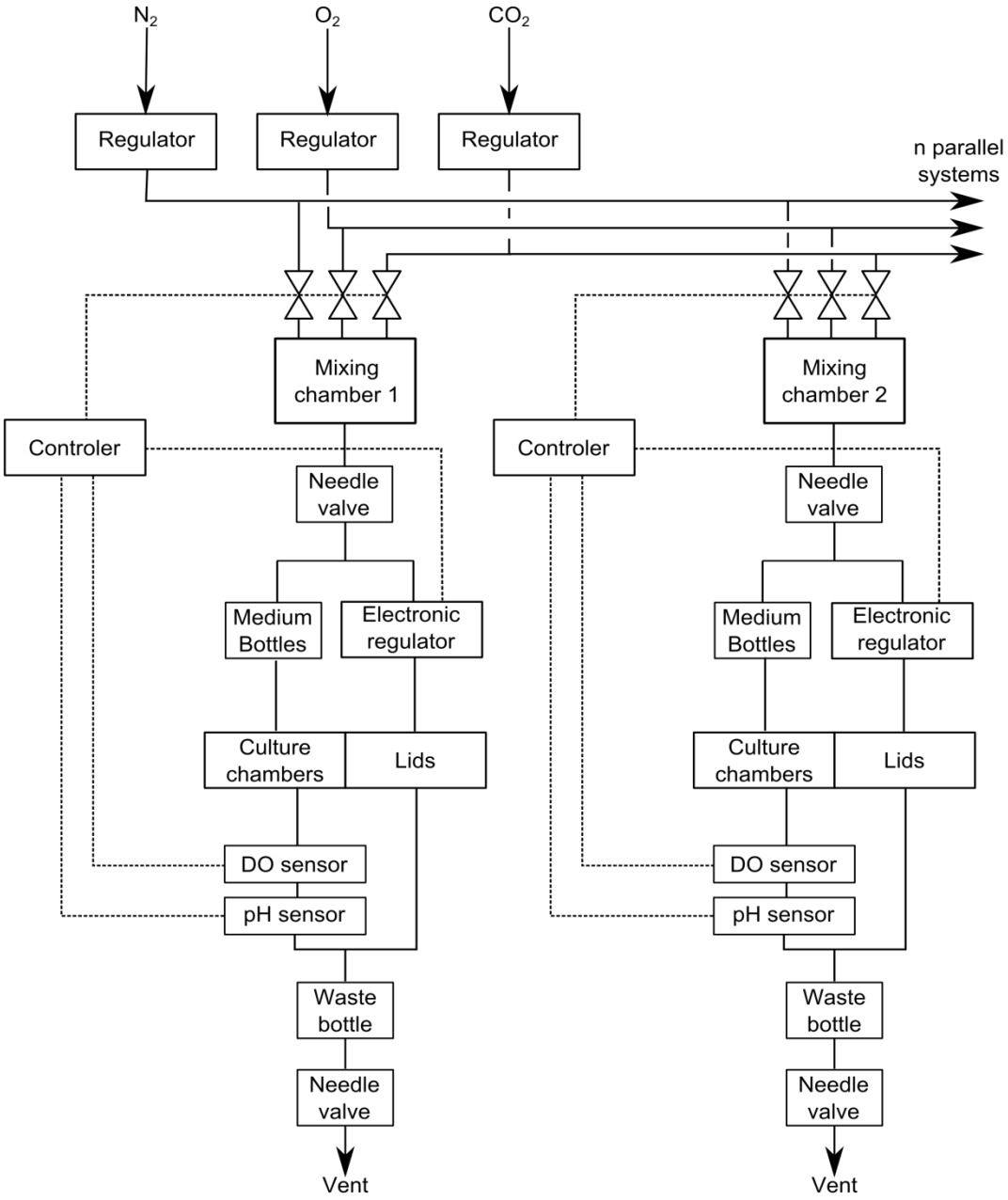

Figure 5.4 - Schematic of gas flow in a conceptual commercial system.

A schematic of gas flow and control in a conceptual commercial system. Cycling three on/off valves with different timings allows control over the concentration of each gas in the mixing chamber (mixed by diffusion). Gas concentrations can be adjusted based on feedback from sensors at the chamber outlets. A needle valve reduces the pressure after the mixing chamber. After the needle valve, gas is split to both the medium bottles and to the lids. The gas flowing through the lids is also used to pressurise the waste bottle. The pressure of the stream to the lids is reduced by an electronic regulator allowing control over the medium flow rate. A final needle valve prevents excessive gas flow through the vent on the waste bottle.

Environmental Control

Gas is used not only to drive the perfused medium, but also to control dissolved oxygen and pH in the culture chamber. Therefore, it should be possible to

control the gas composition separately for each set of parallel culture chambers. This can be achieved by having a single manually regulated supply of each gas component connected to small gas mixing chambers (one for each parallel set of culture chambers) by electrically actuated on/off valves (Figure 5.4). Cycling the valves for each gas open for different amounts of time would control the composition in the mixing chamber. The mixing chamber could feed both the medium reservoirs, and the head spaces of gas permeable lids. The head space gas could also be used to pressurise the waste bottles, as discussed earlier. The lid head space and waste bottle would need a lower pressure than the pressure in the culture chamber. Achieving this with an electronic pressure regulator would also allow control over medium flow rate.

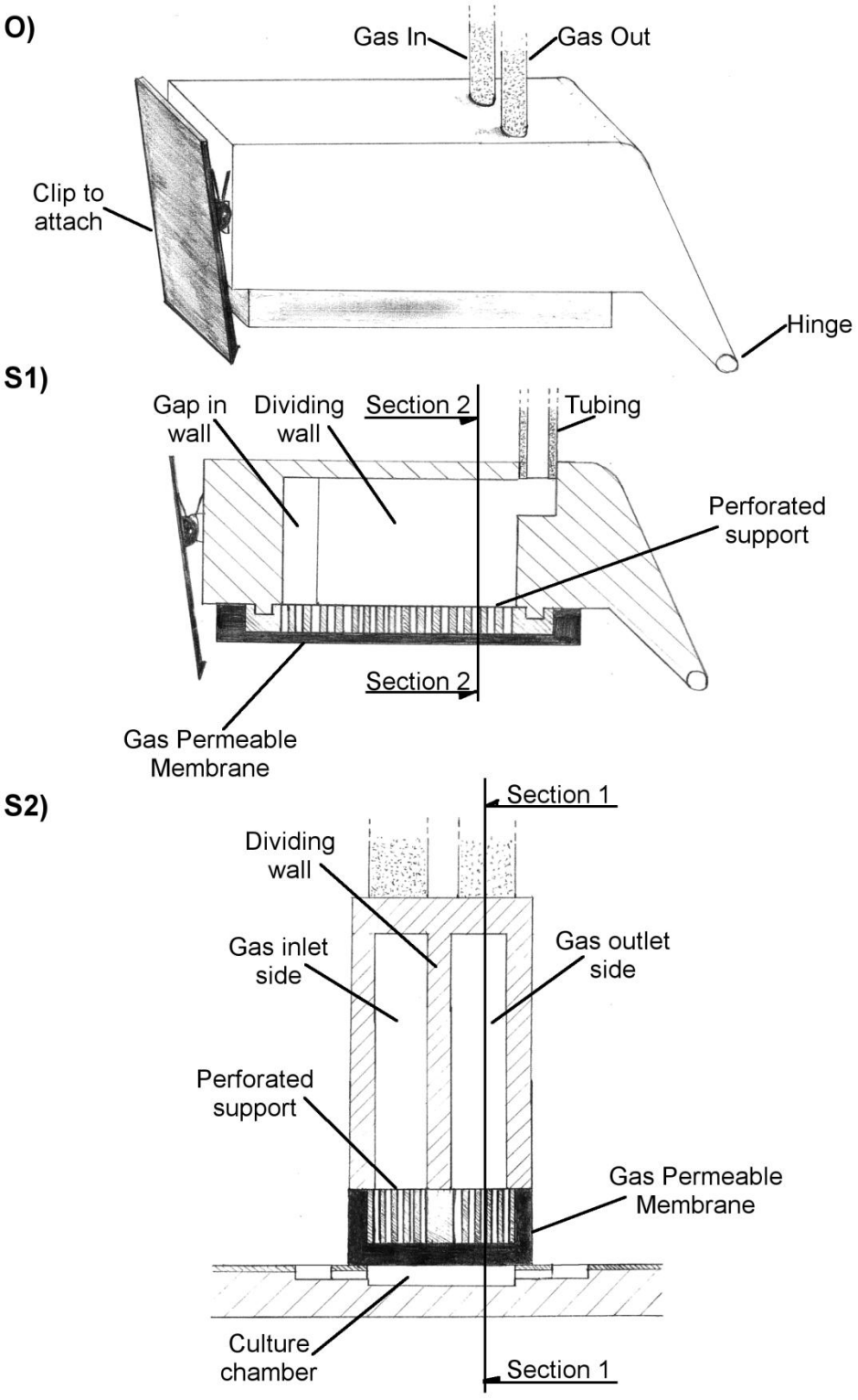

Figure 5.5 - Lid concept for a commercial system.

Orthographic [O] and section views [S1,S2] of a concept for a commercial resalable lid. Section 2 [S2] shows the connector in situ on a TC-PS component. The lid is anchored at one end by a hinge and at the other by a clip, both of which attach to the structure under the TC-PS component. Gas flows along one side of the lid from the inlet then back along the other side to the outlet. A thin gas permeable membrane is positioned flush with the top of the TC-PC component. The membrane is supported by a perforated layer of rigid plastic.

Continuing with environmental control, gas compositions could be controlled by feedback from dissolved oxygen and pH measurements. Flow through sensors situated downstream from the culture chambers could provide information on bulk DO and pH values. The gas composition could then be adjusted accordingly. This information would also provide valuable insight into cell metabolism. Oxygen control could also be improved by the use of thinner PDMS membranes (currently 4.12 mm thick). A shallow chamber in open configuration would allow for such membranes, as well as easier lid ‘insertion’ (Figure 5.5). However, thinner membranes will require more structural support to prevent deformation or breakage under the pressure differential of perfusion culture. Finally, the temperature control method introduced in the previous chapter could be extended to a commercial system; simply heating the surface the TC-PS sits on,, in the areas around the culture chambers.

Concept

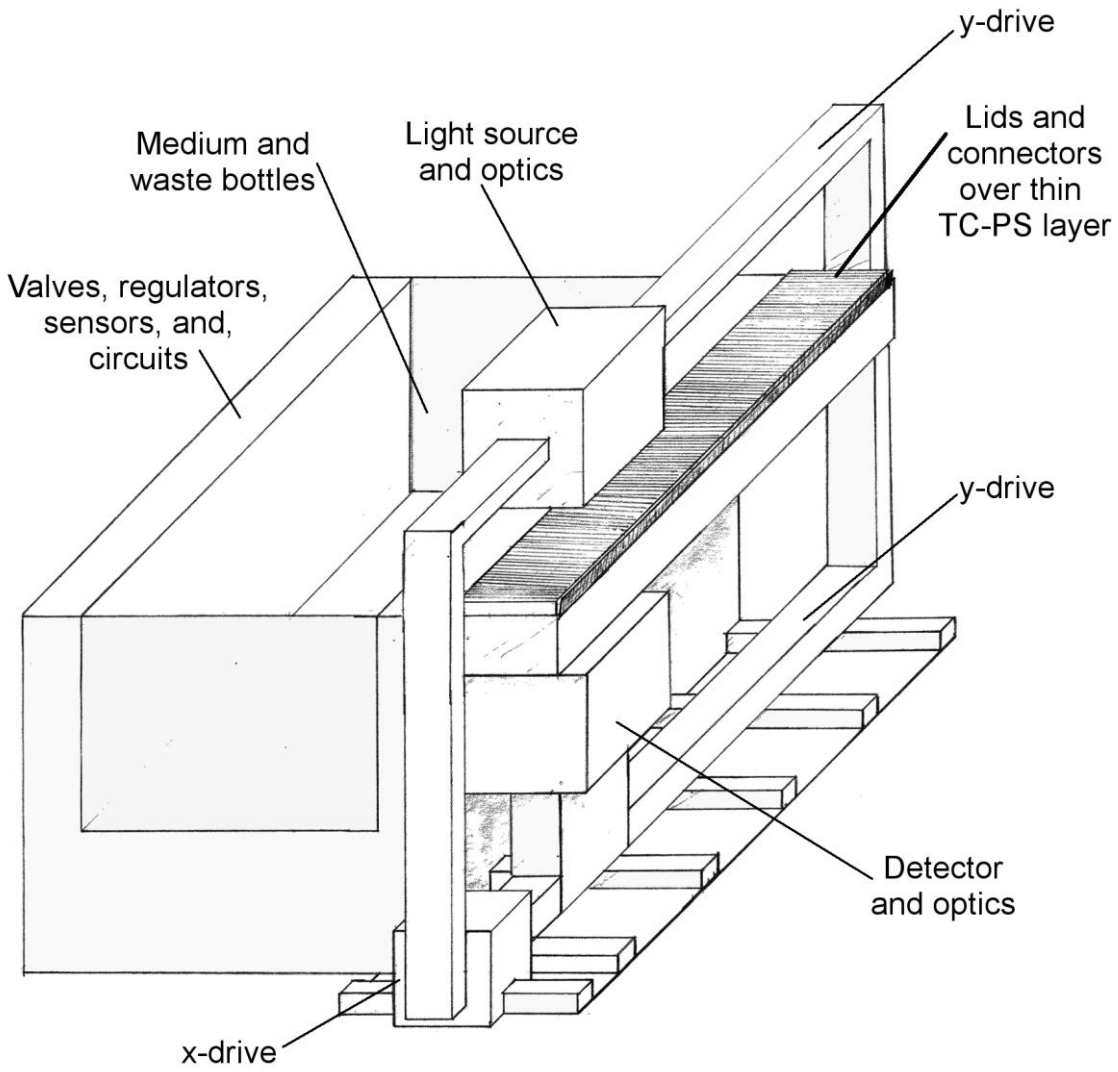

Figure 5.6 - Concept of a commercial system for process development.

An orthographic view of a concept for a commercial process development system. A TC-PS component (too thin to see at this scale), containing the culture chambers, sits on a heated glass surface with fluidic connectors and lids clipped on top. The TC-PS component has 27 rows, with each row containing either one wide culture chamber, or multiple narrower culture chambers operated in parallel. The system incorporates monitoring by microscopy with, *x* and *y* drives to move the light source and detection optics. A large space is allocated for storage of the medium and waste bottles. The surrounding space would contain the valves, regulators, sensors, circuits, and other control hardware.

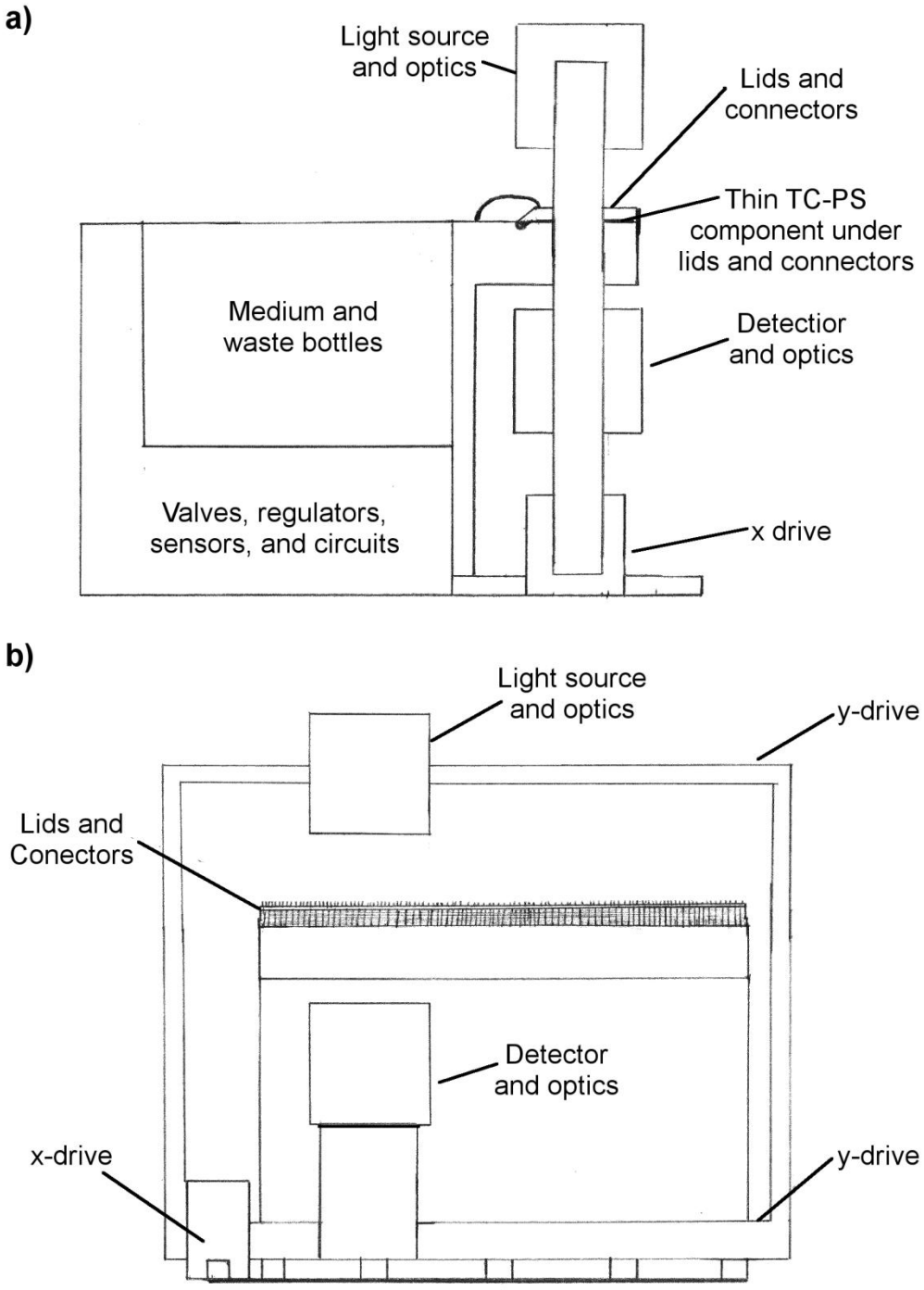

Figure 5.7 - Front and side views of conceptual commercial process development system.

Front [a] and side [b] views of the concept for a commercial process development system pictured above. A TC-PS component (too thin to see at this scale), containing the culture chambers, sits on a heated glass surface with fluidic connectors and lids clipped on top. The TC-PS component has 27 rows, with each row containing either one wide culture chamber, or multiple narrower culture chambers operated in parallel. The system incorporates monitoring by microscopy with, *x* and *y* drives to move the light source and detection optics. A large space is set aside for storage of the medium and waste bottles. The surrounding space would contain the valves, regulators, sensors, circuits, and other control hardware.

Figures 5.2-5.7 show a conceptual design based on the considerations discussed above. The complete concept system shown in Figures 5.6-5.7 consists of 27 rows, with each row containing one wide culture chamber, or multiple narrower culture chambers operated in parallel. The approximate dimensions of the concept system are 0.5×0.5×0.5 m. The concept system incorporates online monitoring by microscopy (phase contrast or digital holographic) and versatile control over process parameters.

5.2 A Small Scale Production System

The above design could be extended to a small scale production system by scaling up and out. The extent to which the length of a culture chamber can be increased will be limited by the sensitivity of the desired process to differences in concentrations of consumed and secreted molecules. However, there is no such limitation on the width dimension of the culture chamber. Sheets of wide, short, parallel culture chambers could be used to produce similar numbers of cells to static multilayer systems with the high level of control offered by the microfabricated system.

For example, working with a 15 mm length dimension of the chamber footprint (a 4 mm chamber plus connections) and increasing the chamber width to 400 mm, a single 400×400 mm sheet would have a culture area of 416 cm^2. Twenty such sheets, stacked vertically, would have 8320 cm^2 of culture area, enough to produce 4×10^9 mESCs (high confluence cell density of 5×10^5 $cells.cm^{-2}$, other cell lines will vary). This is more than enough for a dose of a patient specific treatment or for multiple doses of some allogeneic treatments (dose size 8×10^4 - 1×10^9 cells; (Mason and Dunnill, 2009)). Therefore, such a scaled up and out system may prove appropriate for the production of patient specific treatments or low dose allogeneic treatments for rare conditions.

Assuming similar culture progress in identical culture chambers, a production system would not require the same independent control as a process development system i.e. all culture chambers could be controlled together. A production system could therefore use a single gas mixing chamber and electronic regulator, and a single set of large interchangeable medium bottles. This reduced complexity of the control system contrasts the increased complexity of monitoring with microscope images. A separate imaging system for each sheet of chambers would be neither cost nor space effective. Instead the system would need the capacity to image multiple sheets with a single imaging system.

Concept

The figure below (Figure 5.8) outlines a conceptual design of a production scale system. Multiple stacked sheets of culture chambers (4×400 mm) are operated in parallel form a single set of medium bottles. An elevating platform can withdraw any sheet from the stack and transfer it to an imaging station, allowing monitoring by microscopy. A liquid handling robot may allow automation of seeding and harvesting. For environmental control the whole system is housed in a sterile chamber heated to 37°C.

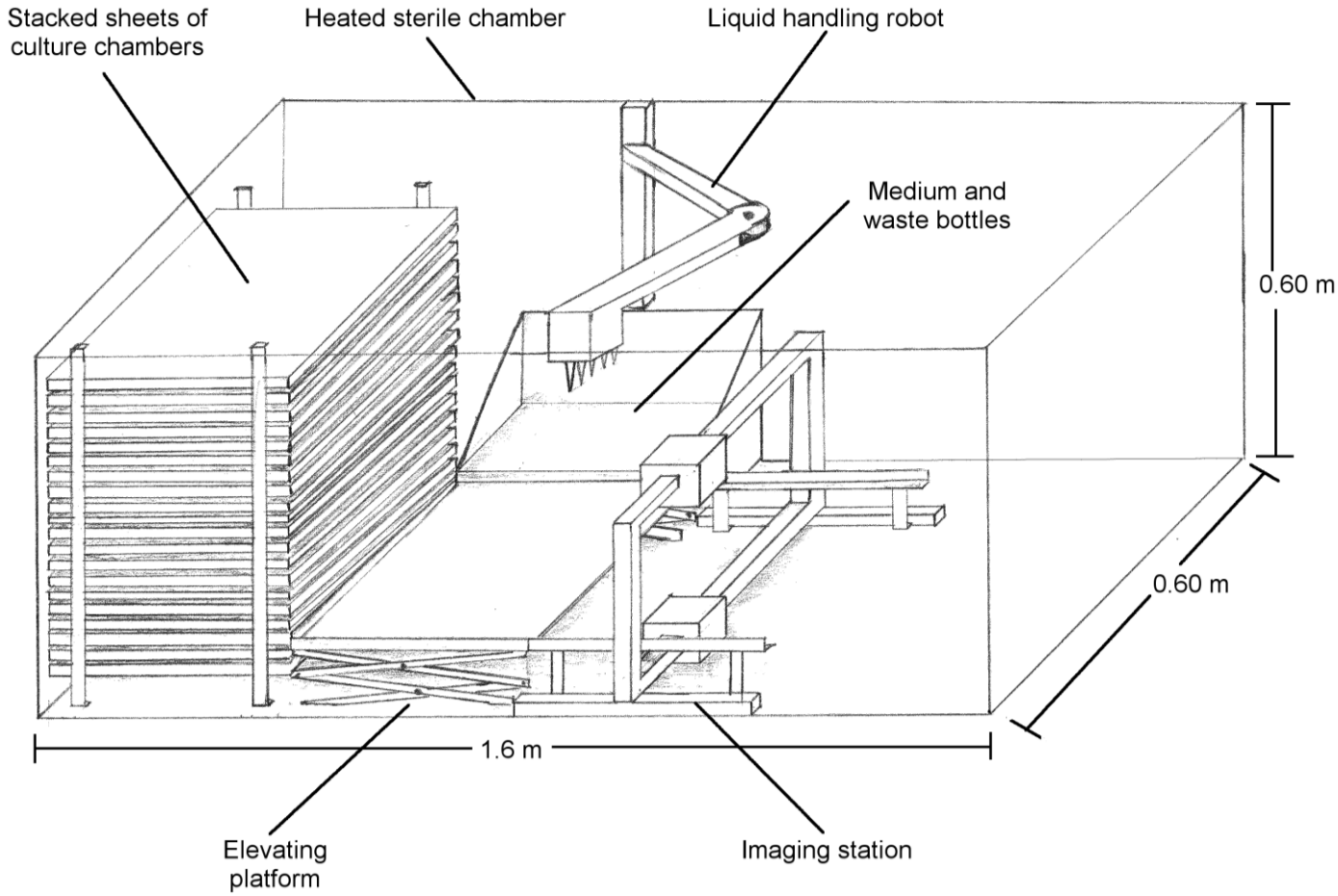

Figure 5.8 - Concept for a production scale system.

A conceptual production scale culture system based on the prototype process development system presented above. Multiple stacked sheets of culture chambers (4×400 mm) are operated in parallel form a single set of medium bottles. An elevating platform can withdraw any sheet from the stack and transfer it to an imaging station, allowing monitoring by microscopy. A liquid handling robot may allow automation of seeding and harvesting. The whole system is housed in a sterile chamber heated to 37°C.

6. Concluding Remarks

6.1 Summary of Results

This research project aimed to build on existing technologies to develop a microfabricated adherent cell culture system for stem cell process development. The multipotency and self renewal of stem cells make them a potentially limitless source of human cells, suitable for both screening and regenerative medicine applications. However, processing stem cells is challenging due to; the complexity of whole cell products, the breadth of process parameters, and the typical use of adherent culture. It is hypothesised that a microfabricated adherent culture system could facilitate process development with minimal use of resources, including scarcely available cell lines and expensive growth factors. Furthermore, microfluidic systems offer advantages in spatial and temporal control of the microenvironment that may benefit process development. Through this project, an existing microfabricated culture system has been further developed. The improved reliability, comparability with standard culture systems, and control over process parameters of the new system should make it a useful tool for process development.

The existing prototype system was critically evaluated; considering the design and opportunities for improvement, modelling fluid velocity, shear stress, and dissolved oxygen, and demonstrating the seeding and perfusion culture of embryonic stem cells. The system showed considerable promise for the perfusion culture of adherent embryonic stem cells. The use of reversible compression seals facilitates both traditional culture methods (static seeding) and materials (TC-PS). Furthermore, the prototype culture device facilitates the seeding and expansion of human embryonic stem cells, co-cultured on inactivated mouse embryonic fibroblasts, for one day of static and two days of perfusion culture. However, the culture system had multiple areas of potential improvement, including both reliability and control over medium velocity distribution and pericellular dissolved oxygen.

The prototype system was then improved, based on this evaluation. Improvements increased the reliability, ease of use, monitoring capabilities, and control over key process parameters. Modelling supported frame bending as the most likely cause of leaking and burst pressure variation in the prototype system. Therefore a new device holder was fabricated out of aluminium to reduce bending to acceptable levels. The opportunity was also taken to make culture devices easier to assemble, by reducing the number of screws and the sensitivity to screw torque. Improvements to the design of the PDMS chip and resealable lid were made to improve control over medium velocity distribution and pericellular dissolved oxygen respectively. These improvements were based on modelling of the process parameters.

The design of the new device holder was also influenced by a redesign of the surrounding process and control platform; the holder was designed such that two holders could position six culture chambers in the area that can be imaged by a motorised inverted fluorescent microscope. This microscope was used to enhance the monitoring capabilities of the culture system allowing automated time lapse imaging of multiple positions within the culture chambers. In addition to monitoring improvements, the external fluidics and the control hardware and software were redesigned to improve the ease and flexibility of operation.

The effects of the system improvements were evaluated by re-investigating the seeding and perfusion culture of mouse embryonic stem cells. On average, the improved culture system shows similar seeding behaviour to the commonly used T-25 tissue culture flask. Therefore, experiments in these two systems can be conducted with the same average starting point for the sake of comparability. However, the small volume of the microfabricated devices results in more variability in the starting cell confluency.

Initial culture experiments showed that, while the improved culture system is easier to use, its flow resistance is variable over the course of multi-day perfusion culture experiments. It was therefore necessary to implement feedback control over the medium flow rate. With flow control in place,

confluency monitoring showed 7% variation between experiments in the time taken to reach a confluency of 0.5 and 9% confluency in the time taken to reach a confluency of 0.8. While this indicates reasonable repeatability, confluency curves also showed clear variations between experiments. The reasons for these experiment to experiment variations are unclear and require further investigation.

The overall growth rates, and the distributions of growth rate, show evidence that the introduction of a gas permeable lid (with an open polycarbonate element) increases both the magnitude and uniformity of growth rate, particularly in late stage culture. Likewise there is some evidence that the improved PDMS chip decreases the magnitude and uniformity of growth rate. These observations are consistent with pericellular dissolved oxygen being the most limiting factor in the expansion of the cells. However, the evidence of these design induced differences is weak due to the high experiment to experiment variability. Furthermore, it was not possible to draw conclusions on the first 12 hours of culture due to the presence of bubbles in some culture devices.

The last design challenge to be overcome was a method of temperature control for the culture chambers. A heating system was developed that is independent of disposable parts, does not overly complicate the assembly or operation of the culture devices, and could be operated while conducting manual operations such as cell seeding. The chief limitation of the new heating system is that thermal gradients exist in the culture system, requiring the monitoring of a site offset from the culture chamber and relation of that position to the culture chamber.

Finally, consideration was given to the requirements, and opportunities for design improvement, that arise if the system is to be commercialised; firstly as a process development system and then as a production system. Design concepts based on these considerations are included this report in order to guide future work with the culture system. In its current state the microfabricated

adherent culture system has improved reliability, ease of use, comparability with traditional culture systems, and control over process parameters, which should make it a useful tool for process development. Many of these features have been demonstrated in the investigation of design changes on the growth rate of mouse embryonic stem cells.

6.2 Future Work

Future work invited by this research can be broken down into; extension of the investigations made into the microfabricated culture system, expansion of those investigations, application of the system to process development, and commercialisation of the system. Firstly, extending the investigations presented here, the perfusion culture experiments of chapter four should be repeated in increased numbers. A higher number of repeats may make the evidence of design induced differences in growth rate more conclusive. Repeat experiments may also shed light on the cause of the experiment to experiment variability observed. Efforts should also be made, through inclusion of the preheat and bubble trap unit and improvements to the method of priming, to minimise the inclusion of bubbles at the start of perfusion. This would allow analysis to be extended into early monolayer culture.

At the same time the investigation could be expanded to include effects on the average expression and spatial distribution of pluripotency markers. The maintenance of pluripotency is a more important factor than growth rate in the expansion of embryonic stem cells. Cell fate may also prove to be more or less sensitive to factors such as pericellular dissolved oxygen and shear stress. Cells could also be expanded in the microfabricated culture system through multiple passages to investigate the occurrence of karyotipic changes. Another area where investigation of the culture system could be expanded, is cell seeding. While it was established that mouse embryonic stem cells seed in a similar time and to a similar average confluency to a tissue culture flask, the variability in the post seeding confluency is high. Techniques to reduce this variability could be investigated.

The potential applications of the culture system to process development are broad, in terms of both process parameters and stem cell processes. The design is especially well suited to looking at the effects of soluble factors by controlling them within very narrow ranges. It would be particularly interesting to integrate dissolved oxygen sensors either at the outlet or on the culture surface to allow precise control over pericellular dissolved oxygen. Processes known to be affected by gas phase oxygen concentration could then be re-investigated to find optimal pericellular values.

Finally, if it is to be widely adopted for process development applications, the system needs to be commercialised. Concepts of a commercial design are laid out in chapter 5. Implementation of the design changes, and development of the commercial system would be best carried out by, or in conjunction with, industrial partners with experience of mass producing parts, and assembling and marketing commercial cell culture systems. If subsequent research with the process development system shows its control advantages are necessary for some developed processes, then a production system could also be developed (a concept is shown in chapter 5).

7. Appendix 1 – Technical Drawings from Chapter 2

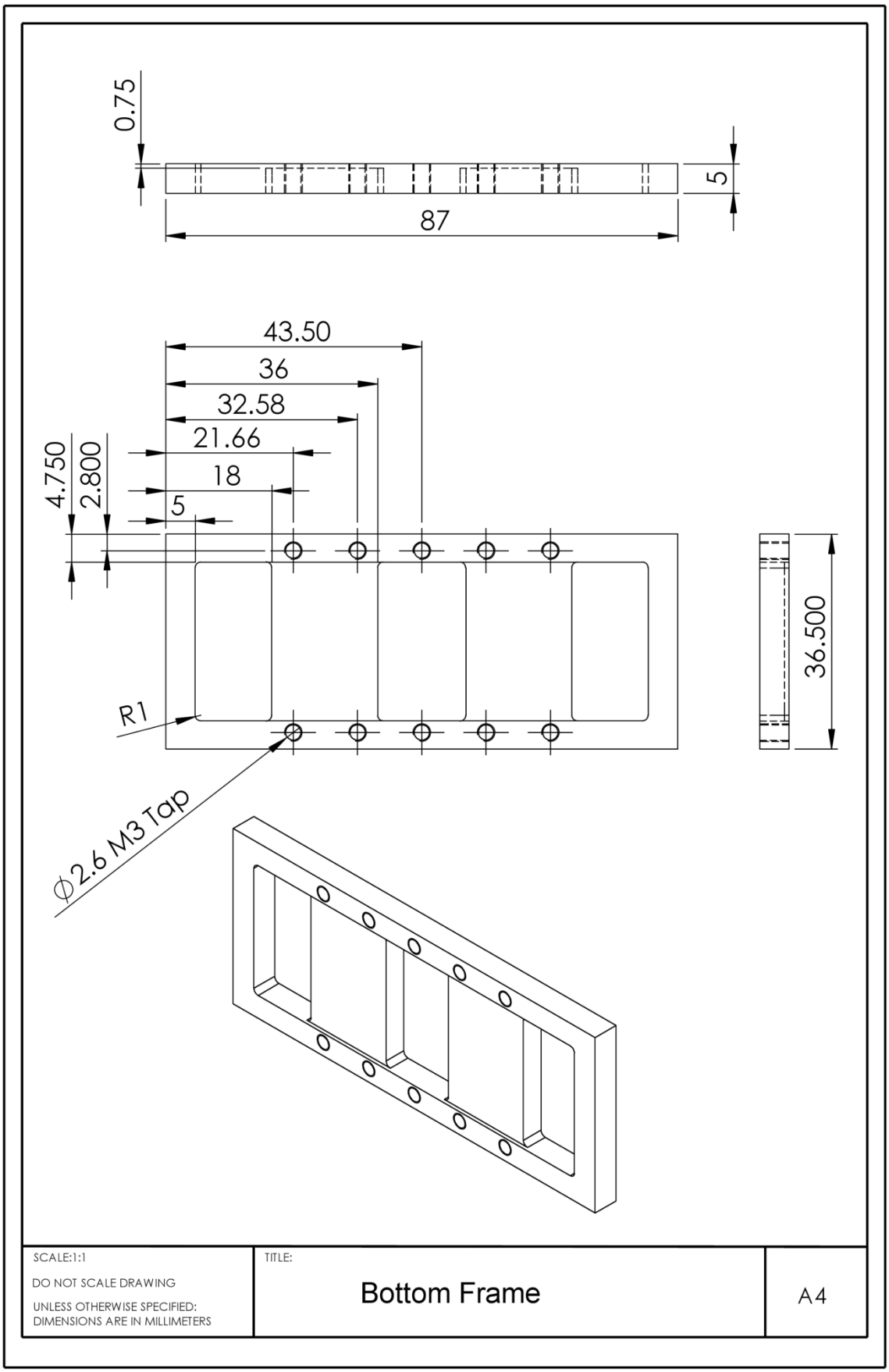

Figure 7.1 - Technical drawing of prototype bottom frame.

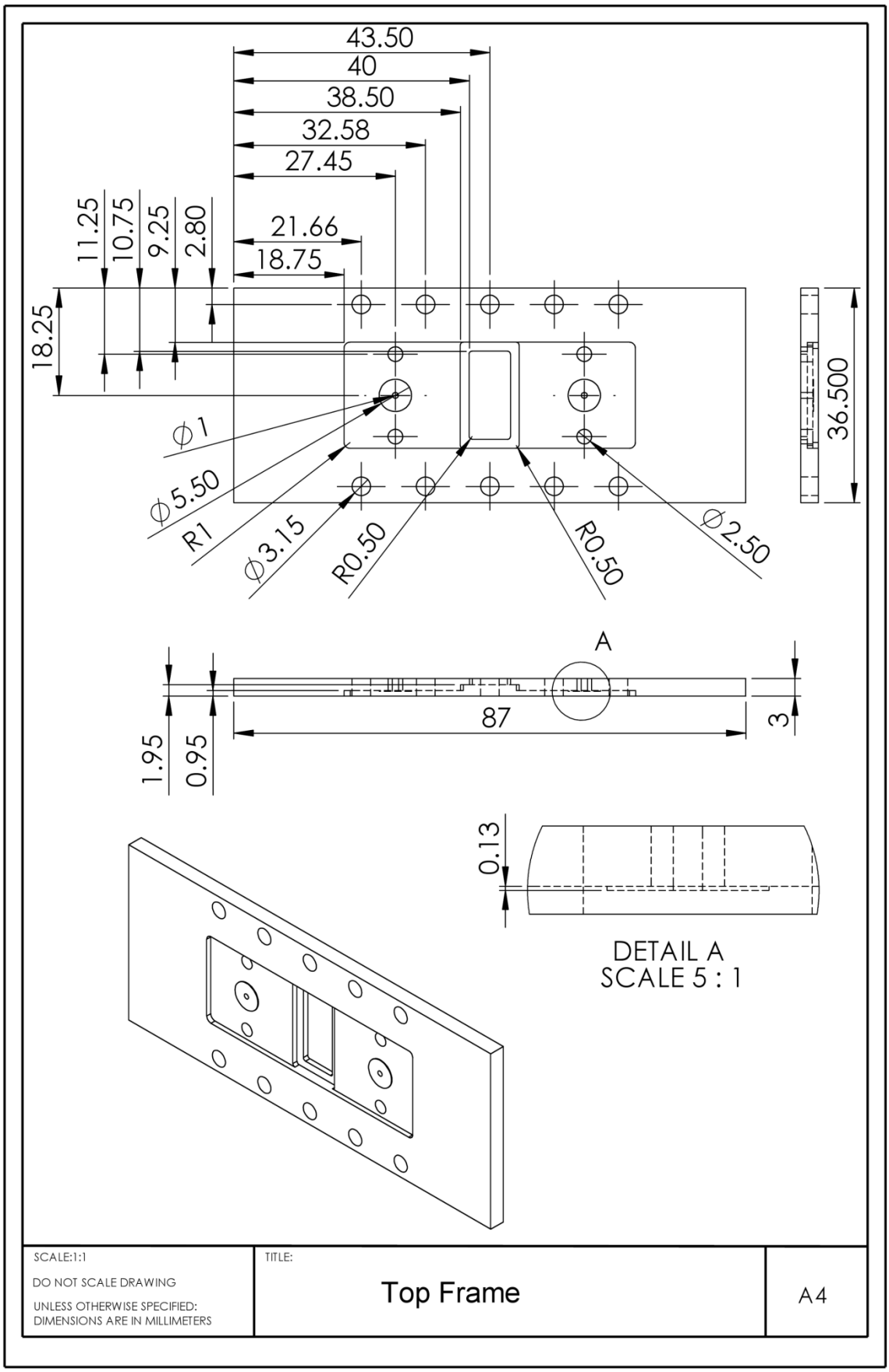

Figure 7.2 - Technical drawing of prototype top frame.

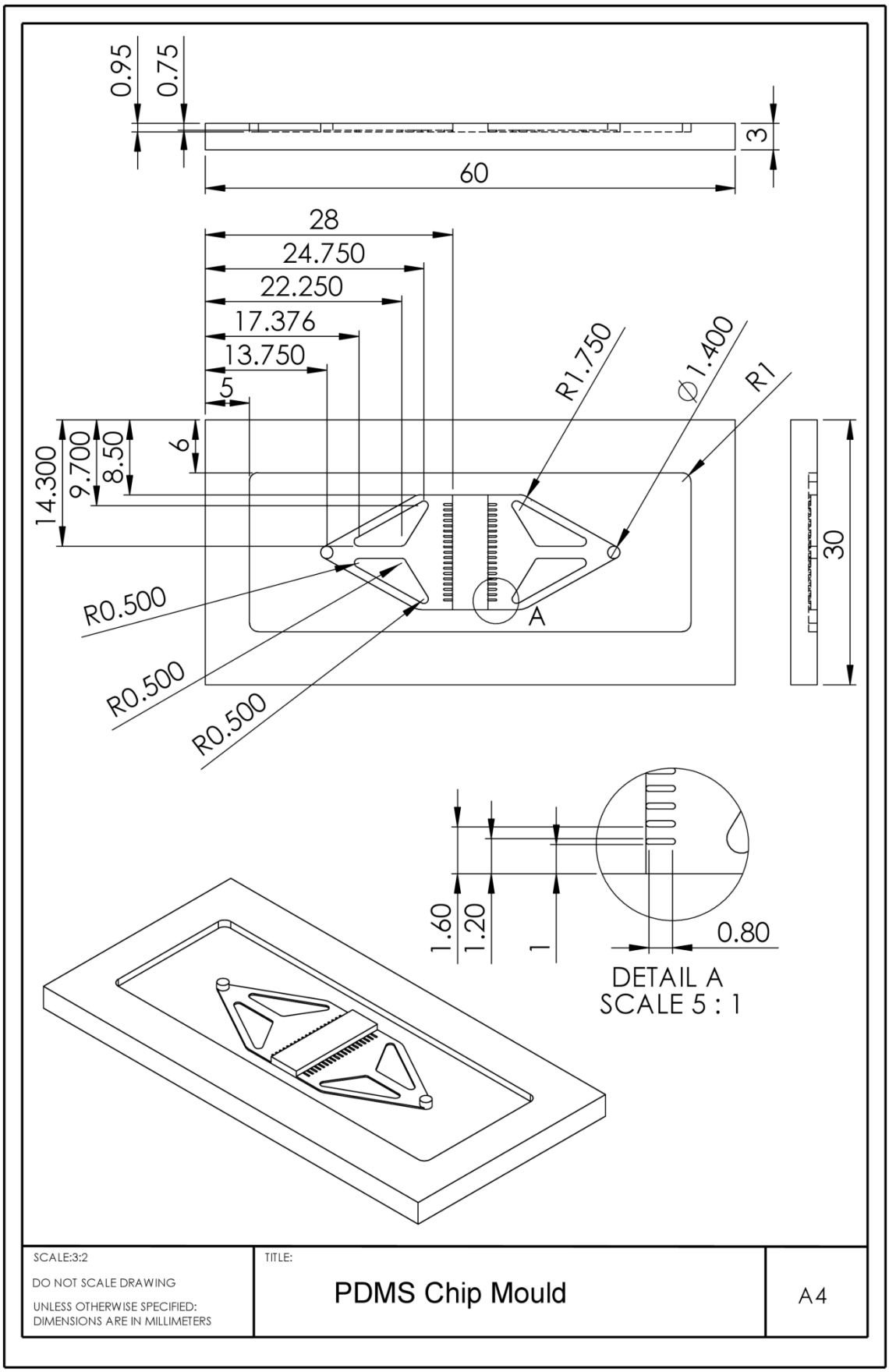

Figure 7.3 - Technical drawing of prototype PDMS chip mould.

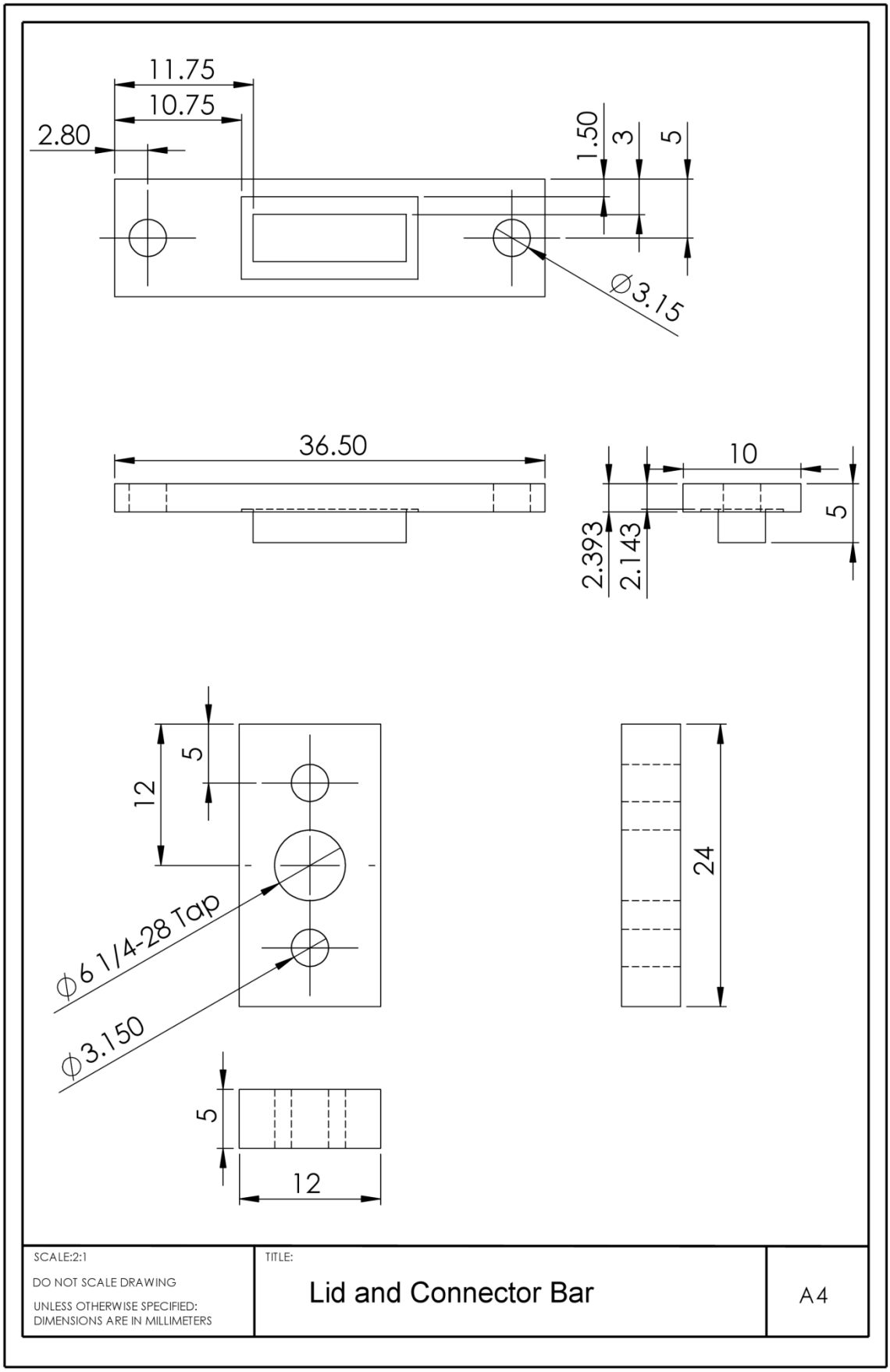

Figure 7.4 - Technical drawings of prototype lid & connector bar.

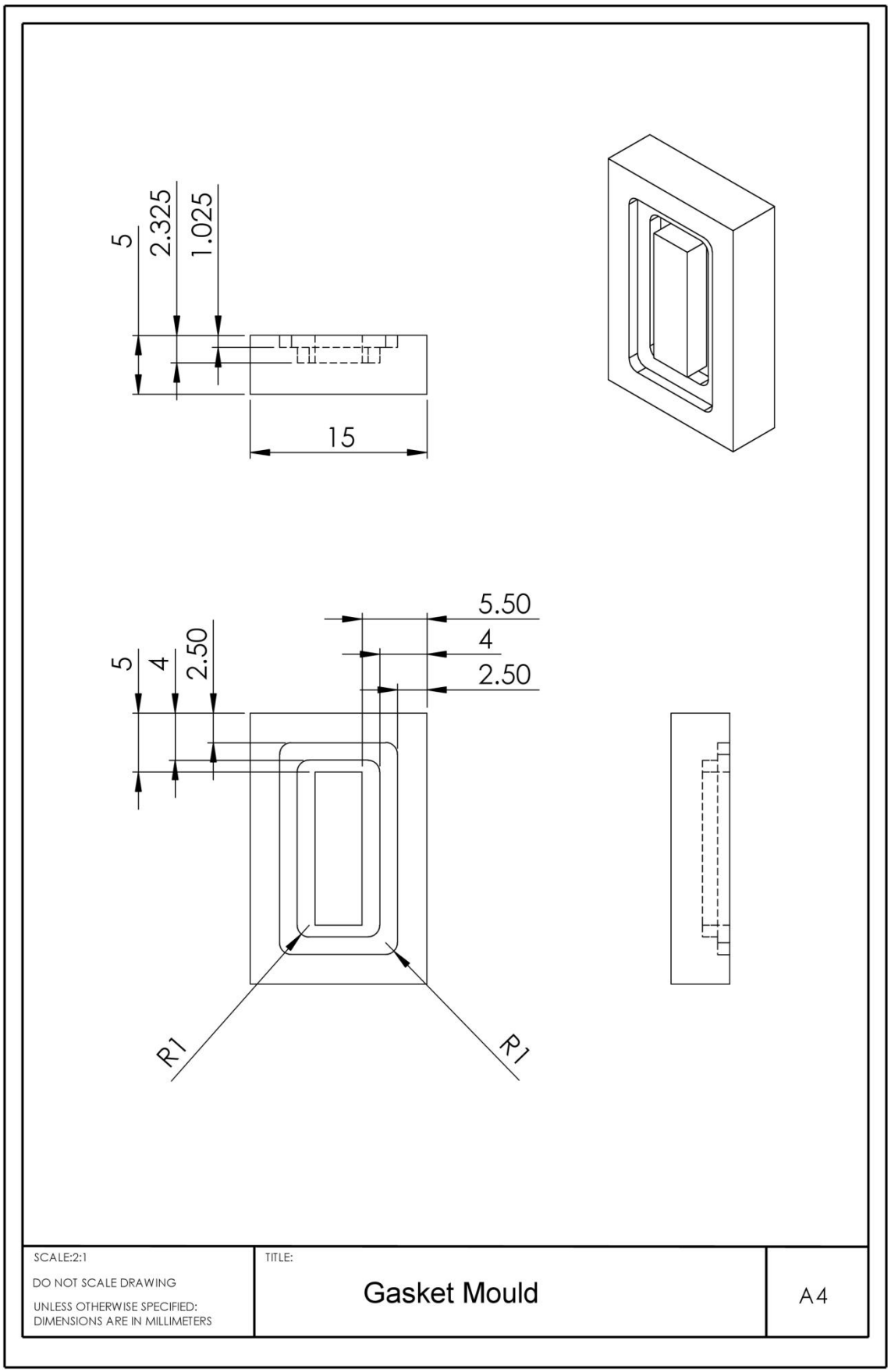

Figure 7.5 - Technical drawing of prototype gasket mould.

8. Appendix 2 – Technical Drawings from Chapter 3

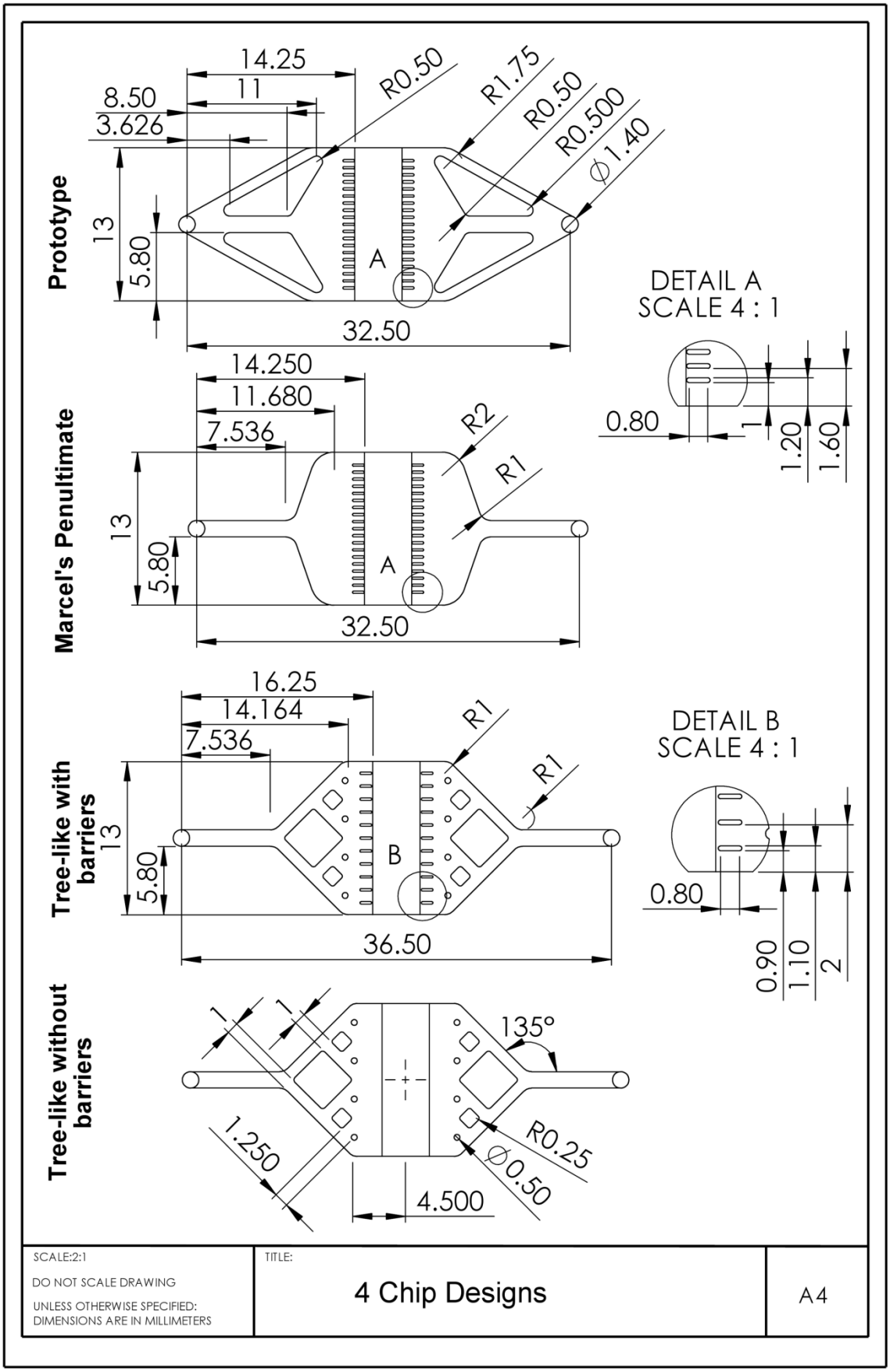

Figure 8.1 - Technical drawings of the four PDMS chip designs modelled.

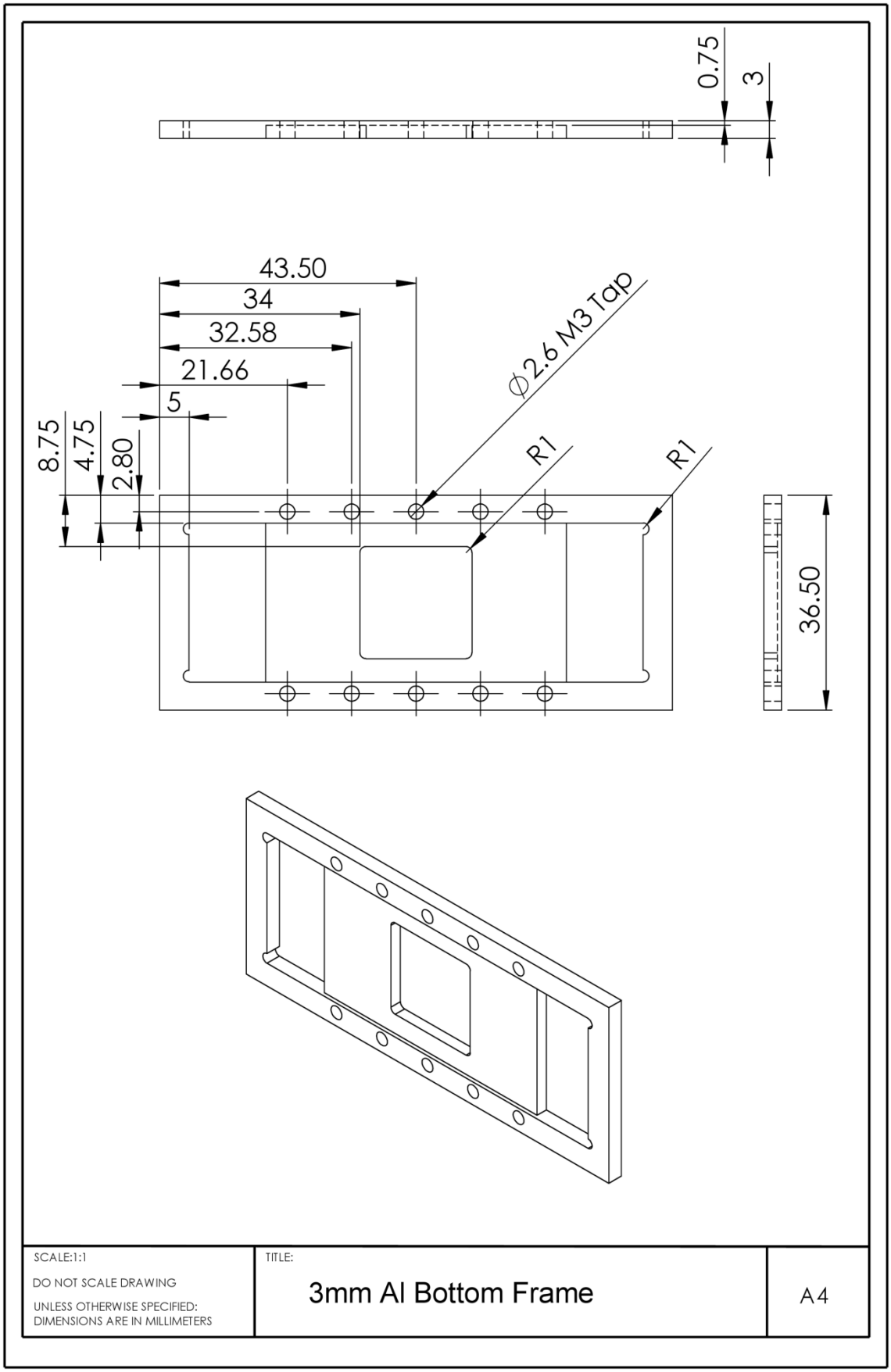

Figure 8.2 - Technical drawing of aluminium version of prototype bottom frame.

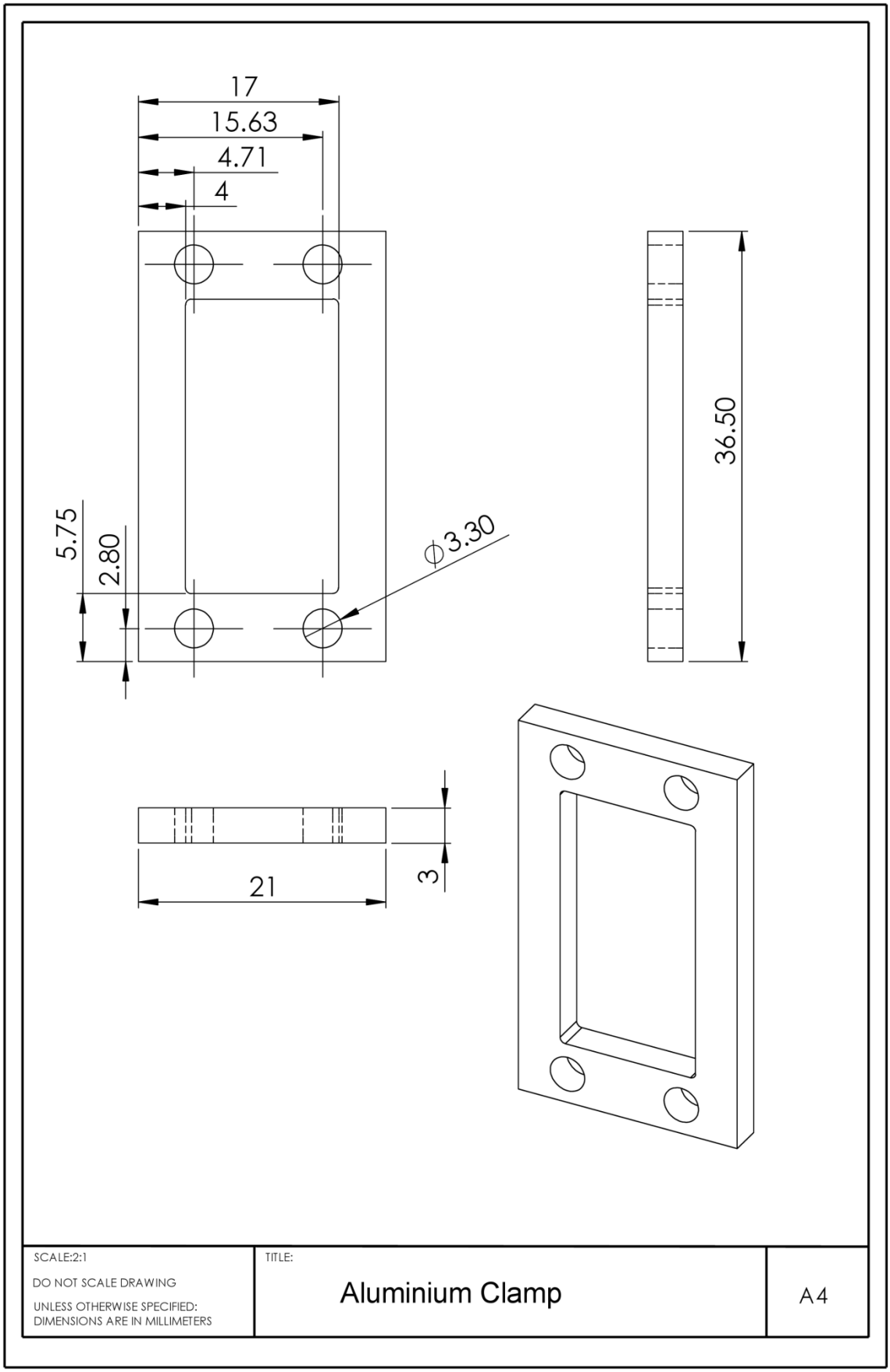

Figure 8.3 - Technical drawing of aluminium clamp.

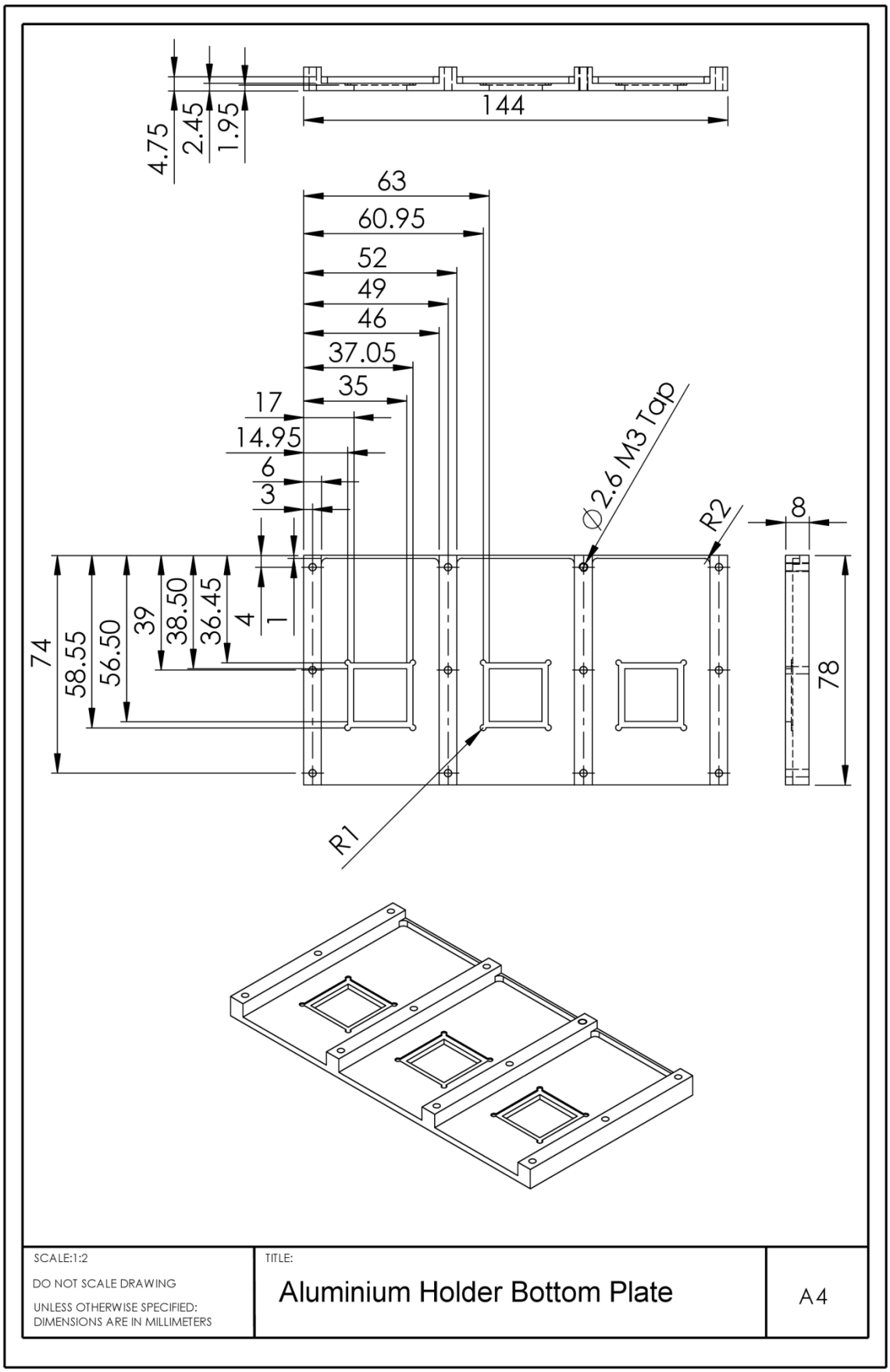

Figure 8.4 - Technical drawing of aluminium holder bottom plate.

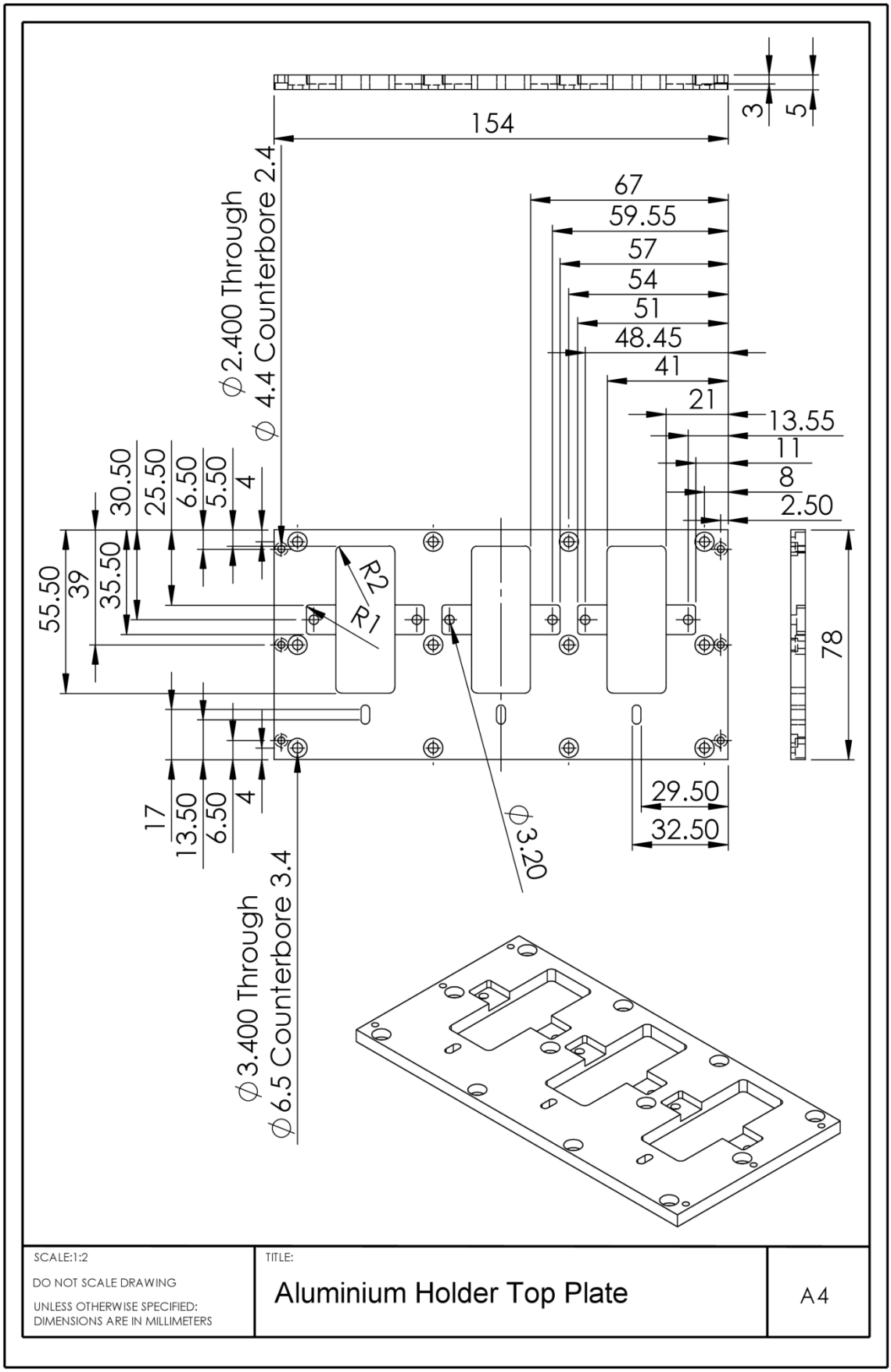

Figure 8.5 - Technical drawing of aluminium holder top plate.

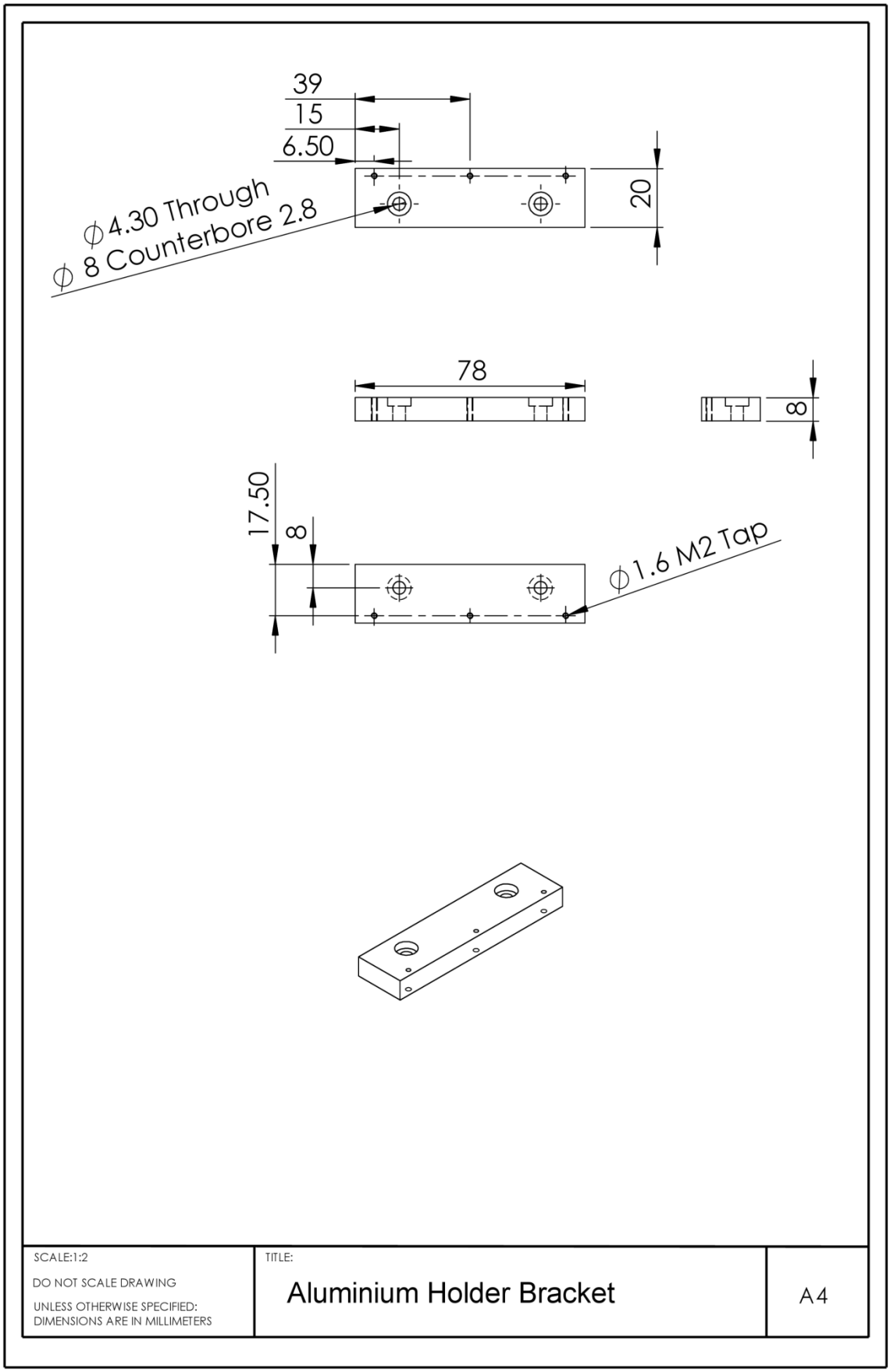

Figure 8.6 - Technical drawing of aluminium holder bracket.

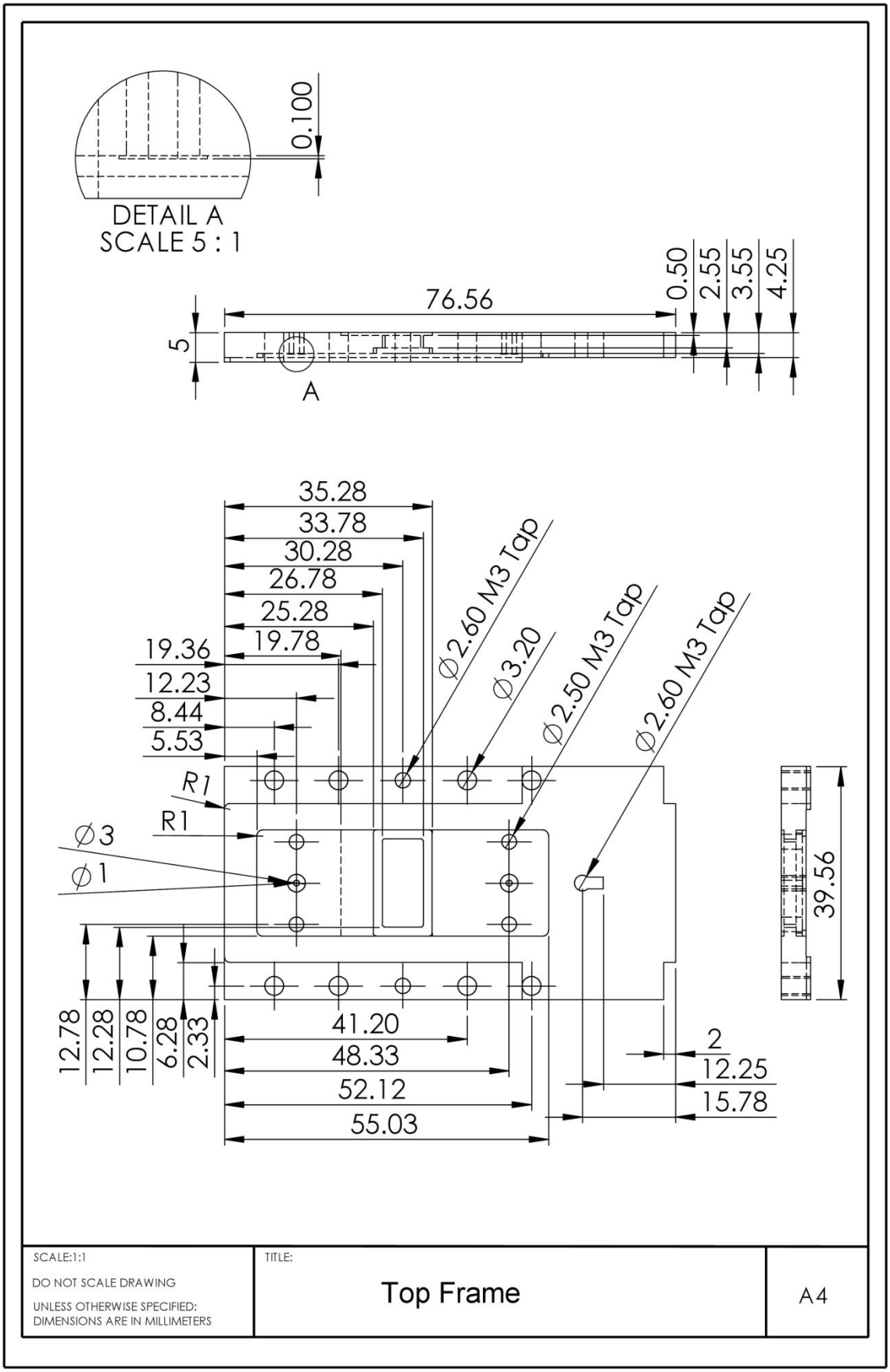

Figure 8.7 - Technical drawing of improved design top frame.

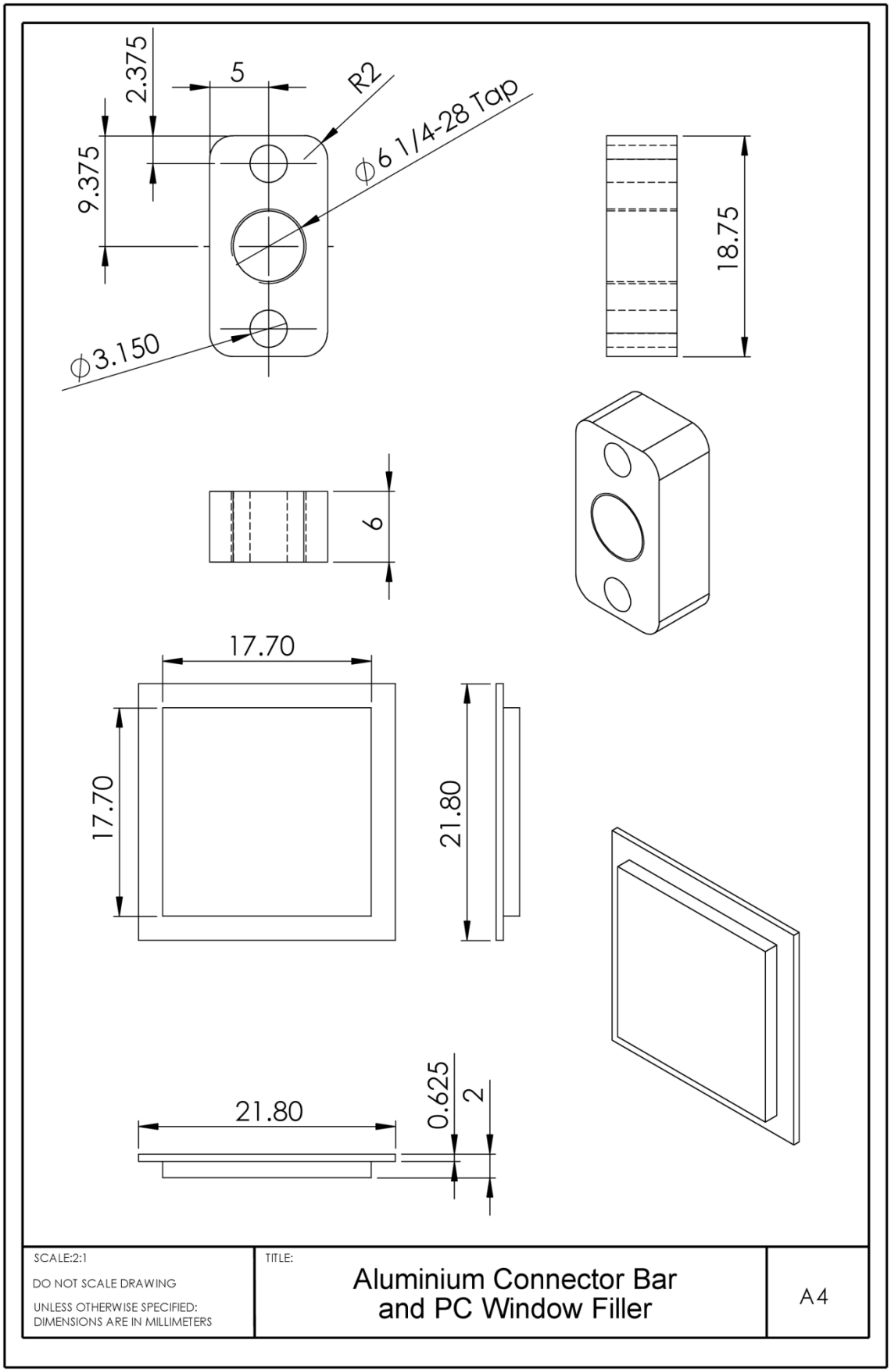

Figure 8.8 - Technical drawings of aluminium connector bar & polycarbonate window filler.

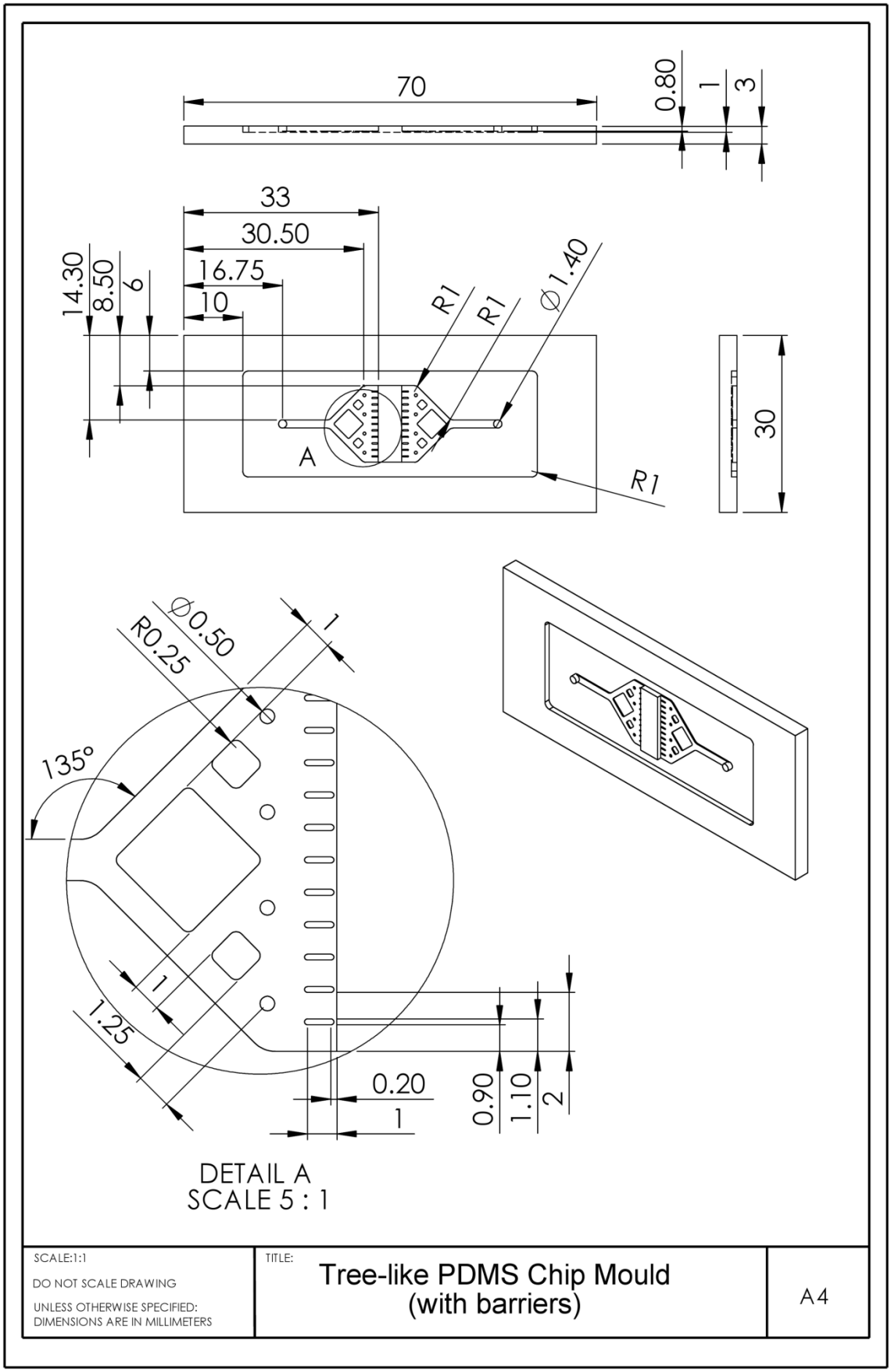

Figure 8.9 - Technical drawing of mould for tree-like PDMS chip.

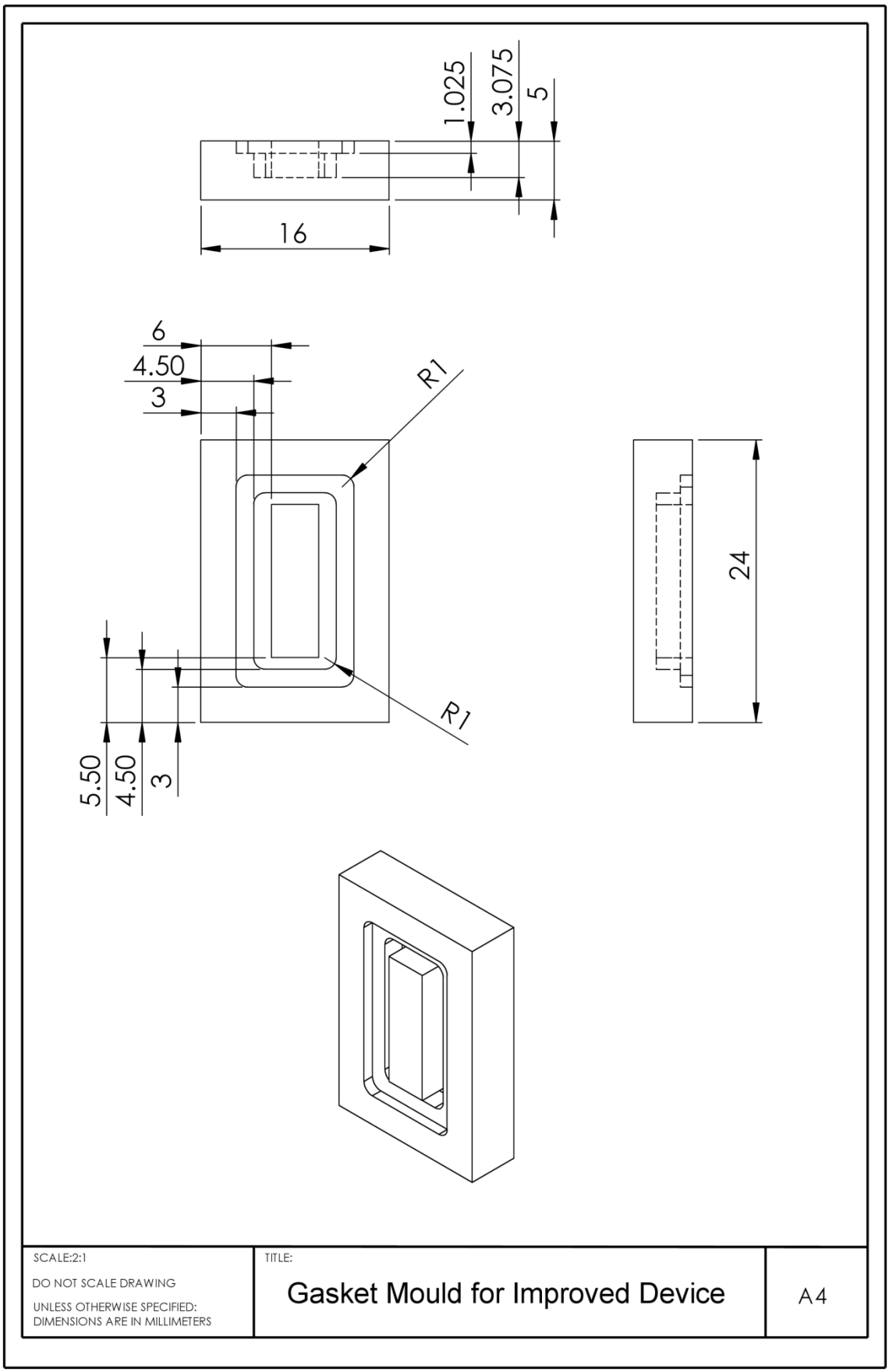

Figure 8.10 - Technical drawing of gasket mould for improved culture device.

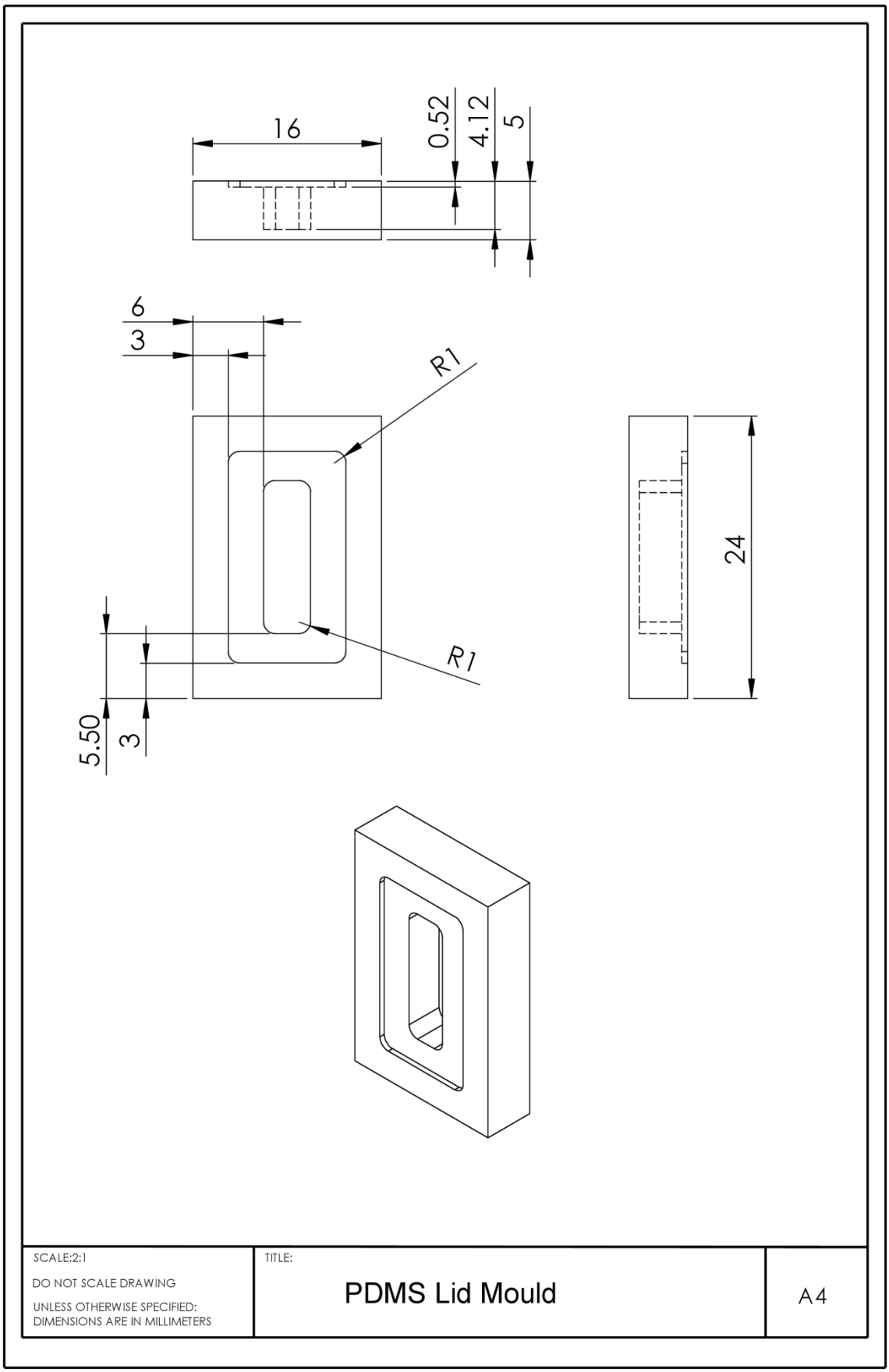

Figure 8.11 - Technical drawing of mould for PDMS lid component.

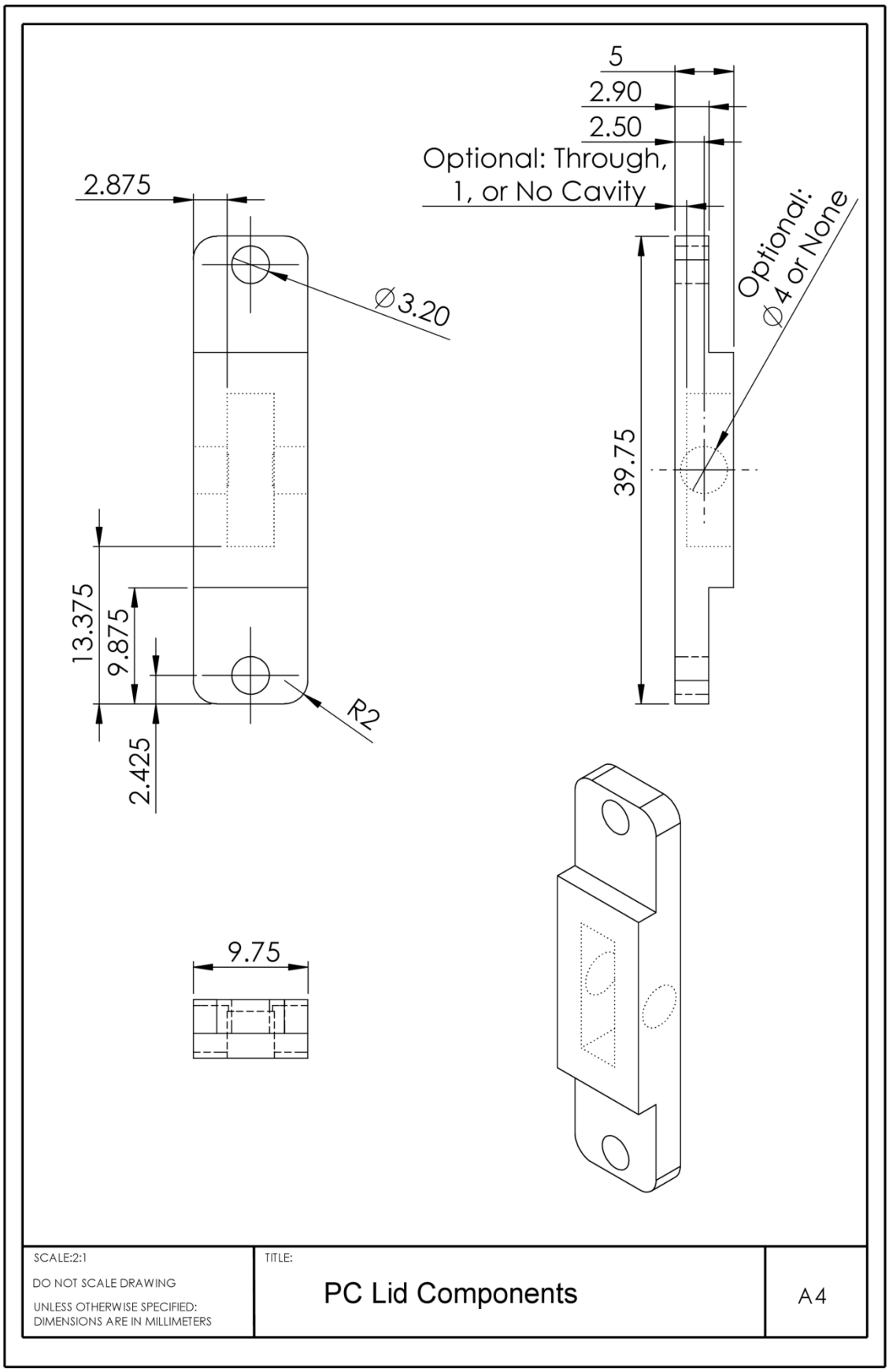

Figure 8.12 - Technical drawing of polycarbonate lid component with options for closed, open, or gas connection.

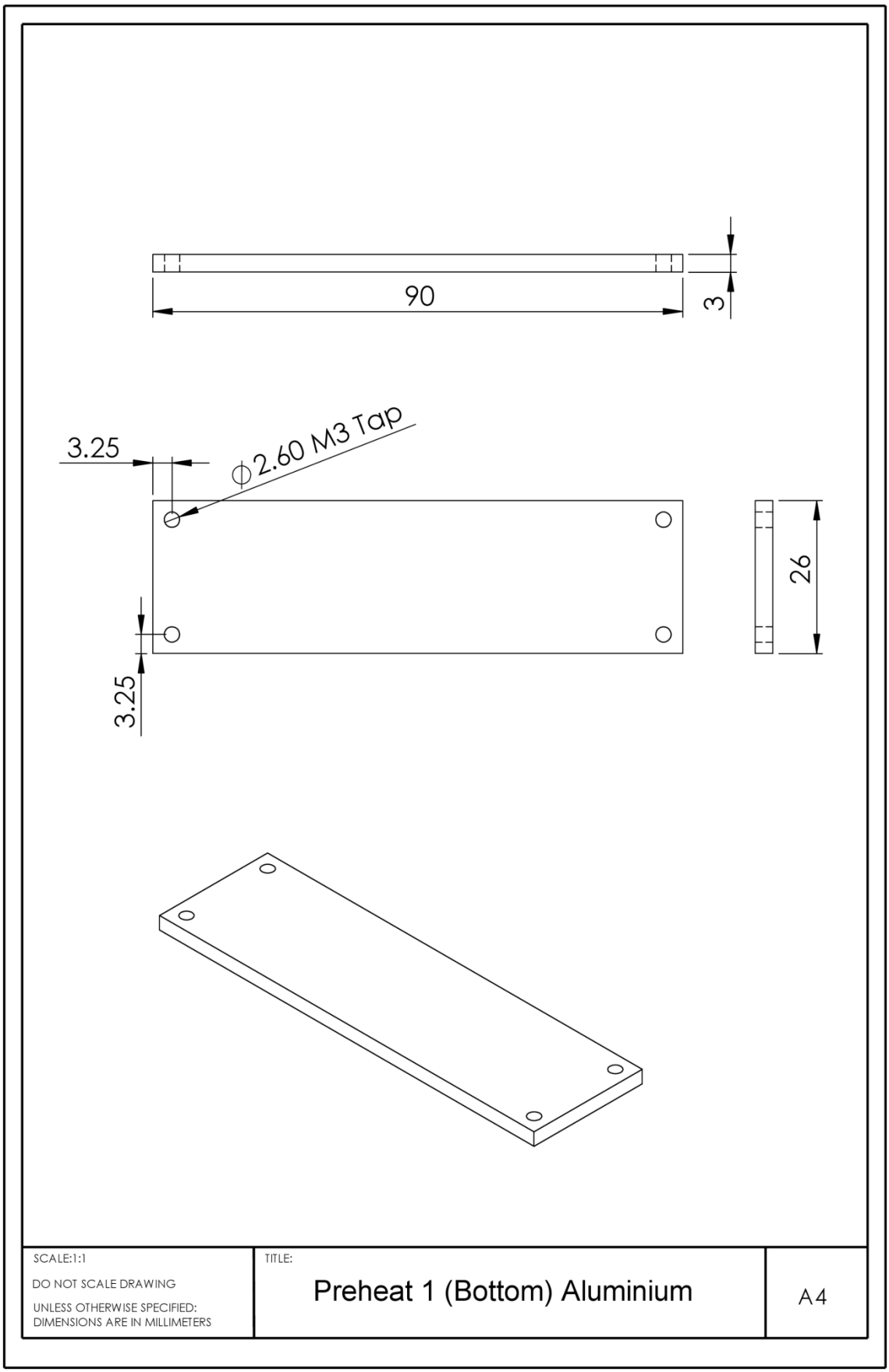

Figure 8.13 - Technical drawing of layer 1 (bottom) of the preheat and bubble trap unit.

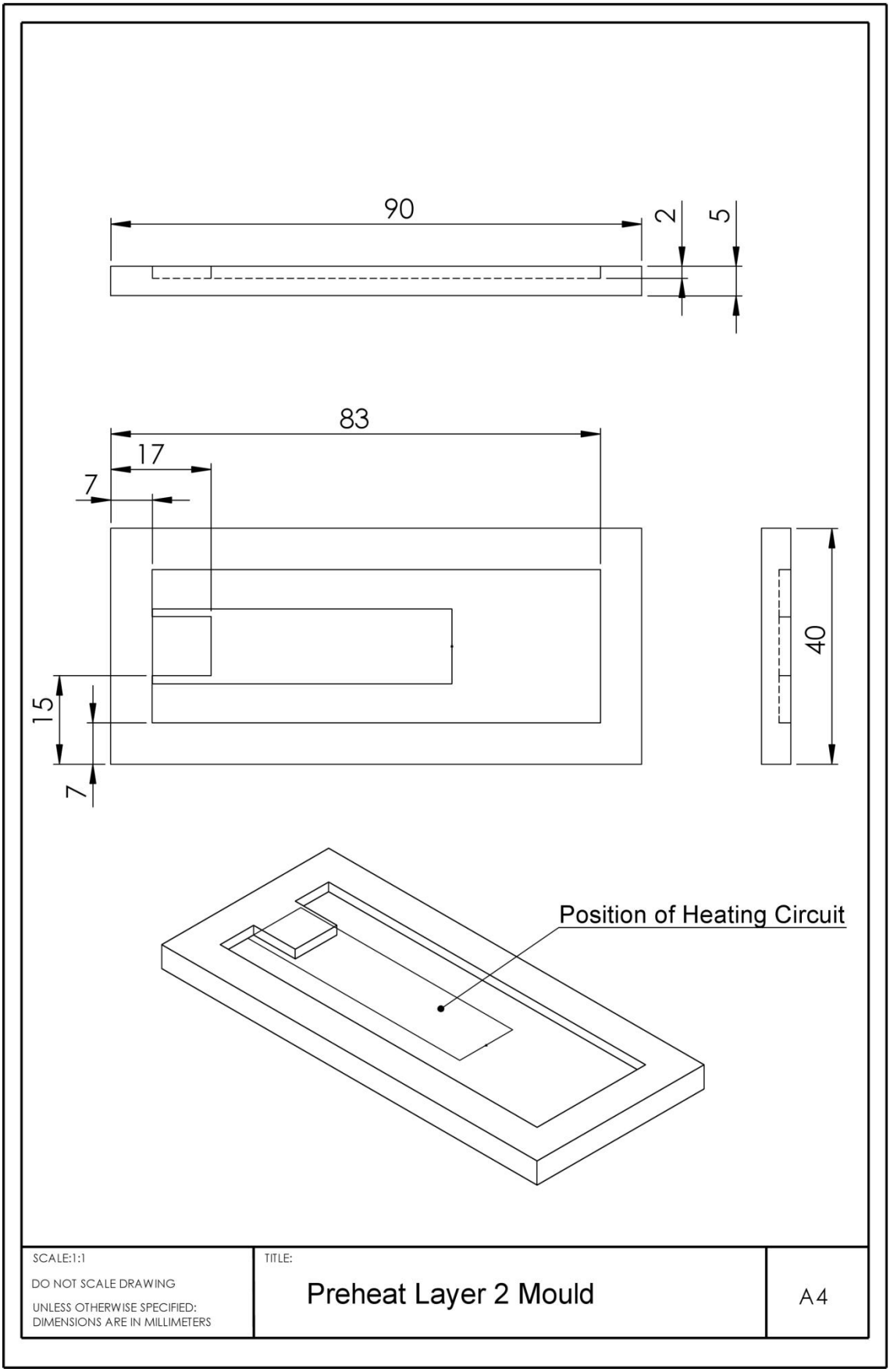

Figure 8.14 - Technical drawing of mould for layer 2 of the preheat and bubble trap unit.

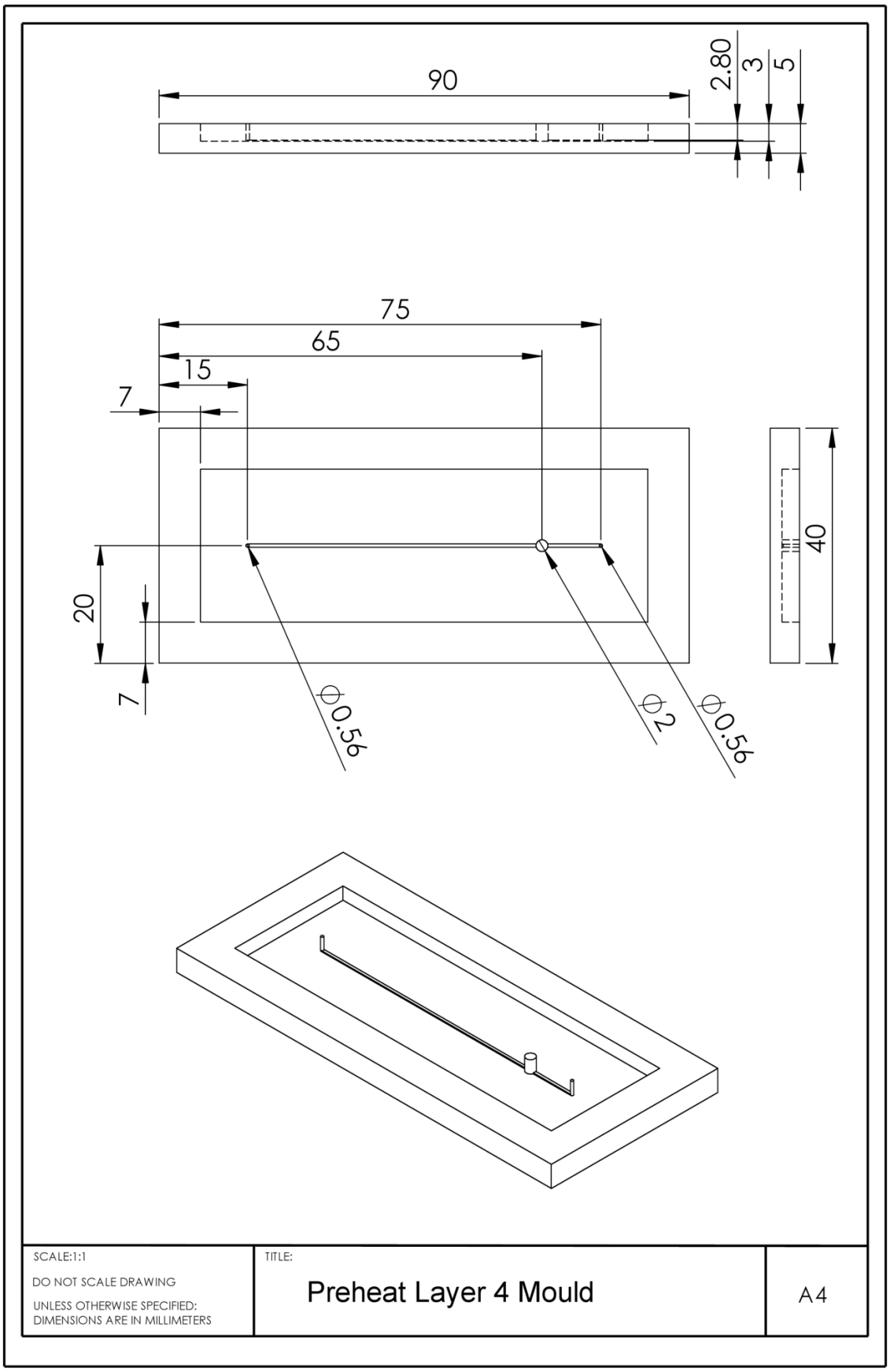

Figure 8.15 - Technical drawing of mould for layer 4 of the preheat and bubble trap element (plasma bonded to layer 3, a 0.12 mm spin-coated layer of PDMS).

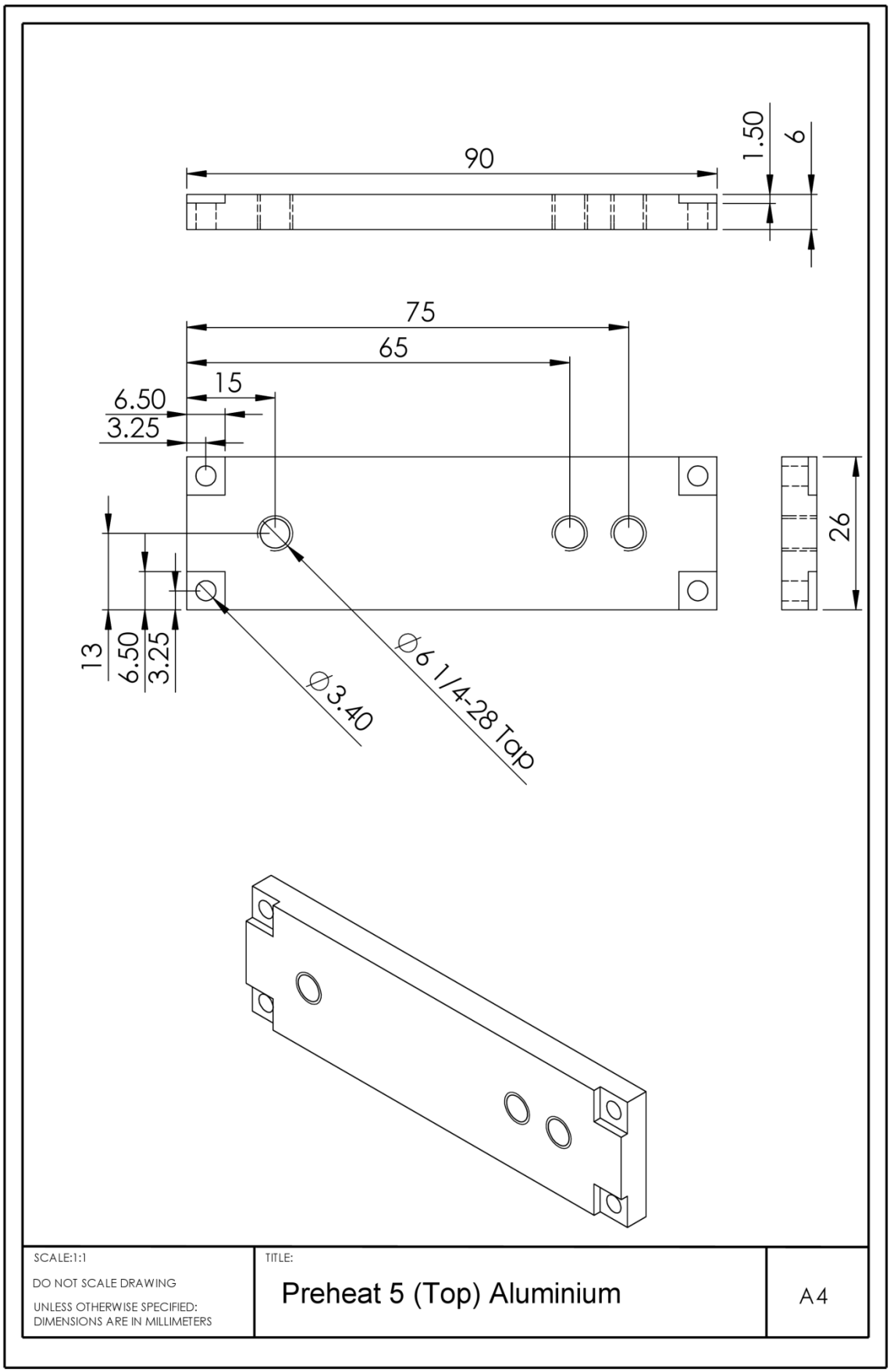

Figure 8.16 - Technical drawing of layer 5 (top) of the preheat and bubble trap unit.

9. Appendix 3 – Cross-sections and Second Moments of Inertia for Bending Calculations

Multiple cross-sections are used across the width of the components modelled in bending calculations. Second moments of inertia were calculated for each rectangular feature and then adjusted for the features distance from the centre axis to give second moments of inertia about the same axis. The adjusted second moments of inertia were multiplied by the appropriate elastic modulus and the product added or subtracted from the previous total as appropriate.

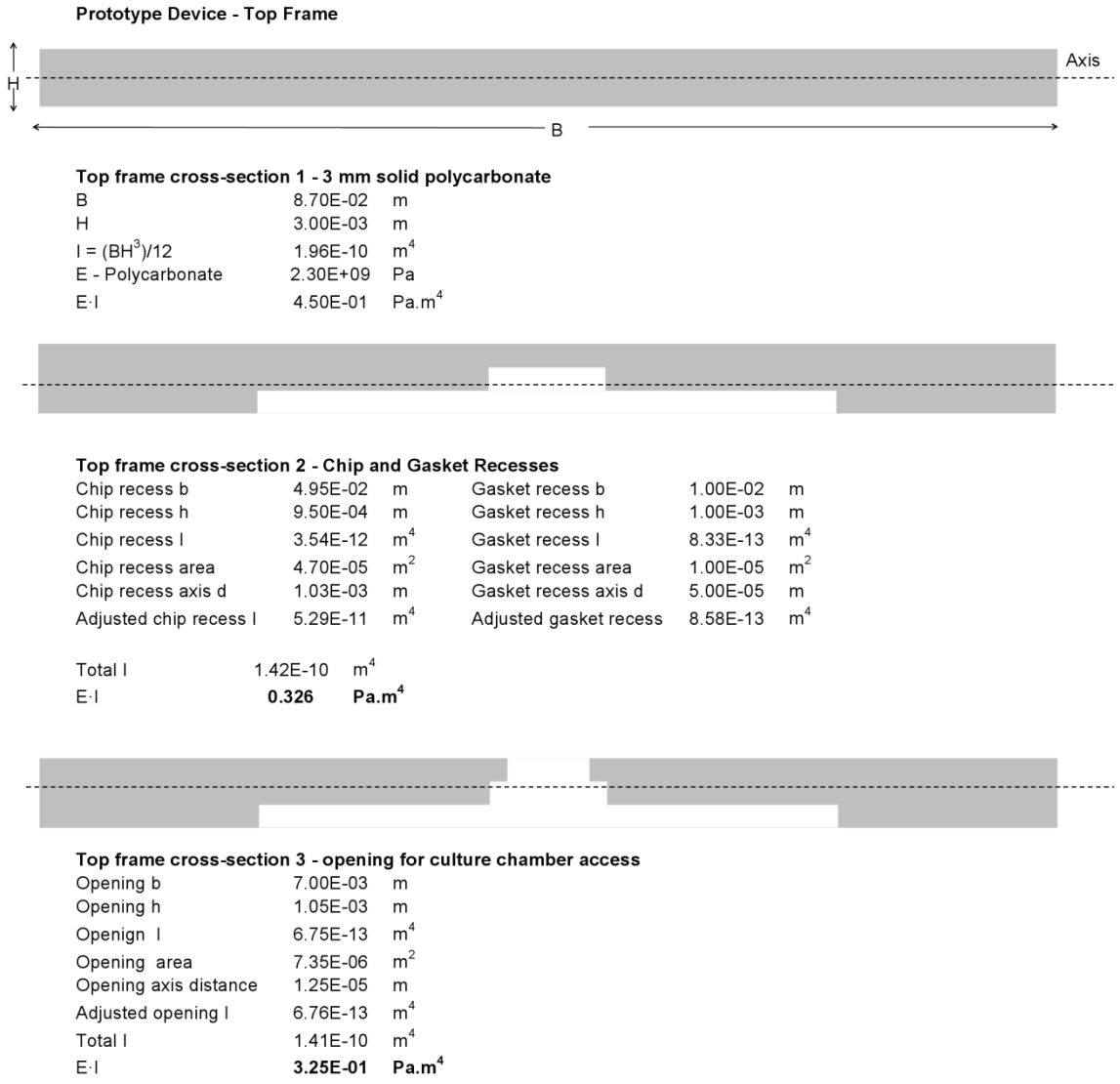

Figure 9.1 – Cross-sections of the prototype top frame used for bending calculations.

Three cross-sections were used across the width of the top frame; a solid rectangle, a rectangle less the gasket and chip recesses, and a rectangle less the opening to access the culture chamber and the gasket and chip recesses.

Prototype Device - Top Frame

Bottom frame cross-section 1- 5 mm solid polycarbonate

B	8.70E-02	m
H	5.00E-03	m
I	9.06E-10	m^4
E - Polycarbonate	2.30E+09	Pa
E·I	**2.08E+00**	**Pa.m^4**

Bottom frame cross-section 2 - slide recess

Slide recess b	7.70E-02	m
Slide recess h	7.50E-04	m
Slide recess I	2.71E-12	m^4
Slide recess area	5.78E-05	m^2
Slide recess axis distan	2.13E-03	m
Adjusted slide recess I	2.63E-10	m^4
Total I	6.43E-10	m^4
E·I	**1.48E+00**	**Pa.m^4**

Bottom frame cross-section 3 - TC-PS Slide

Slide b	7.60E-02	m
Slide h	1.00E-03	m
Slide I	6.33E-12	m^4
Slide area	7.60E-05	m^2
Slide axis distance	2.25E-03	m
Adjusted slide I	3.91E-10	m^4
E - TCPS	3.00E+09	Pa
Total E·I	**2.65E+00**	**Pa.m^4**

Bottom frame cross-section 4 - culture chamber viewing window

Window b	1.90E-02	m
Window h	4.25E-03	m
Window I	1.22E-10	m^4
Window area	8.08E-05	m^2
Window axis d	3.75E-04	m
Adjusted window I	1.33E-10	m^4
E - PC	2.30E+09	Pa
Total E·I	**2.35E+00**	**Pa.m^4**

Figure 9.2 - Cross-sections of the prototype bottom frame and slide used for bending calculations.

Four cross-sections were used across the width of the bottom frame and slide; a solid rectangle, a rectangle less the slide recess, a rectangle less the slide recess plus the slide, and a rectangle less the viewing window and slide recess plus the slide.

Improved Design - Holder Top Plate and Top Frame

Top cross-section 1 - 5 mm solid aluminium

B	7.80E-02	m
H	5.00E-03	m
I	8.13E-10	m^4
E - Aluminium	7.00E+10	Pa
EI	5.69E+01	$Pa.m^4$

Top cross-section 2 - Lid recess and 5 mm polycarbonate top frame

Lid recess b	1.00E-02	m	Top frame b	7.70E-02	m
Lid recess h	3.00E-03	m	Top frame h	5.00E-03	m
Lid recess I	2.25E-11	m^4	Top frame I	8.02E-10	m^4
Lid Recess A	3.00E-05	m^2	Top frame A	3.85E-04	m^2
Lid recess axis d	1.00E-03	m	Top frame axis d	5.00E-03	m
Lid recess adjusted I	5.25E-11	m^4	Top frame adjusted I	1.04E-08	m^4
E - Aluminium	7.00E+10	Pa	E - Polycarbonate	2.30E+09	Pa

EI **7.72E+01** **$Pa.m^4$**

Top cross-section 3 - Slide recess

Slide recess b	7.70E-02	m
Slide recess h	7.50E-04	m
Slide recess I	2.71E-12	m^4
Slide recess A	5.78E-05	m^2
Slide recess axis d	7.13E-03	m
Adjusted slide recess I	2.93E-09	m^4
E - Polycarbonate	2.30E+09	Pa
EI	**7.04E+01**	**$Pa.m^4$**

Figure 9.3 - Cross-sections of the upper components of the improved design used for bending calculations (part 1).

Six cross-sections were used across the width of the upper components which included both the top plate of the aluminium holder and the polycarbonate top frame.

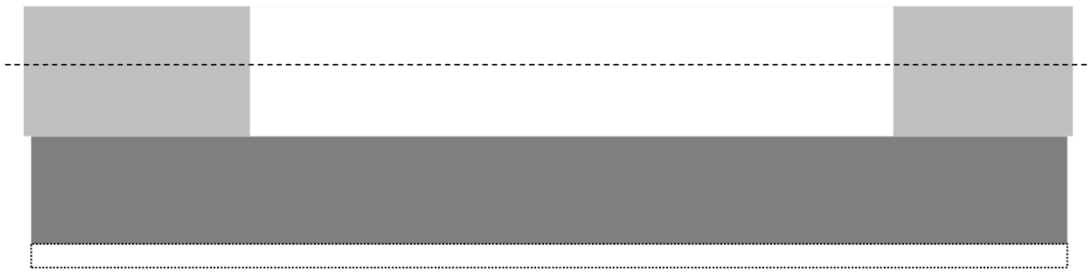

Top cross-section 4 - Top plate window

Window b	5.00E-02	m
Window h	5.00E-03	m
Window I	5.21E-10	m^4
E - Aluminium	7.00E+10	Pa
EI	**3.40E+01**	**$Pa.m^4$**

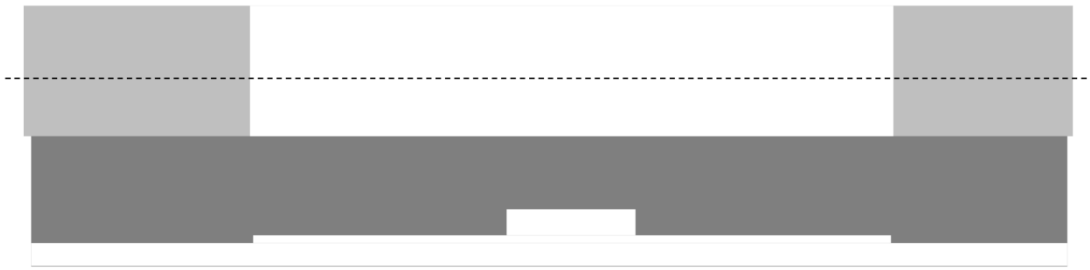

Top cross-section 5 - chip and gasket recesses

Chip recess b	4.95E-02	m	Gasket recess b	1.00E-02	m
Chip recess h	7.00E-04	m	Gasket recess h	1.00E-03	m
Chip recess I	1.41E-12	m^4	Gasket recess I	8.33E-13	m^4
Chip recess A	3.47E-05	m^2	Gasket recess A	1.00E-05	m^2
Chip recess axis d	6.40E-03	m	Gasket recess axis d	5.55E-03	m
Adjusted Chip Recess I	1.42E-09	m^4	Adjusted Gasket reces	3.09E-10	m^4
E - Polycarbonate	2.30E+09	Pa	E - Polycarbonate	2.30E+09	Pa
EI	**3.00E+01**	**$Pa.m^4$**			

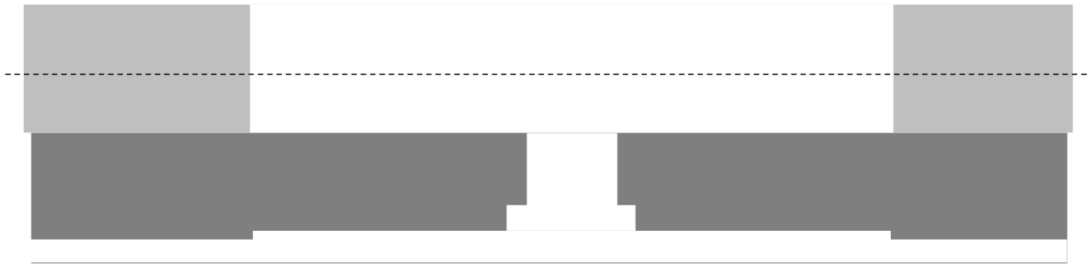

Top cross-section 6 - opening for culture chamber access

Opening b	7.00E-03	m
Opening h	2.55E-03	m
Opening I	9.67E-12	m^4
Opening A	1.79E-05	m^2
Opening axis d	3.78E-03	m
Adjusted opening I	2.64E-10	m^4
E - Polycarbonate	2.30E+09	Pa
EI	**2.94E+01**	**$Pa.m^4$**

9.4 - Cross-sections of the upper components of the improved design used for bending calculations (part 2).

Six cross-sections were used across the width of the upper components which included both the top plate of the aluminium holder and the polycarbonate top frame.

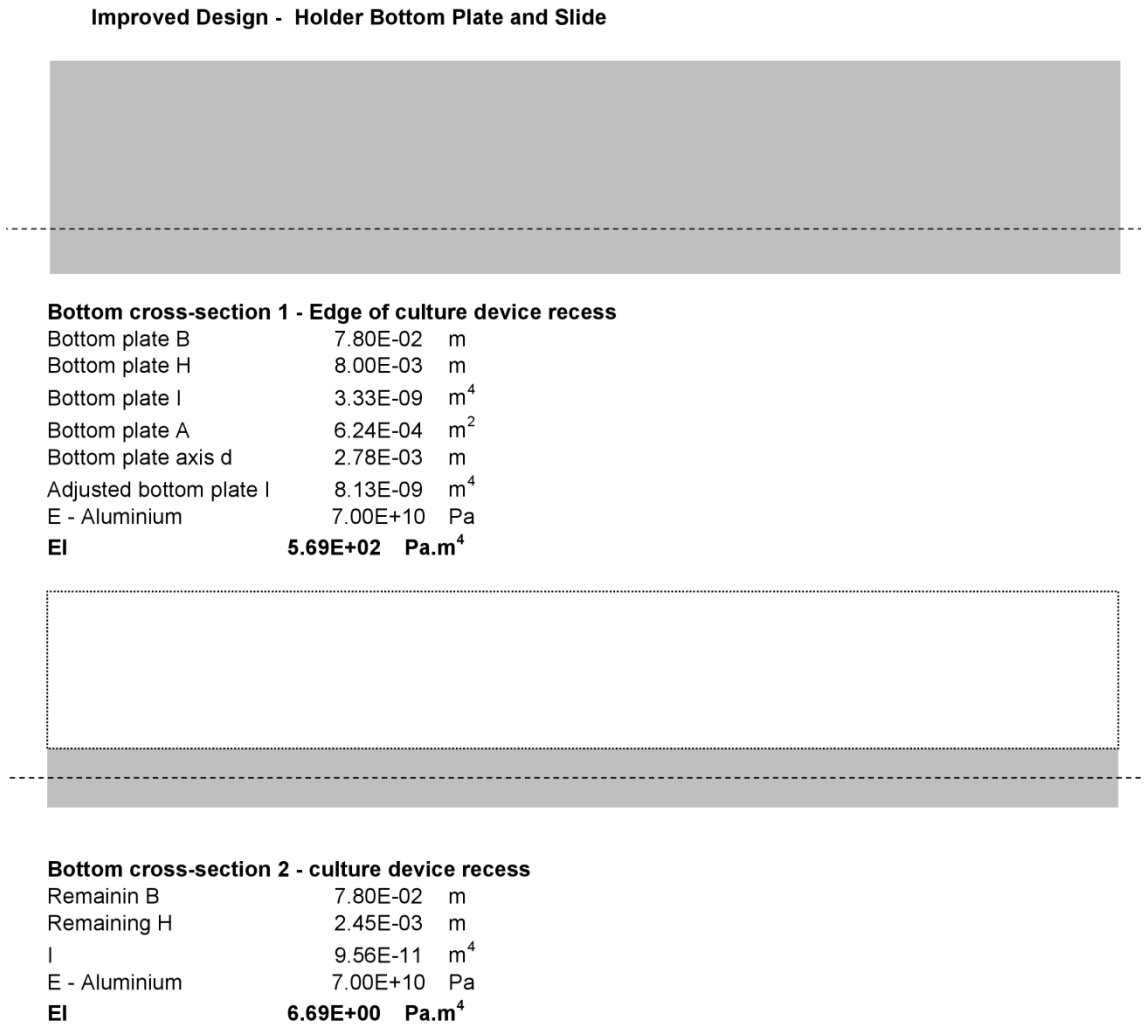

Figure 9.5 - Cross-sections of the lower components of the improved design used for bending calculations (part1).

Four cross-sections were used across the width of the lower components which included both the bottom plate of the aluminium holder and the TC-PS slide.

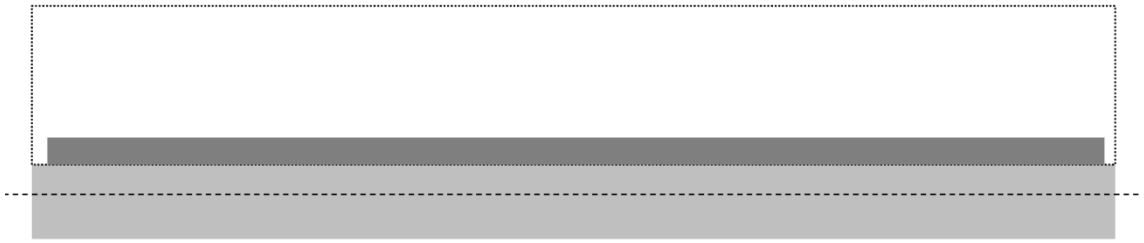

Bottom cross-section 3 - slide

Slide B	7.60E-02	m
Slide H	1.00E-03	m
Slide I	6.33E-12	m^4
Slide A	7.60E-05	m^2
Slide axis d	1.73E-03	m
Adjusted slide I	2.32E-10	m^4
E - TCPS	3.00E+09	Pa
EI	**7.39E+00**	**$Pa.m^4$**

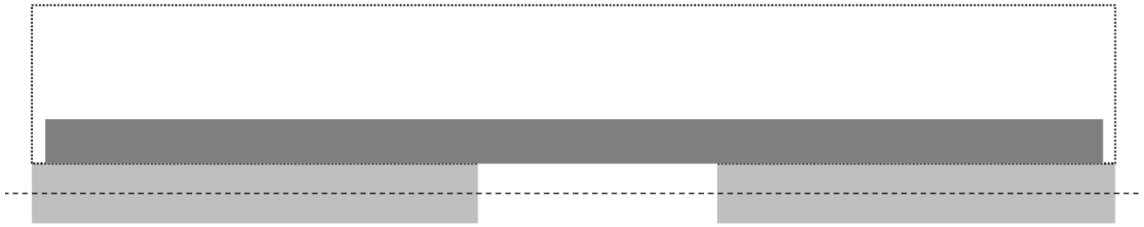

Bottom cross-section 4 - bottom plate viewing window

Window B	1.80E-02	m
Window H	2.45E-03	m
Window I	2.21E-11	m^4
E - Aluminium	7.00E+10	Pa
EI	**5.84E+00**	**$Pa.m^4$**

Figure 9.6 - Cross-sections of the lower components of the improved design used for bending calculations (part1).

Four cross-sections were used across the width of the lower components which included both the bottom plate of the aluminium holder and the TC-PS slide.

10. Appendix 4 – Circuit Diagrams for Improved Culture System

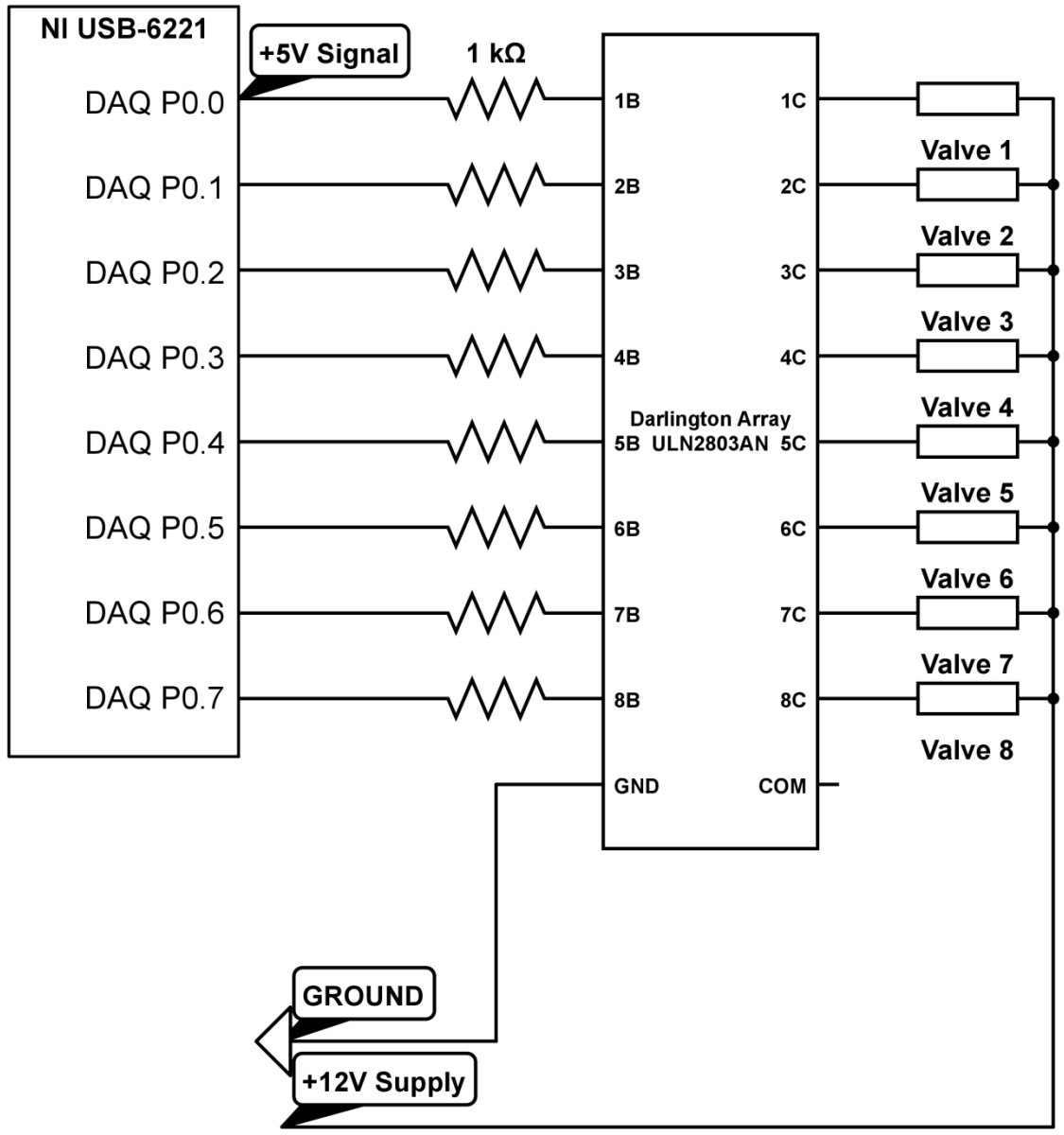

Figure 10.1 - Circuit diagram for valves controlling gas supply in improved platform.

A 5V digital signal from the DAQ (National Instruments, UK) is used to switch the position of valves controlling the gas supply (Pneu-store, UK). The first two valves are to be 2-position 3-way valves (S070B-6CC-M3) controlling which of two gas supplies feeds the gas permeable lids of two parallel device sets. These valves were not installed in the initial build as only one gas supply was used. Valves 3-8 are normal closed on/off valves (LVM10R3Y-6A1-1-Q) to control which gas supplies are connected to which medium bottles. For the initial build with two medium bottles only tow valves were installed. The Darlington Array and resistors were obtained from Farnell, UK. The digital ground of the DAQ is connected to the ground of the 12 V DC power source.

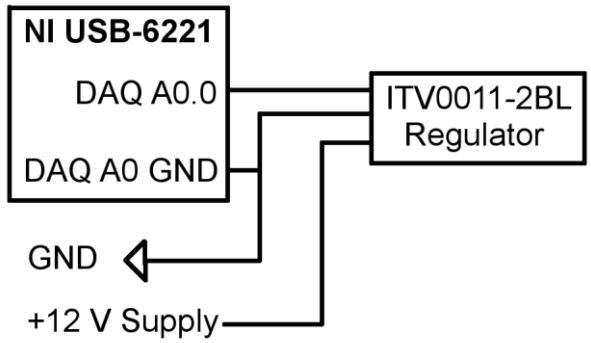

Figure 10.2 - Circuit diagram of electronic regulator.

The electronic regulator (ITV0011-2BL, Pneu-Store, UK) is controlled by a 0-5V analogue output from the DAQ (National Instruments, UK) and powered by the 12 V power supply.

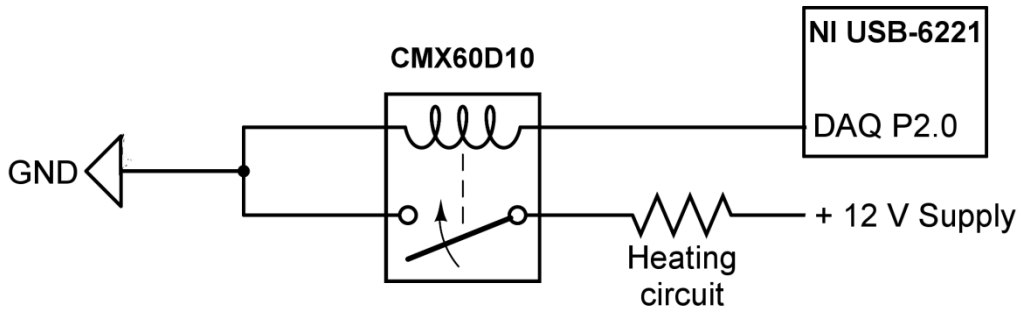

Figure 10.3 - Circuit diagram for heating circuit control.

The flexible heating circuits discussed in chapter 4 are controlled by a digital square wave output from the DAQ (National Instruments, UK) which operates a solid state relay (Farnell, UK) to connect the the 12 V power supply.

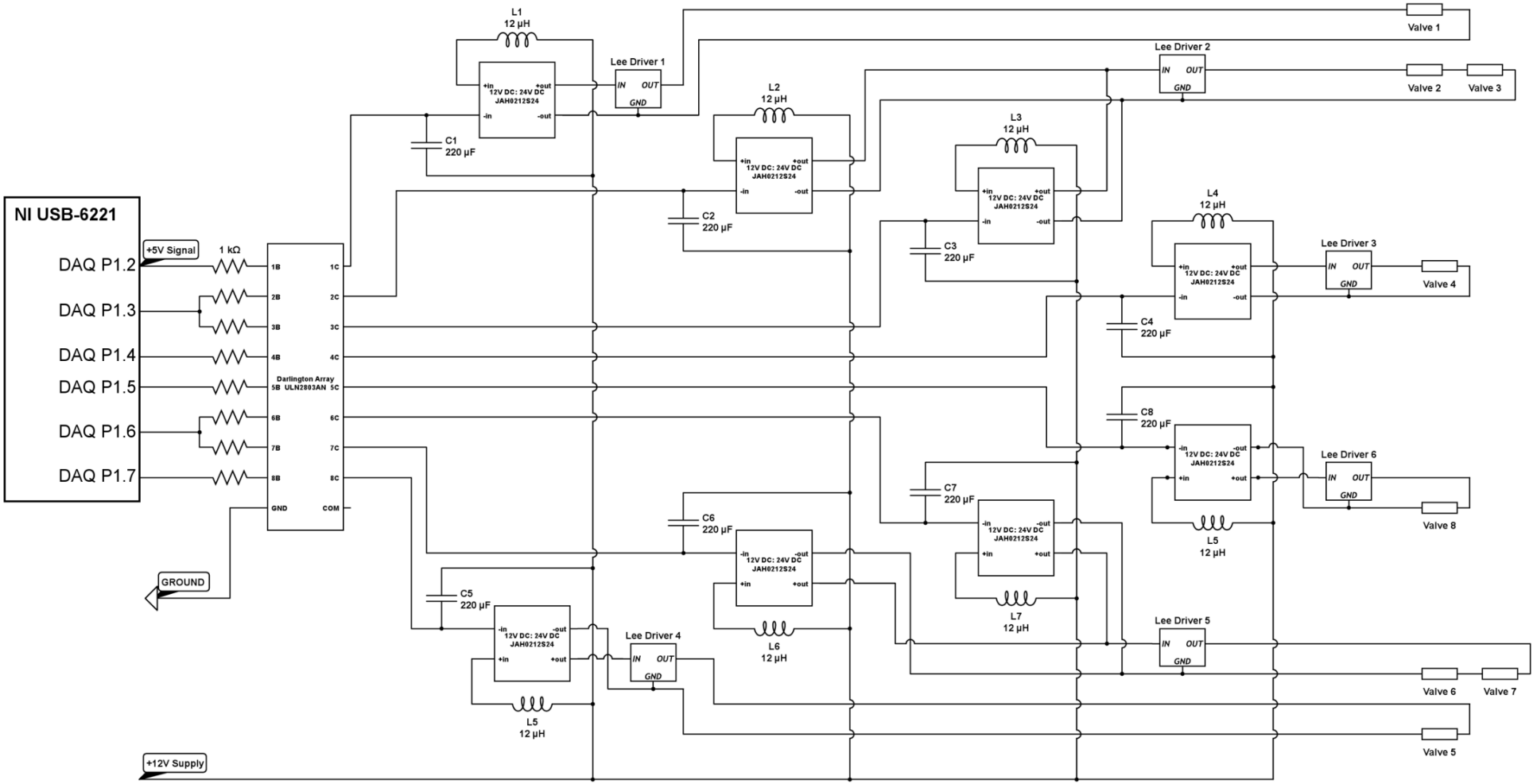

Figure 10.4 - Circuit diagram for control of medium handling valves.

As with the gas handling valves, switching is achieved by sending a 5 V digital output from the DAQ to a Darlington Array. The Darlington Array outputs activate 12V:24V DC:DC converters (JAH0212S34, Farnell, UK) that, in-turn, power the Lee Company (Lee Company, UK) valves via Lee Company drivers (DRVA0000020A). The circuits around the drivers and DC:DC converters are based on specifications supplied by the manufacturer. Valves 1-3 and 5-7 are 2-position 3-way valves (LFRA1230110H) to select the medium bottle used to supply each of two parallel device sets. Valves 4 and 8 are normally closed ON/OFF (LFVA1230113H) valves used to purge the preheat and bubble trap units.

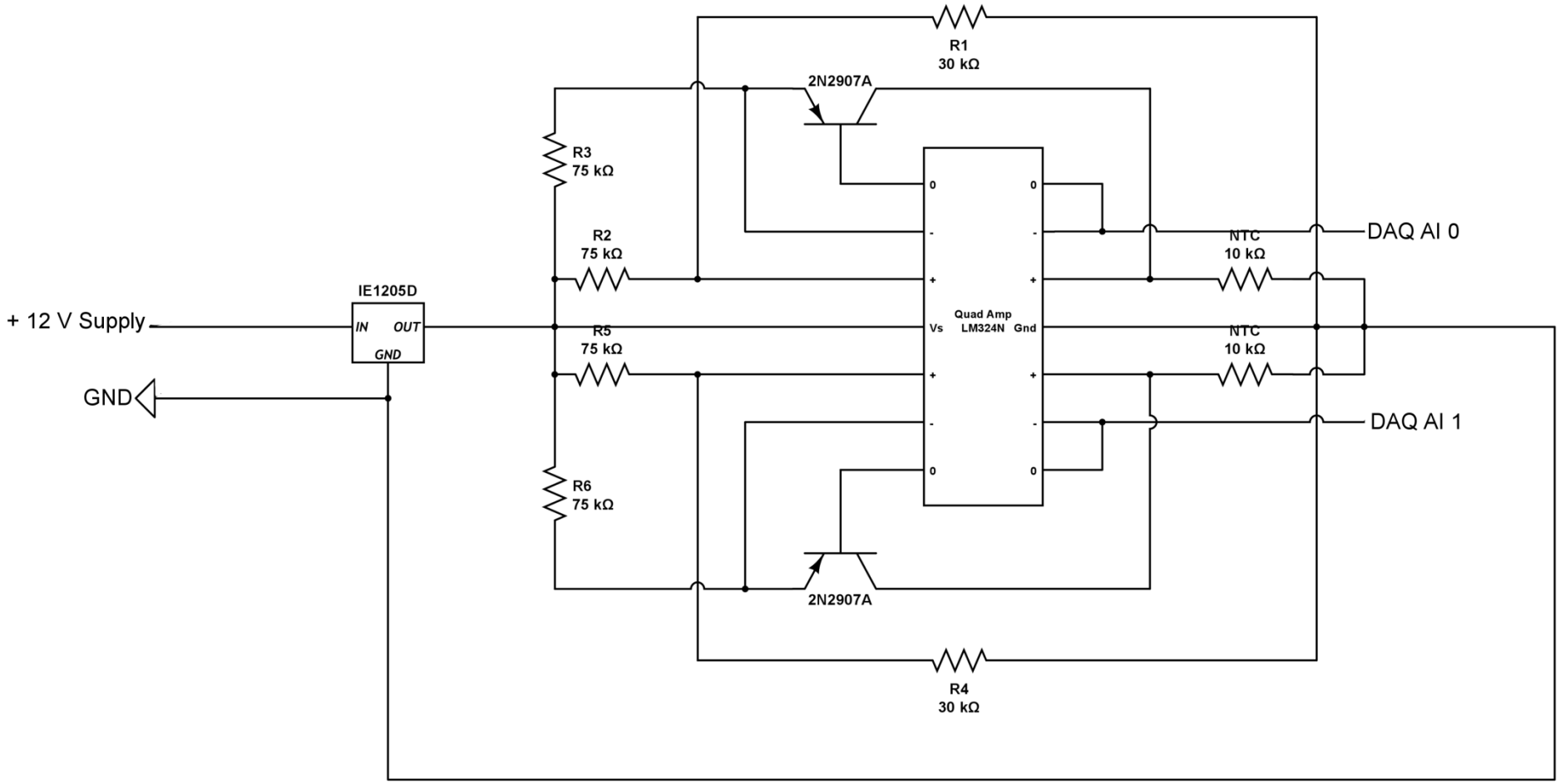

Figure 10.5 - Circuit diagram for thermistor measurements.

The 10 kΩ NTC thermistors (B57863S103F40) provide analogue inputs to the DAQ via this circuit, which is taken from Marcel Reichen's prototype platform (Reichen, 2012). The circuit has been modified to use the single 12 V power supply via a 12V:5V DC:DC converter (IE1205D). All components were obtained from Farnell. UK.

11. Appendix 5 – Publications

A number of publications by the author are related to the work presented in this thesis.

The evaluation of the prototype culture device (chapter 2) is included in:

- REICHEN, M. & MACOWN, R. J., JACCARD, N., SUPER, A., RUBAN, L., GRIFFIN, L. D., VERAITCH, F. S. & SZITA, N. 2012. Microfabricated Modular Scale-Down Device for Regenerative Medicine Process Development. *Plos One,* 7**,** e52246.

The improved culture device, including the aluminium holder and the improvement process (chapter 3), is the topic of:

- MACOWN, R. J., VERAITCH, F. S. & SZITA, N. 2014. Robust, microfabricated culture devices with improved control over the soluble microenvironment for the culture of embryonic stem cells. *Biotechnology Journal,* 9**,** 805-813.

The different versions of image processing software and the automation of monitoring by phase contrast monitoring are covered further in:

- JACCARD, N., GRIFFIN, L. D., KESER, A., MACOWN, R. J., SUPER, A., VERAITCH, F. S. & SZITA, N. 2014. Automated method for the rapid and precise estimation of adherent cell culture characteristics from phase contrast microscopy images. *Biotechnology and Bioengineering,* 111**,** 504-517.
- JACCARD, N., MACOWN, R. J., SUPER, A., GRIFFIN, L. D., VERAITCH, F. S. & SZITA, N. 2014. Automated and Online Characterization of Adherent Cell Culture Growth in a Microfabricated Bioreactor. *J Lab Autom*, 2211068214529288.

Finally, the packaging of the prototype device is discussed in:

- REICHEN, M., SUPER, A., DAVIES, M. J., MACOWN, R. J., O'SULLIVAN, B., KIRK, T. V., MARQUES, M. P. C., DIMOV, N. & SZITA, N. 2014. Characterisation of an Adhesive-free Packaging System for Polymeric Microfluidic Biochemical Devices and Reactors. *Chemical & Biochemical Engineering Quarterly,* 28**,** 189-202.

12. References

ALLEN, J. W., KHETANI, S. R. & BHATIA, S. N. 2005. In Vitro Zonation and Toxicity in a Hepatocyte Bioreactor. *Toxicological Sciences,* 84**,** 110-119.

AMIT, M., CARPENTER, M. K., INOKUMA, M. S., CHIU, C. P., HARRIS, C. P., WAKNITZ, M. A., ITSKOVITZ-ELDOR, J. & THOMSON, J. A. 2000. Clonally derived human embryonic stem cell lines maintain pluripotency and proliferative potential for prolonged periods of culture. *Developmental Biology,* 227**,** 271-278.

ANDREWS, P. W. 1998. Teratocarcinomas and human embryology: pluripotent human EC cell lines. Review article. *APMIS,* 106**,** 158-67; discussion 167-8.

ARNDT, S., SEEBACH, J., PSATHAKI, K., GALLA, H.-J. & WEGENER, J. 2004. Bioelectrical impedance assay to monitor changes in cell shape during apoptosis. *Biosensors and Bioelectronics,* 19**,** 583-594.

AUNINS, J. G., BADER, B., CAOLA, A., GRIFFITHS, J., KATZ, M., LICARI, P., RAM, K., RANUCCI, C. S. & ZHOU, W. C. 2003. Fluid mechanics, cell distribution, and environment in CellCube bioreacors. *Biotechnology Progress,* 19**,** 2-8.

BACABAC, R. G., SMIT, T. H., COWIN, S. C., VAN LOON, J. J. W. A., NIEUWSTADT, F. T. M., HEETHAAR, R. & KLEIN-NULEND, J. 2005. Dynamic shear stress in parallel-plate flow chambers. *Journal of Biomechanics,* 38**,** 159-167.

BAKER, D. E. C., HARRISON, N. J., MALTBY, E., SMITH, K., MOORE, H. D., SHAW, P. J., HEATH, P. R., HOLDEN, H. & ANDREWS, P. W. 2007.

Adaptation to culture of human embryonic stem cells and oncogenesis in vivo. *Nature Biotechnology,* 25**,** 207-215.

BAYATI, V., SADEGHI, Y., SHOKRGOZAR, M. A., HAGHIGHIPOUR, N., AZADMANESH, K., AMANZADEH, A. & AZARI, S. 2011. The evaluation of cyclic uniaxial strain on myogenic differentiation of adipose-derived stem cells. *Tissue and Cell,* 43**,** 359-366.

BECKER, H. & GARTNER, C. 2008. Polymer microfabrication technologies for microfluidic systems. *Analytical and Bioanalytical Chemistry,* 390**,** 89-111.

BERTHIER, E., YOUNG, E. W. K. & BEEBE, D. 2012. Engineers are from PDMS-land, Biologists are from Polystyrenia. *Lab on a Chip,* 12**,** 1224-1237.

BITAR, M., BROWN, R. A., SALIH, V., KIDANE, A. G., KNOWLES, J. C. & NAZHAT, S. N. 2007. Effect of Cell Density on Osteoblastic Differentiation and Matrix Degradation of Biomimetic Dense Collagen Scaffolds. *Biomacromolecules,* 9**,** 129-135.

BRACK, A. S., CONBOY, I. M., CONBOY, M. J., SHEN, J. & RANDO, T. A. 2008. A Temporal Switch from Notch to Wnt Signaling in Muscle Stem Cells Is Necessary for Normal Adult Myogenesis. *Cell Stem Cell,* 2**,** 50-59.

BRADLEY, A., EVANS, M., KAUFMAN, M. H. & ROBERTSON, E. 1984. Formation Of Germ-Line Chimeras From Embryo-Derived Teratocarcinoma Cell-Lines. *Nature,* 309**,** 255-256.

BREIMAN, L. 2001. Random Forests. *Machine Learning,* 45**,** 5-32.

BRINSTER, R. L. 1976. Participation Of Teratocarcinoma Cells In Mouse Embryo Development. *Cancer Research,* 36**,** 3412-3414.

BROXMEYER, H. E., DOUGLAS, G. W., HANGOC, G., COOPER, S., BARD, J., ENGLISH, D., ARNY, M., THOMAS, L. & BOYSE, E. A. 1989. Human umbilical cord blood as a potential source of transplantable hematopoietic stem/progenitor cells. *Proceedings of the National Academy of Sciences,* 86**,** 3828-3832.

BRUGGER, W. M. W. H. S. B. R. J. M. R. K. L. 1993. Ex vivo expansion of enriched peripheral blood CD34+ progenitor cells by stem cell factor, interleukin-1 beta (IL-1 beta), IL-6, IL-3, interferon-gamma, and erythropoietin. *Blood,* 81**,** 2579-2584.

BUTA, C., DAVID, R., DRESSEL, R., EMGÅRD, M., FUCHS, C., GROSS, U., HEALY, L., HESCHELER, J., KOLAR, R., MARTIN, U., MIKKERS, H., MÜLLER, F.-J., SCHNEIDER, R. K., SEILER, A. E. M., SPIELMANN, H. & WEITZER, G. 2013. Reconsidering pluripotency tests: Do we still need teratoma assays? *Stem Cell Research,* 11**,** 552-562.

CAI, J. L., WEISS, M. L. & RAO, M. S. 2004. In search of "stemness". *Experimental Hematology,* 32**,** 585-598.

CAMERON, A. R., FRITH, J. E. & COOPER-WHITE, J. J. 2011. The influence of substrate creep on mesenchymal stem cell behaviour and phenotype. *Biomaterials,* 32**,** 5979-5993.

CAN, A. & KARAHUSEYINOGLU, S. 2007. Concise Review: Human Umbilical Cord Stroma with Regard to the Source of Fetus-Derived Stem Cells. *Stem Cells,* 25**,** 2886-2895.

CANCEDDA, R., DOZIN, B., GIANNONI, P. & QUARTO, R. 2003. Tissue engineering and cell therapy of cartilage and bone. *Matrix Biology,* 22**,** 81-91.

CHEN, KEVIN G., MALLON, BARBARA S., MCKAY, RONALD D. G. & ROBEY, PAMELA G. 2014. Human Pluripotent Stem Cell Culture: Considerations for Maintenance, Expansion, and Therapeutics. *Cell Stem Cell,* 14**,** 13-26.

CHEN, M. B., SRIGUNAPALAN, S., WHEELER, A. R. & SIMMONS, C. A. 2013. A 3D microfluidic platform incorporating methacrylated gelatin hydrogels to study physiological cardiovascular cell-cell interactions. *Lab on a Chip,* 13**,** 2591-2598.

CHERRY, R. S. & KWON, K. Y. 1990. Transient Shear Stresses On A Suspension Cell In Turbulence. *Biotechnology and Bioengineering,* 36**,** 563-571.

CHOWDHURY, F., LI, Y., POH, Y.-C., YOKOHAMA-TAMAKI, T., WANG, N. & TANAKA, T. S. 2010. Soft Substrates Promote Homogeneous Self-Renewal of Embryonic Stem Cells via Downregulating Cell-Matrix Tractions. *Plos One,* 5**,** e15655.

CIGOGNINI, D., LOMAS, A., KUMAR, P., SATYAM, A., ENGLISH, A., AZEEM, A., PANDIT, A. & ZEUGOLIS, D. 2013. Engineering in vitro microenvironments for cell based therapies and drug discovery. *Drug Discovery Today,* 18**,** 1099-1108.

CIMETTA, E., FIGALLO, E., CANNIZZARO, C., ELVASSORE, N. & VUNJAK-NOVAKOVIC, G. 2009. Micro-bioreactor arrays for controlling cellular environments: Design principles for human embryonic stem cell applications. *Methods,* 47**,** 81-89.

COLOMB, T., PAVILLON, N., KÜHN, J., CUCHE, E., DEPEURSINGE, C. & EMERY, Y. 2010. Extended depth-of-focus by digital holographic microscopy. *Optics Letters,* 35**,** 1840-1842.

CROUGHAN, M. S., SAYRE, E. S. & WANG, D. I. C. 1989. Viscous reduction of turbulent damage in animal cell culture. *Biotechnology and Bioengineering,* 33**,** 862-872.

CSASZAR, E., KIROUAC, DANIEL C., YU, M., WANG, W., QIAO, W., COOKE, MICHAEL P., BOITANO, ANTHONY E., ITO, C. & ZANDSTRA, PETER W. 2012. Rapid Expansion of Human Hematopoietic Stem Cells by Automated Control of Inhibitory Feedback Signaling. *Cell Stem Cell,* 10**,** 218-229.

DALEY, GEORGE Q. 2012. The Promise and Perils of Stem Cell Therapeutics. *Cell Stem Cell,* 10**,** 740-749.

DERTINGER, S. K. W., CHIU, D. T., JEON, N. L. & WHITESIDES, G. M. 2001. Generation of gradients having complex shapes using microfluidic networks. *Analytical Chemistry,* 73**,** 1240-1246.

DISCHER, D. E., MOONEY, D. J. & ZANDSTRA, P. W. 2009. Growth Factors, Matrices, and Forces Combine and Control Stem Cells. *Science,* 324**,** 1673-1677.

DOS SANTOS, F., CAMPBELL, A., FERNANDES-PLATZGUMMER, A., ANDRADE, P. Z., GIMBLE, J. M., WEN, Y., BOUCHER, S., VEMURI, M. C., DA SILVA, C. L. & CABRAL, J. M. S. 2014. A xenogeneic-free bioreactor system for the clinical-scale expansion of human mesenchymal stem/stromal cells. *Biotechnology and Bioengineering***,** n/a-n/a.

DOUVILLE, N. J., ZAMANKHAN, P., TUNG, Y.-C., LI, R., VAUGHAN, B. L., TAI, C.-F., WHITE, J., CHRISTENSEN, P. J., GROTBERG, J. B. & TAKAYAMA, S. 2011. Combination of fluid and solid mechanical stresses contribute to cell death and detachment in a microfluidic alveolar model. *Lab on a Chip,* 11**,** 609-619.

DRAPER, J. S., PIGOTT, C., THOMSON, J. A. & ANDREWS, P. W. 2002. Surface antigens of human embryonic stem cells: changes upon differentiation in culture*. *Journal of Anatomy,* 200**,** 249-258.

EGAWA, N., KITAOKA, S., TSUKITA, K., NAITOH, M., TAKAHASHI, K., YAMAMOTO, T., ADACHI, F., KONDO, T., OKITA, K., ASAKA, I., AOI, T., WATANABE, A., YAMADA, Y., MORIZANE, A., TAKAHASHI, J., AYAKI, T., ITO, H., YOSHIKAWA, K., YAMAWAKI, S., SUZUKI, S., WATANABE, D., HIOKI, H., KANEKO, T., MAKIOKA, K., OKAMOTO, K., TAKUMA, H., TAMAOKA, A., HASEGAWA, K., NONAKA, T., HASEGAWA, M., KAWATA, A., YOSHIDA, M., NAKAHATA, T., TAKAHASHI, R., MARCHETTO, M. C. N., GAGE, F. H., YAMANAKA, S. & INOUE, H. 2012. Drug Screening for ALS Using Patient-Specific Induced Pluripotent Stem Cells. *Science Translational Medicine,* 4**,** 145ra104.

EL-ALI, J., SORGER, P. K. & JENSEN, K. F. 2006. Cells on chips. *Nature,* 442**,** 403-411.

ELLERSTROM, C., STREHL, R., NOAKSSON, K., HYLLNER, J. & SEMB, H. 2007. Facilitated expansion of human embryonic stem cells by single-cell enzymatic dissociation. *Stem Cells,* 25**,** 1690-1696.

EVANS, M. J. & KAUFMAN, M. H. 1981. Establishment in culture of pluripotential cells from mouse embryos. *Nature,* 292**,** 154-156.

EZASHI, T., DAS, P. & ROBERTS, R. M. 2005. Low O2 tensions and the prevention of differentiation of hES cells. *Proc Natl Acad Sci U S A,* 102**,** 4783-8.

FDA. 2015. *Cellular & Gene Therapy Products - Approved Products* [Online]. U.S. Food and Drug Administration. Available: http://www.fda.gov/BiologicsBloodVaccines/CellularGeneTherapyProducts/ApprovedProducts/default.htm [Accessed 03/20/2015 2015].

FIGALLO, E., CANNIZZARO, C., GERECHT, S., BURDICK, J. A., LANGER, R., ELVASSORE, N. & VUNJAK-NOVAKOVIC, G. 2007. Micro-bioreactor array for controlling cellular microenvironments. *Lab on a Chip,* 7**,** 710-719.

FLAIM, C. J., CHIEN, S. & BHATIA, S. N. 2005. An extracellular matrix microarray for probing cellular differentiation. *Nature Methods,* 2**,** 119-125.

FLURI, D. A., TONGE, P. D., SONG, H., BAPTISTA, R. P., SHAKIBA, N., SHUKLA, S., CLARKE, G., NAGY, A. & ZANDSTRA, P. W. 2012. Derivation, expansion and differentiation of induced pluripotent stem cells in continuous suspension cultures. *Nat Meth,* 9**,** 509-516.

FONG, W., TAN, H., CHOO, A. & OH, S. 2005. Perfusion cultures of human embryonic stem cells. *Bioprocess and Biosystems Engineering,* 27**,** 381-387.

FORRISTAL, C. E., CHRISTENSEN, D. R., CHINNERY, F. E., PETRUZZELLI, R., PARRY, K. L., SANCHEZ-ELSNER, T. & HOUGHTON, F. D. 2013.

Environmental Oxygen Tension Regulates the Energy Metabolism and Self-Renewal of Human Embryonic Stem Cells. *Plos One,* 8**,** e62507.

FREDRICKSON, C. K. & FAN, Z. H. 2004. Macro-to-micro interfaces for microfluidic devices. *Lab on a Chip,* 4**,** 526-533.

FYNES, K., TOSTOES, R., RUBAN, L., WEIL, B., MASON, C. & VERAITCH, F. S. 2014. The Differential Effects of 2% Oxygen Preconditioning on the Subsequent Differentiation of Mouse and Human Pluripotent Stem Cells. *Stem Cells Dev*.

GAGE, B. K., WEBBER, T. D. & KIEFFER, T. J. 2013. Initial Cell Seeding Density Influences Pancreatic Endocrine Development During *in vitro* Differentiation of Human Embryonic Stem Cells. *Plos One,* 8**,** e82076.

GARBERN, JESSICA C. & LEE, RICHARD T. 2013. Cardiac Stem Cell Therapy and the Promise of Heart Regeneration. *Cell Stem Cell,* 12**,** 689-698.

GHOSH, S., DEAN, A., WALTER, M., BAO, Y., HU, Y., RUAN, J. & LI, R. 2010. Cell density-dependent transcriptional activation of endocrine-related genes in human adipose tissue-derived stem cells. *Experimental Cell Research,* 316**,** 2087-2098.

GIULITTI, S., MAGROFUOCO, E., PREVEDELLO, L. & ELVASSORE, N. 2013. Optimal periodic perfusion strategy for robust long-term microfluidic cell culture. *Lab on a Chip,* 13**,** 4430-4441.

GONZALEZ-GARCIA, C., MORATAL, D., OREFFO, R. O., DALBY, M. J. & SALMERON-SANCHEZ, M. 2012. Surface mobility regulates skeletal stem cell differentiation. *Integr Biol (Camb),* 4**,** 531-9.

GRIFFIN, L., LILLHOLM, M., CROSIER, M. & VAN SANDE, J. 2009. Basic Image Features (BIFs) Arising from Approximate Symmetry Type. *In:* TAI, X.-C., MØRKEN, K., LYSAKER, M. & LIE, K.-A. (eds.) *Scale Space and Variational Methods in Computer Vision.* Springer Berlin Heidelberg.

HAZELTINE, L. B., SELEKMAN, J. A. & PALECEK, S. P. 2013. Engineering the human pluripotent stem cell microenvironment to direct cell fate. *Biotechnology Advances,* 31**,** 1002-1019.

HEATH, C. & KISS, R. 2007. Cell Culture Process Development: Advances in Process Engineering. *Biotechnology Progress,* 23**,** 46-51.

HERNON, C. A., DAWSON, R. A., FREEDLANDER, E., SHORT, R., HADDOW, D. B., BROTHERSTON, M. & MACNEIL, S. 2006. Clinical experience using cultured epithelial autografts leads to an alternative methodology for transferring skin cells from the laboratory to the patient. *Regenerative Medicine,* 1**,** 809-821.

HIYAMA, E. & HIYAMA, K. 2007. Telomere and telomerase in stem cells. *Br J Cancer,* 96**,** 1020-1024.

HONG, J., KANDASAMY, K., MARIMUTHU, M., CHOI, C. S. & KIM, S. 2011. Electrical cell-substrate impedance sensing as a non-invasive tool for cancer cell study. *Analyst,* 136**,** 237-245.

HUG, T. S. 2003. Biophysical methods for monitoring cell-substrate interactions in drug discovery. *Assay Drug Dev Technol,* 1**,** 479-88.

HUH, D., FUJIOKA, H., TUNG, Y.-C., FUTAI, N., PAINE, R., GROTBERG, J. B. & TAKAYAMA, S. 2007. Acoustically detectable cellular-level lung injury

induced by fluid mechanical stresses in microfluidic airway systems. *Proceedings of the National Academy of Sciences,* 104**,** 18886-18891.

HUH, D., HAMILTON, G. A. & INGBER, D. E. 2011. From 3D cell culture to organs-on-chips. *Trends in Cell Biology,* 21**,** 745-754.

HUH, D., MATTHEWS, B. D., MAMMOTO, A., MONTOYA-ZAVALA, M., HSIN, H. Y. & INGBER, D. E. 2010. Reconstituting Organ-Level Lung Functions on a Chip. *Science,* 328**,** 1662-1668.

HUH, D., TORISAWA, Y.-S., HAMILTON, G. A., KIM, H. J. & INGBER, D. E. 2012. Microengineered physiological biomimicry: Organs-on-Chips. *Lab on a Chip,* 12**,** 2156-2164.

HUNG, P. J., LEE, P. J., SABOUNCHI, P., AGHDAM, N., LIN, R. & LEE, L. P. 2005. A novel high aspect ratio microfluidic design to provide a stable and uniform microenvironment for cell growth in a high throughput mammalian cell culture array. *Lab on a Chip,* 5**,** 44-48.

HYSLOP, L. A., ARMSTRONG, L., STOJKOVIC, M. & LAKO, M. 2005. Human embryonic stem cells: biology and clinical implications. *Expert Reviews in Molecular Medicine,* 7**,** 1-21.

ITSKOVITZ-ELDOR, J., SCHULDINER, M., KARSENTI, D., EDEN, A., YANUKA, O., AMIT, M., SOREQ, H. & BENVENISTY, N. 2000. Differentiation of human embryonic stem cells into embryoid bodies comprising the three embryonic germ layers. *Molecular Medicine,* 6**,** 88-95.

ITZHAKI, I., MAIZELS, L., HUBER, I., ZWI-DANTSIS, L., CASPI, O., WINTERSTERN, A., FELDMAN, O., GEPSTEIN, A., ARBEL, G.,

HAMMERMAN, H., BOULOS, M. & GEPSTEIN, L. 2011. Modelling the long QT syndrome with induced pluripotent stem cells. *Nature,* 471**,** 225-9.

JACCARD, N., GRIFFIN, L. D., KESER, A., MACOWN, R. J., SUPER, A., VERAITCH, F. S. & SZITA, N. 2014a. Automated method for the rapid and precise estimation of adherent cell culture characteristics from phase contrast microscopy images. *Biotechnology and Bioengineering,* 111**,** 504-517.

JACCARD, N., SZITA, N. & GRIFFIN, L. 2014. Trainable segmentation of phase contrast microscopy images based on local Basic Image Features histograms. *In:* REYES-ALDASORO, C. C. & SLABAUGH, G., eds. Proceedings of the 18th Conference on Medical Image Understanding and Analysis., 9-11 July 2014b London.

JEON, J. S., BERSINI, S., WHISLER, J. A., CHEN, M. B., DUBINI, G., CHAREST, J. L., MORETTI, M. & KAMM, R. D. 2014. Generation of 3D functional microvascular networks with human mesenchymal stem cells in microfluidic systems. *Integrative Biology*.

JORDAN, M., EPPENBERGER, H. M., SUCKER, H., WIDMER, F. & EINSELE, A. 1994. Interactions between animal cells and gas bubbles: The influence of serum and pluronic F68 on the physical properties of the bubble surface. *Biotechnology and Bioengineering,* 43**,** 446-454.

KAMEI, K. I., GUO, S. L., YU, Z. T. F., TAKAHASHI, H., GSCHWENG, E., SUH, C., WANG, X. P., TANG, J. G., MCLAUGHLIN, J., WITTE, O. N., LEE, K. B. & TSENG, H. R. 2009. An integrated microfluidic culture device for quantitative analysis of human embryonic stem cells. *Lab on a Chip,* 9**,** 555-563.

KEHAT, I., KENYAGIN-KARSENTI, D., SNIR, M., SEGEV, H., AMIT, M., GEPSTEIN, A., LIVNE, E., BINAH, O., ITSKOVITZ-ELDOR, J. & GEPSTEIN, L. 2001. Human embryonic stem cells can differentiate into myocytes with structural and functional properties of cardiomyocytes. *Journal of Clinical Investigation,* 108**,** 407-414.

KEHOE, D. E., JING, D. H., LOCK, L. T. & TZANAKAKIS, E. S. 2010. Scalable Stirred-Suspension Bioreactor Culture of Human Pluripotent Stem Cells. *Tissue Engineering Part A,* 16**,** 405-421.

KESSINGER, A. A. J. O. 1991. The evolving role of autologous peripheral stem cell transplantation following high-dose therapy for malignancies [editorial]. *Blood,* 77**,** 211-213.

KILIAN, K. A., BUGARIJA, B., LAHN, B. T. & MRKSICH, M. 2010. Geometric cues for directing the differentiation of mesenchymal stem cells. *Proceedings of the National Academy of Sciences,* 107**,** 4872-4877.

KIM, H. J. & INGBER, D. E. 2013. Gut-on-a-Chip microenvironment induces human intestinal cells to undergo villus differentiation. *Integrative Biology,* 5**,** 1130-1140.

KIM, L., TOH, Y. C., VOLDMAN, J. & YU, H. 2007a. A practical guide to microfluidic perfusion culture of adherent mammalian cells. *Lab on a Chip,* 7**,** 681-694.

KIM, M. K. 2010. Principles and techniques of digital holographic microscopy. *Journal of Photonics for Energy***,** 018005-018005-50.

KIM, W.-S., PARK, B.-S., SUNG, J.-H., YANG, J.-M., PARK, S.-B., KWAK, S.-J. & PARK, J.-S. 2007b. Wound healing effect of adipose-derived stem cells: A critical role of secretory factors on human dermal fibroblasts. *Journal of Dermatological Science,* 48**,** 15-24.

KIMURA, H., YAMAMOTO, T., SAKAI, H., SAKAI, Y. & FUJII, T. 2008. An integrated microfluidic system for long-term perfusion culture and on-line monitoring of intestinal tissue models. *Lab on a Chip,* 8**,** 741-746.

KIROUAC, D. C. & ZANDSTRA, P. W. 2008. The Systematic Production of Cells for Cell Therapies. *Cell Stem Cell,* 3**,** 369-381.

KNAZEK, R. A., GULLINO, P. M., KOHLER, P. O. & DEDRICK, R. L. 1972. Cell Culture on Artificial Capillaries: An Approach to Tissue Growth in vitro. *Science,* 178**,** 65-67.

KOIZUMI, N., INATOMI, T., SUZUKI, T., SOTOZONO, C. & KINOSHITA, S. 2001. Cultivated corneal epithelial stem cell transplantation in ocular surface disorders. *Ophthalmology,* 108**,** 1569-1574.

KORIN, N., BRANSKY, A., DINNAR, U. & LEVENBERG, S. The culture of human embryonic stem cells in microchannel perfusion bioreactors. *In:* NICOLAU, D. V., ed. Biomedical Applications of Micro- and Nanoengineering III, 2006 Adelaide, Australia. SPIE, 64160N.

KORIN, N., BRANSKY, A., DINNAR, U. & LEVENBERG, S. 2009a. Periodic "flow-stop" perfusion microchannel bioreactors for mammalian and human embryonic stem cell long-term culture. *Biomedical Microdevices,* 11**,** 87-94.

KORIN, N., BRANSKY, A., KHOURY, M., DINNAR, U. & LEVENBERG, S. 2009b. Design of Well and Groove Microchannel Bioreactors for Cell Culture. *Biotechnology and Bioengineering,* 102**,** 1222-1230.

KUNAS, K. T. & PAPOUTSAKIS, E. T. 1990. Damage mechanisms of suspended animal cells in agitated bioreactors with and without bubble entrainment. *Biotechnology and Bioengineering,* 36**,** 476-483.

KUNAS, K. T., PAPOUTSAKIS, E. T. & ELEFTHERIOS TERRY PAPOUTSAKIS, I. B. 2009. Damage mechanisms of suspended animal cells in agitated bioreactors with and without bubble entrainment. *Biotechnology and Bioengineering,* 102**,** 977-987.

KURPINSKI, K., CHU, J., HASHI, C. & LI, S. 2006. Anisotropic mechanosensing by mesenchymal stem cells. *Proceedings of the National Academy of Sciences,* 103**,** 16095-16100.

LANCASTER, M. A., RENNER, M., MARTIN, C.-A., WENZEL, D., BICKNELL, L. S., HURLES, M. E., HOMFRAY, T., PENNINGER, J. M., JACKSON, A. P. & KNOBLICH, J. A. 2013. Cerebral organoids model human brain development and microcephaly. *Nature,* 501**,** 373-379.

LEE, A. S., TANG, C., RAO, M. S., WEISSMAN, I. L. & WU, J. C. 2013a. Tumorigenicity as a clinical hurdle for pluripotent stem cell therapies. *Nat Med,* 19**,** 998-1004.

LEE, J., ABDEEN, A. A., ZHANG, D. & KILIAN, K. A. 2013b. Directing stem cell fate on hydrogel substrates by controlling cell geometry, matrix mechanics and adhesion ligand composition. *Biomaterials,* 34**,** 8140-8148.

LI, X., CHU, J., YANG, L. & LI, S. 2012. Anisotropic Effects of Mechanical Strain on Neural Crest Stem Cells. *Annals of Biomedical Engineering,* 40**,** 598-605.

LIU, G.-H., BARKHO, B. Z., RUIZ, S., DIEP, D., QU, J., YANG, S.-L., PANOPOULOS, A. D., SUZUKI, K., KURIAN, L., WALSH, C., THOMPSON, J., BOUE, S., FUNG, H. L., SANCHO-MARTINEZ, I., ZHANG, K., III, J. Y. & BELMONTE, J. C. I. 2011. Recapitulation of premature ageing with iPSCs from Hutchinson-Gilford progeria syndrome. *Nature,* 472**,** 221-225.

LU, H., GUO, L., WOZNIAK, M. J., KAWAZOE, N., TATEISHI, T., ZHANG, X. & CHEN, G. 2009. Effect of cell density on adipogenic differentiation of mesenchymal stem cells. *Biochemical and Biophysical Research Communications,* 381**,** 322-327.

MACOWN, R. J., VERAITCH, F. S. & SZITA, N. 2014. Robust, microfabricated culture devices with improved control over the soluble microenvironment for the culture of embryonic stem cells. *Biotechnology Journal,* 9**,** 805-813.

MANN, C., YU, L., LO, C.-M. & KIM, M. 2005. High-resolution quantitative phase-contrast microscopy by digital holography. *Optics Express,* 13**,** 8693-8698.

MARTIN, Y., ELDARDIRI, M., LAWRENCE-WATT, D. J. & SHARPE, J. R. 2011. Microcarriers and their potential in tissue regeneration. *Tissue Eng Part B Rev,* 17**,** 71-80.

MARTÍNEZ-MORALES, P. L., REVILLA, A., OCAÑA, I., GONZÁLEZ, C., SAINZ, P., MCGUIRE, D. & LISTE, I. 2013. Progress in Stem Cell Therapy for Major Human Neurological Disorders. *Stem Cell Reviews and Reports,* 9**,** 685-699.

MARTYNOVA, L., LOCASCIO, L. E., GAITAN, M., KRAMER, G. W., CHRISTENSEN, R. G. & MACCREHAN, W. A. 1997. Fabrication of plastic microfluid channels by imprinting methods. *Anal Chem,* 69**,** 4783-9.

MASON, C. & DUNNILL, P. 2008. A brief definition of regenerative medicine. *Regenerative Medicine,* 3**,** 1-5.

MASON, C. & DUNNILL, P. 2009. Quantities of cells used for regenerative medicine and some implications for clinicians and bioprocessors. *Regenerative Medicine,* 4**,** 153-157.

MATHIEU, J., ZHOU, W., XING, Y., SPERBER, H., FERRECCIO, A., AGOSTON, Z., KUPPUSAMY, K. T., MOON, R. T. & RUOHOLA-BAKER, H. 2014. Hypoxia-inducible factors have distinct and stage-specific roles during reprogramming of human cells to pluripotency. *Cell Stem Cell,* 14**,** 592-605.

MATSUOKA, F., TAKEUCHI, I., AGATA, H., KAGAMI, H., SHIONO, H., KIYOTA, Y., HONDA, H. & KATO, R. 2014. Characterization of time-course morphological features for efficient prediction of osteogenic potential in human mesenchymal stem cells. *Biotechnol Bioeng,* 111**,** 1430-9.

MCCORMICK, R. M., NELSON, R. J., ALONSO-AMIGO, M. G., BENVEGNU, D. J. & HOOPER, H. H. 1997. Microchannel electrophoretic separations of DNA in injection-molded plastic substrates. *Anal Chem,* 69**,** 2626-30.

MELKOUMIAN, Z., WEBER, J. L., WEBER, D. M., FADEEV, A. G., ZHOU, Y., DOLLEY-SONNEVILLE, P., YANG, J., QIU, L., PRIEST, C. A., SHOGBON, C., MARTIN, A. W., NELSON, J., WEST, P., BELTZER, J. P., PAL, S. & BRANDENBERGER, R. 2010. Synthetic peptide-acrylate surfaces for long-term

self-renewal and cardiomyocyte differentiation of human embryonic stem cells. *Nat Biotech,* 28**,** 606-610.

MERKEL, T. C., BONDAR, V. I., NAGAI, K., FREEMAN, B. D. & PINNAU, I. 2000. Gas sorption, diffusion, and permeation in poly(dimethylsiloxane). *Journal of Polymer Science Part B: Polymer Physics,* 38**,** 415-434.

MICHAELS, J. D., MALLIK, A. K. & PAPOUTSAKIS, E. T. 1996. Sparging and agitation-induced injury of cultured animals cells: Do cell-to-bubble interactions in the bulk liquid injure cells? *Biotechnology and Bioengineering,* 51**,** 399-409.

MILLMAN, J. R., TAN, J. H. & COLTON, C. K. 2009. The effects of low oxygen on self-renewal and differentiation of embryonic stem cells. *Curr Opin Organ Transplant,* 14**,** 694-700.

MINTZ, B. & ILLMENSEE, K. 1975. Normal Genetically Mosaic Mice Produced From Malignant Teratocarcinoma Cells. *Proceedings of the National Academy of Sciences of the United States of America,* 72**,** 3585-3589.

MITALIPOVA, M. M., RAO, R. R., HOYER, D. M., JOHNSON, J. A., MEISNER, L. F., JONES, K. L., DALTON, S. & STICE, S. L. 2005. Preserving the genetic integrity of human embryonic stem cells. *Nat Biotech,* 23**,** 19-20.

MIYOSHI, N., ISHII, H., NAGANO, H., HARAGUCHI, N., DEWI, DYAH L., KANO, Y., NISHIKAWA, S., TANEMURA, M., MIMORI, K., TANAKA, F., SAITO, T., NISHIMURA, J., TAKEMASA, I., MIZUSHIMA, T., IKEDA, M., YAMAMOTO, H., SEKIMOTO, M., DOKI, Y. & MORI, M. 2011. Reprogramming of Mouse and Human Cells to Pluripotency Using Mature MicroRNAs. *Cell Stem Cell,* 8**,** 633-638.

MONDRAGON-TERAN, P., BABOO, J. Z., MASON, C., LYE, G. J. & VERAITCH, F. S. 2011. The full spectrum of physiological oxygen tensions and step-changes in oxygen tension affects the neural differentiation of mouse embryonic stem cells. *Biotechnology Progress,* 27**,** 1700-1708.

MORRISON, S. J. & KIMBLE, J. 2006. Asymmetric and symmetric stem-cell divisions in development and cancer. *Nature,* 441**,** 1068-1074.

NETO, E., ALVES, C. J., SOUSA, D. M., ALENCASTRE, I. S., LOURENCO, A. H., LEITAO, L., RYU, H. R., JEON, N. L., FERNANDES, R., AGUIAR, P., ALMEIDA, R. D. & LAMGHARI, M. 2014. Sensory neurons and osteoblasts: close partners in a microfluidic platform. *Integr Biol (Camb),* 6**,** 586-95.

NIENOW, A. 2006. Reactor Engineering in Large Scale Animal Cell Culture. *Cytotechnology,* 50**,** 9-33.

NISHIKAWA, M., KOJIMA, N., KOMORI, K., YAMAMOTO, T., FUJII, T. & SAKAI, Y. 2008. Enhanced maintenance and functions of rat hepatocytes induced by combination of on-site oxygenation and coculture with fibroblasts. *Journal of Biotechnology,* 133**,** 253-260.

NSIAH, B. A., AHSAN, T., GRIFFITHS, S., COOKE, M., NEREM, R. M. & MCDEVITT, T. C. 2014. Fluid shear stress pre-conditioning promotes endothelial morphogenesis of embryonic stem cells within embryoid bodies. *Tissue Eng Part A,* 20**,** 954-65.

OH, S. K., KIM, H. S., PARK, Y. B., SEOL, H. W., KIM, Y. Y., CHO, M. S., KU, S. Y., CHOI, Y. M., KIM, D. W. & MOON, S. Y. 2005. Methods for expansion of human embryonic stem. *Stem Cells,* 23**,** 605-609.

OH, S. K. W., CHEN, A. K., MOK, Y., CHEN, X. L., LIM, U. M., CHIN, A., CHOO, A. B. H. & REUVENY, S. 2009. Long-term microcarrier suspension cultures of human embryonic stem cells. *Stem Cell Research,* 2**,** 219-230.

OSORNO, R. & CHAMBERS, I. 2011. Transcription factor heterogeneity and epiblast pluripotency. *Philos Trans R Soc Lond B Biol Sci,* 366**,** 2230-7.

PAGUIRIGAN, A. L. & BEEBE, D. J. 2008. Microfluidics meet cell biology: bridging the gap by validation and application of microscale techniques for cell biological assays. *Bioessays,* 30**,** 811-821.

PAUL, S. M., MYTELKA, D. S., DUNWIDDIE, C. T., PERSINGER, C. C., MUNOS, B. H., LINDBORG, S. R. & SCHACHT, A. L. 2010. How to improve R&D productivity: the pharmaceutical industry's grand challenge. *Nat Rev Drug Discov,* 9**,** 203-214.

PAVILLON, N., KÜHN, J., MORATAL, C., JOURDAIN, P., DEPEURSINGE, C., MAGISTRETTI, P. J. & MARQUET, P. 2012. Early Cell Death Detection with Digital Holographic Microscopy. *Plos One,* 7**,** e30912.

PEASE, S. & WILLIAMS, R. L. 1990. Formation of germ-line chimeras from embryonic stem-cells maintained with recombinant leukemia inhibitory factor. *Experimental Cell Research,* 190**,** 209-211.

PENG, C.-C., LIAO, W.-H., CHEN, Y.-H., WU, C.-Y. & TUNG, Y.-C. 2013. A microfluidic cell culture array with various oxygen tensions. *Lab on a Chip,* 13**,** 3239-3245.

PETERSON, S. E. & LORING, J. F. 2014. Genomic Instability in Pluripotent Stem Cells: Implications for Clinical Applications. *Journal of Biological Chemistry,* 289**,** 4578-4584.

PETRONIS, S., STANGEGAARD, M., CHRISTENSEN, C. B. V. & DUFVA, M. 2006. Transparent polymeric cell culture chip with integrated temperature control and uniform media perfusion. *Biotechniques,* 40**,** 368-376.

PEYTON, S. R., KALCIOGLU, Z. I., COHEN, J. C., RUNKLE, A. P., VAN VLIET, K. J., LAUFFENBURGER, D. A. & GRIFFITH, L. G. 2011. Marrow-Derived stem cell motility in 3D synthetic scaffold is governed by geometry along with adhesivity and stiffness. *Biotechnology and Bioengineering***,** n/a-n/a.

PLACZEK, M. R., CHUNG, I. M., MACEDO, H. M., ISMAIL, S., BLANCO, T. M., LIM, M., CHA, J. M., FAUZI, I., KANG, Y., YEO, D. C. L., MA, C. Y. J., POLAK, J. M., PANOSKALTSIS, N. & MANTALARIS, A. 2009. Stem cell bioprocessing: fundamentals and principles. *Journal of the Royal Society Interface,* 6**,** 209-232.

PMT. 2014. *Making The World's Smallest Tools. 5µm And Up.* [Online]. Performance Micro Tool. Available: http://www.pmtnow.com/ [Accessed 23rd July 2014].

POWERS, D. E., MILLMAN, J. R., HUANG, R. B. & COLTON, C. K. 2008. Effects of oxygen on mouse embryonic stem cell growth, phenotype retention, and cellular energetics. *Biotechnology and Bioengineering,* 101**,** 241-254.

PRONKO, P. P., DUTTA, S. K., SQUIER, J., RUDD, J. V., DU, D. & MOUROU, G. 1995. Machining of sub-micron holes using a femtosecond laser at 800 nm. *Optics Communications,* 114**,** 106-110.

PRZYBYLA, L. & VOLDMAN, J. 2012. Probing embryonic stem cell autocrine and paracrine signaling using microfluidics. *Annu Rev Anal Chem (Palo Alto Calif),* 5**,** 293-315.

PYLE, A. D., LOCK, L. F. & DONOVAN, P. J. 2006. Neurotrophins mediate human embryonic stem cell survival. *Nat Biotech,* 24**,** 344-350.

RAO, G., MOREIRA, A. & BRORSON, K. 2009. Disposable bioprocessing: The future has arrived. *Biotechnology and Bioengineering,* 102**,** 348-356.

RAPPAZ, B., BRETON, B., SHAFFER, E. & TURCATTI, G. 2014. Digital holographic microscopy: a quantitative label-free microscopy technique for phenotypic screening. *Comb Chem High Throughput Screen,* 17**,** 80-8.

RATHORE, A. S. & WINKLE, H. 2009. Quality by design for biopharmaceuticals. *Nat Biotech,* 27**,** 26-34.

REGEHR, K. J., DOMENECH, M., KOEPSEL, J. T., CARVER, K. C., ELLISON-ZELSKI, S. J., MURPHY, W. L., SCHULER, L. A., ALARID, E. T. & BEEBE, D. J. 2009. Biological implications of polydimethylsiloxane-based microfluidic cell culture. *Lab on a Chip,* 9**,** 2132-2139.

REICHEN, M. 2012. *Multiplexed microfabricated cell culture device for stem cell process development.* Doctoral Thesis, UCL (University College London).

REICHEN, M., MACOWN, R. J., JACCARD, N., SUPER, A., RUBAN, L., GRIFFIN, L. D., VERAITCH, F. S. & SZITA, N. 2012. Microfabricated Modular Scale-Down Device for Regenerative Medicine Process Development. *Plos One,* 7**,** e52246.

REICHEN, M., VERAITCH, F. S. & SZITA, N. 2013. Development of a multiplexed microfluidic platform for the automated cultivation of embryonic stem cells. *J Lab Autom,* 18**,** 519-29.

REILLY, G. C. & ENGLER, A. J. 2010. Intrinsic extracellular matrix properties regulate stem cell differentiation. *Journal of Biomechanics,* 43**,** 55-62.

REUBINOFF, B. E., PERA, M. F., FONG, C. Y., TROUNSON, A. & BONGSO, A. 2000. Embryonic stem cell lines from human blastocysts: somatic differentiation in vitro. *Nature Biotechnology,* 18**,** 399-404.

ROBERTS, I., BAILA, S., RICE, R. B., JANSSENS, M., NGUYEN, K., MOENS, N., RUBAN, L., HERNANDEZ, D., COFFEY, P. & MASON, C. 2012. Scale-up of human embryonic stem cell culture using a hollow fibre bioreactor. *Biotechnology Letters,* 34**,** 2307-2315.

SACKMANN, E. K., FULTON, A. L. & BEEBE, D. J. 2014. The present and future role of microfluidics in biomedical research. *Nature,* 507**,** 181-189.

SADRZADEH, M., SHAHIDI, K. & MOHAMMADI, T. 2010. Synthesis and Gas Permeation Properties of a Single Layer PDMS Membrane. *Journal of Applied Polymer Science,* 117**,** 33-48.

SAIAS, L., AUTEBERT, J., MALAQUIN, L. & VIOVY, J. L. 2011. Design, modeling and characterization of microfluidic architectures for high flow rate, small footprint microfluidic systems. *Lab on a Chip,* 11**,** 822-32.

SCADDEN, D. T. 2006. The stem-cell niche as an entity of action. *Nature,* 441**,** 1075-1079.

SCHNEIDER, F., FELLNER, T., WILDE, J. & WALLRABE, U. 2008. Mechanical properties of silicones for MEMS. *Journal of Micromechanics and Microengineering,* 18**,** 065008.

SCHNERCH, A., CERDAN, C. & BHATIA, M. 2010. Distinguishing Between Mouse and Human Pluripotent Stem Cell Regulation: The Best Laid Plans of Mice and Men. *Stem Cells,* 28**,** 419-430.

SCHWARTZ, S. D., HUBSCHMAN, J.-P., HEILWELL, G., FRANCO-CARDENAS, V., PAN, C. K., OSTRICK, R. M., MICKUNAS, E., GAY, R., KLIMANSKAYA, I. & LANZA, R. 2012. Embryonic stem cell trials for macular degeneration: a preliminary report. *The Lancet,* 379**,** 713-720.

SERRA, M., BRITO, C., CORREIA, C. & ALVES, P. M. 2012. Process engineering of human pluripotent stem cells for clinical application. *Trends in Biotechnology,* 30**,** 350-359.

SERRA, M., BRITO, C., SOUSA, M. F. Q., JENSEN, J., TOSTOES, R., CLEMENTE, J., STREHL, R., HYLLNER, J., CARRONDO, M. J. T. & ALVES, P. M. 2010. Improving expansion of pluripotent human embryonic stem cells in perfused bioreactors through oxygen control. *Journal of Biotechnology,* 148**,** 208-215.

SHIMOBABA, T., YAMANASHI, H., KAKUE, T., OIKAWA, M., OKADA, N., ENDO, Y., HIRAYAMA, R., MASUDA, N. & ITO, T. 2013. In-line digital holographic microscopy using a consumer scanner. *Sci. Rep.,* 3.

SIA, S. K. & WHITESIDES, G. M. 2003. Microfluidic devices fabricated in poly(dimethylsiloxane) for biological studies. *Electrophoresis,* 24**,** 3563-3576.

SIMARIA, A. S., HASSAN, S., VARADARAJU, H., ROWLEY, J., WARREN, K., VANEK, P. & FARID, S. S. 2014. Allogeneic cell therapy bioprocess economics and optimization: Single-use cell expansion technologies. *Biotechnology and Bioengineering,* 111**,** 69-83.

SIMON, M. C. & KEITH, B. 2008. The role of oxygen availability in embryonic development and stem cell function. *Nat Rev Mol Cell Biol,* 9**,** 285-96.

SINGELYN, J. M., DEQUACH, J. A., SEIF-NARAGHI, S. B., LITTLEFIELD, R. B., SCHUP-MAGOFFIN, P. J. & CHRISTMAN, K. L. 2009. Naturally derived myocardial matrix as an injectable scaffold for cardiac tissue engineering. *Biomaterials,* 30**,** 5409-16.

SMITH, J., LADI, E., MAYER-PROSCHEL, M. & NOBLE, M. 2000. Redox state is a central modulator of the balance between self-renewal and differentiation in a dividing glial precursor cell. *Proceedings of the National Academy of Sciences of the United States of America,* 97**,** 10032-10037.

SMITH, L. A., LIU, X., HU, J. & MA, P. X. 2009. The influence of three-dimensional nanofibrous scaffolds on the osteogenic differentiation of embryonic stem cells. *Biomaterials,* 30**,** 2516-2522.

SOUTHWELL, D. G., NICHOLAS, C. R., BASBAUM, A. I., STRYKER, M. P., KRIEGSTEIN, A. R., RUBENSTEIN, J. L. & ALVAREZ-BUYLLA, A. 2014. Interneurons from Embryonic Development to Cell-Based Therapy. *Science,* 344.

STEINER, D., KHANER, H., COHEN, M., EVEN-RAM, S., GIL, Y., ITSYKSON, P., TURETSKY, T., IDELSON, M., AIZENMAN, E., RAM, R., BERMAN-ZAKEN, Y. & REUBINOFF, B. 2010. Derivation, propagation and controlled

differentiation of human embryonic stem cells in suspension. *Nature Biotechnology,* 28**,** 361-U88.

STOLBERG, S. & MCCLOSKEY, K. E. 2009. Can Shear Stress Direct Stem Cell Fate? *Biotechnology Progress,* 25**,** 10-19.

SUN, L. Y., LIN, S. Z., LI, Y. S., HARN, H. J. & CHIOU, T. W. 2011. Functional Cells Cultured on Microcarriers for Use in Regenerative Medicine Research. *Cell Transplantation,* 20**,** 49-62.

SUN, W. & ZWEIGERDT, R. 2009. *Human Embryonic Stem Cell-Derived Cardiomyocytes for Cell Therapy and Drug Discovery*, John Wiley & Sons, Inc.

SUNG, J. H., YU, J., LUO, D., SHULER, M. L. & MARCH, J. C. 2010. Microscale 3-D hydrogel scaffold for biomimetic gastrointestinal (GI) tract model. *Lab on a Chip*.

SUPER, A. 2014. *Oxygen monitoring in a microfluidic culture device for stem cell bioprocess development* Doctoral Thesis, UCL (University College London).

TAAPKEN, S. M., NISLER, B. S., NEWTON, M. A., SAMPSELL-BARRON, T. L., LEONHARD, K. A., MCINTIRE, E. M. & MONTGOMERY, K. D. 2011. Karyotypic abnormalities in human induced pluripotent stem cells and embryonic stem cells. *Nat Biotech,* 29**,** 313-314.

TAKAHASHI, K., TANABE, K., OHNUKI, M., NARITA, M., ICHISAKA, T., TOMODA, K. & YAMANAKA, S. 2007. Induction of Pluripotent Stem Cells from Adult Human Fibroblasts by Defined Factors. *Cell,* 131**,** 861-872.

TAKAHASHI, K. & YAMANAKA, S. 2006. Induction of Pluripotent Stem Cells from Mouse Embryonic and Adult Fibroblast Cultures by Defined Factors. *Cell,* 126**,** 663-676.

TAN, G.-D. S., TOH, G. W., BIRGERSSON, E., ROBENS, J., VAN NOORT, D. & LEO, H. L. 2013. A thin-walled polydimethylsiloxane bioreactor for high-density hepatocyte sandwich culture. *Biotechnology and Bioengineering,* 110**,** 1663-1673.

TANZEGLOCK, T., SOOS, M., STEPHANOPOULOS, G. & MORBIDELLI, M. 2009. Induction of mammalian cell death by simple shear and extensional flows. *Biotechnology and Bioengineering,* 104**,** 360-370.

THOMSON, H. 2007. Bioprocessing of embryonic stem cells for drug discovery. *Trends in Biotechnology,* 25**,** 224-230.

THOMSON, J. A., ITSKOVITZ-ELDOR, J., SHAPIRO, S. S., WAKNITZ, M. A., SWIERGIEL, J. J., MARSHALL, V. S. & JONES, J. M. 1998. Embryonic stem cell lines derived from human blastocysts. *Science,* 282**,** 1827-1827.

TIBBITT, M. W. & ANSETH, K. S. 2009. Hydrogels as extracellular matrix mimics for 3D cell culture. *Biotechnology and Bioengineering,* 103**,** 655-663.

TITMARSH, D., HIDALGO, A., TURNER, J., WOLVETANG, E. & COOPER-WHITE, J. 2011. Optimization of flowrate for expansion of human embryonic stem cells in perfusion microbioreactors. *Biotechnology and Bioengineering,* 108**,** 2894-2904.

TITMARSH, D. M., HUDSON, J. E., HIDALGO, A., ELEFANTY, A. G., STANLEY, E. G., WOLVETANG, E. J. & COOPER-WHITE, J. J. 2012.

Microbioreactor Arrays for Full Factorial Screening of Exogenous and Paracrine Factors in Human Embryonic Stem Cell Differentiation. *Plos One,* 7**,** e52405.

TKACHENKO, E., GUTIERREZ, E., GINSBERG, M. H. & GROISMAN, A. 2009. An easy to assemble microfluidic perfusion device with a magnetic clamp. *Lab on a Chip,* 9**,** 1085-1095.

TOH, Y.-C. & VOLDMAN, J. 2011. Fluid shear stress primes mouse embryonic stem cells for differentiation in a self-renewing environment via heparan sulfate proteoglycans transduction. *The FASEB Journal,* 25**,** 1208-1217.

TOUBOUL, T., HANNAN, N. R. F., CORBINEAU, S., MARTINEZ, A., MARTINET, C., BRANCHEREAU, S., MAINOT, S., STRICK-MARCHAND, H., PEDERSEN, R., DI SANTO, J., WEBER, A. & VALLIER, L. 2010. Generation of Functional Hepatocytes from Human Embryonic Stem Cells Under Chemically Defined Conditions that Recapitulate Liver Development. *Hepatology,* 51**,** 1754-1765.

TSAO, C.-W. & DEVOE, D. 2009. Bonding of thermoplastic polymer microfluidics. *Microfluidics and Nanofluidics,* 6**,** 1-16.

VAN DER MEER, A. D., ORLOVA, V. V., TEN DIJKE, P., VAN DEN BERG, A. & MUMMERY, C. L. 2013. Three-dimensional co-cultures of human endothelial cells and embryonic stem cell-derived pericytes inside a microfluidic device. *Lab on a Chip,* 13**,** 3562-3568.

VAN DER SANDEN, B., DHOBB, M., BERGER, F. & WION, D. 2010. Optimizing Stem Cell Culture. *Journal of Cellular Biochemistry,* 111**,** 801-807.

VAN HEEREN, H. 2012. Standards for connecting microfluidic devices? *Lab on a Chip,* 12**,** 1022-1025.

VERAITCH, F. S., SCOTT, R., WONG, J. W., LYE, G. J. & MASON, C. 2008. The impact of manual processing on the expansion and directed differentiation of embryonic stem cells. *Biotechnology and Bioengineering,* 99**,** 1216-1229.

VILLA-DIAZ, L. G., TORISAWA, Y. S., UCHIDA, T., DING, J., NOGUEIRA-DE-SOUZA, N. C., O'SHEA, K. S., TAKAYAMA, S. & SMITH, G. D. 2009. Microfluidic culture of single human embryonic stem cell colonies. *Lab on a Chip,* 9**,** 1749-1755.

VOLAREVIC, V., LJUJIC, B., STOJKOVIC, P., LUKIC, A., ARSENIJEVIC, N. & STOJKOVIC, M. 2011. Human stem cell research and regenerative medicine--present and future. *Br Med Bull,* 99**,** 155-68.

WAGERS, AMY J. 2012. The Stem Cell Niche in Regenerative Medicine. *Cell Stem Cell,* 10**,** 362-369.

WARREN, L., MANOS, P. D., AHFELDT, T., LOH, Y.-H., LI, H., LAU, F., EBINA, W., MANDAL, P. K., SMITH, Z. D., MEISSNER, A., DALEY, G. Q., BRACK, A. S., COLLINS, J. J., COWAN, C., SCHLAEGER, T. M. & ROSSI, D. J. 2010. Highly Efficient Reprogramming to Pluripotency and Directed Differentiation of Human Cells with Synthetic Modified mRNA. *Cell Stem Cell,* 7**,** 618-630.

WATANABE, K., UENO, M., KAMIYA, D., NISHIYAMA, A., MATSUMURA, M., WATAYA, T., TAKAHASHI, J. B., NISHIKAWA, S., NISHIKAWA, S.-I., MUGURUMA, K. & SASAI, Y. 2007. A ROCK inhibitor permits survival of dissociated human embryonic stem cells. *Nat Biotech,* 25**,** 681-686.

WHITESIDES, G. M. 2006. The origins and the future of microfluidics. *Nature,* 442**,** 368-373.

WHITESIDES, G. M., OSTUNI, E., TAKAYAMA, S., JIANG, X. & INGBER, D. E. 2001. Soft Lithography in Biology and Biochemistry. *Annual Review of Biomedical Engineering,* 3**,** 335-373.

WHYTE, J. L., BALL, S. G., SHUTTLEWORTH, C. A., BRENNAN, K. & KIELTY, C. M. 2011. Density of human bone marrow stromal cells regulates commitment to vascular lineages. *Stem Cell Research,* 6**,** 238-250.

WILLIAMSON, A., SINGH, S., FERNEKORN, U. & SCHOBER, A. 2013. The future of the patient-specific Body-on-a-chip. *Lab on a Chip,* 13**,** 3471-3480.

XU, B.-Y., HU, S.-W., QIAN, G.-S., XU, J.-J. & CHEN, H.-Y. 2013. A novel microfluidic platform with stable concentration gradient for on chip cell culture and screening assays. *Lab on a Chip,* 13**,** 3714-3720.

YAMAMOTO, K., SOKABE, T., WATABE, T., MIYAZONO, K., YAMASHITA, J. K., OBI, S., OHURA, N., MATSUSHITA, A., KAMIYA, A. & ANDO, J. 2005. Fluid shear stress induces differentiation of Flk-1-positive embryonic stem cells into vascular endothelial cells in vitro. *American Journal of Physiology-Heart and Circulatory Physiology,* 288**,** H1915-H1924.

YANES, O., CLARK, J., WONG, D. M., PATTI, G. J., SANCHEZ-RUIZ, A., BENTON, H. P., TRAUGER, S. A., DESPONTS, C., DING, S. & SIUZDAK, G. 2010. Metabolic oxidation regulates embryonic stem cell differentiation. *Nature Chemical Biology,* 6**,** 411-417.

YEO, D., KIPARISSIDES, A., CHA, J. M., AGUILAR-GALLARDO, C., POLAK, J. M., TSIRIDIS, E., PISTIKOPOULOS, E. N. & MANTALARIS, A. 2013. Improving Embryonic Stem Cell Expansion through the Combination of Perfusion and Bioprocess Model Design. *Plos One,* 8**,** e81728.

YOSHIMITSU, R., HATTORI, K., SUGIURA, S., KONDO, Y., YAMADA, R., TACHIKAWA, S., SATOH, T., KURISAKI, A., OHNUMA, K., ASASHIMA, M. & KANAMORI, T. 2014. Microfluidic perfusion culture of human induced pluripotent stem cells under fully defined culture conditions. *Biotechnology and Bioengineering,* 111**,** 937-947.

YOUNG, E. W. K. & BEEBE, D. J. 2010. Fundamentals of microfluidic cell culture in controlled microenvironments. *Chemical Society Reviews,* 39**,** 1036-1048.

YOUNG, E. W. K. & SIMMONS, C. A. 2010. Macro- and microscale fluid flow systems for endothelial cell biology. *Lab on a Chip,* 10**,** 143-160.

YU, D. X., MARCHETTO, MARIA C. & GAGE, FRED H. 2013. Therapeutic Translation of iPSCs for Treating Neurological Disease. *Cell Stem Cell,* 12**,** 678-688.

YU, J. Y., VODYANIK, M. A., SMUGA-OTTO, K., ANTOSIEWICZ-BOURGET, J., FRANE, J. L., TIAN, S., NIE, J., JONSDOTTIR, G. A., RUOTTI, V., STEWART, R., SLUKVIN, II & THOMSON, J. A. 2007. Induced pluripotent stem cell lines derived from human somatic cells. *Science,* 318**,** 1917-1920.

ZHANG, B., KRAWETZ, R. & RANCOURT, D. E. 2013. Would the real human embryonic stem cell please stand up? *Bioessays,* 35**,** 632-638.

ZHANG, D. & KILIAN, K. A. 2013. The effect of mesenchymal stem cell shape on the maintenance of multipotency. *Biomaterials,* 34**,** 3962-3969.

ZHOU, H. Y., WU, S. L., JOO, J. Y., ZHU, S. Y., HAN, D. W., LIN, T. X., TRAUGER, S., BIEN, G., YAO, S., ZHU, Y., SIUZDAK, G., SCHOLER, H. R., DUAN, L. X. & DING, S. 2009. Generation of Induced Pluripotent Stem Cells Using Recombinant Proteins. *Cell Stem Cell,* 4**,** 381-384.

ZHOU, J. & NIKLASON, L. E. 2012. Microfluidic artificial "vessels" for dynamic mechanical stimulation of mesenchymal stem cells. *Integrative Biology,* 4**,** 1487-1497.

ZIPORI, D. 2009. *Biology of Stem Cells and the Molecular Basis of the Stem State*, Humana Press Inc.